

# **On the mechanism and quantitative toxicity evolution of catalytic TAML and NewTAML Hydrogen Peroxide oxidative destruction of micropollutants in river water and municipal wastewater**

Dissertation by  
**Yogesh Somasundar**

In Partial Fulfillment of the Requirements for the Degree of  
**Doctor of Philosophy**

Thesis Advisor  
**Terrence J. Collins**

Department of Chemistry, Carnegie Mellon University  
Pittsburgh, PA

Submitted February, 2020

# ABSTRACT

Anthropogenic activities over the centuries have led to depletion of Earth's natural resources and damage to ecology at alarming magnitudes and accelerating rates. Contamination of freshwater is a major component of the ecological injuries which is the most economically accessible point for transformative cleanup to support the survival of mankind and other species. In addition to preventive efforts to conserve water bodies, the world is turning towards replenishing and reusing water through wastewater treatment. Unfortunately, conventional wastewater treatments are not designed to remove micropollutants (MPs) – substances that produce undesired effects, including endocrine disruption, in organisms at low doses (or low concentrations in water for aquatic life), typically parts per trillion (ng/L) – low parts per billion (µg/L) concentrations. Advanced oxidation processes that are capable of removing MPs are very expensive or work at acidic conditions which make them unsuitable for economical wastewater treatment applications. This thesis is an effort towards advancing water purification and reclamation, including real wastewater studies, utilizing sustainably designed catalysts, viz., TAMLs and NewTAMLs, that mimic the chemistries of oxidizing enzymes. Tetraamido macrocyclic ligand (TAML) activators are mechanistically faithful, small molecule replicas of peroxidase and cytochrome P450 enzymes. They are capable of oxidizing numerous MPs in conjunction with hydrogen peroxide applications conducted at nM catalyst concentrations. Over 25 years TAMLs have been iteratively improved to surpass TAMLs with NewTAMLs as by far and away the best peroxidase mimics that are non-halogenated, exhibit superior reactivities and longer lifetimes. A tunable kill switch introduced in NewTAMLs helps to control the lifetimes of the catalysts, including allowing quicker or much slower degradations.

Propranolol is heavily prescribed  $\beta$  blocker drug and persistent MP. It is used herein as a model micropollutant for characterizing the reactivities of various TAMLs and NewTAMLs. At 11.2

ppm hydrogen peroxide, 100nM of the more reactive TAMLs and NewTAMLs are capable of oxidizing 15 ppb propranolol to mineralization in 5 and 30 minutes in buffered water and river water, respectively. The best performing NewTAML with a partially muted kill switch (work is proceeding in the IGS to turn it off completely) provided similar performances to the previous best TAML, but at 1/10<sup>th</sup> the concentration (NewTAML 10 nM, TAML 100 nM). A set of 38 MPs were evaluated simultaneously in real wastewaters of Tucson, AZ with 5 treatments of NewTAML/H<sub>2</sub>O<sub>2</sub> followed temporally for 6 hours. 4 treatments of ozone viz., 2, 4, 6, and 8 ppm were analyzed after 72 h of ozone dosage (not effective contact time) to compare the NewTAML and ozone treatments. Detailed kinetic analyses of the 38 MPs revealed that (i) most of the reaction is completed within the first 30-60 min for NewTAMLs after which the catalyst is inactivated. (ii) The best performing 200 nM NewTAML/22.4 ppm H<sub>2</sub>O<sub>2</sub> outperformed across the board compared to 2 ppm ozone, the current standard dose used in Neugut Plant in Dübendorf Switzerland. From the performance of NewTAML/H<sub>2</sub>O<sub>2</sub> described in this work, it can be projected that 70 nM of NewTAML and 15 ppm of H<sub>2</sub>O<sub>2</sub> can effectively treat 22,500 tonnes of wastewater, the daily amount produced by 150,000 Europeans.

Digging deeper into the kinetic and mechanistic aspects of propranolol oxidation helped us to discover and characterize substrate inhibition in TAMLs using UV-vis, fluorescence, MS, NMR and DFT calculations. Additionally, propranolol-TAML associates were isolated for the very first time. It was determined that substrate inhibition is not a significant factor at ppt-ppb of substrates which is the typically identified concentrations in wastewaters. Oxidation products were identified, isolated where possible and kinetically characterized at each step of oxidation process leading to minerals. Kinetic rate constants at each step of the oxidation was utilized to build theoretical simulation profiles which agreed with experimental composition profiles. Mass (%-composition of intermediates) and toxicity profiles for the overall degradation helped provide a comprehensive view of the sustainable oxidation process. Redox potentials of various TAMLs

and NewTAMLs have been correlated to their reactivities and substrate interactions using Linear Free Energy Relationships (LFER). To conserve time for rapid evaluation of decontamination of various colorless MPs, an alternative kinetic model based on parallel or competitive reactions has been developed to follow the reaction progress of these colorless MPs using UV-Vis spectroscopy with phenol and propranolol as the model colorless substrates. In totality, this thesis serves to (i) advance the mechanistic understanding of TAML catalyzed oxidations, (ii) provide a holistic approach to decontamination processes – mass/toxicity versus time profiles should be considered together, to provide more complete information on potential environmental effects of decontamination procedures, (iii) provide extensive data supporting the applicability of NewTAML/  $\text{H}_2\text{O}_2$  as a viable wastewater treatment technology with experiments on complex real waters including lab water, river water and wastewater.



# ACKNOWLEDGEMENTS

Foremost, I would like to convey my gratitude to the Department of Chemistry, Carnegie Mellon University for providing me an opportunity to pursue grad school after working in a corporate setup. This was not an easy transition for me since I had to revisit the textbooks that I had kept aside for a while. I would like to express my sincere gratitude to the Institute for Green Science (IGS) and especially my advisor Professor Terry Collins for giving me ample time and resources to work with. The fact that I was not from a top academic institution in India did not prevent Terry from accepting me into IGS. His belief in my potential motivated me to work hard and grow as a researcher and a mentor in the group. Thank you Terry for allowing me to explore my research interests in the group, at my own pace, and at my own command. I have a completely different perspective on Sustainability after working with Terry. He has led by example for me when it comes to interacting with peers and students. This translated into how I mentored several undergraduate students in the group.

My thesis work would not have been possible without the constant guidance and inputs from the kinetics maestro Professor Aleksander Ryabov. Before Sasha's class, I never imagined kinetics could give you so much information about a reaction. Sasha has taught me to be fearless with seeking answers. Sasha is masterful at the art of telling a story and I have learned a lot observing him develop a story by knitting together the pieces of my experimental work. Thank you Sasha for being very patient with my first drafts of reports, research proposals, and presentations. While Terry showed me the broad perspective of TAMLs and their possibilities, Sasha kept me grounded with the data at hand, within the purview of the comprehensive picture.

Besides Terry and Sasha, I would like to thank my doctoral thesis committee members Professors Stefan Bernhard and Ryan Sullivan for their guidance, regular feedback and insightful questions all along this journey. Perspectives from both of you gave new dimensions and enriched

the quality of my research. I would like to thank the Richard King Mellon Presidential Fellowship for providing financial support for my research at CMU. I would also like to thank the graduate program committee for developing a holistic program for the development of grad students.

I would like to extend my sincere thanks to Dr. Matthew Mills who mentored me and taught me all the analytical instruments in lab. He was my go-to person for every glitch in my research, at least in the initial phase. Along with Sasha, Matt was very instrumental in training me on experimental design and data analysis. I have learned to work efficiently as a grad student by observing Matt and I attribute my work ethics to him. The work described in Chapters 3 was initiated by Dr. Mills and Abby Burton and the work described in Chapter 7 was initiated by Dr. Mills and Ximena Olivares. The extensive nature of the research in both these chapters are my thesis work though. In addition to assessing my research, I would also like to thank Matt for assessing my cooking experimentations. Chapters 4, 5 and 6 would never have been a reality without NewTAMLs synthesized by Dr. Genoa Warner. In addition to these chapters, I have collaborated with Genoa on multiple projects involving NewTAMLs which will be published in the near future. It started off with Genoa being the really supportive lab senior but now she is more of a friend that I can call anytime to talk research and beyond. Thank you Genoa for being such a good friend. My original research proposal was given a good shape because of Genoa. I wish you, Georgia and Taylor the best in the world. Dr. Liang Tang in addition to being a great lab senior was instrumental to my NMR studies in Chapter 2. She had a calming effect on me during my progress report requirements. I have had very insightful discussions with Dr. Matthew DeNardo during my research at IGS. He was a key person to initiate the discussions which ultimately led to the collaborative work with the University of Arizona, discussed in Chapter 5. I would like to thank Dr. Longzhu Shen for DFT studies discussed in Chapters 2 and 6. I would like to thank the current IGS members Paul Kornbluh and Hannah Frame with whom I have enjoyed doing the practice talks

and whiteboard discussions. Hannah will take over some of the projects that I initiated and I wish her the best in these projects.

I would like to thank Terry for giving me an opportunity to mentor several undergrads as a grad student at IGS. This thesis has a significant contribution from the undergrad army that I have mentored over years. Alexis Hoane performed the UV studies of substrate interactions in Chapter 2 and quenching studies discussed in Chapter 6. I am very happy for her numerous grad school admits and I wish her the very best with grad school. Iris Lu has contributed significantly towards chapter 7 which was technically very challenging. She also performed the preliminary experiments on polymer supported TAMLs which is not discussed in the thesis. Lisa Qian also contributed towards Chapter 7 with initial experiments. Evan Kaaret performed the redox potential measurements of a few catalysts in Chapter 6. Cindy Weng, although not being a chemist, was instrumental to the data collection for the oxidation of insecticide Imidacloprid. This was a collaborative project with Dr. Genoa Warner. Jeff Bradley has significantly contributed towards the kinetic studies involving iodinated contrast agents. Jolie Miller contributed towards identification of oxidation products of contrast agents. David Zhang determined the rate constants for oxidation of one of the intermediates mentioned in Chapter 3. All the undergrads have also contributed towards developing a second reference library of rate constants, after Orange II, for catalytic oxidation of Safranin O with TAMLs and NewTAMLs.

I extend my sincere thanks to all the collaborators that I have worked with during my PhD. Chapter 5 was a collaborative work with Professor Shane Snyder, Dr. Minkyu Park, and Dr. Kevin Daniels at the University of Arizona. Although not discussed in this thesis, I would like to thank Professor Susan Nagel and Jennifer Cornelius for the collaborative work on detoxifying fracking produced waters with NewTAML treatment. The work is expected to be published in the near future. I would like to thank Professor Krzysztof Matyjaszewski, Dr. Grzegorz Szczepaniak and Sushil Lathwal with whom I have collaborated to develop polymer-supported TAMLs for water

treatment. The work is in the preliminary stages and we hope to publish the work in the future. I would like to thank Professor Ryan Sullivan, Bailey Bowers and Lydia Jahl with whom I have collaborated for PFOS breakdown utilizing NewTAML treatment. I want to thank Professor Lyuba Varticovski and Dr. Diana Stavreva at the National Institutes for Health (NIH) for collaborative efforts on high throughput receptor studies. I would also like to thank Professor Karen Stump, Professor Gizelle Sherwood, Carolyn Neiderlander and Lillian Crawford with whom I was associated as a teaching assistant for the first 2 years of my PhD.

All through my PhD, I have used instruments in various labs both within and outside the department. I would especially like to thank Professor Mark Bier at Center for Molecular Analysis (CMA) and Professor Roberto Gil (NMR Center) for providing key instrumentation that aided my research. In addition to them, I would also like to thank the Guo Lab, Armitage Lab, Matyjaszewski Lab, Das Lab, Sydlik Lab, Noonan Lab, Hendrich Lab and the Gregory Lab (Civil and Environmental Engineering) wherein I have used various instruments at different stages of my PhD. This thesis would never be a possibility had it not been for the contributions from the people who ensure the smooth functioning of the department. Thank you Dr. Rea Freeland for constantly checking with my progress and ensuring timely completion. Valerie Bridge, Timothy Sager, Lorna Williams, Jessica Derenburger, Sara Wainer, Patsey Haddock, Kristin Edwards, Beryl Omune, Paul Smith, Ray Butko, and Melissa Powell have all contributed towards the progress of my PhD.

Saving the most important for the last, I want to thank my family and friends whose contribution is immeasurable. My mom Usha has been my inspiration throughout. No words can describe her contribution. I would like to thank my mentor, Mr. Aporesh Acharya from whom I have learnt the values to lead my life. My siblings and their better halves, Gayathri, Sunil, Karthik, Poojitha and my nephew Rana have all ensured that I remain sane and have always been very supportive of my decisions in life. It will be incomplete if I do not thank the contributions of all my

friends in life who have celebrated my success and failures with equal vigor. To all my friends I will like to say that, this would not have been possible without all of you.

# TABLE OF CONTENTS

ABSTRACT .....	ii
ACKNOWLEDGEMENTS.....	v
TABLE OF CONTENTS.....	x
LIST OF FIGURES.....	xv
LIST OF SCHEMES.....	xviii
LIST OF TABLES.....	xix

## CHAPTER 1

<b>The current water treatment scenario and bio-inspired TAML activators as sustainable solutions for the micropollutant menace.....</b>	<b>1</b>
1.1 BIODIVERSITY AND HUMAN IMPACT.....	2
1.1.1 Threats posed by Humans .....	2
1.2 LESSON FROM HISTORY: THE NEAR EXTINCTION AND RESURGENCE OF THE BALD EAGLE .....	4
1.3 DRINKING WATER CRISIS: A FACT CHECK .....	5
1.4 MICROPOLLUTANTS AS A WATER TREATMENT CHALLENGE .....	6
1.4.1 Micropollutants as endocrine disruptors or other toxicity inducing chemicals .....	6
1.4.2 Inefficiency of conventional wastewater treatment methods.....	9
1.4.3 Unusual high production and usage of chemicals.....	9
1.4.4 Micropollutants as persistent organic pollutants (POPs) .....	11
1.4.4.1 Utilizing tree swallows as indicators for contaminant exposure and bioaccumulation .....	11
1.4.5 Advanced oxidation processes (AOP) for the treatment of micropollutants .....	12
1.5 TAML ACTIVATORS AS A SUSTAINABLE SOLUTION FOR TREATING MICROPOLLUTANTS.....	16
1.5.1 History of TAMLs in oxidizing MPs.....	18
1.5.2 London wastewater experiments.....	20
1.6 ITERATIVE DESIGN FROM TAMLs TO NEWTAMLs .....	22
1.6.1 Linear relationship between reactivity and life .....	22
1.6.2 Kill Switch in NewTAMLs.....	25
1.7 SUBSTRATE INHIBITION IN TAML CATALYSIS .....	27

1.8 OXIDATION INTERMEDIATES AND THEIR ENVIRONMENTAL FATE FOR TAML CATALYZED REACTIONS .....	30
1.9 PREDICTING REACTION PROGRESS WITH PROPERTIES OF TAML USING LFER PLOTS .....	32
1.10 ANALYSIS OF COLORLESS MPs IN TAML CATALYZED OXIDATIONS.....	34
1.11 RESEARCH SUMMARY .....	35
1.12 REFERENCES .....	38

## CHAPTER 2

<b>Structural, Mechanistic and Ultra-dilute Catalysis Portrayal of Substrate Inhibition in the TAML–Hydrogen Peroxide Catalytic Oxidation of the Persistent Drug and Micropollutant, Propranolol.....</b>	<b>53</b>
2.1 INTRODUCTION .....	54
2.2 RESULTS .....	57
2.2.1 Kinetics of the TAML-Catalyzed Oxidation of propranolol by H <sub>2</sub> O <sub>2</sub> Reveals Substrate Inhibition.....	57
2.2.2 UV-Vis and Fluorescence Spectroscopies. ....	60
2.2.3 <sup>1</sup> H NMR Spectroscopy. ....	62
2.2.4 Isolation and Composition of the Propranolol-TAML Adducts. ....	64
2.2.5 DFT Simulations. ....	65
2.3 DISCUSSION .....	66
2.4 CONCLUSIONS.....	71
2.5 EXPERIMENTAL.....	73
2.5.1 Materials. ....	73
2.5.2 Instrumentation. ....	73
2.5.3 Kinetics Studies. ....	75
2.5.4 Isolation of Propranolol-TAML [P-TAML] Adducts. ....	75
2.5.5 DFT Calculations. ....	75
2.6 APPENDIX.....	77
2.7 REFERENCES .....	86

## CHAPTER 3

<b>To Sustainability via Analytical and Kinetic Characterization of Propranolol Fragments during Its TAML-Catalyzed Oxidation by H<sub>2</sub>O<sub>2</sub>. Mass and Toxicity vs Time Profiles .....</b>	<b>93</b>
3.1 INTRODUCTION .....	94

3.2 RESULTS AND DISCUSSION .....	97
3.2.1 UPLC and GC-MS Identification of Fragments of TAML-Catalyzed Oxidation of Propranolol by H <sub>2</sub> O <sub>2</sub> . ....	97
3.2.2 Ionic Chromatography Identification of Fragments of TAML-Catalyzed Oxidation of Propranolol by H <sub>2</sub> O <sub>2</sub> . ....	99
3.2.3 Tracing of Acetone by <sup>1</sup> H NMR. ....	100
3.2.4 Building Concentration versus Time Profiles for ‘UPLC’ Products of TAML-catalyzed Oxidation of Propranolol by H <sub>2</sub> O <sub>2</sub> . ....	101
3.2.5 Kinetics of Oxidation by H <sub>2</sub> O <sub>2</sub> of Products of Propranolol Degradation, Uncatalyzed (NO <sub>2</sub> ) and <b>1c</b> -Catalyzed (NOH, NO <sub>2</sub> epo, NO <sub>2</sub> (OH)). ....	102
3.2.6 Computer Simulation of the Concentration/Time Profiles of Propranolol and Its Degradation Fragments. ....	104
3.2.7 "Dark (Toxic) Side of the Moon" .....	106
3.2.8 Mechanistic Considerations. ....	109
3.3 CONCLUSIONS.....	111
3.4 EXPERIMENTAL.....	112
3.4.1 Materials. ....	112
3.4.2 Instrumentation. ....	112
3.4.3 Analyses for Propranolol Fragments.....	113
3.4.4 Kinetics of Oxidation of Propranolol Fragments. ....	114
3.4.5 Isolation of 1,4-Naphthoquinone. ....	114
3.5 APPENDIX.....	116
3.6 REFERENCES .....	124

## CHAPTER 4

<b>Use of the micropollutant, propranolol, as a test system for comparative evaluation of the technical performances of TAMLs and NewTAMLs to identify the best overall candidate for real waste water treatment.....</b>	<b>128</b>
4.1 INTRODUCTION .....	129
4.2 RESULTS AND DISCUSSION .....	132
4.2.1 Buffered studies at propranolol $5 \times 10^{-5}$ M (~15 ppm) at pH 7 .....	132
4.2.2 Determination of kinetic rate constants for NewTAMLs at pH 7.....	133
4.2.3 Buffered studies at propranolol $5.3 \times 10^{-8}$ M (~15 ppb).....	137
4.2.4 Unbuffered studies in Allegheny river water .....	138
4.2.5 Safety perspective: .....	141
4.3 CONCLUSIONS.....	143



4.4 EXPERIMENTAL .....	145
4.4.1 Materials. ....	145
4.4.2 Catalyzed Degradation of Propranolol by H <sub>2</sub> O <sub>2</sub> . ....	145
4.4.3 Instrumentation. ....	146
4.5 REFERENCES .....	147

## CHAPTER 5

<b>Sustainable Ultra-Dilute Oxidation Catalysis (SUDOC) utilizing NewTAML activators for Global water treatment: A Landmark study with Tucson wastewater .....</b>	<b>150</b>
5.1 INTRODUCTION .....	151
5.2 RESULTS AND DISCUSSION .....	154
5.2.1 Comparative evaluation of <b>2d</b> /H <sub>2</sub> O <sub>2</sub> treatments and Ozone treatments .....	154
5.2.2 Improvement factor of 200 nM <b>2d</b> /22.4 ppm H <sub>2</sub> O <sub>2</sub> over 2 ppm ozone.....	156
5.2.3 Kinetic analyses of <b>2d</b> / H <sub>2</sub> O <sub>2</sub> and Ozone treatments utilizing trimethoprim as a model MP.....	158
5.2.4 Correlating structure of MPs with their attenuation.....	161
5.2.5 Effect of <b>2d</b> /H <sub>2</sub> O <sub>2</sub> treatments on Dissolved Organic Carbon in Water.....	164
5.2.6 How many tonnes of wastewater can be treated? .....	167
5.3 CONCLUSIONS.....	168
5.4 EXPERIMENTAL.....	170
5.4.1 Materials, Chemicals and Reagents .....	170
5.4.2 Sample Collection and Preparation.....	170
5.4.3 Indicator Micropollutants for Analyses .....	171
5.4.4 Instrumentation .....	171
5.4.5 Ozone treatments .....	172
5.4.6 <b>2d</b> / H <sub>2</sub> O <sub>2</sub> treatment:.....	173
5.5 APPENDIX.....	174
5.6 REFERENCES .....	183

## CHAPTER 6

<b>Predicting Properties of Iron(III) TAML Activators of Peroxides from Their III/IV and IV/V Reduction Potentials.....</b>	<b>186</b>
6.1 INTRODUCTION .....	187
6.2 RESULTS AND DISCUSSION .....	189
6.2.1 Cyclic Voltammetry Measurements.....	189

6.2.2 Formal Reduction Potentials $E^{\circ}$ and $pK_a$ 's. ....	192
6.2.3 Formal Reduction Potentials $E^{\circ}$ and Stern-Volmer Quenching Constants $K_{SV}$ . ....	194
6.2.4 Calculated Ionization Potentials (IPs), HOMOs of Iron(III, IV and IV) TAMLs and Formal Reduction Potentials $E^{\circ}$ . ....	195
6.2.5 Reactivity Comparisons. ....	197
6.3 CONCLUSION.....	200
6.4 EXPERIMENTAL.....	201
6.4.1 Materials .....	201
6.4.2 Instrumentation and Measurements. ....	201
6.4.3 Theoretical Calculations. ....	201
6.5 APPENDIX.....	203
6.6 REFERENCES .....	207

## CHAPTER 7

<b>Determination by UV-vis spectroscopy of rate constants for colorless substrates for their TAML catalyzed oxidations by <math>H_2O_2</math></b> .....	210
7.1 INTRODUCTION .....	211
7.2 RESULTS AND DISCUSSION .....	215
7.2.1 Direct determination of second order rate constant, $k_{II}$ .....	215
7.2.2 Indirect determination of second order rate constant, $k_{II}^S$ .....	217
7.2.2.1 Kinetics of a TAML catalyzed parallel oxidation of two substrates. ....	217
7.2.3 Significance of substrate inhibition of <b>1a</b> . ....	222
7.2.4 Interference from the oxidation products. ....	229
7.3 CONCLUSIONS.....	231
7.4 EXPERIMENTAL.....	233
7.4.1 Materials. ....	233
7.4.2 Instrumentation. ....	233
7.4.3 Direct kinetic analyses using UPLC. ....	234
7.4.4 Indirect kinetic analyses via parallel reaction approach using UV-vis spectroscopy. ....	234
7.5 APPENDIX.....	235
7.6 REFERENCES .....	239

# LIST OF FIGURES

Figure 1.1 Total compounds in the CAS registry and Roundup herbicide usage across USA. ....	10
Figure 1.2 Classes of MPs oxidized by TAML/H <sub>2</sub> O <sub>2</sub> and NewTAML/H <sub>2</sub> O <sub>2</sub> treatments to date. ..	19
Figure 1.3 TAML catalyzed oxidation of estrogen and pharmaceuticals in London wastewaters.	20
Figure 1.4 Iterative design from TAML to NewTAML activators.....	23
Figure 2.1 Comparative evaluation of TAMLs in degradation of propranolol .....	57
Figure 2.2 .Kinetics of TAML catalyzed degradation of propranolol by H <sub>2</sub> O <sub>2</sub> .....	59
Figure 2.3 Quenching of propranolol fluorescence by TAMLs.....	62
Figure 2.4 <sup>1</sup> H NMR spectra of propranolol and TAML solution.....	63
Figure 2.5 The structural composition of propranolol-TAML adducts. ....	64
Figure 2.6 Projected impact of substrate inhibition on TAML .....	69
Figure 2.7 Determination of initial rate in TAML catalysis .....	77
Figure 2.8 Significance of TAML concentrations in TAML catalyzed oxidations. ....	77
Figure 2.9 TAML catalyzed propranolol oxidation as a function of propranolol concentration. ..	78
Figure 2.10 Analysis of propranolol TAML interaction by UV-vis spectroscopy. ....	78
Figure 2.11 Formation of propranolol-TAML adducts.....	79
Figure 2.12 <sup>1</sup> H NMR spectra of diethylamine and TAML solution.....	79
Figure 2.13 <sup>1</sup> H NMR spectra of FeCl <sub>3</sub> and propranolol solution. ....	80
Figure 2.14 <sup>1</sup> H NMR spectra of propranolol and non-aromatic TAML solution. ....	80
Figure 2.15 <sup>1</sup> H NMR spectra of isopropanol and TAML solution .....	81
Figure 2.16 ESI-MS of propranolol-fluorinated TAML adduct .....	81
Figure 2.17 ESI-MS of propranolol-diaromatic TAML adduct.....	82
Figure 2.18 UV-vis spectra of redissolved propranolol-TAML adduct in methanol.....	82
Figure 2.19 Infrared spectra of propranolol-fluorinated TAML adduct. ....	83
Figure 2.20 Infrared spectra of propranolol-diaromatic TAML adduct.....	84
Figure 2.21 Ion chromatogram for the propranolol-TAML adduct. ....	84
Figure 2.22 <sup>1</sup> H NMR spectra of Orange II and TAML solution.....	85
Figure 3.1 UPLC chromatograms for TAML catalyzed propranolol degradation by H <sub>2</sub> O <sub>2</sub> . ....	97
Figure 3.2 Ionic chromatograms for TAML catalyzed propranolol degradation by H <sub>2</sub> O <sub>2</sub> . ....	100
Figure 3.3 Concentration vs time profiles for propranolol and the products of its degradation. .	101
Figure 3.4 Simulated vs experimental reaction profiles for propranolol degradation. ....	105
Figure 3.5 Calculated toxicity versus time profile for propranolol degradation.....	107

Figure 3.6 Peak areas at 254 nm over time for propranolol and its oxidation products .....	116
Figure 3.7 Determination of 1,4-naphthoquinone by $^1\text{H}$ NMR and GC-MS analyses.....	117
Figure 3.8 Determination of oxidation products by spiking experiments.....	118
Figure 3.9 Gas chromatogram of the products of TAML catalyzed oxidation of propranolol. ....	118
Figure 3.10 Mass spectrum of the peak for 2,3-dihydro-2,3-epoxy-naphthalene-1,4-dione. ....	119
Figure 3.11 Determination of 2-hydroxynaphthalene-1,4-dione by GC-MS analysis.....	120
Figure 3.12 Determination of 1-naphthol by GC-MS analysis.....	121
Figure 3.13 Determination of acetone by $^1\text{H}$ NMR analysis .....	122
Figure 3.14 Kinetics of catalyzed or uncatalyzed oxidation of propranolol oxidation products .	122
Figure 3.15 EPR spectrum of TAML catalyzed 1-naphthol oxidation reaction mixture.....	123
Figure 4.1 Comparative evaluation of TAMLs and NewTAMLs in propranolol oxidation.....	133
Figure 4.2 Kinetics of NewTAML catalyzed propranolol oxidation.....	134
Figure 4.3 Comparison of TAMLs or NewTAMLs in oxidation of 15 ppb propranolol.....	137
Figure 4.4 Comparison of TAMLs and NewTAMLs' performance in Allegheny river water....	139
Figure 4.5 Life time of TAMLs and NewTAMLs in Allegheny river water.....	140
Figure 5.1 Structures and mechanism of TAMLs <b>1</b> and NewTAMLs <b>2</b> .....	152
Figure 5.2 Attenuation of MPs in wastewater by NewTAML/ $\text{H}_2\text{O}_2$ and ozone treatments.....	155
Figure 5.3 Kinetics of oxidation of trimethoprim by NewTAML/ $\text{H}_2\text{O}_2$ and ozone treatments...	159
Figure 5.4 Correlation of attenuation with $\text{pK}_{\text{a}1}$ of micropollutants .....	161
Figure 5.5 Correlation of attenuation, with the HOMO energy levels of micropollutants .....	162
Figure 5.6 Attenuation of MPs with HOMO values in the NewTAML HOMO energy levels ...	163
Figure 5.7 Excitation-emission spectra of wastewater after NewTAML/ $\text{H}_2\text{O}_2$ treatment .....	165
Figure 5.8 Kinetics of attenuation of MPs by NewTAML/ $\text{H}_2\text{O}_2$ and ozone treatments .....	180
Figure 5.9 Attenuation of MPs by various ozone treatments.....	181
Figure 5.10 Dependence of attenuation of MPs on NewTAML concentrations.....	181
Figure 5.11 Structure of Diphenylmethane and its analogues .....	182
Figure 5.12 UV 254 absorbances of wastewater after NewTAML/ $\text{H}_2\text{O}_2$ treatment .....	182
Figure 6.1 Cyclic voltammogram of NewTAML catalyst in MeCN.....	189
Figure 6.2 Correlation of IV/V and III/IV reduction potentials of TAMLs and NewTAMLs ....	191
Figure 6.3 Correlation of reduction potentials with $\text{pK}_{\text{a}}$ of TAMLs and NewTAMLs .....	193
Figure 6.4 Correlation of redox potentials with $K_{\text{SV}}$ for propranolol fluorescence quenching ....	194
Figure 6.5 Calculated IPs of iron(III) TAMLs vs their measured $\text{Fe}^{\text{III/IV}}$ reduction potentials. ...	196
Figure 6.6 Plots of $\log k_{\text{II}}$ (pH 7, 25 °C) against $E^{\text{III/IV}}$ for propranolol and Orange II .....	198

Figure 6.7 Plot of $\log k_1$ (pH 7, 25 °C) against $E^{\text{III/IV}}$ for Orange II .....	199
Figure 6.8 Cyclic voltammograms of TAML at different scan rates .....	203
Figure 6.9 Peak currents versus square root of scan rate for TAML .....	203
Figure 6.10 Cyclic voltammogram showing both anodic and cathodic peaks in TAMLs .....	204
Figure 6.11 Calculated IPs of TAMLs versus their measured $\text{Fe}^{\text{IV/V}}$ reduction potentials. ....	204
Figure 6.12 Correlations between IPs and HOMOs for $\text{Fe}^{\text{III}}$ and $\text{Fe}^{\text{IV}}$ TAML species. ....	205
Figure 7.1 Kinetics of phenol degradation by $\text{H}_2\text{O}_2$ catalyzed by TAML. ....	216
Figure 7.2 Initial rate of Orange II bleaching by TAML/ $\text{H}_2\text{O}_2$ vs propranolol.concentration.....	218
Figure 7.3 Projected impact of propranolol on TAML activation in Orange II solution .....	223
Figure 7.4 Initial rate of Orange II bleaching by TAML/ $\text{H}_2\text{O}_2$ vs phenol concentration.....	224
Figure 7.5 Initial rate of Safranin O bleaching vs propranolol concentration.....	226
Figure 7.6 Initial rate of Orange II bleaching vs propranolol concentration using $k_{\text{I,eff}}$ .....	227
Figure 7.7 Projected impact of propranolol on TAML activation in Safranin O solution, .. f	235
Figure 7.8 Projected impact of Orange II on TAML activation in phenol solution,.....	235
Figure 7.9 Projected impact of Safranin O on TAML activation in phenol solution.....	236
Figure 7.10 Determination of indirect rate constant, $k_{\text{II}}^{\text{phenol}}$ from Orange II bleaching. ....	236
Figure 7.11 Determination of indirect rate constant, $k_{\text{II}}^{\text{prop}}$ from Safranin O bleaching.....	237
Figure 7.12 Initial rate of Safranin O bleaching as a function of phenol using $k_{\text{I,eff}}$ .....	237
Figure 7.13 Significance of solubility and oxidation products in indirect rate measurements. ...	238

# LIST OF SCHEMES

Scheme 1.1 Mechanism of a typical TAML catalyzed peroxide oxidation of substrates .....	17
Scheme 1.2 Stoichiometric mechanism of single substrate inhibition in an enzymatic process....	27
Scheme 1.3 Stoichiometric mechanism of two substrate inhibition in an enzymatic process. ....	27
Scheme 1.4 Stoichiometric mechanism of TAML catalysis with substrate inhibition .....	28
Scheme 2.1 Stoichiometric Mechanism of TAML catalysis with propranolol inhibition .....	58
Scheme 2.2 Postulated Features of Quenching of Propranolol Fluorescence by TAMLs .....	61
Scheme 3.1 Typical stoichiometric mechanism of oxidative catalysis by TAML activators. ....	95
Scheme 3.2 Oxidation of the naphthalene unit of propranolol in TAML catalyzed oxidation....	104
Scheme 3.3 Postulated mechanism of oxidative hydrolysis of propranolol to 1-naphthol .....	109
Scheme 4.1 Stoichiometric mechanism of oxidative catalysis by TAMLs and NewTAMLs .....	134
Scheme 6.1 Deprotonation of six- (A) and five-coordinate aqua iron(III) TAML complexes. ....	192
Scheme 6.2 General mechanism of catalysis by TAML activators .....	192
Scheme 7.1 Mechanism of TAML-catalyzed hydrogen peroxide oxidation of a substrate. ....	213
Scheme 7.2 Reaction mechanism of TAML-catalyzed oxidation of multiple substrates .....	217

# LIST OF TABLES

Table 1.1 Micropollutants and their concentration ranges found in waters across globe. ....	8
Table 1.2 Micropollutants and their removal by various advanced oxidation processes.....	13
Table 1.3 Rate constants for oxidation of Orange II.catalyzed by TAMLs and NewTAMLs.....	24
Table 2.1 Rate Constants for propranolol oxidation catalyzed by TAMLs. ....	60
Table 2.2 Stoichiometry of [propranolol,TAML] adducts.....	83
Table 2.3 Equilibrium constants, $K$ and Free energy change, $\Delta G^\circ$ in propranolol oxidation.....	85
Table 3.1 Experimental and theoretical rate constants for propranolol and oxidation products..	103
Table 4.1 Rate constants for oxidation of propranolol catalyzed by TAMLs and NewTAMLs..	135
Table 5.1 Attenuation of MPs with NewTAML/H <sub>2</sub> O <sub>2</sub> and 2 ppm ozone over 6h. ....	156
Table 5.2 Improvement factors for NewTAML/H <sub>2</sub> O <sub>2</sub> over 2 ppm ozone after 6h treatment .....	157
Table 5.3 Regional fluorescence integration boundaries for DOC in wastewater .....	165
Table 5.4 Fluorescence decrease of wastewater with various NewTAML/H <sub>2</sub> O <sub>2</sub> treatments.....	166
Table 5.5 Micropollutants that were analyzed in this study.....	171
Table 5.6 ESI-MS parameters utilized for compounds and their isotopic surrogates.....	174
Table 5.7 Instrumental parameters for triple quadrupole (QQQ) operations. ....	176
Table 6.1 Reduction potentials and and HOMOs of iron(III) and iron(IV) TAMLs. ....	190
Table 6.2 Stern-Volmer constants $K_{sv}$ for quenching propranolol fluorescence by TAMLs.....	205
Table 6.3 Rate constants $k_I$ and $k_{II}$ for oxidation of propranolol catalyzed by various TAMLs. .	206
Table 6.4 Rate constants, $k_I$ and $k_{II}$ for oxidation of Orange II catalyzed by various TAMLs ....	206
Table 7.1 Rate constants by direct analyses for TAML catalyzed oxidations of substrates .....	216
Table 7.2 Rate constants by indirect analyses for TAML catalyzed oxidations of substrates.....	220

# **Chapter 1**

**The current water treatment scenario and  
bio-inspired TAML activators as  
sustainable solutions for the  
micropollutant menace.**



## **1.1 BIODIVERSITY AND HUMAN IMPACT**

Biodiversity refers to the variety of life, i.e., all species on earth, viz., plants, animals, microorganisms, and humans. Scientists currently estimate about 8.7 million species live on earth, of which 1.2 million have been identified.<sup>1</sup> We humans constitute just 1 of the 1.2 million species. However, over recent generations human activities have heavily reduced the Earth's biodiversity. According to the Intergovernmental Science-Policy Platform on Biodiversity and Ecosystem Services (IPBES, an independent body of 130 governments) report to be published soon, where the summary was approved at the 7th session of the IPBES Plenary meeting in Paris, 29 April – 4 May 2019, nature is declining globally at alarming rates with unprecedented species extinction rates.<sup>2-4</sup> Scientific experts believe that the extinction rates are 1000 – 10,000 times higher than the natural extinction rate without humans<sup>5</sup>—75 % of terrestrial environments and 66% of the marine environments have been affected by human actions. The report further adds that nearly 33 % of coral reefs, sharks and shark relatives, and >33 % of marine mammals and 40 % of amphibians are threatened with extinction. At least 680 vertebrate species have been declared extinct since 1600. Adding to the tragedy, 10 % and 3.5 % of domesticated breeds of mammals and birds respectively were extinct by 2016.<sup>3</sup> In another independent News Feature published in Nature,<sup>6</sup> there have been 765 extinct species since 1500 comprised of 79 mammals, 145 birds, 36 amphibians and 505 other species. In addition to this, 1199 mammalian species, 1373 birds species, 1957 amphibian species and 993 insect species are marked as threatened species.<sup>6</sup>

### ***1.1.1 Threats posed by Humans***

The main threats for this rapid increase in species extinction include over-exploitation such as fishing and hunting (37%), habitat degradation such as deforestation for houses (31 %), habitat loss (13 %), climate change (7 %), invasive species (5 %), pollution (4 %) and diseases (2 %).<sup>6</sup> Anthropogenic activities play a big role in most of these factors. While the % values may not give a complete story, pollution, climate change and population growth immensely impact biodiversity

wherever these occur. The National Oceanic and Atmospheric Administration (NOAA) reported July 2019 as the hottest month on record for the planet with an approximate 1.71°F (0.95 °C) average higher temperature than the July average of the 20<sup>th</sup> century.<sup>7</sup> The past two decades also saw a >3 mm increase in the average global sea level.<sup>2-4</sup> There has been a 100 % increase in greenhouse gas emissions since 1980, contributing to global temperature raise. Water pollution has been a heavy burden on biodiversity. More than 80 % of global wastewater is discharged untreated into the environment. There has been a 10-fold increase in plastic pollution since 1980.<sup>2-4</sup> Discharges of 300–400 million tons of heavy metals, solvents, toxic sludge, industrial effluents are dumped annually into the world's waters. There has been >100% growth of urban areas since 1992 and ca. 50,000 large dams and ca. 17 million reservoirs have been constructed at the latest count.<sup>2-4</sup> Although mining operations comprise <1 % of the total land, they invariably have serious implications on the surrounding biodiversity. There are ca. 6500 offshore oil and gas mining installations.<sup>2-4</sup> In addition to affecting the biodiversity, waters utilized in fracking processes are mostly not reusable and fracking processes also contaminates the ground water with methane and other impurities.<sup>8</sup>

## **1.2 LESSON FROM HISTORY: THE NEAR EXTINCTION AND RESURGENCE OF THE BALD EAGLE**

The USA adopted the Bald Eagle as its national symbol in 1782.<sup>9</sup> At that time, about 100,000 nesting eagles were present in the USA. However, with decreases in water fowl populations and increases in eagle hunting to protect poultry and domestic livestock, a Bald Eagle Protection Act was passed in 1940 by which time a threat to the eagle's extinction had been determined. Matters only got worse with the introduction of Dichlorodiphenyltrichloroethane (DDT) as a pesticide after world war II.<sup>9,10</sup> The profuse use on almost every imaginable species, including humans, brought severe ecological impacts. DDT bioaccumulated in the adipose tissue in Bald Eagles from the fish they consumed, which in turn absorbed DDT from waters contaminated with DDT from agricultural runoff. In consequence, bald eagle eggs typically had very thin shells which cracked upon incubation or did not hatch at all. This led to a sharp decline in their population over 3 decades until DDT was banned across the USA in 1972. By 1963, due to various factors, but most significantly as a result of DDT contamination, there were only 487 bald eagle nesting pairs and they were an endangered species.<sup>9</sup> In 1995, two decades following after ban, the number of bald eagles rose and they were perceived as threatened and not endangered. In 2006, the number of nesting pairs of bald eagles had risen to 9789 pairs.<sup>9</sup> While bald Eagles took the center stage for their significance, other birds such as the peregrine falcon and brown pelican were also impacted by DDT and are making a comeback.<sup>11-14</sup>

### **1.3 DRINKING WATER CRISIS: A FACT CHECK**

Water is a basic resource indispensable for all life on Earth. Of all the water across globe, 97% is sea water and only the remaining 3% is freshwater, the most economical and accessible option for humans and other terrestrial animals. However, in efforts to expand human civilization over centuries, both marine and fresh waters have been contaminated by anthropogenic activities like those associated with the industrial revolution and the many impacts of shipping, off shore oil and natural gas mining, plastics pollution, etc., to name but a few. In today's world, water pollution is omnipresent and contaminated freshwaters directly impact the survival of mankind and animals. According to the World Health Organization (WHO), globally at least 2 billion people use drinking water sources contaminated with feces and 785 million people lack basic drinking water services.<sup>15</sup> Currently, 144 million people are dependent on surface water as a drinking water source and it is projected that by 2025 half of the world's population will be inhabiting water-stressed areas.<sup>15</sup> Access to safe drinking water is a key component of the sustainable development goals for multinational forums such as the United Nations and WHO, etc. Preventive efforts need to be taken in order to conserve remaining uncontaminated freshwaters. However, in the current scenario, this alone will not suffice to meet the daily requirements of living things. With increasing anthropogenic activities, falling water tables and continued contamination of surface waters, the world is turning toward water reclamation through wastewater treatment for other uses and upon adding further water treatment processes to drinking water purification. This thesis is an effort towards advancing water reclamation, including real wastewater studies, utilizing sustainably designed catalysts that mimic the chemistries of oxidizing enzymes.<sup>16</sup>

## 1.4 MICROPOLLUTANTS AS A WATER TREATMENT CHALLENGE

Micropollutants (MPs) are substances that produce undesired effects in studied organisms at low doses or low concentrations in water (for aquatic life), typically parts per trillion (ng/L) – low parts per billion (µg/L) concentrations.<sup>17–19</sup> While MPs can occur naturally, or be of anthropogenic origin—inorganic, organic, metals, etc.,<sup>20</sup>—the focus of this thesis work will be on anthropogenic, organic MPs. As noted in Table 1.1, most of these MPs are encountered on a daily basis in the form of pesticides, pharmaceuticals, personal care products, electronic components or a simple hospital visit for an X ray scan. However, their extensive everyday use also ensures their greater disposal to wastewaters-industrial effluents, domestic sewage, hospital discharge; or directly to surface waters-agricultural runoffs, animal husbandry, combined sewer overflow, etc. Inefficient conventional wastewater treatment methods for these MPs have ensured their presence in surface waters globally.<sup>21–24</sup> Table 1.1 summarizes the most common MPs of various primary utilities found in surface waters across the globe.

### ***1.4.1 Micropollutants as endocrine disruptors or other toxicity inducing chemicals***

*Endocrine disruptors are defined as chemicals that may interfere with the body's endocrine system and produce adverse developmental, reproductive, neurological, and immune effects in both humans and wildlife – National Institute of Environmental Health Sciences (NIEHS).*<sup>25</sup>

Several of the chemicals listed in Table 1.1 and Table 1.2 are encountered on an everyday basis and have been reported to be endocrine disruptors. Because these compounds, as MPs, are present in ppt-ppb concentrations, typically the hormone operational concentrations within animals, they may exhibit maximum response at such low doses if the affinities for the hormone receptor proteins are similar. Traditional toxicological studies have believed in “dose makes the poison” and thus that low doses, much below the lowest observed adverse effect (LOAEL) should be nontoxic.<sup>20,26</sup> This holds true if the dose-response curve is indeed monotonic linear. However, [nonmonotonicity is a fundamental dose-response modus operandi of the endocrine hormone](#)

[system](#). In most cases of nonmonotonic responses, low doses induce toxicological responses not found at higher doses. For endocrine hormones and endocrine disruptors, the “dose makes poison” prescription is invalid. Bisphenol A continues to be a flagbearer for endocrine disruption effects and has been reported to affect the prostate, mammary gland, brain development, behavior and reproduction in rats and humans in this extensively detailed review article.<sup>20</sup> Because of growing concern in the public about the negative impacts of BPA, BPA-free plastic containers are being produced,<sup>27</sup> often unfortunately [using replacements for BPA that are also endocrine disruptors](#). Propranolol, the most heavily prescribed  $\beta$  blocker in the USA, has been shown to be an endocrine disruptor with water concentrations of 0.5 ppb and 1 ppb interfering with egg production in Japanese Medaka fish.<sup>28</sup> Triclosan, an antibacterial, omnipresent in personal care products, was found to increase the uterine weight in female wistar rats, signaling an estrogenic effect.<sup>29</sup> In another study it was found to impact the serum thyroid and testosterone levels in male wistar rats.<sup>30</sup>

p,p'-DDE (Dichlorodiphenyldichloroethylene), which is the primary metabolite of DDT, has been reported to interfere with the sexual differentiation in male rats<sup>31</sup> and also interfere with the conversion of testosterone to dihydrotestosterone.<sup>32</sup> PCBs have been reported to be carcinogenic to rats. Humans exposed to PCBs have been reported to develop severe dermatological effects, mutagenic effects and, in extreme cases, exposures have been lethal.<sup>33,34</sup> A suspected estrogenic mode of action was reported for DDE as well.<sup>35</sup> Glyphosate, the world's top selling herbicide, has been determined to be potentially carcinogenic properties in animals.<sup>36</sup> In 2015, the International Agency for Research on Cancer (IARC) published a monograph concluding that Glyphosate is a potential carcinogen, classifying it as a group 2A carcinogen.<sup>37</sup> Glyphosate has also been reported to be an endocrine disruptor at 0.5 ppm on androgen receptor in MDA-MB453-kb2 cells.<sup>38</sup>

Table 1.1 Examples of micropollutants and their concentration ranges found in surface waters, ground waters and drinking waters (wherever data available) across globe.

Micropollutant	Primary Utility	Concentration in water (surface, ground or wastewater, drinking water where data available) $\mu\text{g L}^{-1}$	Countries where detected in water	Reference
Propranolol	Pharmaceutical ( $\beta$ blocker)	0.05-0.388	USA, UK, European Union, Switzerland	This work and 39–43
Dichloro diphenyl trichloroethane DDT (Legacy chemical)	Pesticide (chlorinated)	0.014-811	Iran, Mexico, Egypt, India	44–47
Imidacloprid	Pesticide (neonicotinoid)	0-0.15	European Union, Switzerland	40–43
Nonylphenol	Surfactant	0.023-32.8	Greece, Korea, USA, China, Japan	21,48–51
Bisphenol A	Industrial chemical	0.004-0.28	Greece, USA, Thailand, Germany, European Union, Korea, Mexico, Austria, China, USA, Spain, India	39,40,43,48,52–56
Phthalates	Industrial chemical	0.0001-339	Bangladesh, USA, Egypt	57–61
Chlorpyrifos	Pesticide (organophosphorous)	0.012-9.31	Russia, China, USA	62–66
Polychlorinated biphenyls (PCBs)	Transformers, capacitors	0.000012- 2.473	China, Sweden, Germany, USA, Italy, France	67–69
17 $\alpha$ ethynyl estradiaol (EE2)	Synthetic estrogen (ovulation inhibitor, birth control pill)	0-0.003	USA, Canada, Hong Kong, China, South Africa	70–72
Polybrominated diphenyl ethers (PBDEs)	Flame retardants	0.002-218.2	USA, Germany	73–78
Iopamidol	Industrial chemical, contrast agents	2.7-20.8	USA, India, Mexico	This work and 79–82
N,N-diethyl-meta-toluamide (DEET)	Personal care, insect repellent	0.0016-5.28	Greece, USA, Switzerland, UK, European Union	This work and 57,83
Triclosan	Personal care, antibacterial	0.06-4.26	UK	This work and 39–43,48,84,85
Metaldehyde	Pesticide, slug or snail poison	0.016-2.7	Mexico, France, USA	86,87
Glyphosate	Herbicide	0.12-1.41	European Union, France, Spain, Switzerland, USA	88–90
Atrazine	Pesticide (organochlorine)	0.001-3.6	USA, UK, European Union, Korea, Spain	21,40,84,91–94
Diclofenac	Pharmaceutical	0.03-3.6		This work and 21,39,40,43,55,84,95

#### ***1.4.2 Inefficiency of conventional wastewater treatment methods***

Conventional wastewater treatments were intended to clear the water of physical and chemical impurities via a series of filtrations, coagulation-flocculation, adsorption and activated sludge treatments to reduce the organic content in water via biodegradation. Disinfection processes were introduced as tertiary or advanced treatment steps to clear water of harmful pathogenic microbes. It can be noted that conventional treatment was never intended for removal of MPs, especially because the ultralow concentrations were not even detectable until recently and were considered harmless until found otherwise.<sup>96-99</sup> While it can be argued that chlorination utilized in disinfection does degrade some MPs, it also produces chlorinated disinfection byproducts which can be persistent and toxic.<sup>100,101</sup> With the growing concerns of MP water contamination, Switzerland has taken strong regulatory steps to reduce the releases of MPs into surface waters, mandating a 50 % reduction in the country's MP releases to surface waters and taxing its population to set up fourth stage ozone or activated carbon plants at 100 of its ca. 650 plants.<sup>102</sup>

#### ***1.4.3 Unusual high production and usage of chemicals***

One of the complexities associated with tackling the challenge of MPs is the massive production, profuse distribution and use of compounds which can behave as MPs. The number of chemicals registered in Chemical Abstracts Service (CAS) registry<sup>103</sup> is over 120 million just for the year 2017 as compared to 2005, wherein roughly 20 million compounds were registered (figure 1.1 ). That is a 6-fold increase in 12 years compared to a 2-fold increase in 15 years from 1990-2015. Most chemicals in use have not been assessed for endocrine disruption toxicity in satisfactory ways by regulatory agencies all of which have reality checks to undergo in the requisite modernization [as exemplified most comprehensively by the USFDA's handling of BPA's endocrine disruption effects](#). In addition, there may be chemicals which are behaving as MPs in water, but have never been detected because of the lack of an analytical method developed to



detect the compound. The pace at which analytical methods allowing science to track the environmental fates of new compounds has never been sufficient to handle the number of chemicals being registered. Even non-targeted analyses require a library of compounds and chemicals that don't make it to the library will never be detected by this approach.

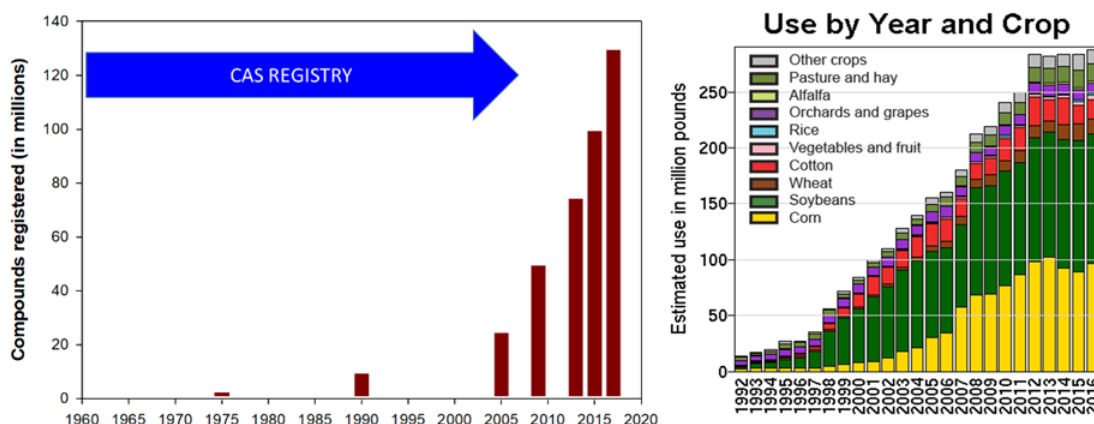


Figure 1.1 (Left) Number of compounds registered in the CAS registry since 1960. (Right) Roundup (herbicide) usage from 1992 – 2016 in various crops across USA.<sup>104</sup>

The matter is complicated further when a chemical is used profusely in spite of being determined to be potentially toxic. Glyphosate, the active component of the herbicide Roundup has been reported to be a potential carcinogen.<sup>36,105</sup> This, however, has not deterred its extensive usage. In the USA alone, this usage has increased for several crops from 25 million pounds in 1994 to an approximate 300 million pounds in 2014.<sup>104</sup> This is a 10-fold increase in usage in two decades, with corn and soybeans being the primary crops for application. This massive usage has led to contamination of sediments<sup>106</sup> and waters<sup>88-90</sup> from the agricultural run offs. Additionally, these pesticides have also become systemic in a few crops,<sup>107</sup> which poses a threat via direct consumption by humans.<sup>105</sup> On the brighter side though, the usage of Roundup from 2012 – 2016 stagnated at approximately 300 million pounds. However, safer alternatives and organic cultivation need to be sped up to reduce the use of this potential carcinogen and endocrine disruptor.<sup>108</sup>

#### ***1.4.4 Micropollutants as persistent organic pollutants (POPs)***

Several pollutants, while exhibiting adverse health effects at extremely low concentrations (Micropollutants), are also persistent organic pollutants (POPs),<sup>109,110</sup> i.e. persist over long periods of time in environmental media, are easily transported via such media, and can bioaccumulate and produce toxic effects. Although, 12 POPs were listed in the Stockholm convention in 2001 to be either banned from production and use (chlorinated pesticides) and unintentional production (dioxins and furans), the after effects of these POPs are still prevalent in sediments and in animals even after more than a decade of its implementation. Recently, polybrominated diphenyl ethers (PBDEs) and perfluorooctanesulfonic acid (PFOS) have been added to the Stockholm convention treaty as well.<sup>111</sup>

##### ***1.4.4.1 Utilizing tree swallows as indicators for contaminant exposure and bioaccumulation***

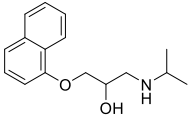
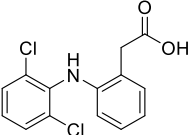
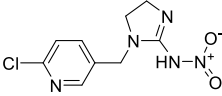
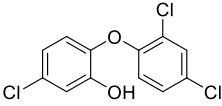
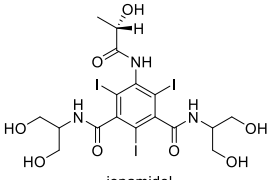
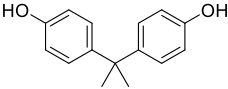
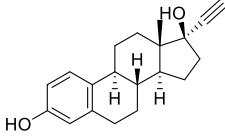
Several POPs have been found to accumulate in body fat and tissues due to their larger partitioning coefficients ( $K_{ow}$ ) which make them sparingly soluble in water and highly soluble in lipids. Several of these MPs, which also behave as endocrine disrupting chemicals (EDCs), like polychlorinated biphenyls (PCBs), dioxins and furans, and dichlorodiphenyldichloroethylene (p,p'-DDE) were recently evaluated for their presence in the eggs of Tree Swallows (*Tachycineta bicolor*) across the Great Lakes Basin from 2010 – 2015.<sup>112</sup> Tree swallows serve as a mid-level consumer providing significant information on the bioaccumulation aspect. They have a very small feeding radius, which made their study across Great Lakes, a pin pointed indication of the contamination of the Great Lakes and its sediments. Additionally, tree swallows bioaccumulate dioxins and furans more readily than some water birds.<sup>113,114</sup> A mean PCB concentration of 7.30 µg/g, wet wt was found in tree swallow egg samples in the Waukegan Harbor, IL, as compared to a background mean concentration of 0.34 µg/g, wet wt in tree swallow eggs across the USA and Canada. A mean concentration of total dioxins and furans (pg/g wet wt) in tree swallow egg

samples was determined to be 1190 pg/g wet wt in Midland, MI as compared to a background reference of 167 pg/g wet wt across USA and Canada. Similarly, a mean concentration of total polybrominated diphenyls (ng/g wet wt) in tree swallow egg samples was found to be 203 ng/g wet wt in Lake Erie MetroPark, MI as compared to a background reference value of 96 ng/g wet wt. A linear correlation was also observed for total PCBs in sediments versus concentration in egg samples. It is important to observe that the egg concentrations were 100 times higher than the corresponding sediment PCB concentrations, due to biomagnification.<sup>112</sup> A mean concentration of total perfluorinated compounds (PFCs) and total perfluorooctanesulfonate (PFOS) in tree swallows nestling plasma was found to be 1649.3 ng/g wet wt, and 1323.7 ng/g wet wt respectively in Oscoda, MI.<sup>115</sup> In the Lakeshore Park, Milwaukee Estuary, WI 5738.6 ng/g wet wt of total polycyclic aromatic hydrocarbons (PAHs) were determined in tree swallow pooled diet samples, of which 2267.1 ng/g wet wt were found to be the alkylated PAHs and 3471.4 ng/g wet wt were found to be parent PAHs.

#### ***1.4.5 Advanced oxidation processes (AOP) for the treatment of micropollutants***

AOP primarily employ reactive species such as  $\bullet\text{OH}$  or  $\bullet\text{SO}_4^-$  or  $\text{O}_2^-$  for oxidizing substrates in water.<sup>116,117</sup> The high reactivity and non-selectivity of these species make them a candidate for MP oxidative destructions. The most commonly used AOPs include Fenton or photo Fenton processes, UV/H<sub>2</sub>O<sub>2</sub> processes and ozone for oxidation of MPs.<sup>118,119</sup> The performance of these AOPs in oxidizing common MPs in water have been summarized in table 1.2.

Table 1.2 Micropollutants and their removal by various advanced oxidation processes

Micropollutant	% removal with Ozone (2 ppm) <sup>120</sup>	% removal with UV/H <sub>2</sub> O <sub>2</sub>	% removal with Fenton/photo Fenton/electro Fenton/O <sub>2</sub> <sup>-</sup>
 propranolol	45	65 <sup>121</sup>	100 <sup>122</sup>
 diclofenac	60	50 <sup>123</sup>	100 <sup>124</sup>
 imidacloprid	>98 <sup>125</sup>	100 <sup>126</sup>	100 <sup>127</sup>
 triclosan	70	90 <sup>128,129</sup>	100 <sup>130</sup>
 iopamidol	10	40 <sup>131</sup>	100 <sup>132</sup>
 bisphenol A	30 <sup>133</sup>	>90 <sup>134</sup>	100 <sup>135</sup>
 ethynyl estradiol	100 <sup>136</sup>	100 <sup>137</sup>	100 <sup>138</sup>

Fenton processes can be driven to provide 100% removal in all cases, as mentioned above. But this requires acidic conditions pH (3-4)<sup>122</sup> for production of  $\bullet\text{OH}$  and also require  $\mu\text{M}$ -mM of Fe in the system.<sup>132</sup> This pH is not typical of wastewaters rendering the processes of very little utility for massive wastewater treatments at neutral pH. Additionally, they employ high mM  $\text{H}_2\text{O}_2$  concentrations which can increase the cost of treatments.<sup>127</sup> Formation of iron salts is typical of Fenton processes and filtering them from the effluent adds further to the treatment costs.

UV/ $\text{H}_2\text{O}_2$  processes employ UV radiation to produce  $\bullet\text{OH}$  from the peroxide bond O-O cleavage in  $\text{H}_2\text{O}_2$  aqueous solutions. This process has shown great removal efficiency for easily oxidized EE2 (100%), BPA (>90 %) and imidacloprid (100 %). Complete removal of persistent imidacloprid with UV/ $\text{H}_2\text{O}_2$  suggested that mechanistically this compound is oxidized better with reactive radicals. Other persistent MPs like propranolol, diclofenac and iopamidol were reduced by 65, 50 and 40 % respectively of their initial concentrations. Low absorption of  $\text{H}_2\text{O}_2$  in the UV region ( $\epsilon_{230} = 72.1 \text{ M}^{-1}\text{cm}^{-1}$  in water)<sup>139</sup> renders usage of high intensity and longer duration of UV doses to produce large concentrations of  $\bullet\text{OH}$ . This makes the treatment an energy intensive process and increases the cost of treatment.<sup>116,140</sup>

Ozone has long been used for disinfection and has been introduced in the recent times for MP oxidation in European countries, e.g. Switzerland and Germany.<sup>141-144</sup> Ozone is a reactive but unstable oxidant. In presence of dissolved organic matter (DOM), ozone produces the reactive hydroxyl radical ( $\bullet\text{OH}$ ). Table 1.2 summarizes the performance of 2 ppm ozone in oxidizing MPs in real wastewaters of Tucson, AZ where 2 ppm is the typical dose used in a treatment plant in Dubendorf, Switzerland-the birth place of ozone treatment of MPs. In the presence of DOC, ozone effected only ca.30, 45, 60, 70, 10 % removal of BPA, Propranolol, Diclofenac, Triclosan and Iopamidol respectively. Iopamidol has been shown to be very hard to oxidize in a different study conducted on wastewaters in Switzerland.<sup>145</sup> While 100 % removal could be obtained for the easily oxidized synthetic estrogen EE2 with 2 ppm ozone without DOC, 100 g/m<sup>3</sup> ozone in

the inlet gas was required to be bubbled for 30 min to effect 98 % removal for recalcitrant Imidacloprid in the absence of DOC. Operationally, ozone is an expensive process requiring corrosion proof equipment and trained professionals for smooth operations.

While AOPs do offer relatively superior performances compared to conventional treatments, they are not economical for applications across the globe. Their utility for removing AOPs as a final step in municipal wastewater treatment is logically dependent on the quality of the rest of the wastewater treatment process which can vary greatly from plant to plant. Additionally, oxidation byproducts require additional toxicological testing at low doses which adds up to the already high costs for operation of these treatment technologies. Thus, there is an imminent requirement for a superior, economical and sustainable alternative for wastewater treatment that can be applicable across globe.

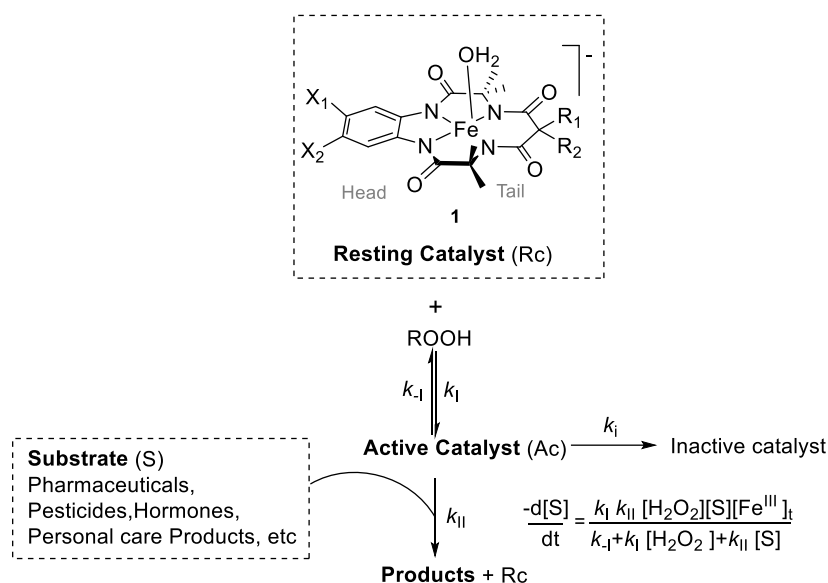
## 1.5 TAML ACTIVATORS AS A SUSTAINABLE SOLUTION FOR TREATING MICROPOLLUTANTS

Tetraamido macrocyclic ligand (TAML) activators (**1**, Scheme 1.1) are mechanistically faithful, small molecule replicas of peroxidase and cytochrome P450 enzymes.<sup>16,146</sup> In mass, TAMLs are typically even lighter than only the central porphyrin unit (active site) of peroxidase enzyme meaning their molar mass is ca. just 1 % the average weight of a peroxidase enzyme. For example, most TAML activators have approximately 500 g molar mass, whereas the light peroxidase, horseradish peroxidase C1 is a 44,173.9-dalton glycoprotein<sup>147</sup>. Heavier peroxidases like lactoperoxidase has a molar mass of [77,500 Da](#) and Human Salivary Peroxidase has multiple forms ranging from 75 to 280 kDa in molar mass. Like the enzymes, TAMLs activate hydrogen peroxide or organic peroxides in solution.<sup>148,149</sup> Activation of dioxygen to perform catalytic oxidation has been reported as well.<sup>150</sup> A typical TAML catalyzed oxidation is illustrated in Scheme 1.1. Since TAML activators are comprised of biochemically common elements,<sup>151</sup> and mimic natural detox processes, any of its own degradation products or oxidation products of substrates will not be expected to have adverse effects on aquatic life other than those already found in natural systems.<sup>151</sup> For example, while bromate is a common phenomenon with ozone treatment of natural waters, TAML catalyzed oxidation of bromide rich waters yielded negligible bromate formation.<sup>116</sup>

The rate constants,  $k_I$  and  $k_{II}$  correspond to activation of the resting catalyst to the active catalyst ( $k_I$ ) and the oxidation of substrate by the active catalyst ( $k_{II}$ ). The exact composition of active catalyst (whether  $\text{Fe}^{\text{IV}}$  or  $\text{Fe}^{\text{V}}$  or  $\text{Fe}^{\text{IV}}$  oxodimer)<sup>152–154</sup> varies depending on the reaction conditions and in general terms involves an iron-oxo complex analogous to compound II for peroxidase enzymes. The most active  $\text{Fe}^{\text{V}}$  oxo has been reported for activation of TAML activators with meta-Chloroperoxybenzoic acid (mCPBA). It has been confirmed through experiments that radicals are not the primary oxidants in TAML/ $\text{H}_2\text{O}_2$  processes.<sup>154–156</sup> The active catalyst oxidizes

the substrates via oxygen transfer to the substrate, electron acceptance or H abstraction from the substrate.<sup>149</sup> The active catalyst can be inactivated either via unimolecular ( $k_i$ ) or intermolecular pathways ( $k_{2i}$ , not shown here)<sup>26,157,158</sup>. The reaction represented by  $k_{2i}$  is typically observed at  $[TAML] > 1 \times 10^{-6}$  M and considering TAML catalytic oxidations for water purification are typically performed at  $[TAML] \ll 1 \times 10^{-6}$  M, this inactivation pathway was not studied in the context of the work presented in this thesis. Hence, wherever the temporal properties of functioning TAML lifetimes are discussed in the forthcoming chapters as well as in the iterative design section below, these refer to only  $k_i$  unimolecular degradation.

Scheme 1.1 Mechanism of a typical TAML catalyzed peroxide oxidation of substrates including rate law utilized for determination of rate constants.



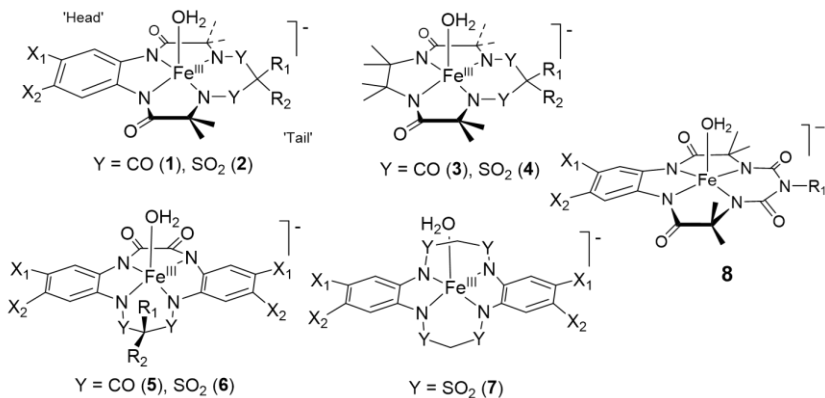
Over a period of 25 years, TAML activators have undergone a series of iterative design cycles (Figure 1.4) using the same design loop<sup>16</sup> that was practiced over the prior 15 years to achieve the prototype TAML activator **1a** with an unsubstituted head and dimethylated tail section.<sup>16,159</sup> Five generations of TAMLs each with a different ligand moiety have been reported to date.<sup>160</sup> A few of the TAMLs from different generations are discussed in this work (Chart 1.1). Beyond the five



TAML generations, our catalysts entered into a new era in 2015 with next generations activators of peroxides called NewTAMLs, which are superior to TAMLs, and were derived by the same iterative design protocol.<sup>161</sup> Structurally, NewTAMLs contain sulfonyl groups in the tail region (Chart 1) and contain either 2 methylene protons or 1 methylene proton which constitute the *kill switch* in NewTAMLs (discussed in detail in the later chapters).

Chart 1.1 Structures of TAML/NewTAML activators discussed in this thesis work

TAML	X <sub>1</sub>	X <sub>2</sub>	R <sub>1</sub>	R <sub>2</sub>
<b>1a</b>	H	H	Me	Me
<b>1b</b>	NO <sub>2</sub>	H	Me	Me
<b>1c</b>	NO <sub>2</sub>	H	F	F
<b>1d</b>	Me	Me	Me	Me
<b>1e</b>	Cl	Cl	F	F
<b>2a</b>	H	H	H	H
<b>2b</b>	NO <sub>2</sub>	H	H	H
<b>2c</b>	H	H	Me	H
<b>2d</b>	NO <sub>2</sub>	H	Me	H
<b>3</b>	-	-	Me	Me
<b>4</b>	-	-	H	H
<b>5</b>	NO <sub>2</sub>	H	Me	Me
<b>6</b>	H	H	H	H
<b>7</b>	H	H	-	-
<b>8</b>	H	H	Me	-



### 1.5.1 History of TAMLs in oxidizing MPs

Over the past two decades TAMLs have been shown (Figure 1.2) to be effective at oxidizing a broad range of MPs like BPA,<sup>162,163</sup> nitrophenols,<sup>164</sup> chlorophenols,<sup>165</sup> surfactants,<sup>162</sup> alkaloids,<sup>166</sup> steroid hormones, especially estrogens,<sup>167</sup> synthetic estrogens,<sup>168</sup> dyes,<sup>160,169–171</sup> pharmaceuticals,<sup>161,172–175</sup> explosives,<sup>176</sup> and biological anthrax surrogates.<sup>177</sup>

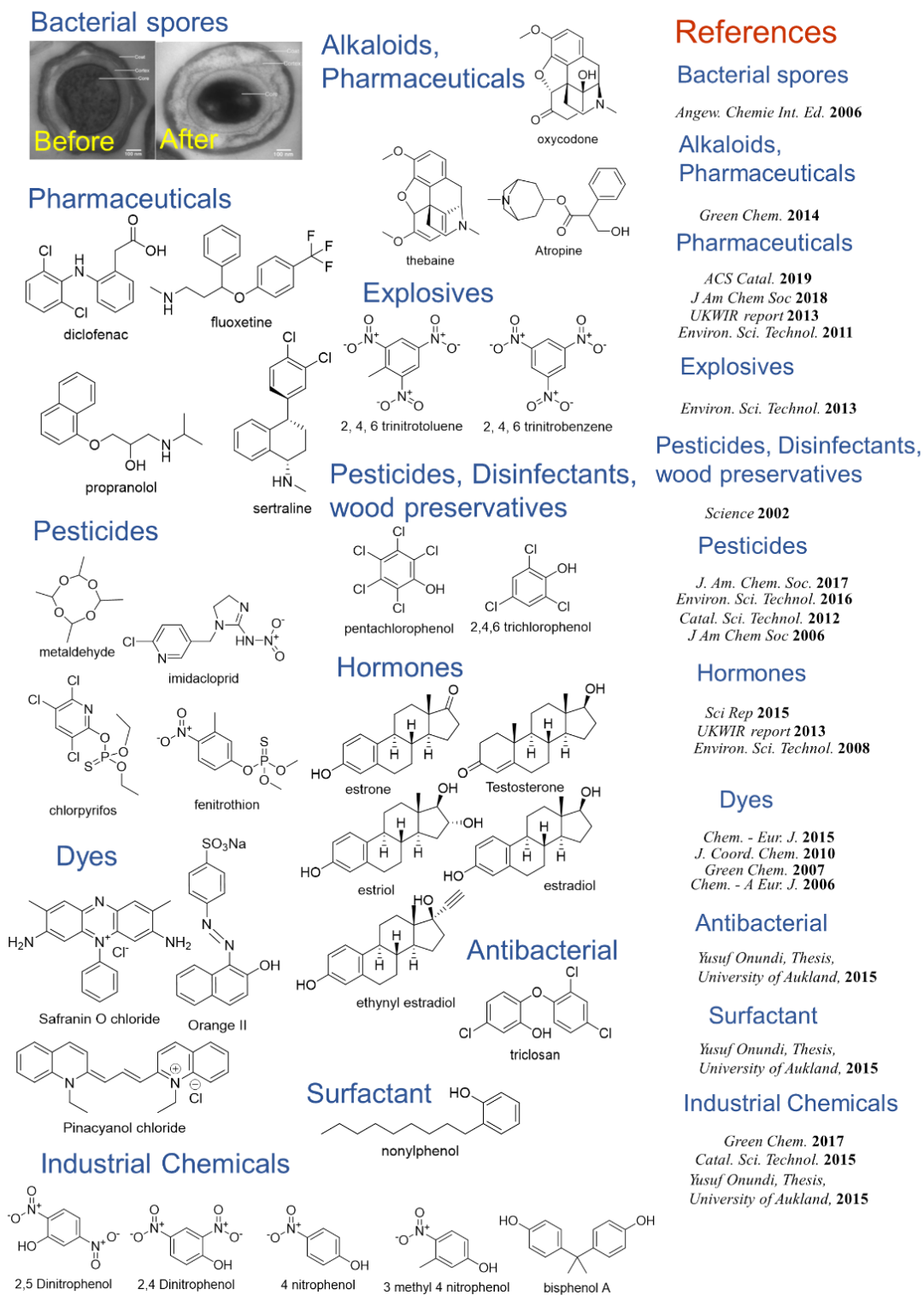


Figure 1.2 Classes of MPs, based on their end point applications, oxidized by TAML/H<sub>2</sub>O<sub>2</sub> and NewTAML/H<sub>2</sub>O<sub>2</sub><sup>161</sup> treatments to date.

### 1.5.2 London wastewater experiments

TAML activators were designed with the aspirational goal of their application in wastewater treatment initially to remove pathogens and then, after their discovery, micropollutants as well. Having achieved superior oxidations at neutral pH for various classes of MPs in isolation, TAML/H<sub>2</sub>O<sub>2</sub> treatment was evaluated for oxidizing MPs in real wastewaters. As part of collaborative efforts with Brunel University, a study was performed on London wastewaters utilizing the prototype **1a** and an iteratively designed superior TAML, **1c**, for a United Kingdom water industry research (UKWIR) project in 2013.<sup>175</sup>

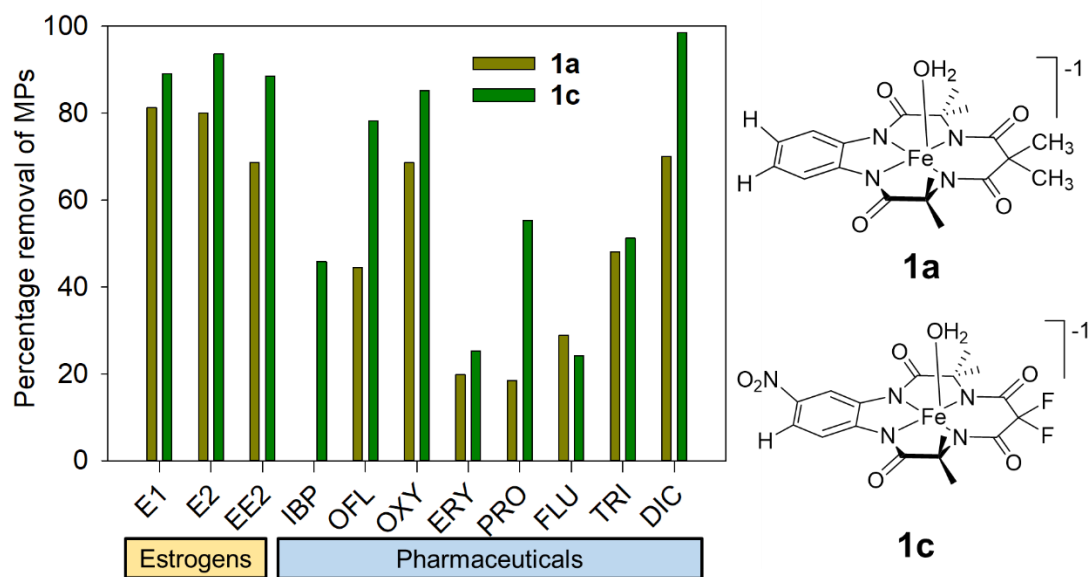


Figure 1.3 Comparative performance of **1a** and **1c** catalyzed hydrogen peroxide oxidation of estrogen and pharmaceuticals in London wastewaters. Adapted from UKWIR report 2013.<sup>175</sup> Reaction conditions: 40 nM [TAML], 20 ppm H<sub>2</sub>O<sub>2</sub>. Abbreviations: estrone (E1), 17 $\beta$ -estradiol (E2), 17 $\alpha$ -ethinylestradiol (EE2), ibuprofen (IBP), ofloxacin (OFL), oxytetracyclin (OXY), Erythromycin (ERY), propranolol (PRO), fluoxetine (FLU), triclosan (TRI) and diclofenac (DIC).

For the estrogens and pharmaceuticals evaluated, in general both TAMLs **1a** and **1c** were effective at oxidizing them at 40 nM [TAML]/20 ppm H<sub>2</sub>O<sub>2</sub>. TAML **1c** showed much superior performance to **1a** across board (Figure 1.3). On an average, more than 50 % reduction was achieved with a higher removal of up to 100% for Diclofenac, a priority pollutant for European wastewaters. Estrogens E1, E2 and EE2, that are responsible for feminization of the fish populations were removed up to 90% with **1c**/H<sub>2</sub>O<sub>2</sub> treatment. The results from this study were compared alongside another study performed in an Ozone pilot plant in Ilkeston, Derbyshire. Although the water quality varied between the plants, 40 nM/20 ppm H<sub>2</sub>O<sub>2</sub> gave a comparable performance to 2 ppm ozone.<sup>175</sup> The significance of this performance is enhanced when the operating costs, safety issues and requirement of highly trained professionals for Ozone treatment are taken into consideration. While **1c** looked like an economical alternative to ozone, it was a fluorinated catalyst. In spite of having cleared the safety studies, **1c** was not taken forward as a precautionary posture over the desire to obtain a sustainable solution for MP water treatment.<sup>151</sup> Hence, began the search for the next generation of catalysts sans halogens, but now with a new reference standard for reactivity and safety.<sup>178</sup>

## 1.6 ITERATIVE DESIGN FROM TAMLs TO NEWTAMLs

Iterative design cycles were employed for TAML activators to constantly learn from the previous catalysts to attain the maximum reactivity and longest life for TAML activators. In initial iterative design cycles (Figure 1.4), catalyst degradation fragments were used for identifying and blocking serially the weakest spot in the catalyst toward oxidative decay.<sup>26,179</sup> However, with the development of superior performing catalysts, an indirect kinetic tool was developed for understanding the reactivity and lifetime of the catalyst since catalytic activities with superior TAMLs require only nM concentration of TAMLs.<sup>157</sup> Correlations between the kinetic rate constants,  $k_I$ ,  $k_{II}$  and  $k_i$  for oxidation of a substrate were used for deriving valuable information regarding the reactivity and life of catalyst (Figure 1.4).<sup>157</sup>

### 1.6.1 Linear relationship between reactivity and life

As mentioned earlier, the reactivity of TAML activators are defined by the rate constants,  $k_I$  and  $k_{II}$ , while the lifetime is defined by the rate constant,  $k_i$ . All three are in turn related to the Lewis acidity at the iron center of the resting catalyst.<sup>157</sup> These rate constants together form the technical performance parameters (TPPs) for any TAML activator. The two key TPPs  $k_{II}$  and  $k_i$  command the relative reactivities of different TAML active catalyst intermediates (Ac) which in turn determines the relative effectiveness of any given catalyst. In a study evaluating 15 TAML activators, a linear free energy relationship (LFER) was observed between  $k_{II}$  and  $k_i$  with a slope  $\sim 1$ .<sup>157</sup> This meant that the most reactive TAML also had the shortest life – “lived faster, died younger”.<sup>157,161</sup> This was clearly observed with the most reactive TAML **5** exhibiting the highest  $k_I$  ( $1900 \pm 100 \text{ M}^{-1} \text{ s}^{-1}$ ) and  $k_{II}$  ( $520000 \pm 70000 \text{ M}^{-1} \text{ s}^{-1}$ ) and also the highest inactivation rate constant,  $k_i$  ( $0.085 \pm 0.006 \text{ s}^{-1}$ ) in the bleaching of Orange II. This can be explained by the fact that both these pathways derive from the same Ac. However, these observations contradicted an oxidative inactivation mechanism for TAMLs, since all TAMLs with varying oxidizable macrocyclic group exhibited the same linear dependence such that it could be deduced that no site

in any of the 15 TAMLs was undergoing oxidative decay.<sup>161,178</sup> Our new hypothesis for TAML inactivation was proposed to be nucleophilic attack at the carbonyl groups (hydrolysis, perhydrolysis) of the carbonamido ligands in the macrocycle at neutral pH.<sup>161</sup>

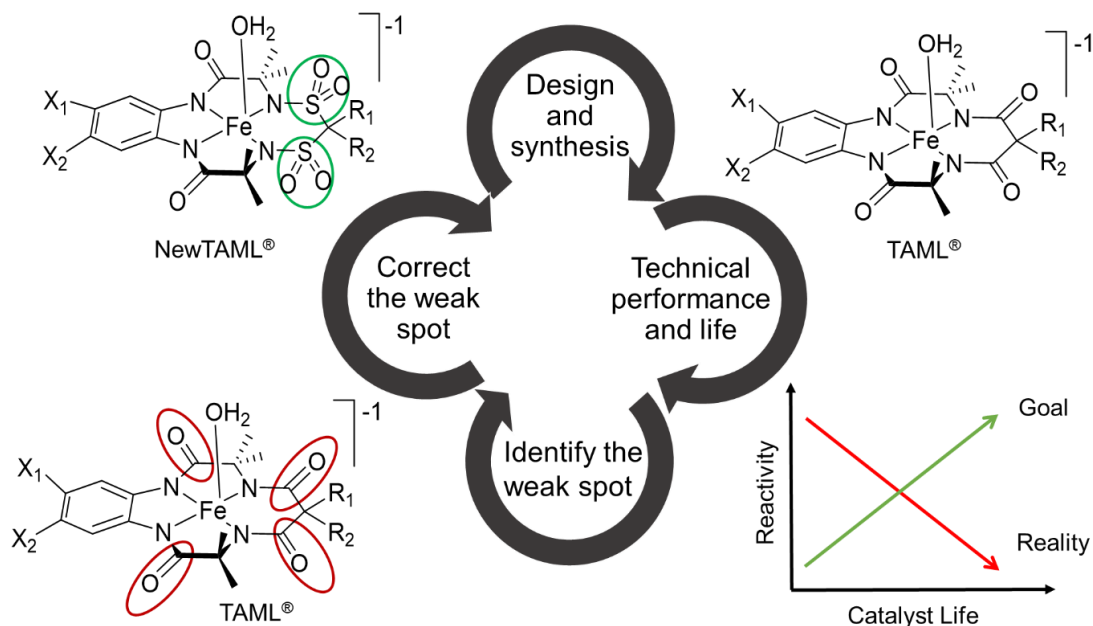


Figure 1.4 Iterative design of TAML activators to yield next generation NewTAML activators

In order to achieve NewTAMLs, we redesigned the TAML macrocycle such that it addressed two key aspects of our endpoint water treatment goals. Firstly, NewTAML macrocycle should be comprised of only biochemically common elements (no halogens) and secondly, the maximum reactivity for NewTAMLs should be optimized for pH 6 -8, typical of wastewaters. For the best performing TAML **1c**, the optimal reactivity was between pH 9 – 10, pretty far from the optimal range for municipal wastewater treatment. To attain the maximum catalytic activity near pH 7, we learned that increased Lewis acidity at iron projects as increased Brønsted acidity at the axial water ligands of TAMLs, which lowers the pH of maximum activity and increases the catalytic rate.<sup>26</sup> This is because the most active form of the catalyst has a deprotonated axial water ligand.

Therefore, under the hypothesis that nucleophilic chemistry is lifetime-limiting, carbonamido-N replacements should be replaced with alternatives that are inductively more electron-withdrawing and also more resistant to nucleophilic attack. To achieve these properties, sulfonamido-N ligands were chosen as the first replacements of carbonamido-N ligands in TAMLs giving NewTAMLs in the process. When not in highly strained rings, sulfonamides are more resistant to nucleophilic degradation than carbonamides<sup>161,180–182</sup> such that slower degradations in NewTAMLs should ensue (decreased  $k_i$ ). Sulfonamides are also more acidic<sup>161</sup> and the deprotonated forms are less  $\sigma$ -donating than carbonamides<sup>161,183</sup> promising higher NewTAML positive charge at iron to deliver faster oxidation catalysis. A comparative evaluation of TPPs of NewTAMLs with analogous TAMLs are detailed in Table 1.3 by the example of oxidation of a reference dye, Orange II used for quick reactivity analyses in the group. All the work including synthesis of NewTAMLs and determination of their TPPs in the oxidation of Orange II is the thesis work of Dr. Genoa R. Warner and is being discussed here only to build a background context for evaluating NewTAMLs with a real world MP, Propranolol.

Table 1.3 Rate constants  $k_I$ ,  $k_{II}$  and  $k_i$  and the ratio of  $k_{II}/k_i$  in the oxidation of Orange II by analogous TAMLs **1** and NewTAMLs **2** at pH 7, 25 °C

TAML	$k_I/\text{M}^{-1} \text{ s}^{-1}$	$k_{II}/\text{M}^{-1} \text{ s}^{-1}$	$10^3 \times k_i/\text{s}^{-1}$	$10^{-7} \times (k_{II}/k_i)/\text{M}^{-1}$	Ref
<b>1a</b>	$31.4 \pm 0.1$	$4950 \pm 20$	$0.30 \pm 0.01$	1.65	157
<b>1b</b>	$152 \pm 5$	$27000 \pm 2000$	$0.34 \pm 0.02$	7.9	157
<b>1c</b>	$350 \pm 2$	$41000 \pm 1000$	$1.1 \pm 0.3$	3.7	157
<b>2a</b>	$330 \pm 20$	$85000 \pm 18000$	$4.3 \pm 0.7$	2	161
<b>2b</b>	$630 \pm 50$	$100000 \pm 20000$	$3.6 \pm 0.7$	2.8	161
<b>2c</b>	$390 \pm 4$	$42000 \pm 1000$	$2.0 \pm 0.5$	2.1	161
<b>2d</b>	$690 \pm 20$	$89000 \pm 2000$	$1.1 \pm 0.1$	8.1	161

In general, higher  $k_{II}$  values were obtained for **2** activators in comparison to their analogous **1** activators. Following the LFER studies, higher  $k_i$  values were also obtained for **2** activators, but this was subsequently determined to arise principally in the unique catalyst innovation called a “kill switch” as discussed below. The  $k_{II}/k_i$  values capture a critical utilitarian element of the behavior of Ac in functioning TAML catalytic cycles—the larger the ratio, the more technically effective the catalyst. The  $k_{II}/k_i$  values for first produced **2a** and **2b** are 2.0 and 2.8 M<sup>-1</sup>, respectively (Table 1.3), mark **2b** as the superior catalyst. However, **1b** and **1c** both have higher  $k_{II}/k_i$  values than either **2a** or **2b** of 7.9 and 3.7 M<sup>-1</sup>, respectively (Table 1.3). This results exclusively from larger  $k_i$  values in **2a,2b** vs **1b,1c** and looked initially like the NewTAMLs with only two of the four carbonamido ligands replaced with sulfonamides was not going to be sufficient for superior performances. But then the kill switch in **2a** and **2b** was discovered to tell us that new ligand iterations would be important to block this intruding decay mechanism.

### 1.6.2 Kill Switch in NewTAMLs

Comparing the TPP pH dependences, specifically for  $k_i$ , for the higher performing TAMLs **1b,1c** and NewTAMLs **2b,2d**, we realized that a novel degradation pathway must be in play in the **2** catalysts which were showing higher  $k_i$  values as compared to analogous TAMLs. The new **2** degradation pathway derives from the acidity of the –CH<sub>2</sub>– group bridging the two sulfonamide-N ligands in **2a** and **2b** which permits the independent, variable control of NewTAML operational lifetimes as a discovered feature we call a “kill switch”.<sup>26,161</sup> Operational acidity in the methylene groups of **2a** and **2b** ligands induced by the electron withdrawing sulfonyl groups was discovered that we expect in manifesting at the most oxidized species in the NewTAML catalytic cycles, namely, the Fe<sup>V</sup>-oxo active intermediates. <sup>1</sup>H NMR and ESI-MS studies confirmed this hypothesis by analyzing the rapid H–D exchange upon contact with D<sub>2</sub>O. We postulate that deprotonation of the –SO<sub>2</sub>CH<sub>2</sub>SO<sub>2</sub>– units of **2a** and **2b** leads to rapid catalyst death under the operating conditions by producing a sulfur ylide carbanion that is oxidatively more sensitive than



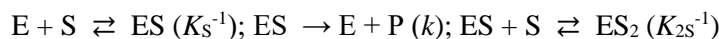
any other species in the catalytic cycle. The kill switch represents a separate reaction from all those occurring at the iron catalytic site, functioning with its own dynamics at a novel reactive location for controllable catalyst inactivation.

*Partially muted kill switches in 2c and 2d:* The structures of **2a** and **2b** were altered to address the kill switch, derived from the acidity of the  $-\text{CH}_2-$  carbon acids at pH 7 by replacing a single methylene C–H in **2a** and **2b** for the more electron-donating C–CH<sub>3</sub> group in the **2c** and **2d** analogues, respectively. The replacements of methyl (**2c** and **2d**) for H (**2a** and **2b**) lowers the acidity of the remaining proton of the bridging carbon in the  $-\text{SO}_2\text{CH}(\text{CH}_3)\text{SO}_2-$  moiety. TPPs for **2c** and **2d** were determined and, as predicted, found to be superior to their counter parts **2a** and **2b** respectively. While there may seem to be a small decrease or similar  $k_{\text{II}}$  values of 85000 vs 42000 and 100000 vs 89000  $\text{M}^{-1}\text{s}^{-1}$  for **2a** vs **2c** and **2b** vs **2d** pairs respectively, there was a reduction in the  $k_i$  value, specifically for the nitro substituted **2b** vs **2d** pair by greater than a factor of 3.<sup>161</sup> When taken in context of the catalysis in solution and the utilitarian parameter,  $k_{\text{II}}/k_i$ , the value for **2d** was found to be 8.1 as opposed to the previously best value for NewTAMLs of 2.8 for **2b**. NewTAML **2d** was also found to have a much significant improvement in the  $k_{\text{II}}/k_i$  value of 3.7 for previously best performing TAML **1c**. Thus, **2d** serves as the current best performing candidate for Orange II oxidation from TPPs perspective over all TAMLs and NewTAMLs. In this work, propranolol, a real world MP and much harder to oxidize substrate than Orange II has been evaluated for TPPs and to derive even better improved candidate for wastewater treatment than **1c**. Real wastewater experiments performed in Tucson, Arizona will be discussed in upcoming chapters.

## 1.7 SUBSTRATE INHIBITION IN TAML CATALYSIS

Competitive, noncompetitive, uncompetitive, mixed, substrate and product inhibitions are the common processes that slow enzymatic activity, the features of which are found in the majority of texts covering kinetics and mechanisms of catalysis by enzymes.<sup>184,185</sup> Such terms are much less commonly applied to metal-complex homogeneous catalysis because competitive, noncompetitive, or uncompetitive models are inapplicable to a low molecular weight catalysts, that typically lack variable binding sites for effector molecules. Substrate inhibition<sup>186</sup> differs in this aspect and is usually considered to arise from binding of a second substrate, S, molecule to an enzyme. The binding imposes a mass-law retardation of the enzymatic activity (Scheme 1.2).

**Scheme 1.2** Stoichiometric mechanism of substrate inhibition in a one substrate enzymatic process

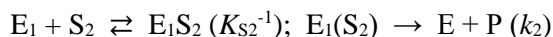
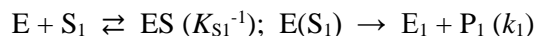


If  $ES_2$  is unreactive, the rate expression is given by

$$\frac{d[P]}{dt} = \frac{k[E][S]}{K_S + [S] + K_{2S}^{-1}[S]^2}$$

Binding of two identical substrate molecules to a low-molecular weight catalyst is made less likely than with enzymes by the relative sizes of the catalysts. However, substrate inhibition could be observed in two-substrate reactions, wherein  $S_1$  is hydrogen peroxide and  $S_2$  is substrate to be oxidized, which occur via a ping-pong mechanism such as, for example, in the case of FAD glucose oxidase<sup>187</sup> or peroxidase enzymes<sup>188</sup> (Scheme 1.3)

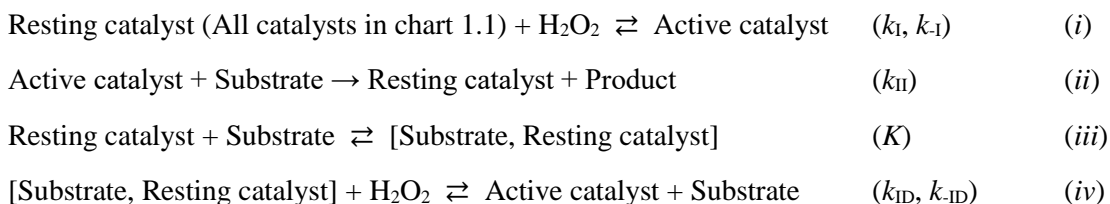
**Scheme 1.3** Stoichiometric mechanism of substrate inhibition in a two substrates enzymatic process.



In fact, there are precedents in metal-complex oxidative catalysis because the second substrate  $S_2$  may bind to a metal center  $M$  and the  $M(S_2)$  complex produced may be significantly less reactive with respect to  $S_1$  ( $H_2O_2$ ) than the free form of  $M$ . As a result, the rate of catalyzed reaction should be retarded by  $S_2$  (Substrate to be oxidized).

The first example of substrate inhibition was identified in the TAML **1a**-catalyzed oxidative bleaching of the Pinacyanol chloride (PNC) blue dye by  $H_2O_2$ .<sup>171</sup> The kinetics of this reaction differed profoundly from the expected and typical of TAML activators rate law in eq 1 (Scheme 1.1), In particular, instead of the anticipated ascending hyperbolic dependence of the rate on PNC concentration, a descending function was observed at pH 9.0; at pH 11 it transformed to a function with extremum. Interpretation of such kinetics necessitated adding events (iii) and (iv) relating to substrate interacting with the catalyst and subsequent activation of catalyst, to Scheme 1. 1 as shown in Scheme 1.4.

Scheme 1.4 Typical stoichiometric mechanism of oxidative catalysis by TAML activators (events (i) and (ii)) and the minimal steps (events (iii) and (iv)) for rationalizing cases of substrate inhibition.



Similar substrate inhibition was also observed, for example in the TAML-catalyzed oxidation of nitrophenols<sup>164</sup> by  $H_2O_2$  and in the bleaching of Orange II by  $H_2O_2$  in the presence of  $[Fe^{III}(\text{octaphenylsulfonato})\text{porphyrazine}]$ .<sup>189</sup> In all cases event (iii) in Scheme 1.4 has been outlined as the most plausible reason for deviations from eq 1.

Though efforts were previously made to prove and justify event (iii) under either noncatalytic conditions or using DFT theoretical modeling,<sup>164</sup> the associate formation between a TAML

activator and any substrate under catalytic conditions has never been proven experimentally. The objective of this work is to (i) obtain direct experimental evidence looking for substrate inhibition as a result of a reversible substrate binding to a TAML complex (ii) determine the impact of substrate inhibition, if found, on TAML activity across substrate MP concentration ranges from high to dilute and ultradilute.

## 1.8 OXIDATION INTERMEDIATES AND THEIR ENVIRONMENTAL FATE FOR TAML CATALYZED REACTIONS

With the growing list of chemicals, several of which are MPs and endocrine disrupting chemicals (EDCs), contaminating water bodies, there is a pressing need for decontamination of these waters.<sup>53,190</sup> There are currently several ongoing efforts in that direction.<sup>145,191</sup> The major focus in all these studies is removal or reduction of each primary pollutant concentration in question. However, decontamination need not necessarily mean detoxification. A decontaminated water body, devoid of any particular contaminant that has been removed by a water treatment process can still be toxic because the degradation intermediates and/or end products are toxic. At the end of the treatment process, an overall testing of the toxicity of the solution is sometimes pursued, and we typically do this with most TAML water purification studies.<sup>163,192,193</sup> TAML activators have shown exemplary performance in destroying pesticidal MPs like fenitrothion,<sup>194</sup> chlorpyrifos<sup>195</sup> and its formulations and metaldehyde;<sup>196</sup> EDCs like EE2;<sup>168</sup> pharmaceuticals like sertraline<sup>174</sup> and diclofenac<sup>175</sup>; industrial chemicals like bisphenol A (BPA),<sup>163</sup> nitrophenols<sup>164</sup> and chlorophenols;<sup>197</sup> explosives like trinitro toluene and trinitro benzene;<sup>176</sup> dyes like Orange II<sup>169</sup> and PNC.<sup>171</sup> While in most of these studies, mineralization of the primary pollutant was achieved, efforts were also made to attain mass balance with respect to final inorganic and organic ions which were found typically to be nitrite, bicarbonate, carbonate, acetate, formate, etc., to name a few.<sup>164,171,174,195,196</sup> Additionally, care has been taken to ensure the final reaction mixture is not toxic which is the general case with mineral ions. This was attained with either multiple aliquots of TAML additions for complete oxidation of a pollutant and its intermediates. Intermediates of oxidation have been identified for TAML-catalyzed peroxide activation of EE2 and sertraline. The point to note here is that while all these studies are essential to any TAML catalytic reaction, these studies provide intermediates and toxicity profile studies in isolation. There is no study that we are aware of wherein a temporal evolution of the evolving product profile of the process including intermediates and their further and final oxidation products has been correlated with the

evolving changes in toxicity. In this work, I have addressed this insufficiency with a study mapping the temporal evolution of products that projects of the evolving overall toxicity based on zebrafish mortality studies for the TAML catalyzed oxidation of Propranolol.

## 1.9 PREDICTING REACTION PROGRESS WITH PROPERTIES OF TAML USING LFER PLOTS

Linear free energy relationships (LFER) are quantitative relationships between the structures of compounds and their reactivities. LFER plots are typically made between energetic equivalents. Hammett plots were among the earliest utilization of LFERs where the equilibrium dissociation constant of substituted benzoic acids ( $\log K$ ) with varying substituents were correlated with the second order rate constant ( $\log k_2$ ) for hydrolysis of substituted ethyl benzoate esters.<sup>198,199</sup> The Brønsted equation correlates second order rate constants  $k_2$  of reactions catalyzed by acids or bases with the  $\text{p}K_a$  value of the catalyst (acid or base).<sup>200</sup> Such LFER plots have also been explored for correlating solvent and medium effects on the rates of a reaction. LFERs have been utilized for a series of TAML activators for correlating reactivity of the active catalyst towards given substrates ( $\log k_{II}$ ) and the reactivity of the resting catalyst in its activation by  $\text{H}_2\text{O}_2$  ( $\log k_I$ ).<sup>157</sup> As discussed earlier, LFER plots of most significance to the group has been the following: (i) the LFER between reactivity of active catalyst toward a given substrate ( $\log k_{II}$ ) and the inactivation of the active catalyst ( $\log k_i$ ). This helped us determine that our inactivation mechanism could not be oxidative leading to the alternative hypothesis that it is nucleophilic hydrolysis of the carbonamido ligands. This understanding was key to developing our next generation called “NewTAML” activators via inputs for the weak spots in TAML activators. (ii) the LFER between reactivity ( $\log k_{II}$ ) and the Lewis acidity at the iron center ( $\text{p}K_a$ ) for TAML activators. This aided in our understanding of the impact of electron poor metal center on the reactivity towards hydrogen peroxide. As such in TAML cases, we have previously used the free energies of the C–H activation ( $\Delta G^\ddagger$ )<sup>201</sup> and the  $\text{p}K_a$  values.<sup>202</sup> However, calculations of ( $\Delta G^\ddagger$ ) and the  $\text{p}K_a$  values is time consuming. Reduction potentials of TAML activators are effortlessly measured via cyclic voltammetry and have been shown to be able to differentiate the two one electron transitions,  $\text{Fe}^{\text{III/IV}}$  and  $\text{Fe}^{\text{IV/V}}$  in acetonitrile.<sup>148</sup> The purpose of this work to utilize the reduction potentials (both  $\text{Fe}^{\text{III/IV}}$  and  $\text{Fe}^{\text{IV/V}}$ ) of TAML activators, spanning various macrocycles

for different generations of TAMLs including the latest NewTAMLs, and correlate it to their various properties such as  $pK_a$ , ionization potentials, HOMO energies, and their reactivities measured by  $k_I$  and  $k_{II}$  to predict the underlying mechanisms and serve as inputs for next generation design.



### 1.10 ANALYSIS OF COLORLESS MPs IN TAML CATALYZED OXIDATIONS

As shown in Scheme 1.1, oxidation of substrates by TAML activators is characterized by the second order rate constant,  $k_{II}$ . The second order rate constant,  $k_{II}$  helps to evaluate reactivities of various TAMLs towards a substrate and also determine the reactivities of different substrates towards a TAML activator. At the IGS,  $k_{II}$  is determined directly via following the decrease in concentration of a substrate utilizing an analytical technique. HPLC is typically used in the group for detection and quantification of colorless MPs (substrates) in water thus allowing following the kinetics of degradation to be studied.<sup>168,172</sup> While HPLC offers great sensitivity, repeatability and capability in substrate detection while simultaneously monitoring the oxidation products, it has certain disadvantages. HPLC analyses require sample preparation in most cases, the run times are typically long and each compound requires a new instrumental method. The kinetics of colored substrates reactions like dyes are analyzed using UV-vis spectroscopy.<sup>169</sup> While UV-Vis does not offer great sensitivity, it performs quick analyses without any sample preparation. This advantage gets manifold when the kinetic analyses have to be performed, especially involving measurements for initial rate approach which deal with < 20 % degradation of the compound. Additionally, UV-Vis is less expensive and requires very little maintenance. For the purpose of quick determinations of  $k_{II}$  for a large number of substrates, a universal UV-Vis spectroscopy can serve as a cost and time efficient technique. Moreover, HPLC would take months, just to generate the instrumental methods for all the individual substrates and mixtures the IGS wants to study. This work utilizes a plausible kinetic model, viz., parallel reaction model,<sup>199</sup> to indirectly measure the  $k_{II}$  for colorless substrates by monitoring the bleaching of a colored substrate via UV-Vis spectroscopy. The parallel reaction model is a kinetic process wherein substrate A (colored) and substrate B (colorless) react with the same reagent, (Activated TAML) in a parallel manner. Varying the [invisible substrate] should negatively impact the rate of dye bleaching in ways that the rate behavior of the invisible substrate can be determined.

### 1.11 RESEARCH SUMMARY

In this work, efforts have been made to add to the repository of TAML/NewTAML catalysis in five ways. Firstly, a detailed characterization of substrate inhibition pathways and correlation of electrochemical properties of TAML with performance in TAML catalysis has been undertaken. Secondly, a first of its kind, full life cycle analysis, of substrate, and oxidation products, with their temporal intermediate and toxicity profiles, in a TAML catalyzed reaction has been completed. Thirdly, identifying the best overall candidate for wastewater treatment via comparative evaluation of TAML and NewTAML activators (developed by Dr. Genoa R. Warner), utilizing a sequential testing protocol developed by me has aided in obtaining proof of patent claims on NewTAMLs. Fourthly, extensive comparative studies between various NewTAML/H<sub>2</sub>O<sub>2</sub> and ozone treatments in oxidizing 38 MPs in real wastewaters of Tucson, Arizona has been a major undertaking that best illustrates to date the immense potential of NewTAML/peroxide in water purification of micropollutants. Finally, an alternative approach to LCMS for kinetic analysis of TAML catalyzed oxidation of invisible MPs via indirect analyses using UV-Vis spectroscopy for faster analyses has been developed.

Chapter 2 describes the comparative evaluation of TAMLs in catalyzing oxidation of a persistent MP and drug, Propranolol. Substrate inhibition is characterized in detail utilizing kinetic analyses and NMR, Fluorescence, UV-Vis, ESI-MS and DFT studies. Substrate inhibition manifests as a decrease in the rate constant for hydrogen peroxide activation and this effect on  $k_1$  can now serve as first point check to see if a substrate is inhibiting in nature. Substrate inhibition can be projected by this study to be insignificant at ultradilute concentrations rendering the utility of TAML/H<sub>2</sub>O<sub>2</sub> as a powerful, green oxidative water treatment technology.

Chapter 3 details a full life cycle analysis of Propranolol and all its oxidation products in a TAML catalyzed oxidation. Simulation profiles for propranolol and its fragments, developed based on the TAML catalytic mechanism, agreed with the experimentally obtained profiles for all

compounds. Time dependent mass and toxicity profiles constructed for propranolol and its fragments illustrate the insufficiency of methodologies that only decrease in concentration of MP, while leaving large degradation products from sustainability perspective.

Chapter 4 describes a comparative evaluation of TAML and NewTAML catalysts to determine the best candidate for wastewater treatment from the perspective of technical and safety performances. A sequential approach, developed by me, has been applied utilizing a hard to oxidize MP, propranolol. NewTAMLs via iterative design contain a tunable kill switch in the macrocyclic framework, which can be deployed to help control their functional lifetimes in water. This is a collaborative study with Dr. Genoa R. Warner, then a graduate student, who synthesized the various NewTAMLs utilized for the study.

Chapter 5 describes a landmark study on oxidizing 38 MPs in real wastewaters of Tucson, Arizona. Seven conditions sets of NewTAML/H<sub>2</sub>O<sub>2</sub> treatments are compared with 4 conditions sets of ozone treatment, including the industrial dose of 2 ppm of ozone used in the Neugat plant in Dübendorf Switzerland where ozone water purification of MPs was significantly developed. The best current NewTAML identified from the previous chapter has been utilized for this work. A detailed kinetic profile has been developed for all NewTAML/H<sub>2</sub>O<sub>2</sub> treatments. This is a collaborative study with Dr. Minkyu Park, Dr. Kevin D. Daniels and Professor Shane A. Snyder at the University of Arizona.

Chapter 6 is an extensive approach to predicting properties, via linear free energy relationships (LFERs), of TAML/NewTAML activators utilizing the Fe<sup>III/IV</sup> and Fe<sup>IV/V</sup> reduction potentials. This provides an alternate to laborious  $\Delta G^\ddagger$  and  $pK_a$  calculations. Correlations have been made for  $pK_a$ 's of the axial aqua ligand at iron(III), the Stern-Volmer constants  $K_{SV}$  for the quenching of a fluorescence of propranolol, calculated ionization potentials of Fe<sup>III</sup> and Fe<sup>IV</sup> TAMLs, rate

constants  $k_I$  and  $k_{II}$  for the oxidation of the resting iron(III) TAML state by  $H_2O_2$  and reactions of the active forms of TAMLs with substrates.

Chapter 7 details an alternative approach to LC-MS, developed in collaboration with Dr. Matthew R. Mills (initiated the work) for quick kinetic analysis for oxidation of colorless substrates using UV-Vis spectroscopy. An indirect approach has been developed by creating a parallel reaction model wherein simultaneous reactions for oxidation of visible substrate (dye) and invisible substrate occur parallel in a reaction and the progress of oxidation of visible substrate should yield us indirectly the progress of oxidation of invisible substrate.

## 1.12 REFERENCES

- (1) Brown, T. Biodiversity <https://www.nationalgeographic.org/encyclopedia/biodiversity/>.
- (2) Díaz, S.; Settele, J.; Brondízio, E. S.; Ngo, H. T.; Agard, J.; Arneth, A.; Balvanera, P.; Brauman, K. A.; Butchart, S. H. M.; Chan, K. M. A.; et al. Pervasive Human-Driven Decline of Life on Earth Points to the Need for Transformative Change. *Science* (80-. ). **2019**, 366 (6471), eaax3100.
- (3) Sustainable development goals <https://www.un.org/sustainabledevelopment/blog/2019/05/nature-decline-unprecedented-report/>.
- (4) *The Evidence Is Clear: Transformative Change Needed Now to Address Nature Crisis and Protect Human Quality of Life*; 2019.
- (5) How many species are we losing? [https://wwf.panda.org/our\\_work/biodiversity/biodiversity/](https://wwf.panda.org/our_work/biodiversity/biodiversity/).
- (6) Monastersky, R. Biodiversity: Life — a Status Report. *Nature* **2014**, 516 (7530), 158–161.
- (7) July 2019 was hottest month on record for the planet <https://www.noaa.gov/news/july-2019-was-hottest-month-on-record-for-planet>.
- (8) Kahrilas, G. A.; Blotevogel, J.; Stewart, P. S.; Borch, T. Biocides in Hydraulic Fracturing Fluids: A Critical Review of Their Usage, Mobility, Degradation, and Toxicity. *Environ. Sci. Technol.* **2015**, 49 (1), 16–32.
- (9) Fact Sheet Natural History, Ecology and Recovery <https://www.fws.gov/midwest/eagle/Nhistory/biologue.html>.
- (10) Ehrlich, P. R.; Dobkin, D. S.; Wheye, D. DDT and Birds [https://web.stanford.edu/group/stanfordbirds/text/essays/DDT\\_and\\_Birds.html](https://web.stanford.edu/group/stanfordbirds/text/essays/DDT_and_Birds.html).
- (11) Environmental Defense Fund <https://www.edf.org/>.
- (12) The Peregrine Fund <https://peregrinefund.org/>.
- (13) The Department of Environmental Protection <https://www.dep.pa.gov/About/Pages/default.aspx>.
- (14) How Important Was Rachel Carson’s Silent Spring in the Recovery of Bald Eagles and Other Bird Species? <https://www.scientificamerican.com/article/rachel-carson-silent-spring-1972-ddt-ban-birds-thrive/>.
- (15) Drinking water Factsheet <https://www.who.int/news-room/fact-sheets/detail/drinking-water>.
- (16) Collins, T. J. Designing Ligands for Oxidizing Complexes. *Acc. Chem. Res.* **1994**, 27 (9), 279–285.
- (17) Daughton, C. G.; Ternes, T. A. Pharmaceuticals and Personal Care Products in the Environment: Agents of Subtle Change? *Environ. Health Perspect.* **1999**, 107 (Suppl 6), 907–938.
- (18) Schwarzenbach, R. P.; Escher, B. I.; Fenner, K.; Hofstetter, T. B.; Johnson, C. A.; von

- Gunten, U.; Wehrli, B. The Challenge of Micropollutants in Aquatic Systems. *Science* (80-. ). **2006**, *313* (5790), 1072 LP – 1077.
- (19) Colborn, T.; vom Saal, F. S.; Soto, A. M. Developmental Effects of Endocrine-Disrupting Chemicals in Wildlife and Humans. *Environ. Health Perspect.* **1993**, *101* (5), 378–384.
  - (20) Vandenberg, L. N.; Colborn, T.; Hayes, T. B.; Heindel, J. J.; Jacobs, D. R.; Lee, D. H.; Shioda, T.; Soto, A. M.; vom Saal, F. S.; Welshons, W. V.; et al. Hormones and Endocrine-Disrupting Chemicals: Low-Dose Effects and Nonmonotonic Dose Responses. *Endocr. Rev.* **2012**, *33* (3), 378–455.
  - (21) Kim, M.-K.; Zoh, K.-D. Occurrence and Removals of Micropollutants in Water Environment. *Environ. Eng. Res.* **2016**, *21* (4), 319–332.
  - (22) Schwarzenbach, R. P.; Egli, T.; Hofstetter, T. B.; von Gunten, U.; Wehrli, B. Global Water Pollution and Human Health. *Annu. Rev. Environ. Resour.* **2010**, *35* (1), 109–136.
  - (23) Pochodylo, A.; Helbling, D. E. *Target and Suspect Screening for Micropollutants in the Hudson River Estuary during the 2015 Recreational Season*; Cornell University, 2015.
  - (24) Chiara, P.; Barbara, M.; Tamar, K.; Anoy's, M.; Denis, T.; Nathalie, C. Occurrence and Fate of Micropollutants in the Vidy Bay of Lake Geneva, Switzerland. Part I: Priority List for Environmental Risk Assessment of Pharmaceuticals. *Environ. Toxicol. Chem.* **2010**, *29* (8), 1649–1657.
  - (25) Endocrine Disruptors  
<https://www.niehs.nih.gov/health/topics/agents/endocrine/index.cfm>.
  - (26) Warner, G. R. SYNTHESIS, PROPERTIES, AND REACTIVITY OF SULFONAMIDE NEWTAML OXIDATION CATALYSTS, Carnegie Mellon University, 2017.
  - (27) BPA free: Water bottles <https://www.target.com/c/water-bottles-sports-outdoors/bpa-free/-/N-5xt53Z5xkqg?Nao=0>.
  - (28) Huggett, D. B.; Brooks, B. W.; Peterson, B.; Foran, C. M.; Schlenk, D. Toxicity of Select Beta Adrenergic Receptor-Blocking Pharmaceuticals (B-Blockers) on Aquatic Organisms. *Arch. Env. Contam Toxicol* **2002**, *43* (2), 229–235.
  - (29) Stoker, T. E.; Gibson, E. K.; Zorrilla, L. M. Triclosan Exposure Modulates Estrogen-Dependent Responses in the Female Wistar Rat. *Toxicol. Sci.* **2010**, *117* (1), 45–53.
  - (30) Zorrilla, L. M.; Gibson, E. K.; Jeffay, S. C.; Crofton, K. M.; Setzer, W. R.; Cooper, R. L.; Stoker, T. E. The Effects of Triclosan on Puberty and Thyroid Hormones in Male Wistar Rats. *Toxicol. Sci.* **2009**, *107* (1), 56–64.
  - (31) Wolf, C.; Lambright, C.; Mann, P.; Price, M.; Cooper, R. L.; Ostby, J.; Gray Jr, L. E. Administration of Potentially Antiandrogenic Pesticides (Procymidone, Linuron, Iprodione, Chlozolinate, p, P'-DDE, and Ketoconazole) and Toxic Substances (Dibutyl- and Diethylhexyl Phthalate, PCB 169, and Ethane Dimethane Sulphonate) during Sexual Differen. *Toxicol. Ind. Health* **1999**, *15* (1–2), 94–118.
  - (32) Lo, S.; King, I.; Alléra, A.; Klingmüller, D. Effects of Various Pesticides on Human 5 $\alpha$ -Reductase Activity in Prostate and LNCaP Cells. *Toxicol. Vitro.* **2007**, *21* (3), 502–508.
  - (33) Borlakoglu, J. T.; Haegele, K. D. Comparative Aspects on the Bioaccumulation,

Metabolism and Toxicity with PCBs. *Comp. Biochem. Physiol. Part C Comp. Pharmacol.* **1991**, 100 (3), 327–338.

- (34) Hardell, L.; Andersson, S.-O.; Carlberg, M.; Bohr, L.; van Bavel, B.; Lindström, G.; Björnfoth, H.; Ginman, C. Adipose Tissue Concentrations of Persistent Organic Pollutants and the Risk of Prostate Cancer. *J. Occup. Environ. Med.* **2006**, 48 (7), 700–707.
- (35) Kester, M. H. A.; Bulduk, S.; Tibboel, D.; Meinl, W.; Glatt, H.; Falany, C. N.; Coughtrie, M. W. H.; Bergman, A. K. E.; Safe, S. H.; Kuiper, G. G. J. M. Potent Inhibition of Estrogen Sulfotransferase by Hydroxylated PCB Metabolites: A Novel Pathway Explaining the Estrogenic Activity of PCBs. *Endocrinology* **2000**, 141 (5), 1897–1900.
- (36) Greim, H.; Saltmiras, D.; Mostert, V.; Strupp, C. Evaluation of Carcinogenic Potential of the Herbicide Glyphosate, Drawing on Tumor Incidence Data from Fourteen Chronic/Carcinogenicity Rodent Studies. *Crit. Rev. Toxicol.* **2015**, 45 (3), 185–208.
- (37) Williams, G. M.; Aardema, M.; Acquavella, J.; Berry, S. C.; Brusick, D.; Burns, M. M.; de Camargo, J. L. V.; Garabrant, D.; Greim, H. A.; Kier, L. D.; et al. A Review of the Carcinogenic Potential of Glyphosate by Four Independent Expert Panels and Comparison to the IARC Assessment. *Crit. Rev. Toxicol.* **2016**, 46 (sup1), 3–20.
- (38) Gasnier, C.; Dumont, C.; Benachour, N.; Clair, E.; Chagnon, M.-C.; Séralini, G.-E. Glyphosate-Based Herbicides Are Toxic and Endocrine Disruptors in Human Cell Lines. *Toxicology* **2009**, 262 (3), 184–191.
- (39) Petrie, B.; Barden, R.; Kasprzyk-Hordern, B. A Review on Emerging Contaminants in Wastewaters and the Environment: Current Knowledge, Understudied Areas and Recommendations for Future Monitoring. *Water Res.* **2015**, 72, 3–27.
- (40) Loos, R.; Gawlik, B. M.; Locoro, G.; Rimaviciute, E.; Contini, S.; Bidoglio, G. EU-Wide Survey of Polar Organic Persistent Pollutants in European River Waters. *Environ. Pollut.* **2009**, 157 (2), 561–568.
- (41) Loos, R.; Carvalho, R.; Comero, S.; António, D. C.; Ghiani, M.; Lettieri, T.; Locoro, G.; Paracchini, B.; Tavazzi, S.; Gawlik, B. M. EU Wide Monitoring Survey on Waste Water Treatment Plant Effluents. **2012**.
- (42) Robert, K.; Marion, J.; Christian, G.; Hollender, J. Assessment of Micropollutants from Municipal Wastewater-Combination of Exposure and Ecotoxicological Effect Data for Switzerland. In *Waste water-evaluation and management*; IntechOpen, 2011.
- (43) Deeb, A. A.; Stephan, S.; Schmitz, O. J.; Schmidt, T. C. Suspect Screening of Micropollutants and Their Transformation Products in Advanced Wastewater Treatment. *Sci. Total Environ.* **2017**, 601–602, 1247–1253.
- (44) Behfar, A.; Nazari, Z.; Rabiee, M. H.; Raeesi, G.; Oveisi, M. R.; Sadeghi, N.; Jannat, B. The Organochlorine Pesticides Residue Levels in Karun River Water. *Jundishapur J. Nat. Pharm. Prod.* **2013**, 8 (1), 41–46.
- (45) Ochoa-Rivero, J. M.; Reyes-Fierro, A. V.; Peralta-Pérez, M. D. R.; Zavala-Díaz de la Serna, F. J.; Ballinas-Casarrubias, L.; Salmerón, I.; Rubio-Arias, H.; Rocha-Gutiérrez, B. A. Levels and Distribution of Pollutants in the Waters of an Aquatic Ecosystem in Northern Mexico. *Int. J. Environ. Res. Public Health* **2017**, 14 (5), 456.
- (46) Dahshan, H.; Megahed, A. M.; Abd-Elall, A. M. M.; Abd-El-Kader, M. A.-G.; Nabawy,

- E.; Elbana, M. H. Monitoring of Pesticides Water Pollution-The Egyptian River Nile. *J. Environ. Heal. Sci. Eng.* **2016**, *14*, 15.
- (47) Mishra, K.; Sharma, R. C. Contamination of Aquatic System by Chlorinated Pesticides and Their Spatial Distribution over North-East India. *Toxicol. Environ. Health Sci.* **2011**, *3* (3), 144.
  - (48) Gatidou, G.; Thomaidis, N. S.; Stasinakis, A. S.; Lekkas, T. D. Simultaneous Determination of the Endocrine Disrupting Compounds Nonylphenol, Nonylphenol Ethoxylates, Triclosan and Bisphenol A in Wastewater and Sewage Sludge by Gas Chromatography–Mass Spectrometry. *J. Chromatogr. A* **2007**, *1138* (1), 32–41.
  - (49) Nakada, N.; Tanishima, T.; Shinohara, H.; Kiri, K.; Takada, H. Pharmaceutical Chemicals and Endocrine Disrupters in Municipal Wastewater in Tokyo and Their Removal during Activated Sludge Treatment. *Water Res.* **2006**, *40* (17), 3297–3303.
  - (50) Wu, Z.; Zhang, Z.; Chen, S.; He, F.; Fu, G.; Liang, W. Nonylphenol and Octylphenol in Urban Eutrophic Lakes of the Subtropical China. *Fresenius Environ. Bull.* **2007**, *16* (3), 227–234.
  - (51) Li, D.; Kim, M.; Shim, W. J.; Yim, U. H.; Oh, J.-R.; Kwon, Y.-J. Seasonal Flux of Nonylphenol in Han River, Korea. *Chemosphere* **2004**, *56* (1), 1–6.
  - (52) Bexfield, L. M.; Toccalino, P. L.; Belitz, K.; Foreman, W. T.; Furlong, E. T. Hormones and Pharmaceuticals in Groundwater Used As a Source of Drinking Water Across the United States. *Environ. Sci. Technol.* **2019**, *53* (6), 2950–2960.
  - (53) Yoon, Y.; Ryu, J.; Oh, J.; Choi, B.-G.; Snyder, S. A. Occurrence of Endocrine Disrupting Compounds, Pharmaceuticals, and Personal Care Products in the Han River (Seoul, South Korea). *Sci. Total Environ.* **2010**, *408* (3), 636–643.
  - (54) Pookpoosa, I.; Jindal, R.; Morknøy, D.; Tantrakarnapa, K. Occurrence and Efficacy of Bisphenol A (BPA) Treatment in Selected Municipal Wastewater Treatment Plants, Bangkok, Thailand. *Water Sci. Technol.* **2015**, *72* (3), 463–471.
  - (55) Deeb, A. A.; Schmidt, T. C. Tandem Anion and Cation Exchange Solid Phase Extraction for the Enrichment of Micropollutants and Their Transformation Products from Ozonation in a Wastewater Treatment Plant. *Anal. Bioanal. Chem.* **2016**, *408* (16), 4219–4232.
  - (56) Weltin, D.; Gehring, M.; Tennhardt, L.; Vogel, D.; Bilitewski, B. Occurrence and Fate of Bisphenol A during Wastewater and Sewage Sludge Treatment in Selected German Wastewater Treatment Plants; Citeseer.
  - (57) Lesser, L. E.; Mora, A.; Moreau, C.; Mahlke, J.; Hernández-Antonio, A.; Ramírez, A. I.; Barrios-Piña, H. Survey of 218 Organic Contaminants in Groundwater Derived from the World's Largest Untreated Wastewater Irrigation System: Mezquital Valley, Mexico. *Chemosphere* **2018**, *198*, 510–521.
  - (58) Luo, Y.; Guo, W.; Ngo, H. H.; Nghiem, L. D.; Hai, F. I.; Zhang, J.; Liang, S.; Wang, X. C. A Review on the Occurrence of Micropollutants in the Aquatic Environment and Their Fate and Removal during Wastewater Treatment. *Sci Total Env.* **2014**, *473–474*, 619–641.
  - (59) Selvaraj, K. K.; Sundaramoorthy, G.; Ravichandran, P. K.; Girijan, G. K.; Sampath, S.; Ramaswamy, B. R. Phthalate Esters in Water and Sediments of the Kaveri River, India: Environmental Levels and Ecotoxicological Evaluations. *Environ. Geochem. Health* **2015**,



37 (1), 83–96.

- (60) Domínguez-Morueco, N.; González-Alonso, S.; Valcárcel, Y. Phthalate Occurrence in Rivers and Tap Water from Central Spain. *Sci. Total Environ.* **2014**, *500–501*, 139–146.
- (61) Sánchez-Avila, J.; Bonet, J.; Velasco, G.; Lacorte, S. Determination and Occurrence of Phthalates, Alkylphenols, Bisphenol A, PBDEs, PCBs and PAHs in an Industrial Sewage Grid Discharging to a Municipal Wastewater Treatment Plant. *Sci. Total Environ.* **2009**, *407* (13), 4157–4167.
- (62) Hossain, M. S.; Chowdhury, M. A. Z.; Pramanik, M. K.; Rahman, M. A.; Fakhruddin, A. N. M.; Alam, M. K. Determination of Selected Pesticides in Water Samples Adjacent to Agricultural Fields and Removal of Organophosphorus Insecticide Chlorpyrifos Using Soil Bacterial Isolates. *Appl. Water Sci.* **2015**, *5* (2), 171–179.
- (63) Bhattacharjee, S.; Fakhruddin, A. N. M.; Chowdhury, M. A. Z.; Rahman, M. A.; Alam, M. K. Monitoring of Selected Pesticides Residue Levels in Water Samples of Paddy Fields and Removal of Cypermethrin and Chlorpyrifos Residues from Water Using Rice Bran. *Bull. Environ. Contam. Toxicol.* **2012**, *89* (2), 348–353.
- (64) Banks, K. E.; Hunter, D. H.; Wachal, D. J. Chlorpyrifos in Surface Waters before and after a Federally Mandated Ban. *Environ. Int.* **2005**, *31* (3), 351–356.
- (65) Bailey, H. C.; Deanovic, L.; Reyes, E.; Kimball, T.; Larson, K.; Cortright, K.; Connor, V.; Hinton, D. E. Diazinon and Chlorpyrifos in Urban Waterways in Northern California, USA. *Environ. Toxicol. Chem.* **2000**, *19* (1), 82–87.
- (66) Malhat, F.; Nasr, I. Monitoring of Organophosphorous Pesticides Residues in Water from the Nile River Tributaries, Egypt. *Am J Water Resour* **2013**, *1* (1), 1–4.
- (67) Carroll, J.; Savinov, V.; Savinova, T.; Dahle, S.; McCrea, R.; Muir, D. C. G. PCBs, PBDEs and Pesticides Released to the Arctic Ocean by the Russian Rivers Ob and Yenisei. *Environ. Sci. Technol.* **2008**, *42* (1), 69–74.
- (68) Xing, Y.; Lu, Y.; Dawson, R. W.; Shi, Y.; Zhang, H.; Wang, T.; Liu, W.; Ren, H. A Spatial Temporal Assessment of Pollution from PCBs in China. *Chemosphere* **2005**, *60* (6), 731–739.
- (69) Zhang, S.; Zhang, Q.; Darisaw, S.; Ehie, O.; Wang, G. Simultaneous Quantification of Polycyclic Aromatic Hydrocarbons (PAHs), Polychlorinated Biphenyls (PCBs), and Pharmaceuticals and Personal Care Products (PPCPs) in Mississippi River Water, in New Orleans, Louisiana, USA. *Chemosphere* **2007**, *66* (6), 1057–1069.
- (70) Janex-Habibi, M.-L.; Huyard, A.; Esperanza, M.; Bruchet, A. Reduction of Endocrine Disruptor Emissions in the Environment: The Benefit of Wastewater Treatment. *Water Res.* **2009**, *43* (6), 1565–1576.
- (71) Nie, Y.; Qiang, Z.; Zhang, H.; Ben, W. Fate and Seasonal Variation of Endocrine-Disrupting Chemicals in a Sewage Treatment Plant with A/A/O Process. *Sep. Purif. Technol.* **2012**, *84*, 9–15.
- (72) Zorita, S.; Mårtensson, L.; Mathiasson, L. Occurrence and Removal of Pharmaceuticals in a Municipal Sewage Treatment System in the South of Sweden. *Sci. Total Environ.* **2009**, *407* (8), 2760–2770.

- (73) North, K. D. Tracking Polybrominated Diphenyl Ether Releases in a Wastewater Treatment Plant Effluent, Palo Alto, California. *Environ. Sci. Technol.* **2004**, 38 (17), 4484–4488.
- (74) Deng, D.; Chen, H.; Tam, N. F. Y. Temporal and Spatial Contamination of Polybrominated Diphenyl Ethers (PBDEs) in Wastewater Treatment Plants in Hong Kong. *Sci. Total Environ.* **2015**, 502, 133–142.
- (75) Hope, B. K.; Pillsbury, L.; Boling, B. A State-Wide Survey in Oregon (USA) of Trace Metals and Organic Chemicals in Municipal Effluent. *Sci. Total Environ.* **2012**, 417–418, 263–272.
- (76) Kim, M.; Guerra, P.; Theocharides, M.; Barclay, K.; Smyth, S. A.; Alae, M. Parameters Affecting the Occurrence and Removal of Polybrominated Diphenyl Ethers in Twenty Canadian Wastewater Treatment Plants. *Water Res.* **2013**, 47 (7), 2213–2221.
- (77) Daso, A. P.; Fatoki, O. S.; Odendaal, J. P.; Olujimi, O. O. Occurrence of Selected Polybrominated Diphenyl Ethers and 2,2',4,4',5,5'-Hexabromobiphenyl (BB-153) in Sewage Sludge and Effluent Samples of a Wastewater-Treatment Plant in Cape Town, South Africa. *Arch. Environ. Contam. Toxicol.* **2012**, 62 (3), 391–402.
- (78) Xiang, N.; Zhao, X.; Meng, X.-Z.; Chen, L. Polybrominated Diphenyl Ethers (PBDEs) in a Conventional Wastewater Treatment Plant (WWTP) from Shanghai, the Yangtze River Delta: Implication for Input Source and Mass Loading. *Sci. Total Environ.* **2013**, 461–462, 391–396.
- (79) Rogowska, J.; Cieszyńska-Semenowicz, M.; Ratajczyk, W.; Wolska, L. Micropollutants in Treated Wastewater. *Ambio* **2019**.
- (80) Völker, J.; Vogt, T.; Castronovo, S.; Wick, A.; Ternes, T. A.; Joss, A.; Oehlmann, J.; Wagner, M. Extended Anaerobic Conditions in the Biological Wastewater Treatment: Higher Reduction of Toxicity Compared to Target Organic Micropollutants. *Water Res.* **2017**, 116, 220–230.
- (81) Duirk, S. E.; Lindell, C.; Cornelison, C. C.; Kormos, J.; Ternes, T. A.; Attene-Ramos, M.; Osiol, J.; Wagner, E. D.; Plewa, M. J.; Richardson, S. D. Formation of Toxic Iodinated Disinfection By-Products from Compounds Used in Medical Imaging. *Environ. Sci. Technol.* **2011**, 45 (16), 6845–6854.
- (82) Ternes, T. A.; Hirsch, R. Occurrence and Behavior of X-Ray Contrast Media in Sewage Facilities and the Aquatic Environment. *Environ. Sci. Technol.* **2000**, 34 (13), 2741–2748.
- (83) Sharma, B. M.; Bečanová, J.; Scheringer, M.; Sharma, A.; Bharat, G. K.; Whitehead, P. G.; Klánová, J.; Nizzetto, L. Health and Ecological Risk Assessment of Emerging Contaminants (Pharmaceuticals, Personal Care Products, and Artificial Sweeteners) in Surface and Groundwater (Drinking Water) in the Ganges River Basin, India. *Sci. Total Environ.* **2019**, 646, 1459–1467.
- (84) Stamatis, N. K.; Konstantinou, I. K. Occurrence and Removal of Emerging Pharmaceutical, Personal Care Compounds and Caffeine Tracer in Municipal Sewage Treatment Plant in Western Greece. *J. Environ. Sci. Health. B.* **2013**, 48 (9), 800–813.
- (85) Wluka, A.-K.; Rudel, H.; Pohl, K.; Schwarzbauer, J. Analytical Method Development for the Determination of Eight Biocides in Various Environmental Compartments and

- Application for Monitoring Purposes. *Environ. Sci. Pollut. Res. Int.* **2016**, 23 (21), 21894–21907.
- (86) Kay, P.; Grayson, R. Using Water Industry Data to Assess the Metaldehyde Pollution Problem. *Water Environ. J.* **2014**, 28 (3), 410–417.
  - (87) Castle, G. D.; Mills, G. A.; Gravel, A.; Jones, L.; Townsend, I.; Cameron, D. G.; Fones, G. R. Review of the Molluscicide Metaldehyde in the Environment. *Environ. Sci. Water Res. Technol.* **2017**, 3 (3), 415–428.
  - (88) Carles, L.; Gardon, H.; Joseph, L.; Sanchís, J.; Farré, M.; Artigas, J. Meta-Analysis of Glyphosate Contamination in Surface Waters and Dissipation by Biofilms. *Environ. Int.* **2019**, 124, 284–293.
  - (89) Rendon-von Osten, J.; Dzul-Caamal, R. Glyphosate Residues in Groundwater, Drinking Water and Urine of Subsistence Farmers from Intensive Agriculture Localities: A Survey in Hopelchén, Campeche, Mexico. *Int. J. Environ. Res. Public Health* **2017**, 14 (6), 595.
  - (90) Kolpin, D. W.; Thurman, E. M.; Lee, E. A.; Meyer, M. T.; Furlong, E. T.; Glassmeyer, S. T. Urban Contributions of Glyphosate and Its Degradate AMPA to Streams in the United States. *Sci. Total Environ.* **2006**, 354 (2), 191–197.
  - (91) Martin Ruel, S.; Esperanza, M.; Choubert, J.-M.; Valor, I.; Budzinski, H.; Coquery, M. On-Site Evaluation of the Efficiency of Conventional and Advanced Secondary Processes for the Removal of 60 Organic Micropollutants. *Water Sci. Technol.* **2010**, 62 (12), 2970–2978.
  - (92) Loos, R.; Carvalho, R.; António, D. C.; Comero, S.; Locoro, G.; Tavazzi, S.; Paracchini, B.; Ghiani, M.; Lettieri, T.; Blaha, L.; et al. EU-Wide Monitoring Survey on Emerging Polar Organic Contaminants in Wastewater Treatment Plant Effluents. *Water Res.* **2013**, 47 (17), 6475–6487.
  - (93) Köck-Schulmeyer, M.; Villagrasa, M.; López de Alda, M.; Céspedes-Sánchez, R.; Ventura, F.; Barceló, D. Occurrence and Behavior of Pesticides in Wastewater Treatment Plants and Their Environmental Impact. *Sci. Total Environ.* **2013**, 458–460, 466–476.
  - (94) Campo, J.; Masiá, A.; Blasco, C.; Picó, Y. Occurrence and Removal Efficiency of Pesticides in Sewage Treatment Plants of Four Mediterranean River Basins. *J. Hazard. Mater.* **2013**, 263, 146–157.
  - (95) Gomez, M. J.; Martinez Bueno, M. J.; Lacorte, S.; Fernandez-Alba, A. R.; Agüera, A. Pilot Survey Monitoring Pharmaceuticals and Related Compounds in a Sewage Treatment Plant Located on the Mediterranean Coast. *Chemosphere* **2007**, 66 (6), 993–1002.
  - (96) Verlicchi, P.; Al Aukidy, M.; Zambello, E. Occurrence of Pharmaceutical Compounds in Urban Wastewater: Removal, Mass Load and Environmental Risk after a Secondary Treatment—a Review. *Sci. Total Environ.* **2012**, 429, 123–155.
  - (97) Onesios, K. M.; Jim, T. Y.; Bouwer, E. J. Biodegradation and Removal of Pharmaceuticals and Personal Care Products in Treatment Systems: A Review. *Biodegradation* **2009**, 20 (4), 441–466.
  - (98) Bolong, N.; Ismail, A. F.; Salim, M. R.; Matsuura, T. A Review of the Effects of Emerging Contaminants in Wastewater and Options for Their Removal. *Desalination* **2009**, 239 (1–3), 229–246.

- (99) Reemtsma, T.; Weiss, S.; Mueller, J.; Petrovic, M.; González, S.; Barcelo, D.; Ventura, F.; Knepper, T. P. Polar Pollutants Entry into the Water Cycle by Municipal Wastewater: A European Perspective. *Environ. Sci. Technol.* **2006**, *40* (17), 5451–5458.
- (100) Krasner, S. W.; Westerhoff, P.; Chen, B.; Rittmann, B. E.; Amy, G. Occurrence of Disinfection Byproducts in United States Wastewater Treatment Plant Effluents. *Environ. Sci. Technol.* **2009**, *43* (21), 8320–8325.
- (101) Rebhun, M.; Heller-Grossman, L.; Manka, J. Formation of Disinfection Byproducts during Chlorination of Secondary Effluent and Renovated Water. *Water Environ. Res.* **1997**, *69* (6), 1154–1162.
- (102) *ICPR Recommendations for Reducing Micropollutants in Waters*; 2019.
- (103) CAS-A Division of the American Chemical Society <https://www.cas.org/>.
- (104) Estimated Annual Agricultural Pesticide Use  
[https://water.usgs.gov/nawqa/pnsp/usage/maps/show\\_map.php?year=2016&map=GLYPHOSATE&hilo=L](https://water.usgs.gov/nawqa/pnsp/usage/maps/show_map.php?year=2016&map=GLYPHOSATE&hilo=L).
- (105) Bai, S. H.; Ogbourne, S. M. Glyphosate: Environmental Contamination, Toxicity and Potential Risks to Human Health via Food Contamination. *Environ. Sci. Pollut. Res.* **2016**, *23* (19), 18988–19001.
- (106) Peruzzo, P. J.; Porta, A. A.; Ronco, A. E. Levels of Glyphosate in Surface Waters, Sediments and Soils Associated with Direct Sowing Soybean Cultivation in North Pampasic Region of Argentina. *Environ. Pollut.* **2008**, *156* (1), 61–66.
- (107) Bøhn, T.; Cuhra, M.; Traavik, T.; Sanden, M.; Fagan, J.; Primicerio, R. Compositional Differences in Soybeans on the Market: Glyphosate Accumulates in Roundup Ready GM Soybeans. *Food Chem.* **2014**, *153*, 207–215.
- (108) Myers, J. P.; Antoniou, M. N.; Blumberg, B.; Carroll, L.; Colborn, T.; Everett, L. G.; Hansen, M.; Landrigan, P. J.; Lanphear, B. P.; Mesnage, R.; et al. Concerns over Use of Glyphosate-Based Herbicides and Risks Associated with Exposures: A Consensus Statement. *Environ. Heal.* **2016**, *15* (1), 19.
- (109) Persistent Organic Pollutants: A Global Issue, A Global Response  
<https://www.epa.gov/international-cooperation/persistent-organic-pollutants-global-issue-global-response#pops>.
- (110) Persistent organic pollutants (POPs)  
[https://www.who.int/foodsafety/areas\\_work/chemical-risks/pops/en/](https://www.who.int/foodsafety/areas_work/chemical-risks/pops/en/).
- (111) The 12 initial POPs under the Stockholm Convention  
<http://chm.pops.int/TheConvention/ThePOPs/The12InitialPOPs/tabid/296/Default.aspx>.
- (112) Custer, C. M.; Custer, T. W.; Dummer, P. M.; Goldberg, D.; Franson, J. C. Concentrations and Spatial Patterns of Organic Contaminants in Tree Swallow (*Tachycineta Bicolor*) Eggs at United States and Binational Great Lakes Areas of Concern, 2010-2015. *Environ. Toxicol. Chem.* **2016**, *35* (12), 3071–3092.
- (113) Custer, C. M.; Custer, T. W.; Dummer, P. M. Patterns of Organic Contaminants in Eggs of an Insectivorous, an Omnivorous, and a Piscivorous Bird Nesting on the Hudson River, New York, USA. *Environ. Toxicol. Chem.* **2010**, *29* (10), 2286–2296.

- (114) Custer, T. W.; Dummer, P. M.; Custer, C. M.; Franson, J. C.; Jones, M. Contaminant Exposure of Birds Nesting in Green Bay, Wisconsin, USA. *Environ. Toxicol. Chem.* **2014**, 33 (8), 1832–1839.
- (115) Custer, T. W.; Custer, C. M.; Dummer, P. M.; Goldberg, D.; Franson, J. C.; Erickson, R. A. Organic Contamination in Tree Swallow (*Tachycineta Bicolor*) Nestlings at United States and Binational Great Lakes Areas of Concern. *Environ. Toxicol. Chem.* **2017**, 36 (3), 735–748.
- (116) Tang, L. L. Activating Oxygen and Degrading the Water Treatment Industry's Most Challenging Micropollutant with TAML Activators and Oxidants, 2016.
- (117) Poyatos, J. M.; Muño, M. M.; Almecija, M. C.; Torres, J. C.; Hontoria, E.; Osorio, F. Advanced Oxidation Processes for Wastewater Treatment: State of the Art. *Water. Air. Soil Pollut.* **2010**, 205 (1–4), 187.
- (118) Parson, S. *Advanced Oxidation Processes for Water and Wastewater Treatment*; IWA Publishing, 2004.
- (119) Miklos, D. B.; Remy, C.; Jekel, M.; Linden, K. G.; Drewes, J. E.; Hübner, U. Evaluation of Advanced Oxidation Processes for Water and Wastewater Treatment – A Critical Review. *Water Res.* **2018**, 139, 118–131.
- (120) Park, M.; Anumol, T.; Daniels, K. D.; Wu, S.; Ziska, A. D.; Snyder, S. A. Predicting Trace Organic Compound Attenuation by Ozone Oxidation: Development of Indicator and Surrogate Models. *Water Res.* **2017**, 119, 21–32.
- (121) Lian, L.; Yao, B.; Hou, S.; Fang, J.; Yan, S.; Song, W. Kinetic Study of Hydroxyl and Sulfate Radical-Mediated Oxidation of Pharmaceuticals in Wastewater Effluents. *Environ. Sci. Technol.* **2017**, 51 (5), 2954–2962.
- (122) Isarain-Chavez, E.; Cabot, P. L.; Centellas, F.; Rodriguez, R. M.; Arias, C.; Garrido, J. A.; Brillas, E. L. B.-I.-C. Electro-Fenton and Photoelectro-Fenton Degradations of the Drug Beta-Blocker Propranolol Using a Pt Anode: Identification and Evolution of Oxidation Products. *J. Hazard. Mater.* **2011**, 185, 1228–1235.
- (123) Vogna, D.; Marotta, R.; Napolitano, A.; Andreozzi, R.; d'Ischia, M. Advanced Oxidation of the Pharmaceutical Drug Diclofenac with UV/H<sub>2</sub>O<sub>2</sub> and Ozone. *Water Res.* **2004**, 38 (2), 414–422.
- (124) Pérez-Estrada, L. A.; Malato, S.; Gernjak, W.; Agüera, A.; Thurman, E. M.; Ferrer, I.; Fernández-Alba, A. R. Photo-Fenton Degradation of Diclofenac: Identification of Main Intermediates and Degradation Pathway. *Environ. Sci. Technol.* **2005**, 39 (21), 8300–8306.
- (125) Bourgin, M.; Violleau, F.; Debrauwer, L.; Albet, J. Ozonation of Imidacloprid in Aqueous Solutions: Reaction Monitoring and Identification of Degradation Products. *J. Hazard. Mater.* **2011**, 190 (1), 60–68.
- (126) Cerreta, G.; Roccamante, M. A.; Oller, I.; Malato, S.; Rizzo, L. Contaminants of Emerging Concern Removal from Real Wastewater by UV/Free Chlorine Process: A Comparison with Solar/Free Chlorine and UV/H<sub>2</sub>O<sub>2</sub> at Pilot Scale. *Chemosphere* **2019**, 236, 124354.
- (127) Segura, C.; Zaror, C.; Mansilla, H. D.; Mondaca, M. A. Imidacloprid Oxidation by Photo-Fenton Reaction. *J. Hazard. Mater.* **2008**, 150 (3), 679–686.

- (128) Carlson, J. C.; Stefan, M. I.; Parnis, J. M.; Metcalfe, C. D. Direct UV Photolysis of Selected Pharmaceuticals, Personal Care Products and Endocrine Disruptors in Aqueous Solution. *Water Res.* **2015**, *84*, 350–361.
- (129) Rozas, O.; Vidal, C.; Baeza, C.; Jardim, W. F.; Rossner, A.; Mansilla, H. D. Organic Micropollutants (OMPs) in Natural Waters: Oxidation by UV/H<sub>2</sub>O<sub>2</sub> Treatment and Toxicity Assessment. *Water Res.* **2016**, *98*, 109–118.
- (130) Sirés, I.; Oturan, N.; Oturan, M. A.; Rodríguez, R. M.; Garrido, J. A.; Brillas, E. Electro-Fenton Degradation of Antimicrobials Triclosan and Triclocarban. *Electrochim. Acta* **2007**, *52* (17), 5493–5503.
- (131) Zhao, X.; Jiang, J.; Pang, S.; Guan, C.; Li, J.; Wang, Z.; Ma, J.; Luo, C. Degradation of Iopamidol by Three UV-Based Oxidation Processes: Kinetics, Pathways, and Formation of Iodinated Disinfection Byproducts. *Chemosphere* **2019**, *221*, 270–277.
- (132) Zhao, C.; Arroyo-Mora, L. E.; DeCaprio, A. P.; Sharma, V. K.; Dionysiou, D. D.; O'Shea, K. E. Reductive and Oxidative Degradation of Iopamidol, Iodinated X-Ray Contrast Media, by Fe(III)-Oxalate under UV and Visible Light Treatment. *Water Res.* **2014**, *67*, 144–153.
- (133) Deborde, M.; Rabouan, S.; Mazellier, P.; Duguet, J.-P.; Legube, B. Oxidation of Bisphenol A by Ozone in Aqueous Solution. *Water Res.* **2008**, *42* (16), 4299–4308.
- (134) Sharma, J.; Mishra, I. M.; Kumar, V. Degradation and Mineralization of Bisphenol A (BPA) in Aqueous Solution Using Advanced Oxidation Processes: UV/H<sub>2</sub>O<sub>2</sub> and UV/S<sub>2</sub>O<sub>8</sub><sup>2-</sup> Oxidation Systems. *J. Environ. Manage.* **2015**, *156*, 266–275.
- (135) Katsumata, H.; Kawabe, S.; Kaneco, S.; Suzuki, T.; Ohta, K. Degradation of Bisphenol A in Water by the Photo-Fenton Reaction. *J. Photochem. Photobiol. A Chem.* **2004**, *162* (2), 297–305.
- (136) Lee, Y.; Zimmermann, S. G.; Kieu, A. T.; von Gunten, U. Ferrate (Fe(VI)) Application for Municipal Wastewater Treatment: A Novel Process for Simultaneous Micropollutant Oxidation and Phosphate Removal. *Environ. Sci. Technol.* **2009**, *43* (10), 3831–3838.
- (137) Zhang, Z.; Feng, Y.; Liu, Y.; Sun, Q.; Gao, P.; Ren, N. Kinetic Degradation Model and Estrogenicity Changes of EE2 (17 $\alpha$ -Ethinylestradiol) in Aqueous Solution by UV and UV/H<sub>2</sub>O<sub>2</sub> Technology. *J. Hazard. Mater.* **2010**, *181* (1), 1127–1133.
- (138) Frontistis, Z.; Xekoukoulotakis, N. P.; Hapeshi, E.; Venieri, D.; Fatta-Kassinos, D.; Mantzavinos, D. Fast Degradation of Estrogen Hormones in Environmental Matrices by Photo-Fenton Oxidation under Simulated Solar Radiation. *Chem. Eng. J.* **2011**, *178*, 175–182.
- (139) George, P. L. B.-ol. The Chemical Nature of the Second Hydrogen Peroxide Compound Formed by Cytochrome c Peroxidase and Horseradish Peroxidase. *Biochem. J.* **1953**, *54*, 267–276.
- (140) James, C.; Germain, E.; Judd, S. Micropollutant Removal by Advanced Oxidation of Microfiltered Secondary Effluent for Water Reuse. *Sep. Purif. Technol.* **2014**, *127*, 77–83.
- (141) Gähr, F.; Hermanutz, F.; Oppermann, W. Ozonation-an Important Technique to Comply with New German Laws for Textile Wastewater Treatment. *Water Sci. Technol.* **1994**, *30* (3), 255.

- (142) Ternes, T. A.; Stüber, J.; Herrmann, N.; McDowell, D.; Ried, A.; Kampmann, M.; Teiser, B. Ozonation: A Tool for Removal of Pharmaceuticals, Contrast Media and Musk Fragrances from Wastewater? *Water Res.* **2003**, *37* (8), 1976–1982.
- (143) Von Sonntag, C.; Von Gunten, U. *Chemistry of Ozone in Water and Wastewater Treatment*; IWA publishing, 2012.
- (144) Sánchez-Polo, M.; Salhi, E.; Rivera-Utrilla, J.; Von Gunten, U. Combination of Ozone with Activated Carbon as an Alternative to Conventional Advanced Oxidation Processes. *Ozone Sci. Eng.* **2006**, *28* (4), 237–245.
- (145) Margot, J.; Kienle, C.; Magnet, A.; Weil, M.; Rossi, L.; de Alencastro, L. F.; Abegglen, C.; Thonney, D.; Chevre, N.; Scharer, M.; et al. Treatment of Micropollutants in Municipal Wastewater: Ozone or Powdered Activated Carbon? *Sci Total Env.* **2013**, *461–462*, 480–498.
- (146) Collins, T. J.; Horwitz, C. P.; Ryabov, A. D.; Vuocolo, L. D.; Gupta, S. S.; Ghosh, A.; Fattaleh, N. L.; Hangan, Y.; Steinhoff, B.; Noser, C. A.; et al. Tetraamido Macrocyclic Ligand Catalytic Oxidant Activators in the Pulp and Paper Industry. *ACS Symposium Series*. Department of Chemistry, Carnegie Mellon University, 4400 Fifth Avenue, Pittsburgh, PA 15213-2683, United States NZ Forest Research Institute, Private Bag 3020, Rotorua, New Zealand Department of Chemistry, University of Auckland, Private Bag 92019, Auckl 2002, pp 47–60.
- (147) Carlsson, G. H.; Nicholls, P.; Svistunenko, D.; Berglund, G. I.; Hajdu, J. Complexes of Horseradish Peroxidase with Formate, Acetate, and Carbon Monoxide. *Biochemistry* **2005**, *44* (2), 635–642.
- (148) Ghosh, A.; Mitchell, D. A.; Chanda, A.; Ryabov, A. D.; Popescu, D. L.; Upham, E. C.; Collins, G. J.; Collins, T. J. Catalase-Peroxidase Activity of Iron(III)-TAML Activators of Hydrogen Peroxide. *J. Am. Chem. Soc.* **2008**, *130* (45), 15116–15126.
- (149) Ryabov, A. D.; Collins, T. J. Mechanistic Considerations on the Reactivity of Green FeIII-TAML Activators of Peroxides. *Adv. Inorg. Chem.* **2009**, *61*, 471–521.
- (150) Tang, L. L.; Gunderson, W. A.; Weitz, A. C.; Hendrich, M. P.; Ryabov, A. D.; Collins, T. J. Activation of Dioxygen by a TAML Activator in Reverse Micelles: Characterization of an Fe(III)Fe(IV) Dimer and Associated Catalytic Chemistry. *J Am Chem Soc* **2015**, *137* (30), 9704–9715.
- (151) Collins, T. Toward Sustainable Chemistry. *Science* (80-. ). **2001**, *291* (5501), 48 LP – 49.
- (152) Kundu, S.; Van Kirk Thompson, J.; Shen, L. Q.; Mills, M. R.; Bominaar, E. L.; Ryabov, A. D.; Collins, T. J. Activation Parameters as Mechanistic Probes in the TAML Iron(V)-Oxo Oxidations of Hydrocarbons. *Chem. - Eur. J.* **2015**, *21* (4), 1803–1810.
- (153) Mills, M. R.; Burton, A. E.; Mori, D. I.; Ryabov, A. D.; Collins, T. J. Iron(IV) or Iron(V)? Heterolytic or Free Radical? Oxidation Pathways of a TAML Activator in Acetonitrile at -40 °C. *J. Coord. Chem.* **2015**, *68* (17–18), 3046–3057.
- (154) Ghosh, A.; De Oliveira, F. T.; Yano, T.; Nishioka, T.; Beach, E. S.; Kinoshita, I.; Münck, E.; Ryabov, A. D.; Horwitz, C. P.; Collins, T. J.; et al. Catalytically Active  $\mu$ -Oxodiiron(IV) Oxidants from Iron(III) and Dioxygen. *J. Am. Chem. Soc.* **2005**, *127* (8), 2505–2513.

- (155) Collins, T. J.; Ryabov, A. D. *Understanding Mechanisms of Green Oxidation Catalysis by Iron-TAML Peroxide Activators*; 2004.
- (156) Collins, T. J. TAML Activators: Mechanisms of Action and Applications; American Chemical Society, 2012; p INOR-491.
- (157) DeNardo, M. A.; Mills, M. R.; Ryabov, A. D.; Collins, T. J. Unifying Evaluation of the Technical Performances of Iron-Tetra-Amido Macrocyclic Ligand Oxidation Catalysts. *J. Am. Chem. Soc.* **2016**, *138* (9), 2933–2936.
- (158) A, D. M. Gaining Insight into the Design of Oxidation Catalysts by c Omparing the Rate and Equilibrium Constants That Define the Technical Performance of a Suite of TAML Activators Including Design Related Studies for Environmental Performance , Carnegie Mellon University: USA, 2016, Vol. PhD.
- (159) Collins, T. J. TAML Oxidant Activators: A New Approach to the Activation of Hydrogen Peroxide for Environmentally Significant Problems. *Acc. Chem. Res.* **2002**, *35* (9), 782–790.
- (160) Warner, G.; Mills, M.; Enslin, C.; Pattanayak, S.; Panda, C.; Sen Gupta, S.; Ryabov, A. D.; Collins, T. J. Reactivity of N-Tailed ('Biuret') TAMLs in Water: Kinetics of the Catalyzed Oxidation of Orange II by H<sub>2</sub>O<sub>2</sub>. Synthesis and X-Ray Characterization of an N-Phenyl Biuret TAML. *Chem. - Eur. J.* **2015**, *21* (16), 6226–6233.
- (161) Warner, G. R.; Somasundar, Y.; Jansen, K. C.; Kaaret, E. Z.; Weng, C.; Burton, A. E.; Mills, M. R.; Shen, L. Q.; Ryabov, A. D.; Pros, G.; et al. Bioinspired, Multidisciplinary, Iterative Catalyst Design Creates the Highest Performance Peroxidase Mimics and the Field of Sustainable Ultradilute Oxidation Catalysis (SUDOC). *ACS Catal.* **2019**, 7023–7037.
- (162) Onundi, Y. Oxidation of Bisphenol A, Triclosan and 4-Nonylphenol by Fe-B\* Activated Peroxide, The University of Auckland, 2015.
- (163) Onundi, Y.; Drake, B. A.; Malecky, R. T.; DeNardo, M. A.; Mills, M. R.; Kundu, S.; Ryabov, A. D.; Beach, E. S.; Horwitz, C. P.; Simonich, M. T.; et al. A Multidisciplinary Investigation of the Technical and Environmental Performances of TAML/Peroxide Elimination of Bisphenol A Compounds from Water. *Green Chem.* **2017**, *19* (18), 4234–4262.
- (164) Kundu, S.; Chanda, A.; Thompson, J. V. K.; Diabes, G.; Khetan, S. K.; Ryabov, A. D.; Collins, T. J. Rapid Degradation of Oxidation Resistant Nitrophenols by TAML Activator and H<sub>2</sub>O<sub>2</sub>. *Catal. Sci. Technol.* **2015**, *5* (3), 1775–1782.
- (165) Sen Gupta, S.; Stadler, M.; Noser, C. A.; Ghosh, A.; Steinhoff, B.; Lenoir, D.; Horwitz, C. P.; Schramm, K.-W.; Collins, T. J. Rapid Total Destruction of Chlorophenols by Activated Hydrogen Peroxide. *Sci. (Washington, DC, U. S.)* **2002**, *296* (5566), 326–328.
- (166) Do Pham, D. D.; Kelso, G. F.; Yang, Y.; Hearn, M. T. W. Studies on the Oxidative N-Demethylation of Atropine, Thebaine and Oxycodone Using a Fe III -TAML Catalyst. *Green Chem.* **2014**, *16* (3).
- (167) Shappell, N. W.; Vrabell, M. A.; Madsen, P. J.; Harrington, G.; Billey, L. O.; Hakk, H.; Larsen, G. L.; Beach, E. S.; Horwitz, C. P.; Ro, K.; et al. Destruction of Estrogens Using Fe-TAML/Peroxide Catalysis. *Environ. Sci. Technol.* **2008**, *42* (4), 1296–1300.



- (168) Mills, M. R.; Arias-Salazar, K.; Baynes, A.; Shen, L. Q.; Churchley, J.; Beresford, N.; Gayathri, C.; Gil, R. R.; Kanda, R.; Jobling, S.; et al. Removal of Ecotoxicity of 17 $\alpha$ -Ethinylestradiol Using TAML/Peroxide Water Treatment. *Sci Rep* **2015**, *5*, 10511.
- (169) Chahbane, N.; Popescu, D. L.; Mitchell, D. A.; Chanda, A.; Lenoir, D.; Ryabov, A. D.; Schramm, K. W.; Collins, T. J. FeIII-TAML-Catalyzed Green Oxidative Degradation of the Azo Dye Orange II by H<sub>2</sub>O<sub>2</sub> and Organic Peroxides: Products, Toxicity, Kinetics, and Mechanisms. *Green Chem.* **2007**, *9* (1), 49–57.
- (170) Chanda, A.; Ryabov, A. D.; Mondal, S.; Alexandrova, L.; Ghosh, A.; Hangan-Balkir, Y.; Horwitz, C. P.; Collins, T. J. Activity-Stability Parameterization of Homogeneous Green Oxidation Catalysts. *Chem. - A Eur. J.* **2006**, *12* (36), 9336–9345.
- (171) Mitchell, D. A.; Ryabov, A. D.; Kundu, S.; Chanda, A.; Collins, T. J. Oxidation of Pinacyanol Chloride by H<sub>2</sub>O<sub>2</sub> Catalyzed by FeIII Complexed to Tetraamidomacrocyclic Ligand: Unusual Kinetics and Product Identification. *J. Coord. Chem.* **2010**, *63* (14–16), 2605–2618.
- (172) Somasundar, Y.; Shen, L. Q.; Hoane, A. G.; Tang, L. L.; Mills, M. R.; Burton, A. E.; Ryabov, A. D.; Collins, T. J. Structural, Mechanistic, and Ultradilute Catalysis Portrayal of Substrate Inhibition in the TAML–Hydrogen Peroxide Catalytic Oxidation of the Persistent Drug and Micropollutant, Propranolol. *J. Am. Chem. Soc.* **2018**, *140* (38), 12280–12289.
- (173) Madsen, P. J.; Popescu, D.-L.; Vrabel, M. A.; Horwitz, C. P.; Collins, T. J. Degradation of Fluoxetine Using FeIII-TAML Activated Hydrogen Peroxide; American Chemical Society, 2007; p IEC-146.
- (174) Shen, L. Q.; Beach, E. S.; Xiang, Y.; Tshudy, D. J.; Khanina, N.; Horwitz, C. P.; Bier, M. E.; Collins, T. J. Rapid, Biomimetic Degradation in Water of the Persistent Drug Sertraline by TAML Catalysts and Hydrogen Peroxide. *Env. Sci Technol* **2011**, *45* (18), 7882–7887.
- (175) Churchley, J.; Collins, T.; Jobling, S. *Catalytic Oxidation of Pharmaceutical Compounds in Wastewater Effluents*; UKWIR: London, 2013.
- (176) Kundu, S.; Chanda, A.; Khetan, S. K.; Ryabov, A. D.; Collins, T. J. TAML Activator/Peroxide-Catalyzed Facile Oxidative Degradation of the Persistent Explosives Trinitrotoluene and Trinitrobenzene in Micellar Solutions. *Env. Sci Technol* **2013**, *47* (10), 5319–5326.
- (177) Deboshri, B.; L., M. A.; Toshihiro, Y.; Anindya, G.; B., B. P.; G., M. E.; K., K. S.; J., C. T. “Green” Oxidation Catalysis for Rapid Deactivation of Bacterial Spores. *Angew. Chemie Int. Ed.* **2006**, *45* (24), 3974–3977.
- (178) Collins, T. J.; DeNardo, M. A.; Warner, G. R.; Gordon-Wylie, S. W.; Ellis, W. C.; Somasundar, Y. Far Superior Oxidation Catalysts Based on Macrocyclic Compounds, October 25, 2018.
- (179) Bartos, M. J.; Gordon-Wylie, S. W.; Fox, B. G.; James Wright, L.; Weintraub, S. T.; Kauffmann, K. E.; Münck, E.; Kostka, K. L.; Uffelman, E. S.; Rickard, C. E. F.; et al. Designing Ligands to Achieve Robust Oxidation Catalysts. Iron Based Systems. *Coord. Chem. Rev.* **1998**, *174* (1), 361–390.

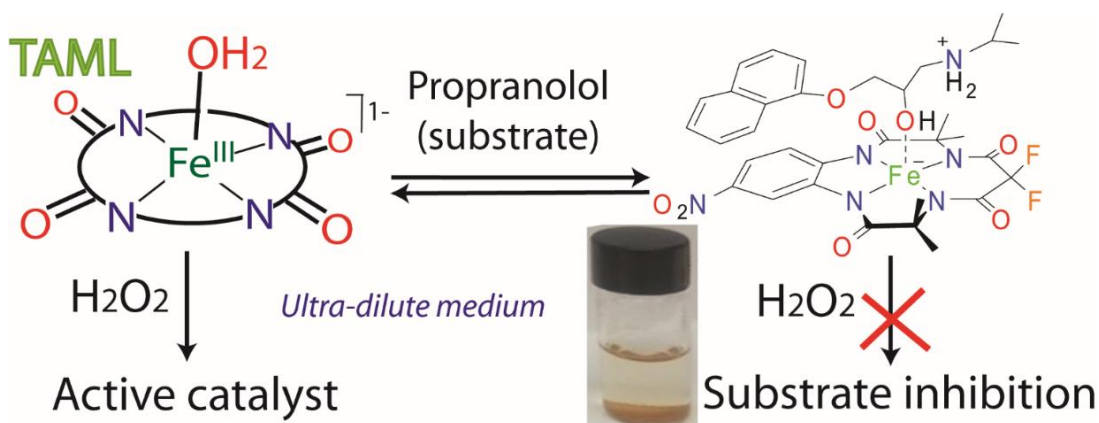
- (180) Ahmed, N.; Tsang, W. Y.; Page, M. I. Acyl vs Sulfonyl Transfer in N-Acyl  $\beta$ -Sultams and 3-Oxo- $\beta$ -Sultams. *Org. Lett.* **2004**, 6 (2), 201–203.
- (181) Baxter, N. J.; Rigoreau, L. J. M.; Laws, A. P.; Page, M. I. Reactivity and Mechanism in the Hydrolysis of  $\beta$ -Sultams. *J. Am. Chem. Soc.* **2000**, 122 (14), 3375–3385.
- (182) Iley, J.; Lopes, F.; Moreira, R. Kinetics and Mechanism of Hydrolysis of N-Amidomethylsulfonamides. *J. Chem. Soc. Perkin Trans. 2* **2001**, No. 5, 749–753.
- (183) Bossu, F. P.; Chellappa, K. L.; Margerum, D. W. Ligand Effects on the Thermodynamic Stabilization of Copper(III)-Peptide Complexes. *J. Am. Chem. Soc.* **1977**, 99 (7), 2195–2203.
- (184) Berezin, I. V.; Martinek, K. *Principles of the Physical Chemistry of Enzymic Catalysis*; Vysshaya Shkola: Moscow, 1977.
- (185) Cornish-Bowden, A. *Fundamentals of Enzyme Kinetics*; Portland Press: London, UK, 1995.
- (186) Cleland, W. W. Substrate Inhibition. *Methods Enzym.* **1979**, 63 (Enzyme Kinet. Mech., Part A), 500–513.
- (187) Wilson, R.; Turner, A. P. F. Glucose-Oxidase - an Ideal Enzyme. *Biosens. Bioelectron.* **1992**, 7 (3), 165–185.
- (188) Dunford, H. B. *Heme Peroxidases*; Wiley-VCH: NY, Chichester, Weinheim, 1999.
- (189) Theodoridis, A.; Maigut, J.; Puchta, R.; Kudrik, E. V; van Eldik, R. Novel Iron(III) Porphyrine Complex. Complex Speciation and Reactions with NO and H<sub>2</sub>O<sub>2</sub>. *Inorg Chem* **2008**, 47 (8), 2994–3013.
- (190) Khetan, S. K.; Collins, T. J. Human Pharmaceuticals in the Aquatic Environment: A Challenge to Green Chemistry. *Chem. Rev.* **2007**, 107 (6), 2319–2364.
- (191) Urtiaga, A. M.; Perez, G.; Ibanez, R.; Ortiz, I. Removal of Pharmaceuticals from a WWTP Secondary Effluent by Ultrafiltration/Reverse Osmosis Followed by Electrochemical Oxidation of the RO Concentrate. *Desalination* **2013**, 331, 26–34.
- (192) Schug, T. T.; Abagyan, R.; Blumberg, B.; Collins, T. J.; Crews, D.; DeFur, P. L.; Dickerson, S. M.; Edwards, T. M.; Gore, A. C.; Guillet, L. J. Designing Endocrine Disruption out of the next Generation of Chemicals. *Green Chem.* **2013**, 15 (1), 181–198.
- (193) Truong, L.; DeNardo, M. A.; Kundu, S.; Collins, T. J.; Tanguay, R. L. Zebrafish Assays as Developmental Toxicity Indicators in the Green Design of TAML Oxidation Catalysts. *Green Chem.* **2013**, 15 (9), 2339–2343.
- (194) Chanda, A.; Khetan, S. K.; Banerjee, D.; Ghosh, A.; Collins, T. J. Total Degradation of Fenitrothion and Other Organophosphorus Pesticides by Catalytic Oxidation Employing Fe-TAML Peroxide Activators. *J Am Chem Soc* **2006**, 128 (37), 12058–12059.
- (195) Kundu, S.; Chanda, A.; Espinosa-Marvan, L.; Khetan, S. K.; Collins, T. J. Facile Destruction of Formulated Chlorpyrifos through Green Oxidation Catalysis. *Catal. Sci. Technol.* **2012**, 2 (6), 1165–1172.
- (196) Tang, L. L.; DeNardo, M. A.; Gayathri, C.; Gil, R. R.; Kanda, R.; Collins, T. J. TAML/H<sub>2</sub>O<sub>2</sub> Oxidative Degradation of Metaldehyde: Pursuing Better Water Treatment

for the Most Persistent Pollutants. *Env. Sci Technol* **2016**, 50 (10), 5261–5268.

- (197) Gupta, S. Sen; Stadler, M.; Noser, C. A.; Ghosh, A.; Steinhoff, B.; Lenoir, D.; Horwitz, C. P.; Schramm, K.-W.; Collins, T. J. Rapid Total Destruction of Chlorophenols by Activated Hydrogen Peroxide. *Science* (80-. ). **2002**, 296 (5566), 326 LP – 328.
- (198) Hammett, L. P. The Effect of Structure upon the Reactions of Organic Compounds. Benzene Derivatives. *J. Am. Chem. Soc.* **1937**, 59 (1), 96–103.
- (199) Ryabov, A. D. *Kinetics and Mechanisms of Chemical and Enzymatic Reactions*; M.V. Lomonosov Moscow State University, Carnegie Mellon University, 2015.
- (200) Buncl, E.; Wilson, H. The Reactivity Selectivity Principle: Should It Ever Be Used? *J. Chem. Educ.* **1987**, 64 (6), 475.
- (201) Kundu, S.; Van Thompson, J. K.; Shen, L. Q.; Mills, M. R.; Bominaar, E. L.; Ryabov, A. D.; Collins, T. J. Activation Parameters as Mechanistic Probes in the TAML Iron(V)-Oxo Oxidations of Hydrocarbons. *Chem. - A Eur. J.* **2015**, 21 (4), 1803–1810.
- (202) Mills, M. R.; Weitz, A. C.; Zhang, D. Z.; Hendrich, M. P.; Ryabov, A. D.; Collins, T. J. A “Beheaded” TAML Activator: A Compromised Catalyst That Emphasizes the Linearity between Catalytic Activity and PKa. *Inorg. Chem.* **2016**, No. 23, 12263–12269.

## Chapter 2

# Structural, Mechanistic and Ultra-dilute Catalysis Portrayal of Substrate Inhibition in the TAML–Hydrogen Peroxide Catalytic Oxidation of the Persistent Drug and Micropollutant, Propranolol





RightsLink®



Home



Help



Email Support



Sign in



Create Account



**Structural, Mechanistic, and Ultradilute Catalysis Portrayal of Substrate Inhibition in the TAML-Hydrogen Peroxide Catalytic Oxidation of the Persistent Drug and Micropollutant, Propranolol**

**Author:** Yogesh Somasundar, Longzhu Q. Shen, Alexis G. Hoane, et al

**Publication:** Journal of the American Chemical Society

**Publisher:** American Chemical Society

**Date:** Sep 1, 2018

Copyright © 2018, American Chemical Society

**PERMISSION/LICENSE IS GRANTED FOR YOUR ORDER AT NO CHARGE**

This type of permission/license, instead of the standard Terms & Conditions, is sent to you because no fee is being charged for your order. Please note the following:

- Permission is granted for your request in both print and electronic formats, and translations.
- If figures and/or tables were requested, they may be adapted or used in part.
- Please print this page for your records and send a copy of it to your publisher/graduate school.
- Appropriate credit for the requested material should be given as follows: "Reprinted (adapted) with permission from (COMPLETE REFERENCE CITATION). Copyright (YEAR) American Chemical Society." Insert appropriate information in place of the capitalized words.
- One-time permission is granted only for the use specified in your request. No additional uses are granted (such as derivative works or other editions). For any other uses, please submit a new request.

[BACK](#)[CLOSE WINDOW](#)

## 2.1 INTRODUCTION

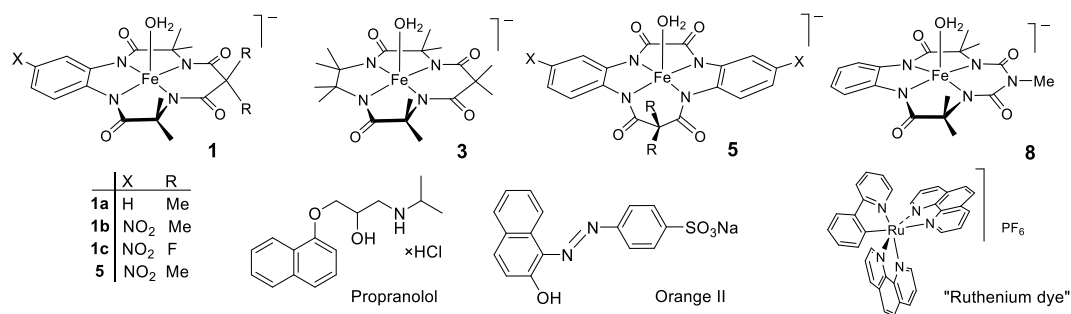
Many chemicals are capable of injuring living things at low doses,<sup>1,2</sup> including certain everyday-everywhere chemicals.<sup>3-9</sup> This realization has given rise to the term “micropollutant” (MP) to signify chemical contaminants in water that elicit adverse effects at low concentrations.<sup>7,10-15</sup> Thus, the need for safe, effective, inexpensive, flexible methods for decomposing these chemicals before their release to environmental waters has become a premier sustainability challenge for chemists.<sup>3,16,25,17-24</sup> TAML oxidation catalysts (Chart 2.1)<sup>26-29</sup> are high performance, small molecule *functional* replicas of the peroxidases, key enzymes used throughout the natural world to oxidatively convert or decompose both toxic and nontoxic chemicals.<sup>30-33</sup> Although typically  $\leq 1\%$  the mass of peroxidases, the technical performance of TAMLs in  $\text{H}_2\text{O}_2$  activation results in many MPs being rapidly destroyed oxidatively under ultra-dilute conditions;  $[\text{TAML}] = 4 \text{ nM} - 5 \text{ }\mu\text{M}$  (commonly  $50 - 100 \text{ nM}$  or ca.  $25 - 50 \text{ ppb}$ ),  $[\text{substrate}] = \text{low ppt} - \text{low ppb}$ ,  $[\text{H}_2\text{O}_2] = \text{low ppm}$ . Unprecedented ultra-dilute catalytic destruction occurs for numerous MPs,<sup>7,12,34-41</sup> including in the degradation of a set of high-concern MPs in London municipal wastewater.<sup>42</sup>

As a practical matter, the more efficient TAML/ $\text{H}_2\text{O}_2$  water purification becomes, the more economic and environmental criteria are favored by allowing less catalyst and oxidant to be used. Thus, as we have explored TAML/ $\text{H}_2\text{O}_2$  ultra-dilute oxidation catalysis, we have been on the lookout for evidence of processes that might slow the water purification rates. Substrate inhibition, where a substrate slows its own oxidation via a separate reaction, is a candidate.<sup>43-46</sup> While a rich variety of substrate inhibitions occur in oxidative enzymatic catalysis,<sup>47-52</sup> similar applications for small-molecule, synthetic catalysts are rare.<sup>53</sup> No inhibition complex corresponding to the slowing TAML/ $\text{H}_2\text{O}_2$  process has been isolated and no structural knowledge exists for any potential such complex.

Propranolol is a  $\beta$ -blocker drug and a common MP of concern.<sup>55-57</sup> Propranolol's therapeutic properties were first discovered by James Black to treat angina pectoris<sup>58</sup> (1988 Nobel Prize in

Physiology and Medicine). Today, propranolol is used, inter alia, for the treatment of cardiovascular disease,<sup>58</sup> hypertension,<sup>59</sup> hand tremors,<sup>59</sup> and migraine.<sup>60</sup> This extensive use, compounded by persistence, leads to contamination of both untreated<sup>55,56,61</sup> and conventionally treated municipal wastewater,<sup>57</sup> surface water,<sup>62</sup> underground well water,<sup>57</sup> and water abstracted for drinking water production.<sup>63</sup> Propranolol disrupts steroid hormone levels, egg production and hatching in Japanese Medaka, a fish species with considerable reproductive genetic similarity to humans.<sup>13</sup> Although numerous studies have explored propranolol removal from water by a variety of techniques,<sup>16,64–68</sup> there remains a pressing need for a method that is suitable for wide adoption.

Chart 2.1 Structure of substrates (propranolol, Orange II and “Ruthenium Dye”) and TAML (ref 54) Activators **1**, **3**, **5** and **8** Used or Discussed in This Study\* (TAML is a Registered Trademark Covering Tetra-carbonAmido-N Macrocyclic Ligand Complexes).



\*The catalysts have been numbered keeping in mind all the chapters in this thesis work.

Any successful TAML/H<sub>2</sub>O<sub>2</sub> water treatment process for MPs must be able to remove propranolol effectively, making it important to understand the discovered inhibition properties and to quantitatively evaluate impacts on degradation rates and process efficiencies that might show up in real world ultra-dilute applications. Thus, we present clear insight into the kinetics of TAML/H<sub>2</sub>O<sub>2</sub> propranolol substrate inhibition for very dilute conditions with projection to ultra-dilute conditions that cannot be studied experimentally and the isolation and structural characterization of several inhibition complexes by ESI-MS, fluorescence, UV-vis, FTIR, <sup>1</sup>H NMR, and IC examination, and DFT calculations. This work also establishes a general method for quantifying substrate inhibition processes for TAML/H<sub>2</sub>O<sub>2</sub> processes.

## 2.2 RESULTS

### 2.2.1 Kinetics of the TAML-Catalyzed Oxidation of propranolol by $H_2O_2$ Reveals Substrate

#### *Inhibition.*

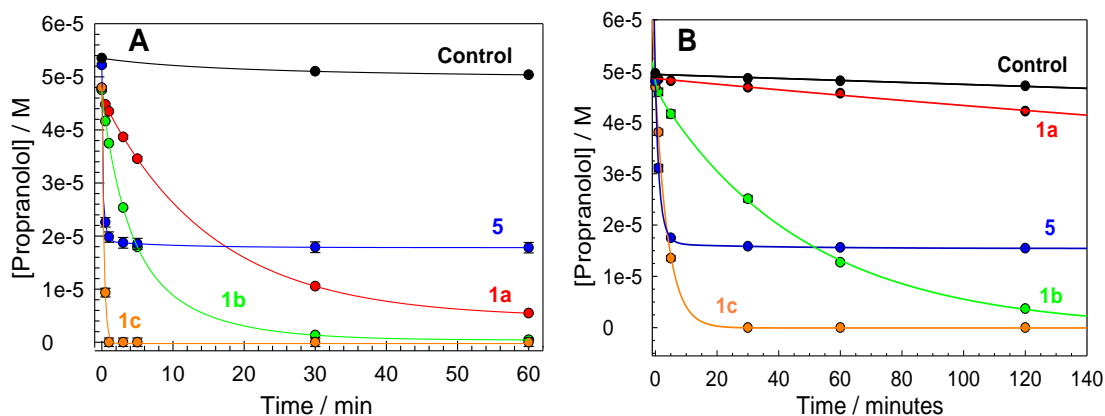


Figure 2.1 Degradation of propranolol by  $H_2O_2$  catalyzed by **1** and **5** at pH 9 (A) and pH 7 (B) measured by UPLC. Conditions: [TAML] =  $1 \times 10^{-6}$  M, [propranolol] =  $5 \times 10^{-5}$  M, [ $H_2O_2$ ] =  $5 \times 10^{-3}$  M, 0.01 M phosphate, 25 °C. All points are an average of three values; standard deviation error bars are mostly not visible as the triplicate points are tightly grouped.

The dynamics of **1** and **5** catalyzed propranolol degradation by  $H_2O_2$  in water were investigated by following the disappearance of the drug by UPLC. At ambient temperature and pH 9, TAMLs **1** and **5** ( $1 \times 10^{-6}$  M) efficiently catalyze propranolol oxidation. Nitro-substituted **1b** and **1c** give superior performances with the elimination of propranolol to the UPLC non-detectable limit under these conditions ( $5.7 \times 10^{-7}$  M, 170 ppb) in 60 and 2 min, respectively (Figure 2.1A). Note in Figure 2.1 that **5** is more active than **1c** at low conversions, but in contrast with **1c**, the non-detect limit was not achieved because this catalyst deactivates faster under these operating conditions.<sup>69</sup>

Several fragments of propranolol degradation have been detected by UPLC. The characterization of these and the pathways of further degradation will be reported separately. The focus here is on the first oxidation event in propranolol's multistep degradation (43 equiv of  $H_2O_2$  are required to mineralize propranolol), achieved by employing the initial rate method. The data of Figure 2.1 are



convenient for screening comparative TAML reactivities—initial rates of propranolol disappearance were obtained using much higher data density (Figure 2.7, appendix).

Scheme 2.1 Typical Stoichiometric Mechanism of TAML Oxidation Catalysis, (i)–(ii), and Minimal Steps (iii)–(iv) for Rationalizing Substrate Inhibitions. (RC = Resting Catalyst (1 or others in chart 2.1), AC = Active Catalyst, S = Substrate, P = Product, [Fe<sup>III</sup>]<sub>t</sub> = total [TAML])



$$-\frac{d[\text{S}]}{dt} = \frac{k_I k_{II} [\text{H}_2\text{O}_2] [\text{S}]}{k_{-I} + k_I [\text{H}_2\text{O}_2] + k_{II} [\text{S}]} [\text{Fe}_t^{\text{III}}] \quad (2.1)$$

The initial rate of TAML/H<sub>2</sub>O<sub>2</sub> oxidation of propranolol is a linear function of the concentration of **1c** in the range of (5–50) × 10<sup>-8</sup> M (Figure 2.8, appendix). Figure 2.2 presents the hyperbolic initial rate dependence on [H<sub>2</sub>O<sub>2</sub>] for **1a**, consistent with eq 2.1 (from events (i) and (ii) in Scheme 2.1) when *k*<sub>-I</sub> is negligible. The rate constants *k*<sub>I</sub> and *k*<sub>II</sub> in Table 2.1 were calculated from a linear double inverse plot *dt/d*[S] versus [H<sub>2</sub>O<sub>2</sub>]<sup>-1</sup> (Figure 2.2 inset). At high H<sub>2</sub>O<sub>2</sub> concentrations, the rate is nearly independent of [H<sub>2</sub>O<sub>2</sub>] and eq 1 becomes eq 2.2,

$$-\frac{d[\text{S}]}{dt} = k_{II} [\text{S}] [\text{Fe}_t^{\text{III}}] \quad (2.2)$$

Thus, the initial rate should depend linearly on [propranolol] as was observed for **1a** at [H<sub>2</sub>O<sub>2</sub>] = 4.25 × 10<sup>-3</sup> M (Figure 2.9, appendix). The rate constant *k*<sub>II</sub> calculated from the slope of a plot of -

$d[S]/dt$  vs  $[S]$  according to eq 2 is  $780 \pm 20 \text{ M}^{-1} \text{ s}^{-1}$ , consistent with the value of  $k_{II}$  obtained by linearizing the hyperbolic dependence in Figure 2.2 ( $800 \pm 30 \text{ M}^{-1} \text{ s}^{-1}$ ) as listed in Table 2.1.

The kinetic data for **1a** at pH 7 (Table 2.1) were similarly obtained. Though the oxidations of propranolol and Orange II follow the same rate law (eq 1),<sup>70</sup> the rate constants  $k_I^{\text{OrII}}$ , which refer to the oxidation of the  $\text{Fe}^{\text{III}}$  of **1a** by  $\text{H}_2\text{O}_2$  to AC in the Orange II catalytic oxidation, are 16 (pH 7) and 19 (pH 9) times higher than  $k_I$  obtained with propranolol. In prior work with a set of nitrophenols,<sup>37</sup> the value of  $k_I$  differed with the nitrophenol structure.

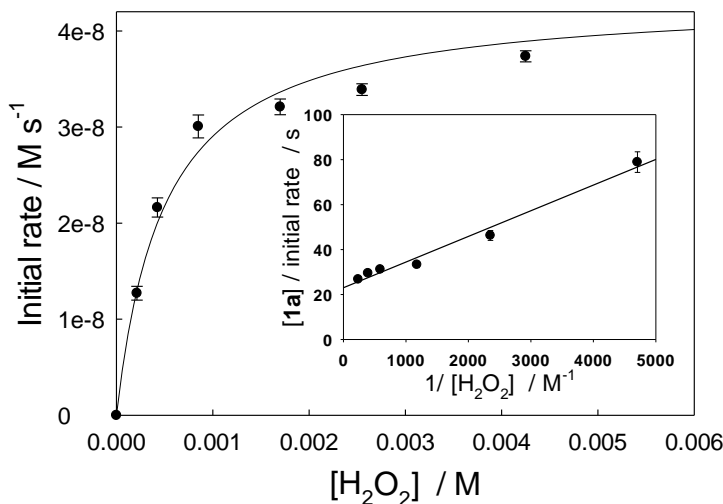


Figure 2.2 . Initial rate of propranolol degradation by  $\text{H}_2\text{O}_2$  catalyzed by **1a** as a function of  $[\text{H}_2\text{O}_2]$  measured by UPLC. Inset shows the double inverse linear plot,  $[\text{1a}]/(\text{initial rate})$  versus  $[\text{H}_2\text{O}_2]^{-1}$  (see text for details). Conditions:  $[\text{1a}] = 1 \times 10^{-6} \text{ M}$ ,  $[\text{propranolol}] = 5 \times 10^{-5} \text{ M}$ , pH 9 (0.01 M phosphate), 25 °C. The solid curve was calculated using the values of  $k_I$  and  $k_{II}$  obtained through the linearization. All the data points are an average of three values with standard deviations shown. Very tight triplicate sets leave some error bars undetectable.

In the absence of a substrate specific interaction, such as substrate–TAML binding,  $k_I$  should always be the same no matter which catalytic oxidation it is extracted from. Therefore, when kinetic analyses are applied to determine  $k_I$  separately with multiple substrates, the substrate that returns the highest  $k_I$  is the substrate with the least inhibitory effect of its own oxidation. To gain further insight into the inhibitions, TAMLs **1b**, **1c** and **5** were also studied for propranolol degradation. In each case, eq 1 was found to hold and the propranolol derived rate constants  $k_I$  were significantly

lower than the  $k_1^{\text{OrII}}$  partners when measured under identical conditions ( $k_1^{\text{OrII}}/k_1 > 1$  in Table 2.1) with the  $k_1^{\text{OrII}}/k_1$  ratio in the range of 4–30. The highest  $k_1^{\text{OrII}}/k_1$  ratio of 30 was observed for **1b** at pH 7. The  $k_1$  rate constants are larger at pH 9 than at pH 7. For **1a-c**,  $k_1$  (pH 9)  $\approx 30 \times k_1$  (pH 7). For **5**,  $k_1$  (pH 9)  $\approx 20 \times k_1$  (pH 7). This has been attributed to the increase in  $k_1$  under alkaline conditions that accompanies the deprotonation of the axial water ligand of TAMLs.<sup>71</sup> We will now present data supporting the conclusion that substrate inhibition in the TAML/H<sub>2</sub>O<sub>2</sub> oxidation of propranolol results from propranolol association with resting state TAML activators.

**Table 2.1** Rate Constants  $k_1$  and  $k_{\text{II}}$  Found for Propranolol in This Work and  $k_1$  Values Reported Previously Using Orange II ( $k_1^{\text{OrII}}$ ) and the Cyclometalated Ruthenium(II) Dye [Ru(*o*-C<sub>6</sub>H<sub>4</sub>-2-py)(phen)<sub>2</sub>]<sup>+</sup> ( $k_1^{\text{Ru}}$ ) at 25 °C.

	pH	$k_1$ M <sup>-1</sup> s <sup>-1</sup>	$10^{-2} \times k_{\text{II}}$ M <sup>-1</sup> s <sup>-1</sup>	$k_1^{\text{OrII}}$ or $k_1^{\text{Ru}}$ M <sup>-1</sup> s <sup>-1</sup>	$k_1^{\text{OrII}}/k_1$ or $k_1^{\text{Ru}}/k_1$
<b>1a</b>	7.0	2.0±0.1	0.7±0.2	31.4±0.1 <sup>a)</sup>	16
	7.0			<b>52±2</b> <sup>c)</sup>	<b>26</b>
	9.0	74±3	8.0±0.3	1400±10 <sup>b)</sup>	19
	9.0			<b>2400±300</b> <sup>c)</sup>	<b>32</b>
<b>1b</b>	7.0	5.0±0.2	1.4±0.2	152±5 <sup>a)</sup>	30
	9.0	149±5	35±1		
<b>1c</b>	7.0	90±10	146±2	350±2 <sup>a)</sup>	4
	9.0	2990±50	680±10		
<b>5</b>	7.0	200±10	53±24	1900±100 <sup>a)</sup>	9.5
	9.0	4200±400	500±40	(16±2)×10 <sup>3</sup> <sup>d)</sup>	4

<sup>a)</sup> Orange II; from ref.<sup>69</sup> <sup>b)</sup> Orange II; from ref.<sup>70</sup> <sup>c)</sup> Cyclometalated ruthenium(II) dye [Ru<sup>II</sup>(*o*-C<sub>6</sub>H<sub>4</sub>-2-py)(phen)<sub>2</sub>]<sup>+</sup><sup>73</sup>; from ref.<sup>71</sup> <sup>d)</sup> Orange II; from ref.<sup>74</sup>

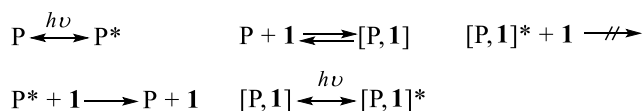
### 2.2.2 UV-vis and Fluorescence Spectroscopies.

TAML–substrate associations have been detected previously in systems where detailed structural and mechanistic characterizations could not be made. Association between **1a** and Pinacyanol

chloride was detected by UV-vis spectroscopy because the chromophore of this dye exhibits very high sensitivity to its environment.<sup>72</sup> However, UV-vis spectroscopy provided no direct evidence for binding of nitrophenols to TAML **1a** where kinetics evidence and DFT calculations support such an interaction.<sup>37</sup> Similarly, the UV-vis technique provides no evidence for propranolol-TAML binding—the spectrum of **1a** ( $5 \times 10^{-5}$  M) in pH 7 water (0.01 M phosphate) did not change as the propranolol concentration was varied in the range  $(3.2\text{--}15.7) \times 10^{-4}$  M (Figure 2.10, appendix).

However, propranolol is fluorescent and TAMLs **1a** and **1b** efficiently quench its fluorescence (Figure 2.3). The corresponding Stern-Volmer plots<sup>75</sup> (insets to Figure 2.3) are curved noticeably upward with the curvature being more pronounced for **1b**. Therefore, for quantitative comparisons, the data obtained at low concentrations of **1** at which the Stern-Volmer plots can be approximated by a straight line were used.

Scheme 2.2 Postulated Features of Quenching of Propranolol Fluorescence by **1** Involving [P,**1**] Adducts.



The Stern-Volmer constants  $K_{SV}$ , i.e. the slopes of these straight lines at 356 nm, equal  $(60 \pm 1) \times 10^2 \text{ M}^{-1}$  and  $(140 \pm 10) \times 10^2 \text{ M}^{-1}$  for **1a** and **1b**, respectively, and can be compared with that for the benchmark quencher, the iodide anion.<sup>76</sup> The  $K_{SV}$  value of  $71 \text{ M}^{-1}$  has been reported for the propranolol/iodide pair.<sup>77</sup> Some key points to note here are (i) **1a** and **1b** are ca. 100–200 times more efficient than iodide at quenching propranolol fluorescence, (ii)  $K_{SV}$  for **1b** is ca. twice that of **1a** from which we deduce that the electron-withdrawing nitro group of **1b**, absent from **1a**, favors the quenching, (iii) unlike with iodide, quenching by **1** is non-monotonic.<sup>78</sup>

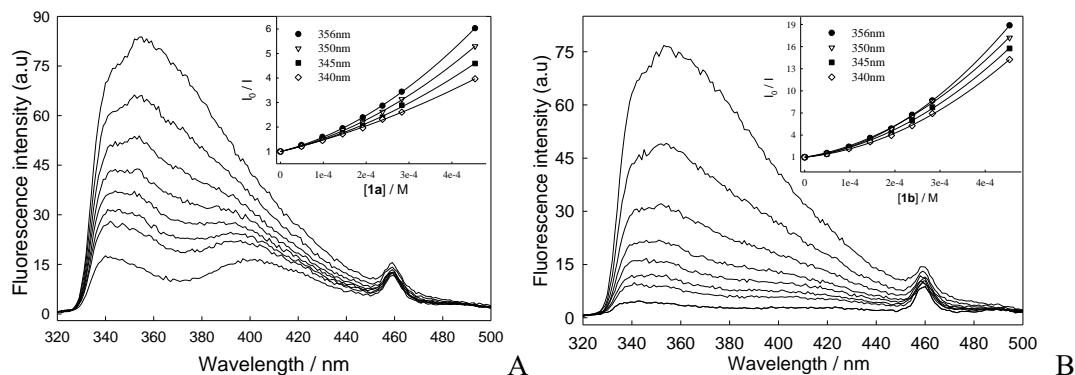


Figure 2.3 Quenching of propranolol fluorescence by **1a** (A) and **1b** (B). Insets show the corresponding Stern-Volmer plots at various wavelengths. Conditions: excitation wavelength 230 nm; [propranolol] 0.075 M; range of **1a** and **1b** concentrations  $(4.95\text{--}45.45) \times 10^{-5}$  M; pH 7 (0.01 M phosphate), 25 °C. Similar studies were not possible for **1c**, and **5** because of the precipitation of the adducts (see Figure 2.11, appendix). The emission at ~460 nm is an artifact associated with the Xe lamp.<sup>79</sup>

A new maximum at 405 nm at higher  $[1]$  is possibly associated with emission from the excited state of the adduct,  $[P,1]^*$  (Scheme 2.2). The 405 nm maximum is less obvious in the case of **1b** quenching (Figure 2.3B) compared to **1a**. Possible explanations include greater quenching of  $[P,1b]^*$  by **1b** (Scheme 2.2) or less fluorescence emission by  $[P,1b]^*$  typical of compounds with the nitro group.<sup>80</sup> This scenario is consistent with a higher positive curvature of the Stern-Volmer plot for **1b** compared to **1a**.

### 2.2.3 <sup>1</sup>H NMR Spectroscopy.

The Fe<sup>III</sup>TAMs **1** and **2** are paramagnetic ( $S = 3/2$ )<sup>81</sup> and expected to line-broaden the <sup>1</sup>H NMR signals of diamagnetic propranolol upon association. Figure 2.4 presents <sup>1</sup>H NMR spectra in D<sub>2</sub>O for pure propranolol and propranolol-**1b** mixtures ( $[1b]$  is 1–2% vs [propranolol]). Line-broadening of the propranolol resonances increased with increasing  $[1b]$ .<sup>82</sup> The aromatic <sup>1</sup>H resonances are broadened much more than the aliphatic signals, suggesting a hydrophobic/ $\pi$ -stacking interaction between the aromatic units of **1b** and propranolol.<sup>83</sup>

The propranolol isopropyl methyl signals are broadened only slightly. In contrast, broadening was found for the  $-\text{CH}_2-$  and  $-\text{CH}_3$  signals of diethylamine with more broadening for the former (Figure 2.12, appendix). This suggests no Fe–N bonding for propranolol. Hydrophobic/ $\pi$ -stacking is qualitatively supported by the following observations: (i) there is no line-broadening at comparable concentrations of iron(III) chloride (Figure 2.13, appendix) or in presence of the ‘beheaded’ TAML activator **3**, which lacks an aromatic group<sup>69,84</sup> (Figure 2.14, appendix), (ii) the propranolol proton signals in the proximity of the OH group (Figure 2.4, H's 12, 13, and 15) are broadened in the presence of **1b**, although the  $^1\text{H}$  NMR spectrum of isopropanol showed no broadening at comparable concentrations (0.015 M, Figure 2.15, appendix). Thus, fluorescence and  $^1\text{H}$  NMR data indicate an association between propranolol and TAMLs in water reinforced by the fact that several adducts precipitate from solution.

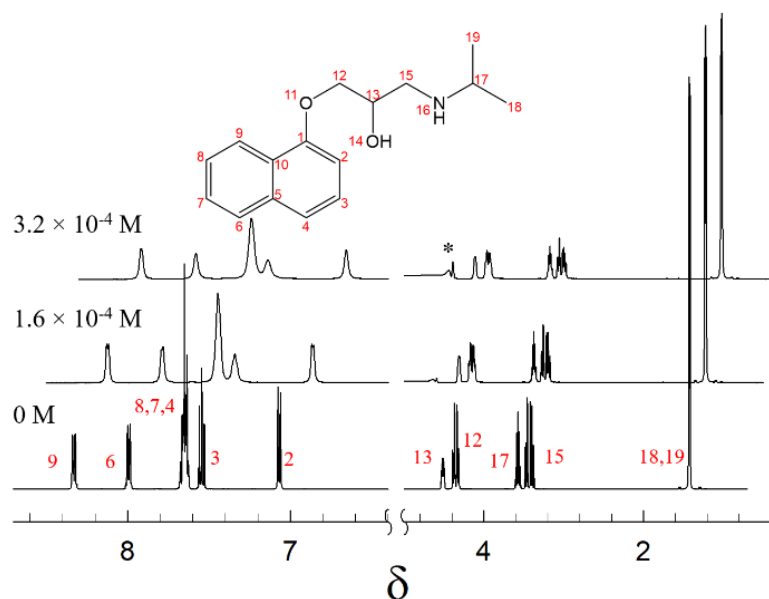


Figure 2.4  $^1\text{H}$  NMR spectra of 0.015 M propranolol (bottom) showing line broadening of signals ( $\delta$ , ppm vs NaTMSP- $\text{d}^4$ ) upon addition of **1b** ( $1.6 \times 10^{-4}$  and  $3.2 \times 10^{-4}$  M, middle and top, respectively). Conditions:  $\text{D}_2\text{O}$ , 25 °C. Peak assignments<sup>85</sup> are shown in the bottom spectrum. Asterisk \* indicates the signal from  $\text{H}_2\text{O}$  introduced with 20  $\mu\text{L}$  aliquots of **1b**. From the bottom spectrum, each higher spectrum is offset by 0.2  $\delta$ .

#### 2.2.4 Isolation and Composition of the propranolol-TAML Adducts.

Under the described conditions (experimental section), [P,1c] and [P,5] precipitated from solution. The adducts are fragile and dissociate to the starting materials when dissolved in methanol.

ESI-MS spectra of [P,1c] and [P,5] methanol solutions showed only free propranolol and TAMLs (Figures 2.16, 2.17, appendix). The UV-vis spectrum of [P,1c] in methanol is a superposition of unperturbed spectra of propranolol and 1c (Figure 2.18, appendix). An approximate 1:1 stoichiometry in the [P,TAML] adducts was determined. (see Table 2.2, Figure 2.18, appendix).

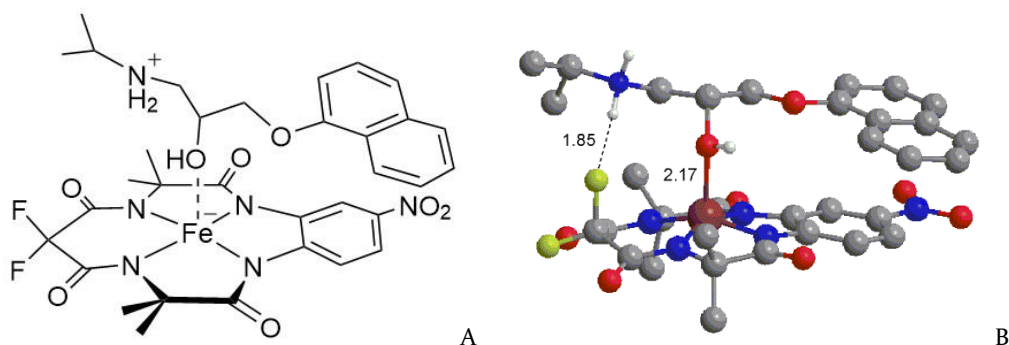


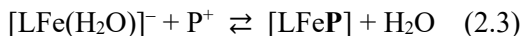
Figure 2.5 . (A) The structural composition of [P,1c] deduced from the spectroscopic studies and used as a starting point for DFT calculations. (B) DFT energy-minimized structure of [P,1c] featuring (i) the hydrophobic/stacking interaction, (ii) the coordinative Fe–O bond, (iii) the F $\cdots$ H hydrogen bond. Charges of propranolol and 1c of +1 and –1, respectively, favor an additional coulombic stabilization. For clarity, H atoms are shown only at amine N and hydroxyl oxygen. Color code: O (red), N (blue), C (grey), Fe (brown), H (white), F (yellow).

FTIR spectra of the solid [P,TAML] adducts differ from propranolol and the parent TAMLs (Figures 2.19 and 2.20, appendix)—a factor complicating comparisons is that propranolol exhibits polymorphism.<sup>86</sup> Nevertheless, several observations are consistent with the DFT calculated structure for [P,1c] below; (i) much reduced 1107 cm<sup>-1</sup> ( $\nu$ (C–OH)) bands in the adducts compared to the parent propranolol spectrum are consistent with an axial Fe<sup>III</sup>–O bond<sup>74</sup> and, (ii) changes in

the 2700–2250 cm<sup>-1</sup>  $\nu(\text{N-H})$  of the propranolol spectrum, ascribed to the ammonium ion  $\text{R}_2\text{NH}_2^{+87}$  are consistent with TAML providing the counter-ion for the *N*-protonated propranolol cation.

### 2.2.5 DFT Simulations.

The structure of the energy-minimized [P,**1c**] (Figure 2.5B) was developed from a postulated structure (Figure 2.5A) constructed based on the evidence above. The aromatic C $\cdots$ C separations of 3.224, 3.269, 3.461 Å is comparable to stacked benzene dimers.<sup>88</sup> The Fe–O bond length of 2.17 Å, is consistent with 2.06 Å obtained for **5** with axial methanol found by X-ray crystallography.<sup>74</sup> The formation of an Fe–O bond in [P,**1c**] requires the displacement of the normally found axial water of **1c** by the hydroxyl group of propranolol as in eq 2.3.



The displacement reaction was found to be exergonic by DFT with  $\Delta G^\circ = -5.9 \text{ kcal mol}^{-1}$ , in good agreement with the experimental values (see below). N–H $\cdots$ F hydrogen bond, typically demonstrated by X-ray crystallography<sup>89</sup>, between propranolol and **1c** was also predicted by DFT with a H $\cdots$ F separation of 1.85 Å that is much lower than the sum of the van-der-Waals radii of H and F (2.56 Å).<sup>90</sup>



## 2.3 DISCUSSION

The combined experimental and theoretical evidence presents a convincing case for the formation and structures of adducts capable of inhibiting the reactivity of small molecule TAML peroxidase mimics, even under what might be considered very dilute conditions ( $10^{-3}$ – $10^{-4}$  M). As analyzed below, a key question for MP treatment with TAML/[H<sub>2</sub>O<sub>2</sub>] pertains to whether these interactions persist under ultra-dilute conditions of TAML usage to date ( $5 \times 10^{-6}$ – $4 \times 10^{-9}$  M) when isolation and characterization of adducts is effectively impossible. The precipitated fragile adducts [P,1c] and [P,5] (Figure 2.11) provide strong corroborating evidence for substrate inhibition in non-enzymatic catalytic reactions as we<sup>37,72</sup> and others<sup>91</sup> have postulated to rationalize kinetic effects observed with other substrates.

The propranolol:TAML ratio was found to be slightly in excess of 1:1—1.2:1 and 1.4:1 for [P,1c] and [P,5], respectively (see Table 2.2, Figure 2.18, appendix). It is reasonable to assume that hydrophobic/stacking may not guarantee a 1:1 stoichiometry. Propranolol may, for example, be attached to **5** in a 2:1 ratio in a component of the solid sample, in which each of the two aromatic units of **5** binds uniquely to the naphthalene units of separate propranolol molecules to produce the 1.4:1 [P,5] stoichiometry.

In chloride analyses of the isolated [P,TAML] adducts, the chloride IC peak overlaps with the methanol solvent peak (Figure 2.21, appendix). However, the analyses clearly show that small amounts of chloride from the parent propranolol salt are incorporated in both [P,1c] and [P,2]. In both cases, the amount of chloride is insufficient to balance the additional charge for the quantity of the second propranolol. We assume the counterion deficit is compensated for by buffer phosphate in any of its various forms.

The very small binding constants typical of chloride binding to Fe<sup>III</sup>TAMLs (e.g.  $K_{Cl}$  for **1a** =  $0.18 \pm 0.04$  M<sup>-1</sup>) indicate that, in catalytic processes, chloride association with the resting state catalyst is a highly unlikely mechanism of inhibition.<sup>28</sup>

Scheme 2.1 explains the kinetics of substrate inhibition. Assuming the reactivity of the adduct toward H<sub>2</sub>O<sub>2</sub> is negligible (step *iv*), steps *i-iii* lead to the rate law as in eq 2.4, where *K* is the binding constant between the catalyst RC and the substrate.

$$-\frac{d[S]}{dt} = \frac{\frac{k_I}{1 + K[S]} k_{II} [H_2O_2] [S]}{\frac{k_I}{1 + K[S]} [H_2O_2] + k_{II} [S]} [Fe_t^{III}] \quad (2.4)$$

When inhibition occurs, the rate constant *k<sub>I</sub>* in eq 1 becomes an effective value *k<sub>I,eff</sub>* = *k<sub>I</sub>*/(1 + *K*[S]), and therefore eq 1 is better presented as eq 2.5.

$$-\frac{d[S]}{dt} = \frac{k_{I,eff} k_{II} [H_2O_2] [S]}{k_{I,eff} [H_2O_2] + k_{II} [S]} [Fe_t^{III}] \quad (2.5)$$

Since *k<sub>I,eff</sub>* = *k<sub>I</sub>* when *K* = 0 (substrate does not bind to catalyst), the question is now opened as to whether substrate inhibition was present but not recognized in prior determinations of *k<sub>I</sub>* using eq 1 with other test substrates. For **1a**, the “ruthenium dye” [Ru<sup>II</sup>(*o*-C<sub>6</sub>H<sub>4</sub>-2-py)(phen)<sub>2</sub>]<sup>+</sup> gives the largest *k<sub>I</sub>* at both pH 7 and 9 (52 and 2400 M<sup>-1</sup> s<sup>-1</sup>, respectively).<sup>71</sup> If “ruthenium dye” behaves as a fast outer-sphere electron-transfer reductant, as we have always assumed, then the *k<sub>I</sub>* values derived using this substrate would represent the pure uninhibited rate constants. The assumption that this is so will stand unless another test substrate leads to a higher *k<sub>I</sub>* value. By comparison, Orange II returns a slightly lower *k<sub>I</sub>* at pH 7 and 9 (31 and 1400 M<sup>-1</sup> s<sup>-1</sup>, respectively).<sup>69,70</sup> At both pHs, the *k<sub>I</sub><sup>Ru</sup>* / *k<sub>I</sub><sup>OrII</sup>* ≈ 1.7, indicating that Orange II mildly inhibits its own **1a**/H<sub>2</sub>O<sub>2</sub> oxidation. Therefore, line-broadening in the <sup>1</sup>H NMR spectrum of Orange II on addition of **1b** was explored and confirmed (Figure 2.22, appendix). The ratios *k<sub>I</sub><sup>X</sup>*/*k<sub>I</sub>* (*X* = Ru or OrII as in the last column of Table

2.1) equal  $(1 + K[S])$  and vary over the four studied TAMLs in the range of 4–32 at  $[ \text{propranolol} ] = 5 \times 10^{-5} \text{ M}$ . Correspondingly, the equilibrium constants  $K$  have been estimated for all pairs in Table 2.1 (see Table 2.3, appendix) to lie in the range of  $(0.6\text{--}6.0) \times 10^5 \text{ M}$  ( $\Delta G^\circ = -(6.5\text{--}7.9) \text{ kcal mol}^{-1}$ ). The energies are similar to the value of  $-5.9 \text{ kcal mol}^{-1}$  estimated by DFT for **1c**. The energies of hydrophobic stacking interactions in benzene dimers are  $-3.4$  and  $-2.5 \text{ kcal mol}^{-1}$  for parallel displaced and parallel stacked structures, respectively, suggesting the hydrophobic/ $\pi$ -stacking may be the dominant inhibitory interaction while receiving reinforcement from the other identified interactions.<sup>88</sup>

In the more general case, when all steps in Scheme 2.1, including step *iv*, are used to derive the rate law, one arrives at eq 2.6. The quadratic term in  $[S]$  in the denominator would produce a strong dependence on the substrate concentration. Providing  $k_I > k_{ID}K[S]$ , the reaction rate should first increase with increasing  $[S]$  at low  $S$  concentrations, but then decrease at high  $S$  concentrations. In fact, this has been observed previously, but not recognized as such, in the kinetics of Orange II oxidation by  $\text{H}_2\text{O}_2$  catalyzed by the *N*-tailed (‘biuret’) TAML activator **8** (Chart 2.1).<sup>92</sup> The planarity of TAML **8** is higher than that of **1** such that hydrophobic/ $\pi$ -stacking interactions could be stronger for **8** and the equilibrium constant  $K$  correspondingly higher.

The majority of experiments to understand the mechanism of the inhibition process were performed at  $[ \text{propranolol} ] = 50 \text{ } \mu\text{M}$ , which was found to be an ideal concentration in the rather narrow  $[ \text{propranolol} ]$  regime where the UPLC measurements with fluorescence detection work well. At higher concentrations, the detector is saturated.

$$-\frac{d[S]}{dt} = \frac{(k_I[S] + k_{ID}K[S]^2)k_{II}[\text{H}_2\text{O}_2][\text{Fe}^{\text{III}}]_t}{k_I[\text{H}_2\text{O}_2] + k_{ID}K[\text{H}_2\text{O}_2][S] + (k_{-ID} + k_{II})[S] + (k_{-ID} + k_{II})K[S]^2} \quad (2.6)$$

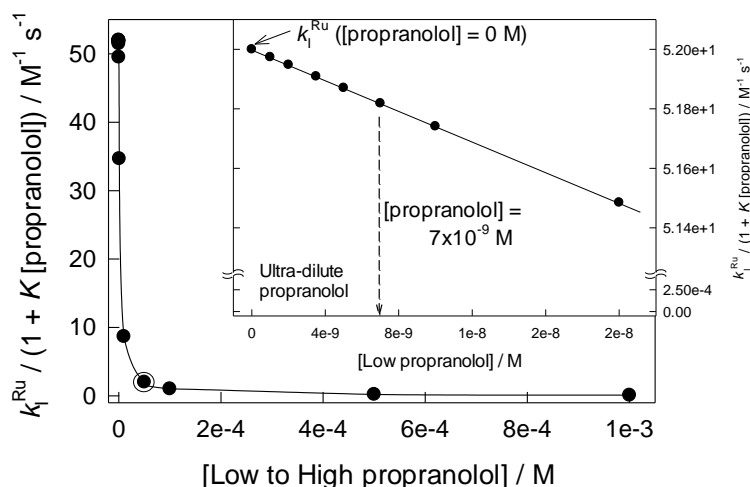


Figure 2.6 Plot showing the experimentally determined  $k_{i,\text{eff}}$  for **1a** for propranolol (circled datum) and the projected impact of propranolol substrate inhibition on the uninhibited  $k_i^{\text{Ru}}$  from  $[\text{propranolol}] = 0$  to low mM. Note,  $k_{i,\text{eff}} = k_i^{\text{Ru}} / (1 + K[\text{propranolol}]) \approx 0$  when  $[\text{propranolol}] \geq 2.0 \times 10^{-4} \text{ M}$ . Inset shows the same projection at very low  $[\text{propranolol}]$ .

At lower concentrations, the sensitivity of the detector and the slowness of the initial rates degrade the utility of the data. We do not consider  $50 \text{ } \mu\text{M}$  to be an ultra-dilute concentration—rather it might be labeled “very dilute”. While conditions can vary, most micropollutants found in conventionally treated London municipal wastewater manifest at  $\leq 2 \text{ ppb}$ .<sup>42</sup> This is equivalent to  $\leq 7 \text{ nM}$  for propranolol, a limit that is ca. 7000-fold more dilute than  $50 \text{ } \mu\text{M}$ . Thus, it became vital to understand how the inhibition process impacts the catalytic cycle across a wide concentration range with special concern for the ultra-dilute regime.

Figure 2.6 shows the calculated impact of substrate inhibition on  $k_i$  over the complete range of relevant propranolol concentrations. The values of the function  $k_{i,\text{eff}} = k_i^{\text{Ru}} / (1 + K[\text{propranolol}])$  are plotted vs  $[\text{propranolol}]$ , where  $k_i^{\text{Ru}}$  can be considered to be the uninhibited  $k_i$  (see above) and  $K$  is the calculated inhibition binding constant based on the experimentally obtained propranolol  $k_{i,\text{eff}}$  of  $2 \text{ M}^{-1}\text{s}^{-1}$  for **1a** at  $[\text{propranolol}] = 50 \text{ } \mu\text{M}$ . In this projection, substrate inhibition manifests as a

decrease in the value of  $k_{l,eff}$  from the uninhibited  $k_l^{Ru}$  as the [propranolol] is raised from 0 through the ultra-dilute zone and upward to low mM values. Starting at  $k_{l,eff} = 2 \text{ M}^{-1}\text{s}^{-1}$ , the value of  $k_{l,eff}$  falls off rapidly as [propranolol] is increased and begins approaching 0 around 200  $\mu\text{M}$ . The form of the Figure 2.6 plot indicates that propranolol substrate inhibition, clearly detectable for [propranolol] = 50  $\mu\text{M}$ , is sufficiently weak as to have virtually no effect for the municipal wastewater relevant MP regime of [propranolol]  $\leq 7 \text{ nM}$ . This is consistent with the finding that TAML/ $\text{H}_2\text{O}_2$  rapidly destroys propranolol in London municipal wastewater.<sup>42</sup> A large study of all observable intermediates of TAML/ $\text{H}_2\text{O}_2$  propranolol degradation has been conducted as the subject of a forthcoming publication and this work shows that no intermediate is capable of interfering with the integrity of the initial rate method in propranolol degradation kinetics.

## 2.4 CONCLUSIONS

TAML activators are peroxidase mimics that function efficiently under ambient conditions in water with ultra-dilute concentrations of catalyst, substrate with very dilute oxidant. We have proven herein that TAML catalysis can be subject to substrate inhibition for propranolol and Orange II at  $\mu\text{M}$  substrate concentration. The impact on catalysis under the low nM substrate concentrations of ultra-dilute conditions is shown to be negligible. The understanding achieved is of central significance to the development of TAML/ $\text{H}_2\text{O}_2$  processes for removing micropollutants from water, a major sustainability challenge for the chemical enterprise. The potential for poisonous inhibition processes has been addressed and concerns about the potential blocking of TAML/ $\text{H}_2\text{O}_2$  water treatment assuaged by the discovery of a methodology for quantifying the strongly conditions dependent substrate inhibition. Micropollutant contamination of municipal wastewater typically involves ca. 100 persistent species about 20 of which are of particularly high concern because of strong adverse impacts on aquatic life. Propranolol is one of these. As detailed TAML/ $\text{H}_2\text{O}_2$  studies of the full degradation chemistries of each key MP is undertaken, the methodology for quantitatively evaluating substrate inhibition kinetically is now available wherever there might be concern that it could be lowering the efficiency. If strong inhibition is ever discovered for any important MP under ultra-dilute conditions, the potential for obviating this by TAML design is supported by the differing behaviors of the four TAMLs studied here for propranolol inhibition.

Propranolol retards its own oxidation via a fast and reversible binding to the ferric resting catalyst. This results in a mass law decrease in the speed of interaction of the catalyst with  $\text{H}_2\text{O}_2$  associated with the rate constant  $k_1$  labeled as  $k_{1,\text{eff}}$  to signal that it is not a pure  $k_1$ . TAML–propranolol adducts form observably at higher concentrations and can even precipitate from aqueous solution. A combination of analytical techniques and DFT calculations suggest that propranolol forms weak adducts with TAMLs **1** and **5** via combinations of the attractive forces of (*i*) hydrophobic/ $\pi$ -stacking

contacts, (ii) a coulombic TAML anion–propranolol cation interaction, (iii) a coordinative iron(III)–oxygen bond and, (iv) C–F...H–N hydrogen bonding (in the case of the fluorine-tailed catalyst **1c**).

Our understanding of the mechanism of TAML catalysis has been built over many years by examining the oxidation of standard substrates, especially Orange II and a cyclometalated ruthenium(II) dye (Chart 2.1). The largest  $k_1$  value determined with the ruthenium dye stands in the case of each TAML for which it has been studied as the value of the pure uninhibited rate constant unless a larger  $k_1$  rate constant is discovered in the future for another substrate. With this assumption, it can be asserted that substrate inhibition for Orange II is weak, if not negligible.

As a final general point for researchers who are studying TAML catalyzed oxidative degradation of pollutants,<sup>93</sup> the processes may be controlled by either the  $k_1$  or  $k_{II}$  steps, or a mixture of the two, where the apportioning of control can be impacted by many experimental variables.<sup>28</sup> Therefore, it is important to be mindful that rate-related comparisons can be valid for mechanistic and theoretical analyses only when a common pure rate control regime has been established, i.e. control by either the  $k_1$  or  $k_{II}$  step. In assessing how the electronic properties of the substrates impact the oxidation by the activated catalyst, the rate-determining step must be  $k_{II}$  associated. Moreover, this work establishing substrate inhibition, presents a new factor that must henceforth be considered in mechanistic studies, especially those conducted at [substrate]  $\geq$   $\mu$ M. Moreover, in principle, any degradation species for any micropollutant might engage in substrate inhibition.

## 2.5 EXPERIMENTAL

### 2.5.1 Materials.

TAML activator **1a** was IGS stock supplies and the other TAMLs were synthesized according to the published procedures: **1b** and **1c**;<sup>94</sup> **5**<sup>74,95</sup> and **3**.<sup>69,84</sup> Buffer solutions were made using KH<sub>2</sub>PO<sub>4</sub> (Acros) or K<sub>2</sub>HPO<sub>4</sub> (Merck); the pH was adjusted with concentrated solutions of KOH or H<sub>3</sub>PO<sub>4</sub>. Hydrogen peroxide (30%) was purchased from Fischer. Catalase from bovine liver (lyophilized powder, 2000-5000 units/mg of protein) was purchased from Sigma. (±)-Propranolol hydrochloride (>99%) and sodium chloride were both purchased from Sigma and used as received. Methanol and water (both HPLC grade) were obtained from Fischer and used for liquid or ion chromatography without additional purification.

### 2.5.2 Instrumentation.

UV-vis measurements were performed using an Agilent 8453 instrument with an attached temperature controller. The pH measurements were made using an Accumet Basic AB15 pH meter from Fischer Scientific. UPLC studies were performed with a Shimadzu LC system with LC 20AB pump, SIL 20A autosampler, CTO 20A column oven, and an RF 20A XS fluorescence detector. A Kinetex (Phenomenex) 5  $\mu$ M EVO C18 100A column (4.6  $\times$  50 mm) was used for all kinetic analyses. The LC method consisted of 1 mL min<sup>-1</sup> flow rate, 35% methanol in pH 3 phosphate buffer (0.01 M), 40 °C column temperature, and fluorescence detection with 230 nm excitation and 340 nm emission (injections 10  $\mu$ L), with automatic peak integration and Lab Solutions software data analysis. <sup>1</sup>H NMR experiments were performed at 25 °C on a Bruker Avance III 500 NMR spectrometer operating at 500.13 MHz. The water signal was suppressed using a pre-saturation routine obtained from the Bruker Pulse Programs Library. Chemical shifts are reported in ppm ( $\delta$ ) relative to HDO which was determined to resonate at 4.7 ppm relative to an internal standard, the sodium salt of 3-(trimethylsilyl)propionic-2,2,3,3-*d*<sub>4</sub> acid, in calibration experiments. The chemical



shifts were determined in this way to avoid interactions of the acid standard with the TAML or [P, TAML] adducts. Each sample was scanned 32 times over 4 min. NMR data was processed with Bruker TopSpin 3.5 software.

Ion chromatography measurements were performed using the ThermoScientific Dionex Ion chromatography system (ICS) 5000+ with Dionex ICS-5000+ dual pump, Dionex ICS-5000+ eluent generator, Dionex ICS-5000+ detector/chromatography module housing a conductivity detector and a Thermo Scientific Dionex AS-AP autosampler. A Dionex IonPac CG12 A  $4 \times 50$  mm guard column and a Dionex AS11HC  $4 \times 250$  mm column were used throughout. Analyses were performed under isocratic conditions with 0.030 M KOH as the mobile phase,  $1.2 \text{ mL min}^{-1}$  flow rate and an oven temperature of  $30^\circ\text{C}$  and  $25 \mu\text{L}$  injection volume. The mobile phase was prepared with deionized water from a Barnstead Nanopure system. Data were analyzed using Chromeleon Chromatography Version 7 software.

Fluorescence measurements were performed at  $25^\circ\text{C}$  using a Cary Eclipse Varian instrument with an excitation wavelength of 230 nm and an emission range from 250 to 800 nm and a slit width of 5 nm.

Mass fragments for the propranolol-TAML adducts were analyzed by electrospray ionization (ESI) MS using a Finnigan Mat mass spectrometer with methanol as an eluent. The spray/source voltage and the capillary temperature were maintained at 4.5 kV and  $200^\circ\text{C}$ , respectively. Dinitrogen at 18.7 arbitrary units was used as a sheath gas. Methanol was used at a flow rate of  $45 \mu\text{L min}^{-1}$ . Mass fragments in both positive and negative modes were explored in the  $m/z$  range of 150–900. An average of 40 scans was performed for each measurement.

Infrared studies of the adducts were performed using an Attenuated Total Reflectance–Fourier Transform Infrared (ATR FTIR) instrument (Perkin Elmer Frontier with a germanium crystal,  $4 \text{ cm}^{-1}$  resolution,  $700\text{--}4000 \text{ cm}^{-1}$  range). Samples were placed directly on a germanium crystal. A

Labconco freeze-dry system (Freezone 4.5 L benchtop lyophilizer) was used to freeze dry the propranolol-TAML adducts at  $-50\text{ }^{\circ}\text{C}$  for 24 h.

### **2.5.3 Kinetics Studies.**

Kinetics studies of propranolol oxidation by  $\text{H}_2\text{O}_2$  catalyzed by **1** or **2** were conducted at  $25\text{ }^{\circ}\text{C}$  in 0.01 M phosphate buffer. Stock solutions of TAML activators ( $5 \times 10^{-3}\text{ M}$ ), propranolol ( $5 \times 10^{-3}\text{ M}$ ), and  $\text{H}_2\text{O}_2$  (1 M) were prepared in HPLC grade water. Solutions of  $\text{H}_2\text{O}_2$  were stored under refrigeration and standardized daily before use by UV spectroscopy at 230 nm in water ( $\epsilon = 72.4\text{ M}^{-1}\text{ cm}^{-1}$ ).<sup>96</sup> Reaction mixtures were prepared by adding corresponding amounts of the stock solutions of propranolol and TAML to the buffer to bring the total volume to 10 mL. The mixture was kept at  $25\text{ }^{\circ}\text{C}$  in a water bath and the reaction was initiated by adding the stock solution of  $\text{H}_2\text{O}_2$ . After certain time intervals, 1 mL aliquots were withdrawn and quenched with catalase (10  $\mu\text{L}$  of 10 mg  $\text{mL}^{-1}$  solution). Propranolol was quantified by UPLC. The initial rates were calculated from linear plots of propranolol concentration vs time when the conversion of propranolol did not exceed 10–20%. Each data point reported is a mean value of three measurements.

### **2.5.4 Isolation of Propranolol-TAML [P-TAML] Adducts.**

A 0.3 mL aliquot of **1c** or **5** ( $5 \times 10^{-3}\text{ M}$ ) was added to 3 mL of a solution of propranolol ( $7.5 \times 10^{-2}\text{ M}$ ) in pH 7 0.01 M phosphate buffer to yield a final **1c** or **5** concentration of  $4.5 \times 10^{-4}\text{ M}$ . Precipitation occurred instantly for **5** while the mixture with **1c** became turbid after a few minutes at room temperature. The mixtures were kept overnight and then centrifuged at 15,000 rpm for 15 min. The solids were washed three times with water and lyophilized overnight.

### **2.5.5 DFT Calculations.**

The structure of **1c** was built using the X-ray data for its analogue without nitro group.<sup>81</sup> The 3D structure of propranolol was created using the open source chemistry toolbox OpenBabel.<sup>97</sup> The geometries of **1c**, propranolol and their adduct were optimized at the DFT level (M06 density

functional)<sup>98</sup> using the triple- $\zeta$  basis set 6-311G implemented in the computational suite Gaussian 09, rev. D.01.<sup>99</sup> Solvent effects were examined using the SMD continuum model.<sup>100</sup> The default convergence criteria were adopted in geometrical optimizations.

## 2.6 APPENDIX

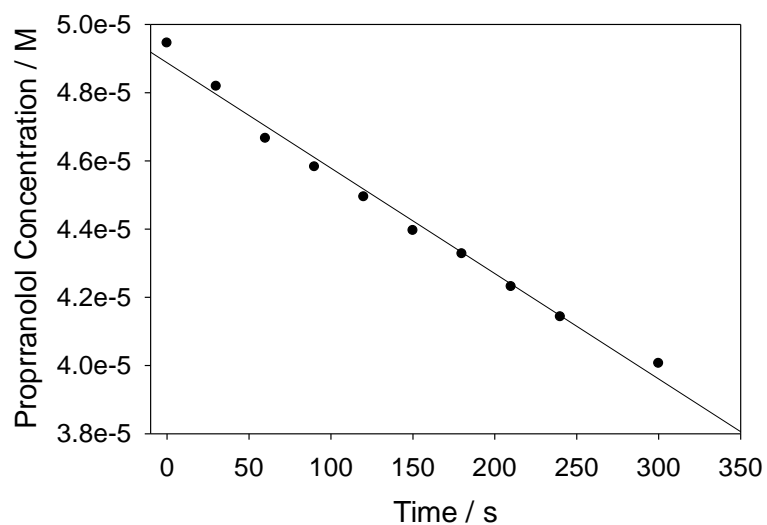


Figure 2.7 Determination of initial rate (slope of the line) when  $\leq 20\%$  reaction is completed. Conditions: [**1a**]  $1 \times 10^{-6}$  M, [propranolol]  $5 \times 10^{-5}$  M, [ $\text{H}_2\text{O}_2$ ]  $1 \times 10^{-3}$  M, pH 9 (0.01 M phosphate),  $25^\circ\text{C}$ .

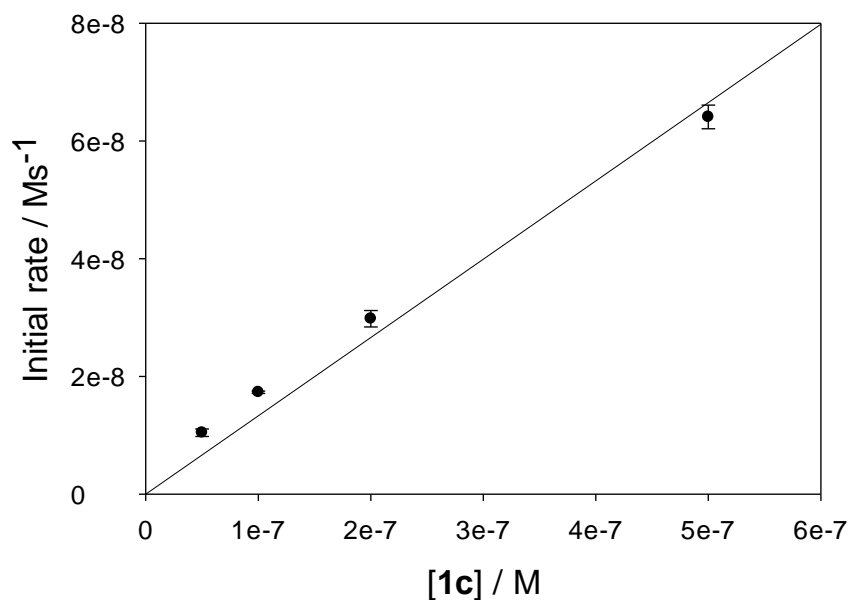


Figure 2.8 Initial rate of propranolol degradation by  $\text{H}_2\text{O}_2$  catalyzed by **1c** as a function of [**1c**]. Conditions: [**1c**]  $(5-50) \times 10^{-8}$  M, [propranolol]  $5 \times 10^{-5}$  M, [ $\text{H}_2\text{O}_2$ ]  $3 \times 10^{-3}$  M, pH 7 (0.01 M phosphate).

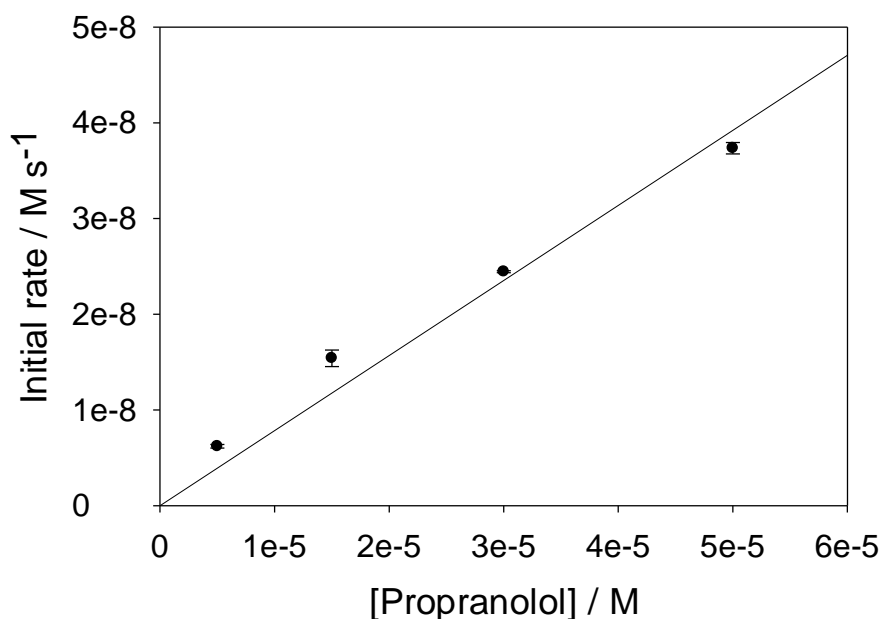


Figure 2.9 Initial rate of propranolol degradation by  $\text{H}_2\text{O}_2$  catalyzed by **1a** as a function of [propranolol]. Conditions: [**1a**]  $1 \times 10^{-6}$  M, [propranolol]  $(5-50) \times 10^{-6}$  M, [ $\text{H}_2\text{O}_2$ ]  $4.25 \times 10^{-3}$  M, pH 9 (0.01 M phosphate).

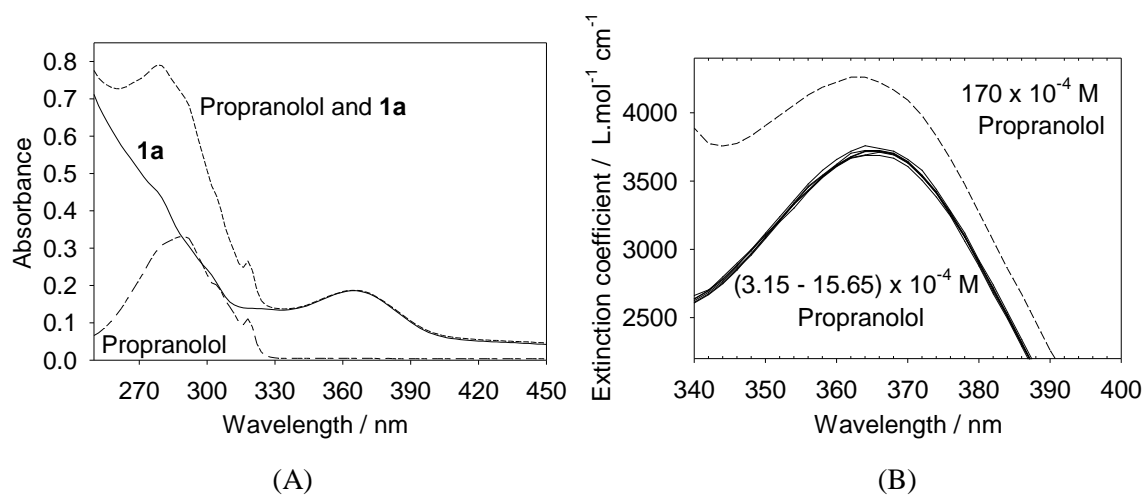


Figure 2.10 (A) UV-vis spectrum of propranolol ( $5 \times 10^{-5}$  M), **1a** ( $5 \times 10^{-5}$  M), and propranolol and **1a** ( $5 \times 10^{-5}$  M each), in pH 7 0.01 M phosphate buffer. (B) the variation of extinction coefficient of **1a** ( $5 \times 10^{-5}$  M) upon titration with propranolol. Solid lines represent propranolol  $(3.2 - 15.7) \times 10^{-4}$  M and the dotted line represents propranolol ( $170 \times 10^{-4}$  M).

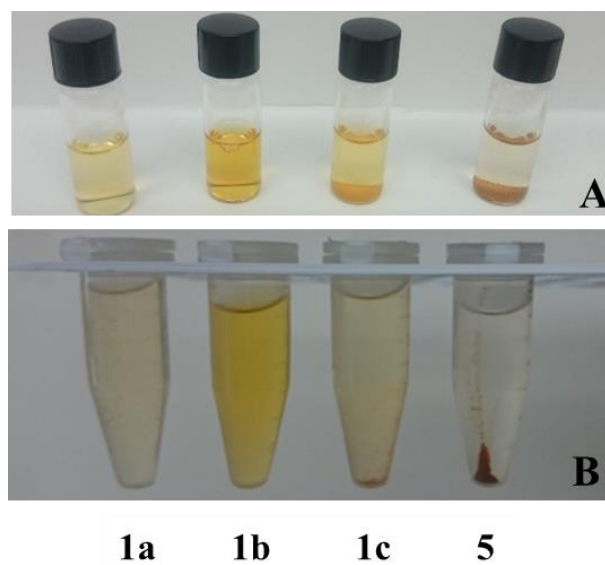


Figure 2.11 Mixtures of propranolol with TAMLs (left to right: **1a**, **1b**, **1c**, **5**) showing the formation of precipitates for **1c** and **5** before (A) and after (B) centrifugation. Conditions: propranolol ( $7.5 \times 10^{-2}$  M), TAMLs ( $4.5 \times 10^{-4}$  M), pH 7.0, room temperature.

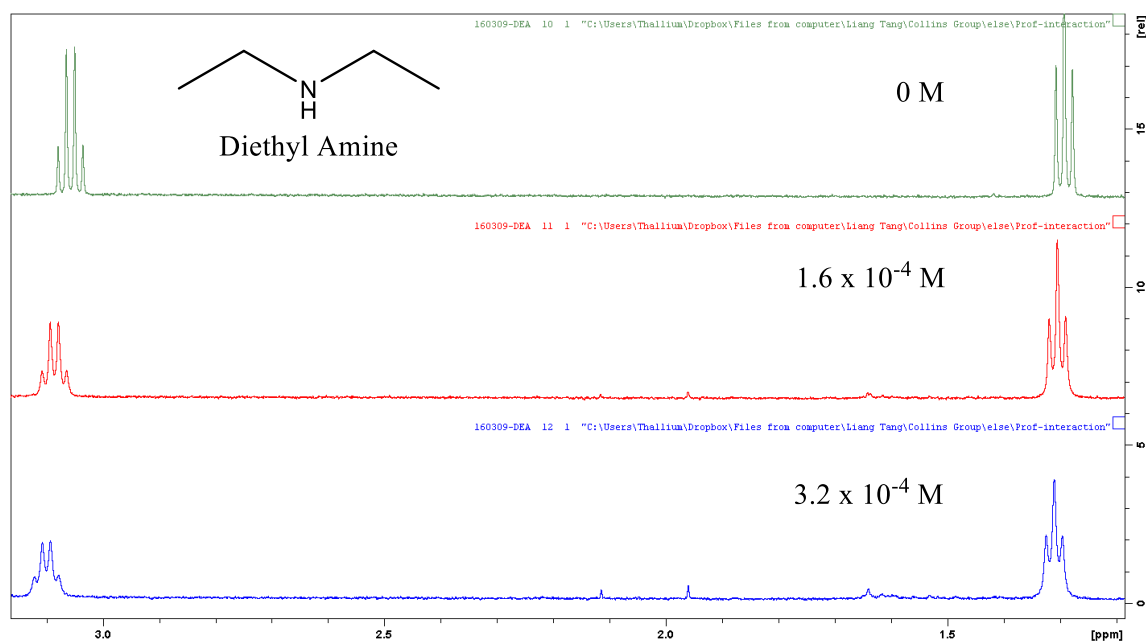


Figure 2.12  $^1\text{H}$  NMR spectra of diethylamine alone (0.015 M, top) and in the presence of **1b** ( $1.6 \times 10^{-4}$  and  $3.2 \times 10^{-4}$  M, middle and bottom, respectively). Conditions:  $\text{D}_2\text{O}$ , 25  $^\circ\text{C}$ .

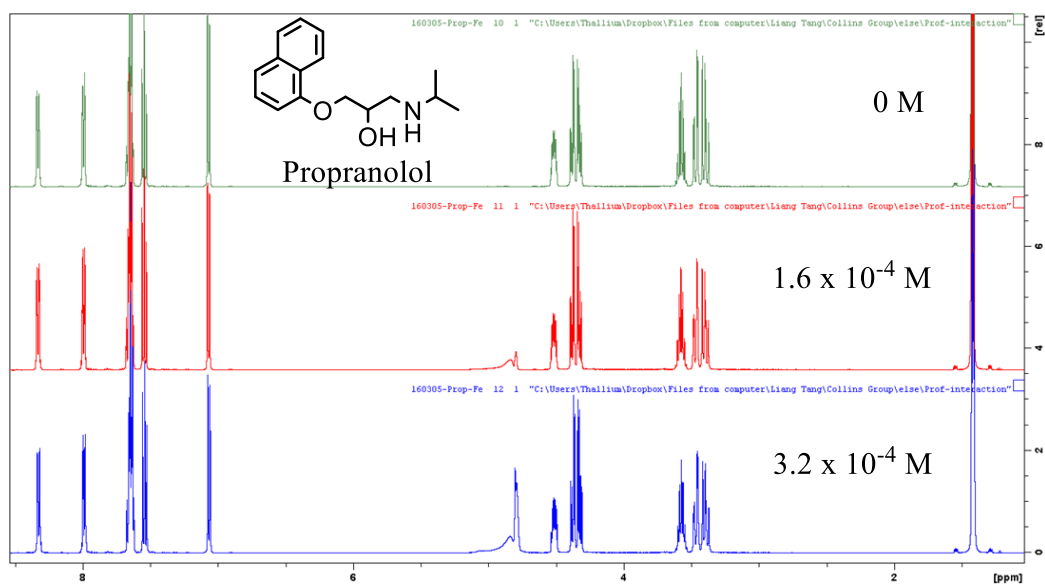


Figure 2.13  $^1\text{H}$  NMR spectra of propranolol alone (0.015 M, top) and in the presence of  $\text{FeCl}_3$  ( $1.6 \times 10^{-4}$  and  $3.2 \times 10^{-4}$  M, middle and bottom, respectively). Conditions:  $\text{D}_2\text{O}$ , 25 °C.

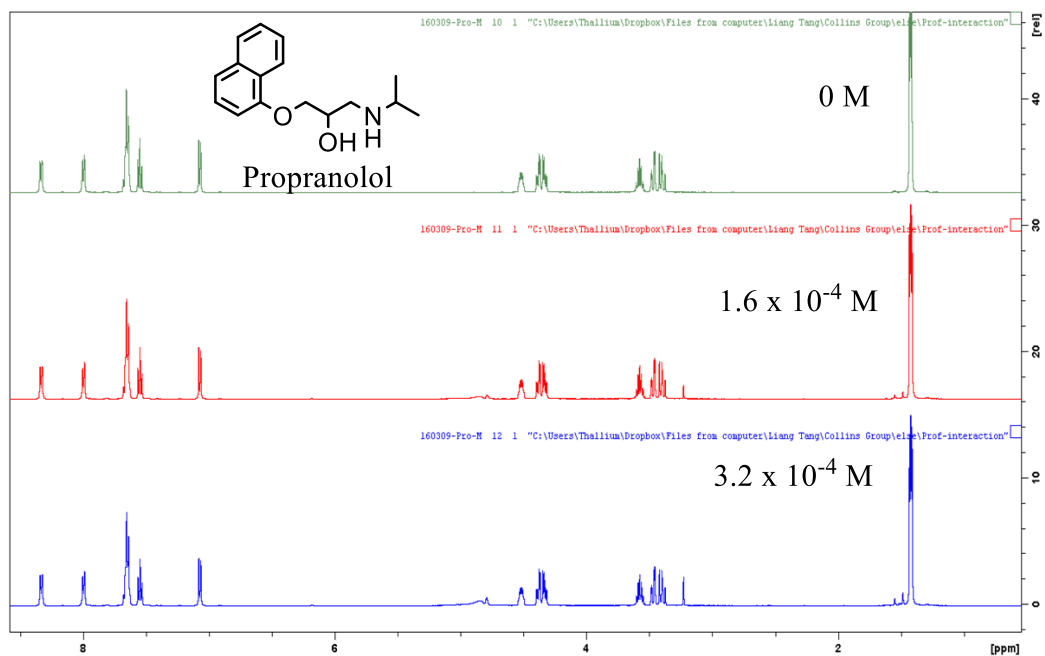


Figure 2.14  $^1\text{H}$  NMR spectra of propranolol alone (0.015 M, top) and in the presence of **3** ( $1.6 \times 10^{-4}$  and  $3.2 \times 10^{-4}$  M, middle and bottom, respectively). Conditions:  $\text{D}_2\text{O}$ , 25 °C.

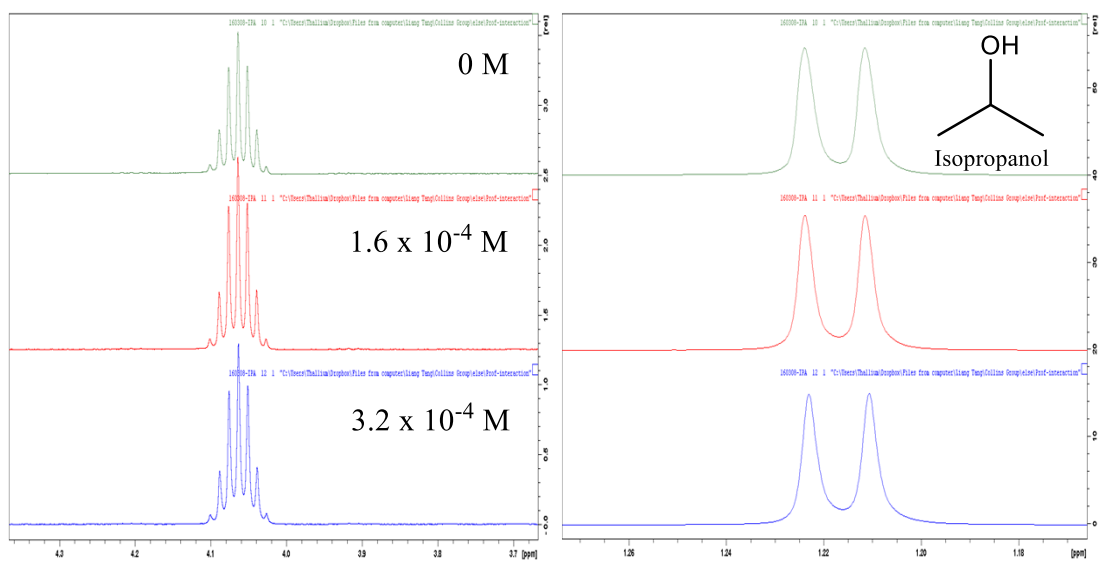


Figure 2.15  $^1\text{H}$  NMR spectra of isopropanol alone (0.015 M, top) and in the presence of **1b** ( $1.6 \times 10^{-4}$  and  $3.2 \times 10^{-4}$  M, middle and bottom, respectively). Conditions:  $\text{D}_2\text{O}$ , 25  $^\circ\text{C}$ .

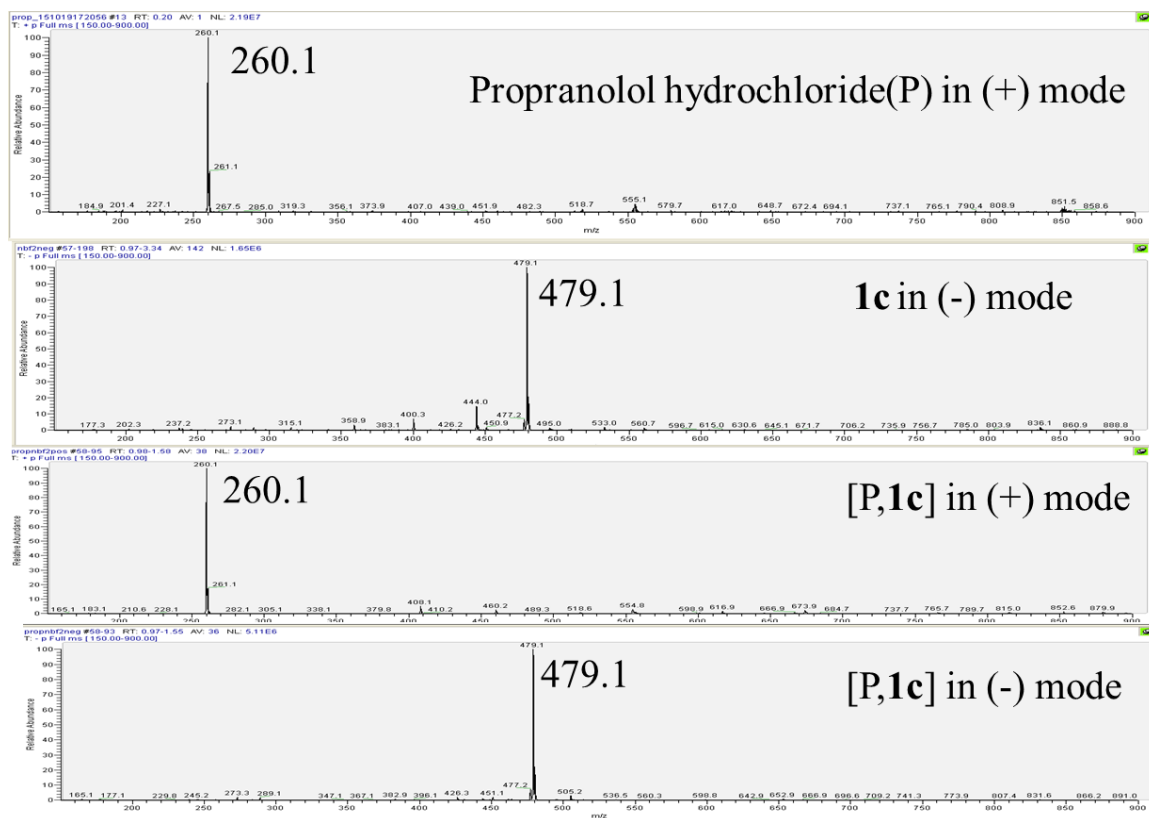


Figure 2.16 ESI-MS of propranolol, **1c** and **[P,1c]** in methanol. Conditions: 10  $\mu\text{L}$  injection, 25  $^\circ\text{C}$ .



°C.

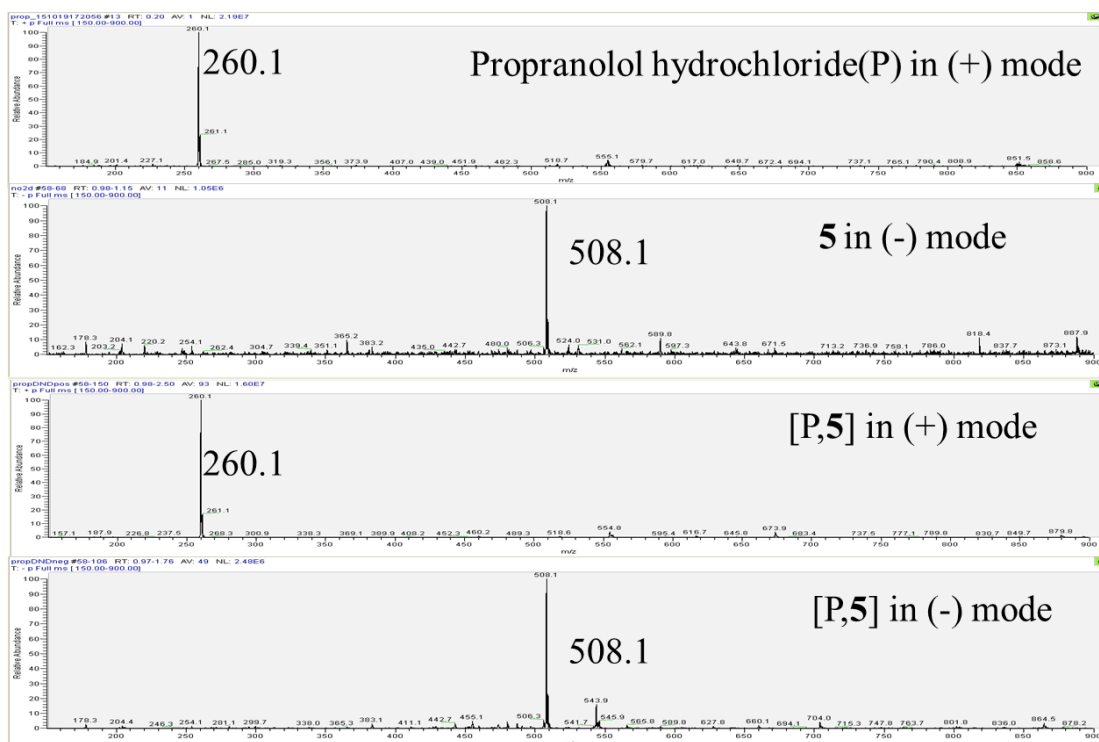


Figure 2.17 ESI-MS of propranolol, **5** and [P,**5**] in methanol. Conditions: 10  $\mu$ L injection, 25 °C.

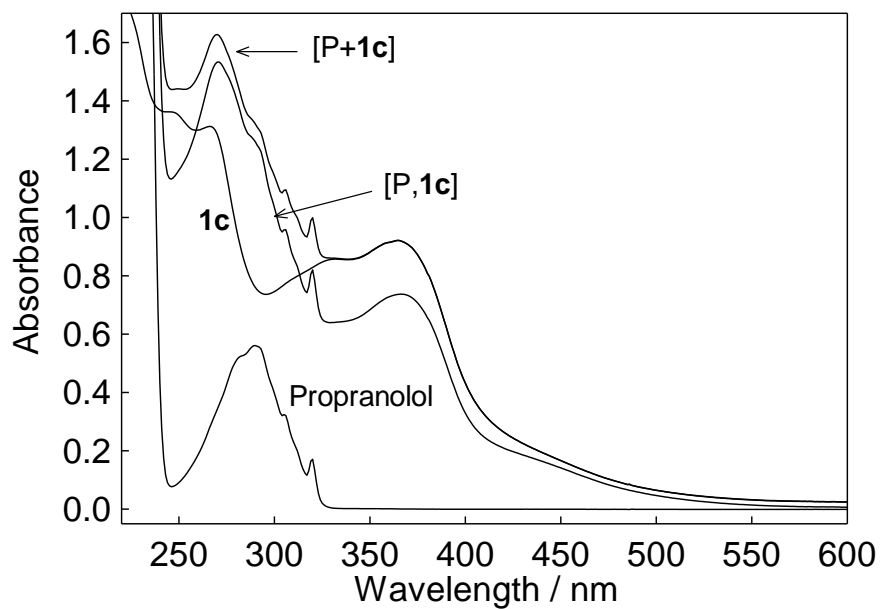


Figure 2.18 UV-vis spectra of propranolol ( $9 \times 10^{-5}$  M), **1c** ( $9 \times 10^{-5}$  M), [P,**1c**] adduct (ca.  $8 \times 10^{-5}$  M) and the sum of the spectra of propranolol and **1c** (both  $9 \times 10^{-5}$  M, P + **1c**). All spectra are in methanol.

Propranolol does not absorb light at 365 nm and therefore the concentration of **1c** in solution can be calculated from absorbance at 365 nm. At 290 nm (maximum for propranolol), the absorbance  $A = c_p \epsilon_p + c_{1c} \epsilon_{1c}$  and the concentration of propranolol  $c_p$  is easy to find since the extinction coefficients  $\epsilon_p$  and  $\epsilon_{1c}$  for propranolol and **1c**, respectively, and the concentration of **1c** ( $c_{1c}$ ) are known. This routine confirmed an approximate 1:1 stoichiometry of the [P,TAML] adducts (Table 2.2). The exact P:TAML ratio was found to be 1.2 and 1.4 for **1c** and **5**, respectively. Based on these stoichiometries, the isolated yields of the adducts equal 42% and 124% for **1c** and **5**, respectively.

Table 2.2 Stoichiometry of [P,TAML] adducts.

Adduct type	Concentration of TAML x 10 <sup>4</sup> M		Average concentration of Propranolol x 10 <sup>4</sup> M			Ratio of Propranolol : TAML	
	365nm	445nm	280nm	290nm	300nm		
P+ <b>1c</b>	0.79	-	1.02	0.95	0.90	0.95(3)	1.2 (3)
P+ <b>5</b>	-	0.84	1.25	1.18	1.08	1.17 (3)	1.4 (3)

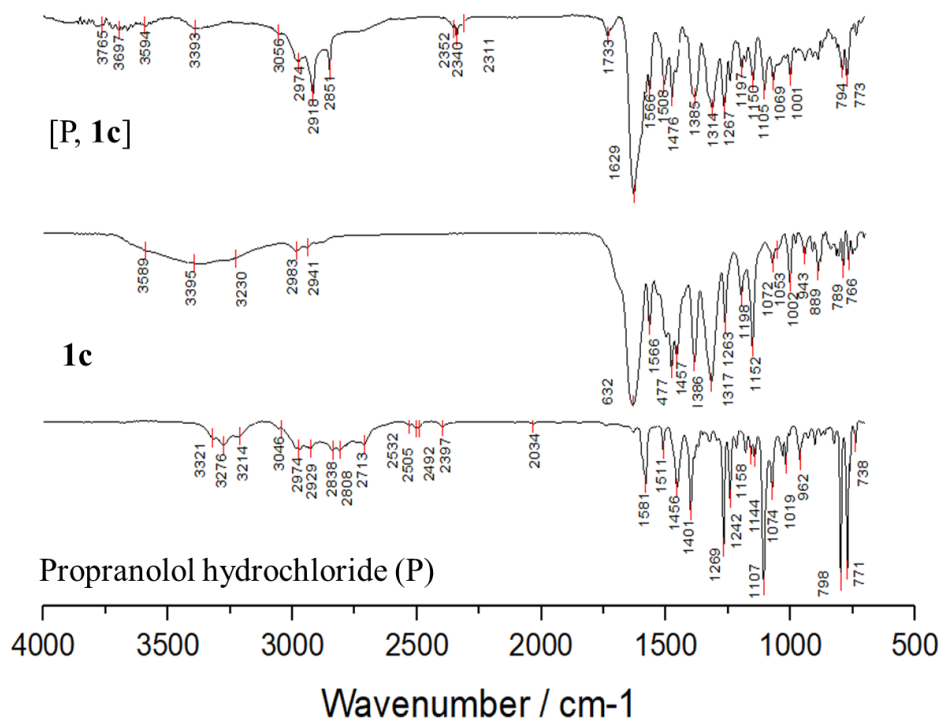


Figure 2.19 Infrared spectra of propranolol (P), **1c** and [P,**1c**]. Conditions: ATR accessory, germanium crystal, 25 °C. (All the spectra are scaled differently).

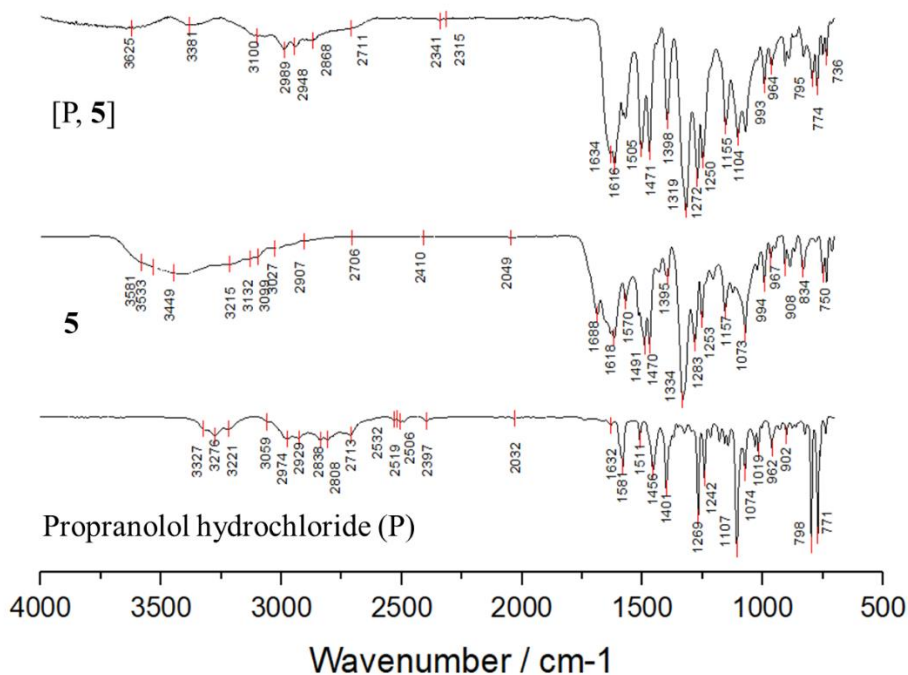


Figure 2.20 Infrared spectra of propranolol (P), **5** and [P,**5**]. Conditions: ATR accessory, germanium crystal, 25 °C. (All the spectra are scaled differently).

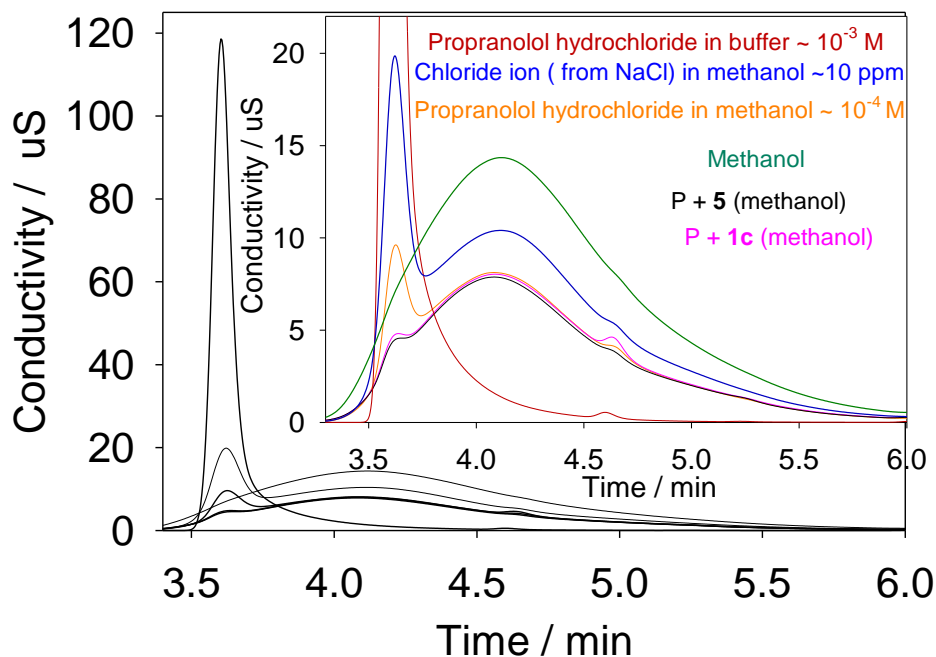


Figure 2.21 . Ion chromatogram for the anionic component of [P,**1c**] and [P,**5**] in methanol. Inset: zoomed in area between 0-20  $\mu\text{S}$ . Conditions: Sample prepared at 25 °C, 25  $\mu\text{L}$  injection. A trace of chloride remains in the isolated adducts as seen in the peak at 3.6 min.

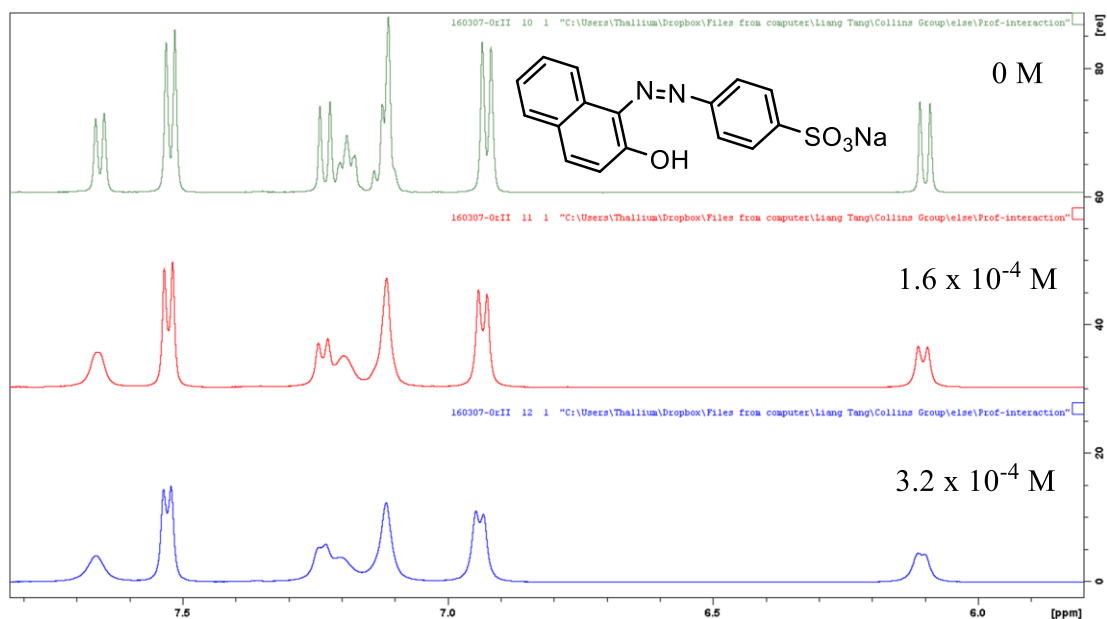


Figure 2.22  $^1\text{H}$  NMR spectra of Orange II alone (0.015 M, top) and in the presence of **1b** ( $1.6 \times 10^{-4}$  and  $3.2 \times 10^{-4}$  M, middle and bottom, respectively). Conditions:  $\text{D}_2\text{O}$ , 25  $^\circ\text{C}$ .

Table 2.3 Rate constants  $k_{\text{I}}$  and  $k_{\text{II}}$  for Propranolol at 25  $^\circ\text{C}$  compared with  $k_{\text{I}}$  values reported previously using other test substrates; calculated equilibrium constants,  $K$  and corresponding free energy change,  $\Delta G^\circ$ .

TAML	pH	$k_{\text{I}}$ $\text{M}^{-1} \text{s}^{-1}$	$10^{-2} \times k_{\text{II}}$ $\text{M}^{-1} \text{s}^{-1}$	$k_{\text{I}}^{\text{OrII}}$ or $k_{\text{I}}^{\text{Ru}}$ $\text{M}^{-1} \text{s}^{-1}$	$k_{\text{I}}^{\text{OrII}}/k_{\text{I}}$ or $k_{\text{I}}^{\text{Ru}}/k_{\text{I}}$	$10^{-5} \times K$ M	$\Delta G^\circ$ kcal mol $^{-1}$
1a	7.0	$2.0 \pm 0.1$	$0.7 \pm 0.2$	$31.4 \pm 0.1^{\text{a}}$	16	3	-7.5
	7.0			$52 \pm 2^{\text{c}}$	26	5	-7.8
	9.0	$74 \pm 3$	$8.0 \pm 0.3$	$1400 \pm 10^{\text{b}}$	19	3.6	-7.6
	9.0			$2400 \pm 300^{\text{c}}$	32	6.2	-7.9
1b	7.0	$5.0 \pm 0.2$	$1.4 \pm 0.2$	$152 \pm 5^{\text{a}}$	30	5.8	-7.9
	9.0	$149 \pm 5$	$35 \pm 1$				
1c	7.0	$90 \pm 10$	$146 \pm 2$	$350 \pm 2^{\text{a}}$	4	0.6	-6.5
	9.0	$2990 \pm 50$	$680 \pm 10$				
5	7.0	$200 \pm 10$	$53 \pm 24$	$1900 \pm 100^{\text{a}}$	9.5	1.7	-7.1
	9.0	$4200 \pm 400$	$500 \pm 40$	$16,000 \pm 2000^{\text{d}}$	4	0.6	-6.5

<sup>a)</sup> Orange II; from ref.<sup>69</sup> <sup>b)</sup> Orange II; from ref.<sup>70</sup> <sup>c)</sup> Cyclometalated ruthenium(II) dye  $[\text{Ru}^{\text{II}}(\text{o-C}_6\text{H}_4\text{-2-py})(\text{phen})_2]^+$ ; from ref.<sup>71</sup> <sup>d)</sup> Orange II; from ref.<sup>74</sup>

## 2.7 REFERENCES

- (1) Colborn, T.; vom Saal, F. S.; Soto, A. M. Developmental Effects of Endocrine-Disrupting Chemicals in Wildlife and Humans. *Environ. Health Perspect.* **1993**, *101* (5), 378–384.
- (2) Vandenberg, L. N.; Colborn, T.; Hayes, T. B.; Heindel, J. J.; Jacobs, D. R.; Lee, D. H.; Shioda, T.; Soto, A. M.; vom Saal, F. S.; Welshons, W. V.; Zoeller, R. T.; Myers, J. P. Hormones and Endocrine-Disrupting Chemicals: Low-Dose Effects and Nonmonotonic Dose Responses. *Endocr. Rev.* **2012**, *33* (3), 378–455.
- (3) Schwarzenbach, R. P.; Escher, B. I.; Fenner, K.; Hofstetter, T. B.; Johnson, C. A.; von Gunten, U.; Wehrli, B. The Challenge of Micropollutants in Aquatic Systems. *Science* (80-. ). **2006**, *313* (5790), 1072 LP – 1077.
- (4) Daughton, C. G.; Ternes, T. A. Pharmaceuticals and Personal Care Products in the Environment: Agents of Subtle Change? *Environ. Health Perspect.* **1999**, *107* (Suppl 6), 907–938.
- (5) Benotti, M. J.; Trenholm, R. A.; Vanderford, B. J.; Holady, J. C.; Stanford, B. D.; Snyder, S. A. Pharmaceuticals and Endocrine Disrupting Compounds in U.S. Drinking Water. *Environ. Sci. Technol.* **2009**, *43* (3), 597–603.
- (6) Kounang, N. Dangerous chemicals hiding in everyday products.  
<https://www.cnn.com/2016/07/01/health/everyday-chemicals-we-need-to-reduce-exposure-to/index.html> (accessed Jul 1, 2017).
- (7) Onundi, Y.; Drake, B. A.; Malecky, R. T.; DeNardo, M. A.; Mills, M. R.; Kundu, S.; Ryabov, A. D.; Beach, E. S.; Horwitz, C. P.; Simonich, M. T.; Truong, L.; Tanguay, R. L.; Wright, L. J.; Singhal, N.; Collins, T. J. A Multidisciplinary Investigation of the Technical and Environmental Performances of TAML/Peroxide Elimination of Bisphenol A Compounds from Water. *Green Chem.* **2017**, *19* (18), 4234–4262.
- (8) Chiara, P.; Barbara, M.; Tamar, K.; Anoys, M.; Denis, T.; Nathalie, C. Occurrence and Fate of Micropollutants in the Vidy Bay of Lake Geneva, Switzerland. Part I: Priority List for Environmental Risk Assessment of Pharmaceuticals. *Environ. Toxicol. Chem.* **2010**, *29* (8), 1649–1657.
- (9) Lesser, L. E.; Mora, A.; Moreau, C.; Mahlknecht, J.; Hernández-Antonio, A.; Ramírez, A. I.; Barrios-Piña, H. Survey of 218 Organic Contaminants in Groundwater Derived from the World's Largest Untreated Wastewater Irrigation System: Mezquital Valley, Mexico. *Chemosphere* **2018**, *198*, 510–521.
- (10) Escher, B. I.; Bramaz, N.; Eggen, R. I. L.; Richter, M. In Vitro Assessment of Modes of Toxic Action of Pharmaceuticals in Aquatic Life. *Environ. Sci. Technol.* **2005**, *39* (9), 3090–3100.
- (11) Fent, K.; Weston, A. A.; Caminada, D. Ecotoxicology of Human Pharmaceuticals. *Aquat. Toxicol.* **2006**, *76* (2), 122–159.
- (12) Tang, L. L.; DeNardo, M. A.; Gayathri, C.; Gil, R. R.; Kanda, R.; Collins, T. J. TAML/H<sub>2</sub>O<sub>2</sub> Oxidative Degradation of Metaldehyde: Pursuing Better Water Treatment for the Most Persistent Pollutants. *Env. Sci Technol* **2016**, *50* (10), 5261–5268.
- (13) Huggett, D. B.; Brooks, B. W.; Peterson, B.; Foran, C. M.; Schlenk, D. Toxicity of Select Beta Adrenergic Receptor-Blocking Pharmaceuticals (B-Blockers) on Aquatic Organisms. *Arch Env. Contam Toxicol* **2002**, *43* (2), 229–235.
- (14) Niemuth, N. J.; Jordan, R.; Crago, J.; Blanksma, C.; Johnson, R.; Klaper, R. D. Metformin Exposure at Environmentally Relevant Concentrations Causes Potential Endocrine Disruption in Adult Male Fish. *Env. Toxicol Chem* **2015**, *34* (2), 291–296.
- (15) Kong, L.; Kadokami, K.; Duong, H. T.; Chau, H. T. C. Screening of 1300 Organic Micro-

- Pollutants in Groundwater from Beijing and Tianjin, North China. *Chemosphere* **2016**, 165, 221–230.
- (16) Margot, J.; Kienle, C.; Magnet, A.; Weil, M.; Rossi, L.; de Alencastro, L. F.; Abegglen, C.; Thonney, D.; Chevre, N.; Scharer, M.; Barry, D. A. Treatment of Micropollutants in Municipal Wastewater: Ozone or Powdered Activated Carbon? *Sci Total Env.* **2013**, 461–462, 480–498.
  - (17) Margot, J.; Rossi, L.; Barry, D. A.; Holliger, C. A Review of the Fate of Micropollutants in Wastewater Treatment Plants. *WIREs Water* **2015**, 2 (5), 457–487.
  - (18) Daughton, C. G. Cradle-to-Cradle Stewardship of Drugs for Minimizing Their Environmental Disposition While Promoting Human Health. I. Rationale for and Avenues toward a Green Pharmacy. *Environ. Health Perspect.* **2003**, 111 (5), 757–774.
  - (19) Khetan, S. K.; Collins, T. J. Human Pharmaceuticals in the Aquatic Environment: A Challenge to Green Chemistry. *Chem. Rev.* **2007**, 107 (6), 2319–2364.
  - (20) Kim, M.-K.; Zoh, K.-D. Occurrence and Removals of Micropollutants in Water Environment. *Environ. Eng. Res.* **2016**, 21 (4), 319–332.
  - (21) Cirja, M.; Ivashechkin, P.; Schäffer, A.; Corvini, P. F. X. Factors Affecting the Removal of Organic Micropollutants from Wastewater in Conventional Treatment Plants (CTP) and Membrane Bioreactors (MBR). *Rev. Environ. Sci. Bio/Technology* **2008**, 7 (1), 61–78.
  - (22) Eggen, R. I. L.; Hollender, J.; Joss, A.; Schärer, M.; Stamm, C. Reducing the Discharge of Micropollutants in the Aquatic Environment: The Benefits of Upgrading Wastewater Treatment Plants. *Environ. Sci. Technol.* **2014**, 48 (14), 7683–7689.
  - (23) Luo, Y.; Guo, W.; Ngo, H. H.; Nghiem, L. D.; Hai, F. I.; Zhang, J.; Liang, S.; Wang, X. C. A Review on the Occurrence of Micropollutants in the Aquatic Environment and Their Fate and Removal during Wastewater Treatment. *Sci Total Env.* **2014**, 473–474, 619–641.
  - (24) Chávez, A.; Maya, C.; Gibson, R.; Jiménez, B. The Removal of Microorganisms and Organic Micropollutants from Wastewater during Infiltration to Aquifers after Irrigation of Farmland in the Tula Valley, Mexico. *Environ. Pollut.* **2011**, 159 (5), 1354–1362.
  - (25) Barbara, M.; Florence, B.; Hans, R.; Dominique, G.; Felipe, de A. L.; Chiara, P.; Nathalie, C.; Tamar, K. Occurrence and Fate of Micropollutants in the Vidy Bay of Lake Geneva, Switzerland. Part II: Micropollutant Removal between Wastewater and Raw Drinking Water. *Environ. Toxicol. Chem.* **2010**, 29 (8), 1658–1668.
  - (26) Collins, T. J. Designing Ligands for Oxidizing Complexes. *Acc. Chem. Res.* **1994**, 27 (9), 279–285.
  - (27) Collins, T. J. TAML Oxidant Activators: A New Approach to the Activation of Hydrogen Peroxide for Environmentally Significant Problems. *Acc. Chem. Res.* **2002**, 35 (9), 782–790.
  - (28) Ryabov, A. D.; Collins, T. J. Mechanistic Considerations on the Reactivity of Green FeIII-TAML Activators of Peroxides. *Adv. Inorg. Chem.* **2009**, 61, 471–521.
  - (29) Ryabov, A. D. Green Challenges of Catalysis via Iron(IV)Oxo and Iron(V)Oxo Species. *Adv. Inorg. Chem.* **2013**, 65, 117–163.
  - (30) Dunford, H. B. *Heme Peroxidases*; Wiley-VCH: NY, Chichester, Weinheim, 1999.
  - (31) Yadav, M.; Rai, N.; Yadav, H. S. The Role of Peroxidase in the Enzymatic Oxidation of Phenolic Compounds to Quinones from Luffa Aegyptiaca (Gourd) Fruit Juice. *Green Chem. Lett. Rev.* **2017**, 10 (3), 154–161.
  - (32) Michon, T.; Chenu, M.; Kellershon, N.; Desmadril, M.; Guéguen, J. Horseradish Peroxidase Oxidation of Tyrosine-Containing Peptides and Their Subsequent Polymerization: A Kinetic Study. *Biochemistry* **1997**, 36 (28), 8504–8513.
  - (33) Kersten, P. J.; Kalyanaraman, B.; Hammel, K. E.; Reinhammar, B.; Kirk, T. K. Comparison of Lignin Peroxidase, Horseradish Peroxidase and Laccase in the Oxidation of Methoxybenzenes. *Biochem. J.* **1990**, 268 (2), 475 LP – 480.

- (34) Mills, M. R.; Arias-Salazar, K.; Baynes, A.; Shen, L. Q.; Churchley, J.; Beresford, N.; Gayathri, C.; Gil, R. R.; Kanda, R.; Jobling, S.; Collins, T. J. Removal of Ecotoxicity of 17alpha-Ethinylestradiol Using TAML/Peroxide Water Treatment. *Sci Rep* **2015**, *5*, 10511.
- (35) Tang, L. L.; DeNardo, M. A.; Schuler, C. J.; Mills, M. R.; Gayathri, C.; Gil, R. R.; Kanda, R.; Collins, T. J. Homogeneous Catalysis Under Ultradilute Conditions: TAML/NaClO Oxidation of Persistent Metaldehyde. *J. Am. Chem. Soc.* **2017**, *139* (2), 879–887.
- (36) Kundu, S.; Chanda, A.; Espinosa-Marvan, L.; Khetan, S. K.; Collins, T. J. Facile Destruction of Formulated Chlorpyrifos through Green Oxidation Catalysis. *Catal. Sci. Technol.* **2012**, *2* (6), 1165–1172.
- (37) Kundu, S.; Chanda, A.; Thompson, J. V. K.; Diabes, G.; Khetan, S. K.; Ryabov, A. D.; Collins, T. J. Rapid Degradation of Oxidation Resistant Nitrophenols by TAML Activator and H<sub>2</sub>O<sub>2</sub>. *Catal. Sci. Technol.* **2015**, *5* (3), 1775–1782.
- (38) Chanda, A.; Khetan, S. K.; Banerjee, D.; Ghosh, A.; Collins, T. J. Total Degradation of Fenitrothion and Other Organophosphorus Pesticides by Catalytic Oxidation Employing Fe-TAML Peroxide Activators. *J Am Chem Soc* **2006**, *128* (37), 12058–12059.
- (39) Deboshri, B.; L., M. A.; Toshihiro, Y.; Anindya, G.; B., B. P.; G., M. E.; K., K. S.; J., C. T. “Green” Oxidation Catalysis for Rapid Deactivation of Bacterial Spores. *Angew. Chemie Int. Ed.* **2006**, *45* (24), 3974–3977.
- (40) Shen, L. Q.; Beach, E. S.; Xiang, Y.; Tshudy, D. J.; Khanina, N.; Horwitz, C. P.; Bier, M. E.; Collins, T. J. Rapid, Biomimetic Degradation in Water of the Persistent Drug Sertraline by TAML Catalysts and Hydrogen Peroxide. *Env. Sci Technol* **2011**, *45* (18), 7882–7887.
- (41) Gupta, S. Sen; Stadler, M.; Noser, C. A.; Ghosh, A.; Steinhoff, B.; Lenoir, D.; Horwitz, C. P.; Schramm, K.-W.; Collins, T. J. Rapid Total Destruction of Chlorophenols by Activated Hydrogen Peroxide. *Science* (80-. ). **2002**, *296* (5566), 326 LP – 328.
- (42) Churchley, J.; Collins, T.; Jobling, S. *Catalytic Oxidation of Pharmaceutical Compounds in Wastewater Effluents*; UKWIR: London, 2013.
- (43) Berezin, I. V.; Martinek, K. *Principles of the Physical Chemistry of Enzymic Catalysis*; Vysshaya Shkola: Moscow, 1977.
- (44) Cornish-Bowden, A. *Fundamentals of Enzyme Kinetics*; Portland Press: London, UK, 1995.
- (45) Fersht, A. *Structure and Mechanism in Protein Science: A Guide to Enzyme Catalysis and Protein Folding*; Freeman: NY, 1999.
- (46) Cleland, W. W. Substrate Inhibition. *Methods Enzym.* **1979**, *63* (Enzyme Kinet. Mech., Part A), 500–513.
- (47) Dalziel, K.; Dickinson, F. M. Substrate Activation and Inhibition in Coenzyme-Substrate Reactions Cyclohexanol Oxidation Catalysed by Liver Alcohol Dehydrogenase. *Biochem. J.* **1966**, *100* (2), 491–500.
- (48) Takashi, H. INDIVIDUAL PEROXISOMAL BT-OXIDATION ENZYMES\*. *Ann. N. Y. Acad. Sci.* **1982**, *386* (1), 5–12.
- (49) Mayberry, J. M.; Mallette, M. F. Inhibition of the Tyrosinase Oxidation of One Substrate by Another. *J. Gen. Physiol.* **1962**, *45* (6), 1239 LP – 1245.
- (50) Keehyun, H.; Octave, L. Extended Monod Kinetics for Substrate, Product, and Cell Inhibition. *Biotechnol. Bioeng.* **1988**, *32* (4), 430–447.
- (51) Müller, C. S.; Knehans, T.; Davydov, D. R.; Bounds, P. L.; von Mandach, U.; Halpert, J. R.; Caflisch, A.; Koppenol, W. H. Concurrent Cooperativity and Substrate Inhibition in the Epoxidation of Carbamazepine by Cytochrome P450 3A4 Active Site Mutants Inspired by Molecular Dynamics Simulations. *Biochemistry* **2015**, *54* (3), 711–721.
- (52) Lin, Y.; Lu, P.; Tang, C.; Mei, Q.; Sandig, G.; Rodrigues, A. D.; Rushmore, T. H.; Shou,

- M. Substrate Inhibition Kinetics for Cytochrome P450-Catalyzed Reactions. *Drug Metab. Dispos.* **2001**, 29 (4 Pt 1), 368–374.
- (53) Crabtree, R. H. Deactivation in Homogeneous Transition Metal Catalysis: Causes, Avoidance, and Cure. *Chem. Rev.* **2015**, 115 (1), 127–150.
  - (54) Collins, T. J.; Gordon-Wylie, S. W.; Horwitz, C. P. Long-Lived Homogenous Amide Containing Macrocyclic Compounds. U.S. Patent 6054580, 2000.
  - (55) Huggett, D. B.; Khan, I. A.; Foran, C. M.; Schlenk, D. Determination of Beta-Adrenergic Receptor Blocking Pharmaceuticals in United States Wastewater Effluent. *Environ. Pollut.* **2002**, 121, 199–205.
  - (56) Gros, M.; Petrović, M.; Barceló, D. Wastewater Treatment Plants as a Pathway for Aquatic Contamination by Pharmaceuticals in the Ebro River Basin (Northeast Spain). *Environ. Toxicol. Chem.* **2007**, 26 (8), 1553–1562.
  - (57) Petrovic, M.; Skrbic, B.; Zivancev, J.; Ferrando-Climent, L.; Barcelo, D. Determination of 81 Pharmaceutical Drugs by High Performance Liquid Chromatography Coupled to Mass Spectrometry with Hybrid Triple Quadrupole-Linear Ion Trap in Different Types of Water in Serbia. *Sci. Total Environ.* **2014**, 468, 415–428.
  - (58) Stapleton, M. P. Sir James Black and Propranolol. The Role of the Basic Sciences in the History of Cardiovascular Pharmacology. *Tex Hear. Inst J* **1997**, 24 (4), 336–342.
  - (59) Pharmaceuticals, W. Inderal  
[https://www.accessdata.fda.gov/drugsatfda\\_docs/label/2011/016418s080,016762s017,017683s0081bl.pdf](https://www.accessdata.fda.gov/drugsatfda_docs/label/2011/016418s080,016762s017,017683s0081bl.pdf) (accessed Jul 1, 2017).
  - (60) Elman, M. J.; Sugar, J.; Fiscella, R.; Deutsch, T. A.; Noth, J.; Nyberg, M.; Packo, K.; Anderson, R. J. The Effect of Propranolol versus Placebo on Resident Surgical Performance. *Trans Am Ophthalmol Soc* **1998**, 96, 283–284.
  - (61) Du, B.; Price, A. E.; Scott, W. C.; Kristofco, L. A.; Ramirez, A. J.; Chambliss, C. K.; Yelderman, J. C.; Brooks, B. W. Comparison of Contaminants of Emerging Concern Removal, Discharge, and Water Quality Hazards among Centralized and on-Site Wastewater Treatment System Effluents Receiving Common Wastewater Influent. *Sci. Total Environ.* **2014**, 466–467, 976–984.
  - (62) Pochodylo, A.; Helbling, D. E. *Target and Suspect Screening for Micropollutants in the Hudson River Estuary during the 2015 Recreational Season*; Cornell University, 2015.
  - (63) Houtman, C. J.; ten Broek, R.; de Jong, K.; Pieterse, B.; Kroesbergen, J. A. Multicomponent Snapshot of Pharmaceuticals and Pesticides in the River Meuse Basin. *Env. Toxicol Chem* **2013**, 32 (11), 2449–2459.
  - (64) Yamamoto, H.; Nakamura, Y.; Moriguchi, S.; Nakamura, Y.; Honda, Y.; Tamura, I.; Hirata, Y.; Hayashi, A.; Sekizawa, J. Persistence and Partitioning of Eight Selected Pharmaceuticals in the Aquatic Environment: Laboratory Photolysis, Biodegradation, and Sorption Experiments. *Water Res* **2009**, 43 (2), 351–362.
  - (65) Isarain-Chavez, E.; Cabot, P. L.; Centellas, F.; Rodriguez, R. M.; Arias, C.; Garrido, J. A.; Brillas, E. L. B.-I.-C. Electro-Fenton and Photoelectro-Fenton Degradations of the Drug Beta-Blocker Propranolol Using a Pt Anode: Identification and Evolution of Oxidation Products. *J. Hazard. Mater.* **2011**, 185, 1228–1235.
  - (66) Kim, I.; Tanaka, H. Use of Ozone-Based Processes for the Removal of Pharmaceuticals Detected in a Wastewater Treatment Plant. *Water Environ. Res.* **2010**, 82 (4), 294–301.
  - (67) Morlay, C.; Laidin, I.; Chesneau, M.; Joly, J.-P. L. B.-0a6. Charbons Actifs et Traitement Des Eaux. *Actual. Chim.* **2006**, 295–296, 95–99.
  - (68) Anquandah, G. A. K.; Sharma, V. K.; Panditi, V. R.; Gardinali, P. R.; Kim, H.; Oturan, M. A. Ferrate(VI) Oxidation of Propranolol: Kinetics and Products. *Chemosphere* **2013**, 91 (1), 105–109.
  - (69) DeNardo, M. A.; Mills, M. R.; Ryabov, A. D.; Collins, T. J. Unifying Evaluation of the



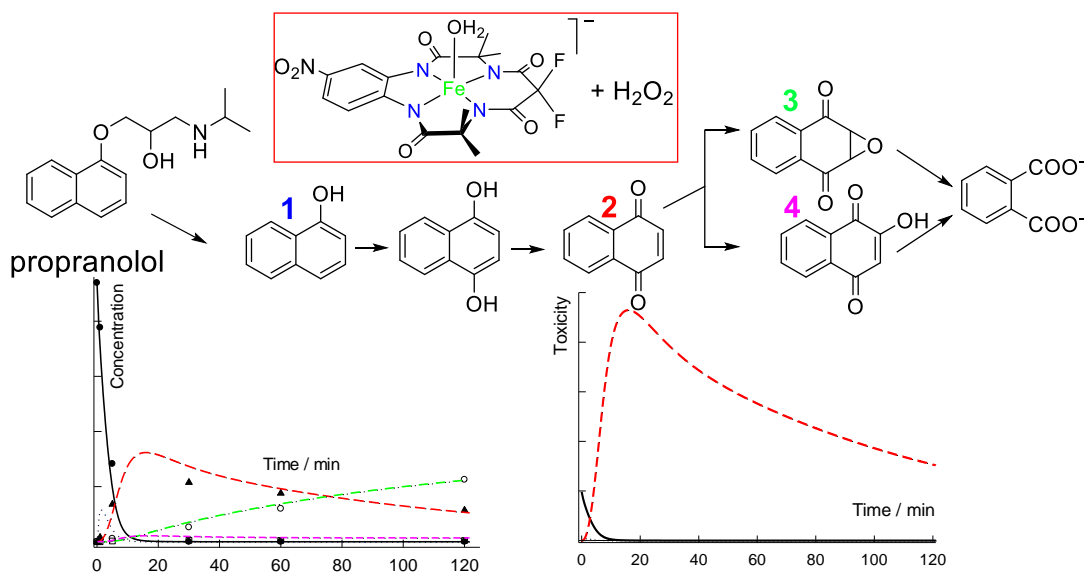
- Technical Performances of Iron-Tetra-Amido Macrocyclic Ligand Oxidation Catalysts. *J. Am. Chem. Soc.* **2016**, *138* (9), 2933–2936.
- (70) Chahbane, N.; Popescu, D. L.; Mitchell, D. A.; Chanda, A.; Lenoir, D.; Ryabov, A. D.; Schramm, K. W.; Collins, T. J. FeIII-TAML-Catalyzed Green Oxidative Degradation of the Azo Dye Orange II by H<sub>2</sub>O<sub>2</sub> and Organic Peroxides: Products, Toxicity, Kinetics, and Mechanisms. *Green Chem.* **2007**, *9* (1), 49–57.
  - (71) Ghosh, A.; Mitchell, D. A.; Chanda, A.; Ryabov, A. D.; Popescu, D. L.; Upham, E. C.; Collins, G. J.; Collins, T. J. Catalase-Peroxidase Activity of Iron(III)-TAML Activators of Hydrogen Peroxide. *J. Am. Chem. Soc.* **2008**, *130* (45), 15116–15126.
  - (72) Mitchell, D. A.; Ryabov, A. D.; Kundu, S.; Chanda, A.; Collins, T. J. Oxidation of Pinacyanol Chloride by H<sub>2</sub>O<sub>2</sub> Catalyzed by FeIII Complexed to Tetraamidomacrocyclic Ligand: Unusual Kinetics and Product Identification. *J. Coord. Chem.* **2010**, *63* (14–16), 2605–2618.
  - (73) Ryabov, A. D.; Sukbarev, V. S.; Alexandrova, L.; Le Lagadec, R.; Pfeffer, M. New Synthesis and New Bio-Application of Cyclometalated Ruthenium(II) Complexes for Fast Mediated Electron Transfer with Peroxidase and Glucose Oxidase. *Inorg. Chem.* **2001**, *40* (25), 6529–6532.
  - (74) Ellis, W. C.; Tran, C. T.; Denardo, M. A.; Fischer, A.; Ryabov, A. D.; Collins, T. J. Design of More Powerful Iron-TAML Peroxidase Enzyme Mimics. *J. Am. Chem. Soc.* **2009**, *131* (50), 18052–18053.
  - (75) Lakowicz, J. R. *Principles of Fluorescence Spectroscopy*; Plenum Press: NY, London, 1983.
  - (76) Eftink, M. R. Fluorescence Quenching: Theory and Applications. *Top. Fluoresc. Spectrosc.* **1991**, *2*, 53–126.
  - (77) Bisby, R. H.; Botchway, S. W.; Crisostomo, A. G.; Karolin, J.; Parker, A. W.; Schröder, L. Interactions of the  $\beta$ -Blocker Drug, Propranolol, with Detergents,  $\beta$ -Cyclodextrin and Living Cells Studied Using Fluorescence Spectroscopy and Imaging. *Spectroscopy* **2010**, *24* (1–2), 137–142.
  - (78) Bani-Yaseen, A. D. Synchronous Spectrofluorimetric Study of the Supramolecular Host-Guest Interaction of Beta-Cyclodextrin with Propranolol: A Comparative Study. *Spectrochim. Acta, Part A* **2015**, *148*, 93–98.
  - (79) Instrumentation for Fluorescence Spectroscopy BT - Principles of Fluorescence Spectroscopy; Lakowicz, J. R., Ed.; Springer US: Boston, MA, 2006; pp 27–61.
  - (80) Seely, G. R. Quenching of Pyrochlorophyll Fluorescence by Nitro Compounds. *J. Phys. Chem.* **1969**, *73* (1), 125–129.
  - (81) Ghosh, A.; Ryabov, A. D.; Mayer, S. M.; Horner, D. C.; Prasuhn Jr, D. E.; Sen Gupta, S.; Vuocolo, L.; Culver, C.; Hendrich, M. P.; Rickard, C. E. F.; Norman, R. E.; Horwitz, C. P.; Collins, T. J. Understanding the Mechanism of H<sup>+</sup>-Induced Demetalation as a Design Strategy for Robust Iron(III) Peroxide-Activating Catalysts. *J. Am. Chem. Soc.* **2003**, *125* (41), 12378–12379.
  - (82) Lauffer, R. B. Paramagnetic Metal-Complexes as Water Proton Relaxation Agents for Nmr Imaging - Theory and Design. *Chem. Rev.* **1987**, *87* (5), 901–927.
  - (83) Ramos, A.; Varani, G. A New Method To Detect Long-Range Protein– RNA Contacts: NMR Detection of Electron– Proton Relaxation Induced by Nitroxide Spin-Labeled RNA. *J. Am. Chem. Soc.* **1998**, *120* (42), 10992–10993.
  - (84) Mills, M. R.; Weitz, A. C.; Zhang, D. Z.; Hendrich, M. P.; Ryabov, A. D.; Collins, T. J. A “Beheaded” TAML Activator: A Compromised Catalyst That Emphasizes the Linearity between Catalytic Activity and PKa. *Inorg. Chem.* **2016**, No. 23, 12263–12269.
  - (85) Wishart, D. S.; Knox, C.; Guo, A. C.; Eisner, R.; Young, N.; Gautam, B.; Hau, D. D.; Psychogios, N.; Dong, E.; Bouatra, S.; Mandal, R.; Sinelnikov, I.; Xia, J.; Jia, L.; Cruz, J.

- A.; Lim, E.; Sobsey, C. A.; Shrivastava, S.; Huang, P.; Liu, P.; Fang, L.; Peng, J.; Fradette, R.; Cheng, D.; Tzur, D.; Clements, M.; Lewis, A.; De Souza, A.; Zuniga, A.; Dawe, M.; Xiong, Y.; Clive, D.; Greiner, R.; Nazyrova, A.; Shaykhutdinov, R.; Li, L.; Vogel, H. J.; Forsythe, I. HMDB: A Knowledgebase for the Human Metabolome. *Nucleic Acids Res* **2009**, *37* (Database issue), D603-10.
- (86) Bartolomei, M.; Bertocchi, P.; Cotta Ramusino, M.; Ciranni Signoretti, E. Thermal Studies on the Polymorphic Modifications of (R,S)-Propranolol Hydrochloride. *Thermochim. Acta* **1998**, *321* (1–2), 43–52.
- (87) Gordon, A. F.; Ford, R. A. *Chemist's Companion*; John Wiley & Sons: NY, 1972.
- (88) Yaya, A.; Tiburu, E. K.; Onwona-Agyeman, B.; Dodoo-Arhin, D.; Efavi, J. . A Comparative Study of DFT/LDA with Higher Levels of Theory on  $\pi$ - $\pi$  Interactions: A Typical Case for the Benzene Dimer. *J. Comput. Model.* **2014**, *4* (3), 27–42.
- (89) Takemura, H.; Kon, N.; Yasutake, M.; Nakashima, S.; Shinmyozu, T.; Inazu, T. The C-F $\cdots$ cation Interaction: An Ammonium Complex of a Hexafluoro Macrocyclic Cage Compound. *Chem. - Eur. J.* **2000**, *6* (13), 2334–2337.
- (90) Pauling, L. *The Nature of the Chemical Bond*, 3d ed.; Cornell University Press: Ithaca, New York, 1960.
- (91) Theodoridis, A.; Maigut, J.; Puchta, R.; Kudrik, E. V; van Eldik, R. Novel Iron(III) Porphyrine Complex. Complex Speciation and Reactions with NO and H<sub>2</sub>O<sub>2</sub>. *Inorg Chem* **2008**, *47* (8), 2994–3013.
- (92) Warner, G.; Mills, M.; Enslin, C.; Pattanayak, S.; Panda, C.; Sen Gupta, S.; Ryabov, A. D.; Collins, T. J. Reactivity of N-Tailed ('Biuret') TAMLs in Water: Kinetics of the Catalyzed Oxidation of Orange II by H<sub>2</sub>O<sub>2</sub>. Synthesis and X-Ray Characterization of an N-Phenyl Biuret TAML. *Chem. - Eur. J.* **2015**, *21* (16), 6226–6233.
- (93) Su, H.; Yu, C.; Zhou, Y.; Gong, L.; Li, Q.; Alvarez, P. J. J.; Long, M. Quantitative Structure–Activity Relationship for the Oxidation of Aromatic Organic Contaminants in Water by TAML/H<sub>2</sub>O<sub>2</sub>. *Water Res.* **2018**, *140*, 354–363.
- (94) Colin P. Horwitz;; Ghosh, A. Synthesis of Macrocyclic Tetraamido Compounds and New Metal Insertion Process. US7060818B2, 2006.
- (95) Ellis, W. C.; Tran, C. T.; Roy, R.; Rusten, M.; Fischer, A.; Ryabov, A. D.; Blumberg, B.; Collins, T. J. Designing Green Oxidation Catalysts for Purifying Environmental Waters. *J. Am. Chem. Soc.* **2010**, *132* (28), 9774–9781.
- (96) George, P. The Chemical Nature of the Second Hydrogen Peroxide Compound Formed by Cytochrome c Peroxidase and Horseradish Peroxidase. 1. Titration with Reducing Agents. *Biochem. J.* **1953**, *54* (2), 267–276.
- (97) O'Boyle, N. M.; Banck, M.; James, C. A.; Morley, C.; Vandermeersch, T.; Hutchison, G. R. Open Babel: An Open Chemical Toolbox. *J. Cheminf.* **2011**, *3*, 33.
- (98) Zhao, Y.; Truhlar, D. G. The M06 Suite of Density Functionals for Main Group Thermochemistry, Thermochemical Kinetics, Noncovalent Interactions, Excited States, and Transition Elements: Two New Functionals and Systematic Testing of Four M06-Class Functionals and 12 Other Function. *Theor. Chem. Acc.* **2008**, *120* (1–3), 215–241.
- (99) Frisch, M. J.; Trucks, G. W.; Schlegel, H. B.; Scuseria, G. E.; Robb, M. A.; Cheeseman, J. R.; Scalmani, G.; Barone, V.; Petersson, G. A.; Nakatsuji, H.; Li, X.; Caricato, M.; Marenich, A. V.; Bloino, J.; Janesko, B. G.; Gomperts, R.; Mennucci, B.; Hratchian, H. P.; Ortiz, J. V.; Izmaylov, A. F.; Sonnenberg, J. L.; Williams-Young, D.; Ding, F.; Lipparini, F.; Egidi, F.; Goings, J.; Peng, B.; Petrone, A.; Henderson, T.; Ranasinghe, D.; Zakrzewski, V. G.; Gao, J.; Rega, N.; Zheng, G.; Liang, W.; Hada, M.; Ehara, M.; Toyota, K.; Fukuda, R.; Hasegawa, J.; Ishida, M.; Nakajima, T.; Honda, Y.; Kitao, O.; Nakai, H.; Vreven, T.; Throssell, K.; Montgomery, J. A., Jr.; Peralta, J. E.; Ogliaro, F.; Bearpark, M. J.; Heyd, J. J.; Brothers, E. N.; Kudin, K. N.; Staroverov, V. N.; Keith, T. A.; Kobayashi,

- R.; Normand, J.; Raghavachari, K.; Rendell, A. P.; Burant, J. C.; Iyengar, S. S.; Tomasi, J.; Cossi, M.; Millam, J. M.; Klene, M.; Adamo, C.; Cammi, R.; Ochterski, J. W.; Martin, R. L.; Morokuma, K.; Farkas, O.; Foresman, J. B.; Fox, D. J. Gaussian 09, Revision D.01. *Gaussian, Inc., Wallingford CT*. 2009.
- (100) Marenich, A. V; Cramer, C. J.; Truhlar, D. G. Universal Solvation Model Based on Solute Electron Density and on a Continuum Model of the Solvent Defined by the Bulk Dielectric Constant and Atomic Surface Tensions. *J. Phys. Chem. B* **2009**, *113* (18), 6378–6396.

## Chapter 3

# To Sustainability via Analytical and Kinetic Characterization of Propranolol Fragments during Its TAML-Catalyzed Oxidation by $\text{H}_2\text{O}_2$ . Mass and Toxicity vs Time Profiles



### 3.1 INTRODUCTION

Our chemically polluted environment demands corrective action.<sup>1</sup> This general thesis is nowadays undeniable — nobody opposes it, at least openly. The problem is multidimensional. The largest dimension requires removal of aggressive chemicals, such as pesticides, herbicides, chlorinated hydrocarbons, drugs, etc., from air, soil, water—from everywhere. Many efforts are targeted at chemical and biochemical decomposition of environmental pollutants. The task is, however, very delicate and complicated. The single-step complete mineralization of a pollutant is barely possible because chemical, biochemical or other method degradations of a pollutant produce intermediates as single steps involve one and two-electron processes. The intermediates, unfortunately, may not degrade further and can be even be more toxic than their precursors. It is clearly insufficient is to destroy a targeted pollutant. Instead, authentic purification requires detailed scientific backing in which (i) the spectrum of each pollutants' intermediates formed prior final nontoxic mineralization are identified, and (ii) the targeted reduction in toxicity is achieved.<sup>2</sup> A key part of authentic purification involves estimation of the lifetimes of the intermediates, as this is key to their potential ecological impact.

A model of fully authenticated water purification is described in this work. By the example of the TAML-catalyzed oxidative degradation of propranolol (Chart 3.1), the widely used  $\beta$ -blocker drug,<sup>3</sup> to mineralization, aromatic intermediates were identified and some were isolated and characterized. Their concentration versus time profiles were constructed and the longevity of intermediates was estimated through a computer simulation of the entire catalytic process. The simulation afforded rate constants  $k_{II,S}$ , which were validated by direct kinetic study of these intermediates, as it is described for propranolol in chapter 2.<sup>4</sup> The experimental rate constants  $k_{II}$  agreed fully with  $k_{II,S}$  values obtained in a computer simulation. The match gives confidence that all the major intermediates were actually identified.

The oxidation system was comprised of hydrogen peroxide as the primary oxidant and an iron(III) TAML activator of hydrogen peroxide (Chart 3.1), a functional replica of peroxidase and peroxide short-circuited cytochrome P450 enzymes.<sup>5-8</sup>

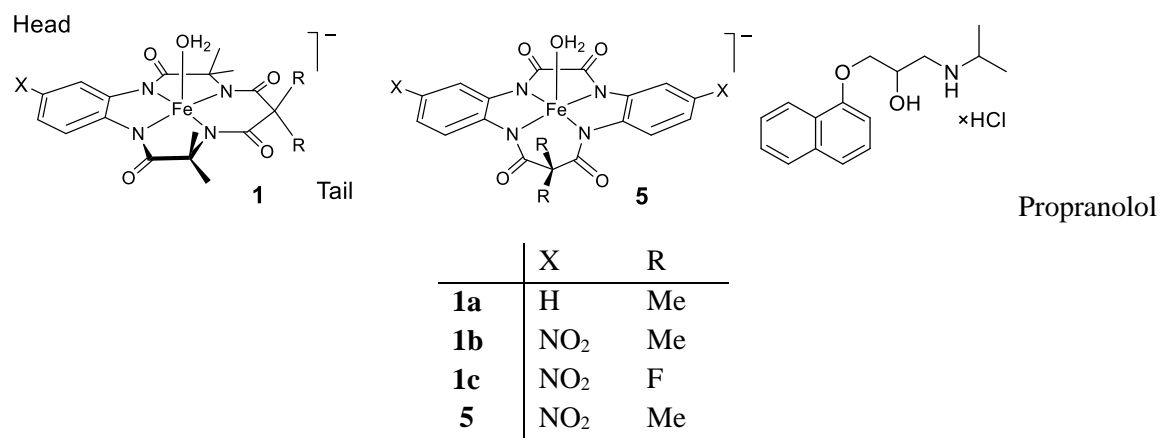
Scheme 3.1 Typical stoichiometric mechanism of oxidative catalysis by TAML activators.

Resting catalyst (such as **1**) + H<sub>2</sub>O<sub>2</sub>  $\rightleftharpoons$  Active catalyst (*k*<sub>I</sub>, *k*<sub>-I</sub>) (i)

Active catalyst + Substrate  $\rightarrow$  Resting catalyst + Product (*k*<sub>II</sub>) (ii)

In water, TAMLs catalyze in a ping-pong manner (Scheme 3.1) the oxidation of a broad spectrum of molecules including micropollutants, compounds that produce undesired effects at low concentrations.

Chart 3.1 Propranolol and TAML activators **1** and **5** used in this study.



The mechanism in Scheme 3.1, when the oxidation is not complicated by extra phenomena, leads to kinetic eq 3.1. The rate constant *k*<sub>-I</sub> is usually negligible.<sup>9</sup>

$$-\frac{d[S]}{dt} = \frac{k_I k_{II} [H_2O_2][S]}{k_{-I} + k_I [H_2O_2] + k_{II} [S]} [Fe_t^{III}] \quad (3.1)$$

Dynamic behavior of propranolol in the TAML/H<sub>2</sub>O<sub>2</sub> systems has been discussed in chapter 2

that was recently published.<sup>4</sup> In that study a focus was on propranolol itself, but a hunt for fragments generated from propranolol with their identification, kinetic characterization, mass/toxicity profiles is described herein.

## 3.2 RESULTS AND DISCUSSION

### 3.2.1 UPLC and GC-MS Identification of Fragments of TAML-Catalyzed Oxidation of Propranolol by $H_2O_2$ .

In chapter 2 we have shown that TAML activators do catalyze oxidation of propranolol by  $H_2O_2$  in aqueous media (pH 7–9) at 25 °C. Particularly efficient is TAML **1c**, which at 1  $\mu$ M loading digests all propranolol in a matter of 30 and 2 min at pH 7 and 9, respectively, as confirmed by UPLC using a fluorescent detector. No intermediates were detected with this technique. When the chromatograms were analyzed spectrophotometrically at 254 nm using a photo-diode array detector (Figure 3.1), several products with retention times exceeding that for propranolol (1.8 min) were observed.

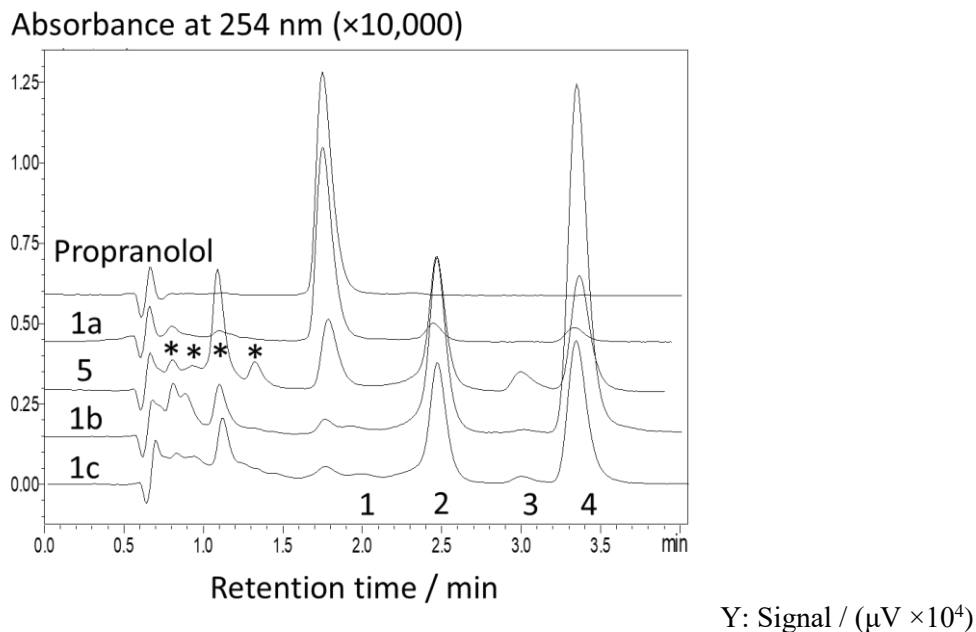


Figure 3.1 UPLC chromatograms of the products of degradation of propranolol by  $H_2O_2$  catalyzed by TAML activators (Chart 3.1) identified at 254 nm using a photo-diode array detector. Conditions: [TAML]  $1 \times 10^{-6}$  M, [propranolol]  $50 \times 10^{-6}$  M, [ $H_2O_2$ ]  $5 \times 10^{-3}$  M pH 7 (0.01 M phosphate),  $23 \pm 2$  °C, reaction time 2 h.



Both TAML activators studied (**1** and **5**) generate identical intermediates, amounts of which vary consistent with diverse catalytic activity of TAMLs toward both propranolol and degradation products. Less intermediate material was observed in case of **1c**, the most active toward propranolol.

The chromatograms have also peaks with retention times < 1.8 min (indicated by asterisks in Figure 3.1). Corresponding compounds are eluted almost immediately suggesting that they are more polar than propranolol, perhaps smaller organic molecules, products of deep fragmentation of propranolol. The ionic chromatography data presented below agree with this. Peaks 1–4 in Figure 3.1 arise from compounds less polar than propranolol and their characterization was our first key goal. To pursue this, several approaches have been applied with references to the results reported by other workers, who identified the products of oxidative degradation of propranolol using methods not involving TAML activators.<sup>10–12</sup>

The areas of peaks 1–4 plus that of propranolol were monitored multiple times over 8 h and plotted versus time. The representative, most diagnostic data for **1c** in Figure 3.6 indicate that the peak 4 compound appears first and is then further oxidized to peak 1–3 compounds. The highest yield of peak-4-material is achieved in a matter of ca. 30 min but its amount then further decreases (Figure 3.6). Note that peaks 1–3 and all other peaks disappear after 8 h in the **1c**/H<sub>2</sub>O<sub>2</sub> system.

The peak-4-material is 1,4-naphthoquinone (NO<sub>2</sub>). It was isolated using larger initial loadings of both propranolol and **1c**, and H<sub>2</sub>O<sub>2</sub> was added in multiple aliquots over ca. 24 h to minimize the catalytic (H<sub>2</sub>O<sub>2</sub> disproportionation) activity of **1c**<sup>13</sup> (see Experimental section). The isolated and purified material was characterized by <sup>1</sup>H NMR and mass-spectrometry (Figure 3.7); its authenticity as the peak-4-compound (Figure 3.1) was confirmed by running the reaction at a low H<sub>2</sub>O<sub>2</sub> concentration, when only peak 4 was detected, and executing UPLC of the reaction mixture

after addition of the 1,4-naphthoquinone standard (a spiking experiment) (Figure 3.8).

Correspondingly, peak 1–3 compounds derive from 1,4-naphthoquinone; their natures were identified by the GC-MS technique and confirmed by UPLC spiking experiments.

The gas chromatogram of the reaction products after their solid phase extraction into methanol contains two intense peaks and several peaks of much lower intensity (Figure 3.9). The major two correspond to unreacted propranolol (16.57 min) and 2,3-dihydro-2,3-epoxynaphthalene-1,4-dione ( $NO_2$ epo), 12.92 min, Figure 3.10; confirmed by matching MS pattern. This  $NO_2$ epo, could then give rise to one of the 1–3 peaks in Figure 3.1 and spiking experiments confirmed that this derivative was associated with peak 2 (Figure 3.8).

The nature of peak 3 compound was suggested by analysis of mass-spectra of the smaller peaks in Figure 3.9. The largest among the smallest peaks, with a retention time of 12.32 min, corresponds to the already identified 1,4-naphthoquinone — its GC-MS spectrum was indistinguishable from that in Figure 3.7C. The 13.08 min peak originates from 2-hydroxynaphthalene-1,4-dione ( $NO_2$ (OH), Figure 3.11), as confirmed by GC and mass-spectral analyses. The spiking experiment in Figure 3.8 associated it with peak 3 (Figure 3.1). Among other products tracked by GC-MS was 1-naphthol ( $NOH$ ), identified by the mass spectrum of the peak with retention time of 12.75 min in Figure 3.9, which was compared with the spectrum of the authentic 1-naphthol sample in Figure 3.12. Peak 1 in Figure 3.1 belongs to phthalic acid (spiking), a common product of oxidative degradation of propranolol identified by many workers.<sup>10,11</sup>

### ***3.2.2 Ionic Chromatography Identification of Fragments of TAML-Catalyzed Oxidation of Propranolol by $H_2O_2$ .***

Phthalic acid and small organic acids were also confirmed by ion chromatography (Figure 3.2; the reaction was run for 24 h). Acetate (10.8 min), oxamate (11.7 min) and phthalate (30.8 min) were reliably identified by running standards separately. The peak (\*\*) at ~36.9 min was not

identified. Phosphate (29 min) from the buffer and chloride (15.6 min) from the propranolol hydrochloride were also detected. Peaks marked with asterisk result from contamination in the original propranolol sample.

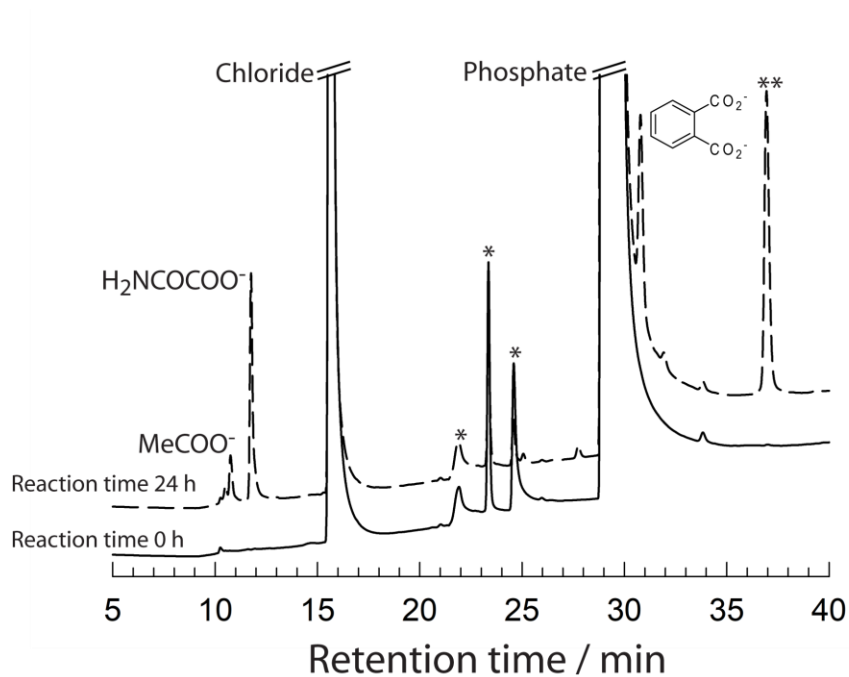


Figure 3.2 Ionic chromatogram of products of degradation of propranolol by  $\text{H}_2\text{O}_2$  catalyzed by **1c** identified using a conductivity detector. Conditions: [**1c**]  $1 \times 10^{-6}$  M, [propranolol]  $500 \times 10^{-6}$  M, [ $\text{H}_2\text{O}_2$ ]  $5 \times 10^{-3}$  M pH 7 (0.01 M phosphate), 25 °C, reaction time 24 h.

### 3.2.3 Tracing of Acetone by $^1\text{H}$ NMR.

We have previously found that products TAML-catalyzed degradation of organic compounds by  $\text{H}_2\text{O}_2$  may contain acetone as in the case of Bisphenol A.<sup>14</sup> Therefore,  $^1\text{H}$  NMR study of the reaction mixture was undertaken and acetone was detected at 2.26 ppm which is close to the common literature value of 2.23 ppm (Figure 3.13).

### 3.2.4 Building Concentration versus Time Profiles for ‘UPLC’ Products of TAML-catalyzed Oxidation of Propranolol by $H_2O_2$ .

Having peaks 1–4 identified, the qualitative concentration profiles in Figure 3.6 were quantified using the UPLC calibration curves for propranolol,  $NO_2$ ,  $NO_2$ epo, and  $NO_2(OH)$  (Figure 3.3, see Scheme 3.2 for abbreviations). The new profile reports on the mass balance during the catalyzed degradation of propranolol.

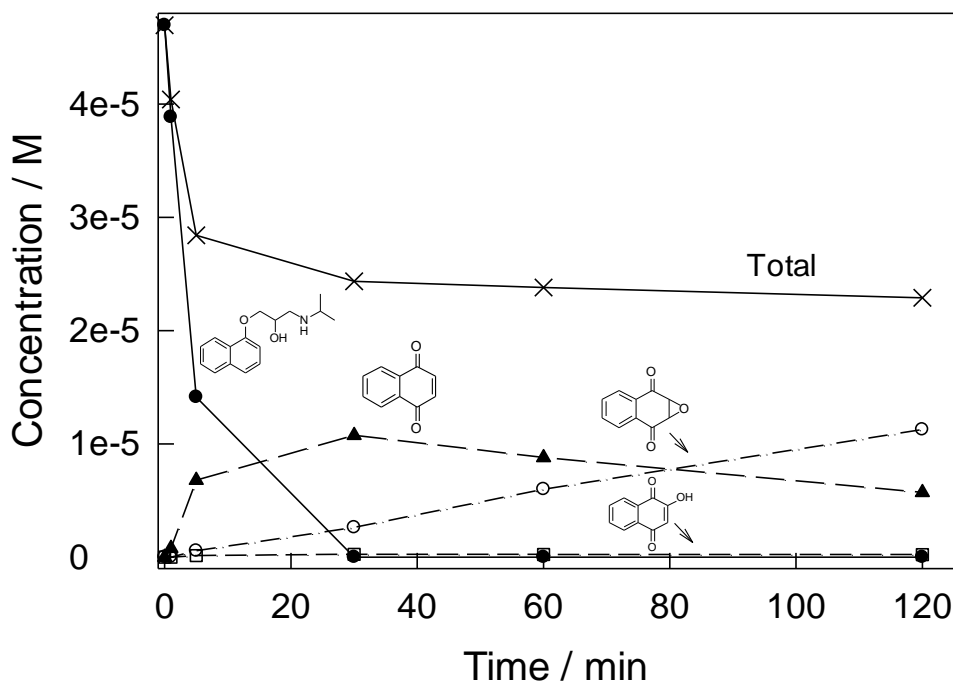


Figure 3.3 Concentration versus time profiles for propranolol and the products of its degradation identified by HPLC during **1c**-catalyzed degradation of propranolol by  $H_2O_2$ . Lines here are for emphasis only. The total line represents the concentration of all organic material in the graph. Conditions: [**1c**]  $1 \times 10^{-6}$  M, [propranolol]  $50 \times 10^{-6}$  M, [ $H_2O_2$ ]  $5 \times 10^{-3}$  M pH 7 (0.01 M phosphate), 25 °C.

The total concentration of all compounds in Figure 3.3 after 5 min is just  $2.84 \times 10^{-5}$  M, which corresponds to 61% of initial propranolol. Therefore, the quantitation of peaks 2–4 (peak 1 could not be quantified because of crowding) in Figure 3.1, is insufficient for complete characterization of degradation fragments of propranolol, at least of its “naphthalene” unit. Thus, it was essential

to add 1-naphthol, which was qualitatively traced by GC-MS, and 1,4-dihydroxynaphthalene  $N(OH)_2$ , an inevitable intermediate separating 1-naphthol and 1,4-naphthoquinone.<sup>15,16</sup>

### **3.2.5 Kinetics of Oxidation by $H_2O_2$ of Products of Propranolol Degradation, Uncatalyzed ( $NO_2$ ) and **1c**-Catalyzed ( $NOH$ , $NO_2epo$ , $NO_2(OH)$ ).**

This sub-study was undertaken with a further goal of a quantitative simulation of the data in Figure 3.3 and comparing 'theoretical' rate constants used in simulations with those measured experimentally. 1-Naphthol,  $NO_2epo$  and  $NO_2(OH)$ , similarly to propranolol, are predominantly oxidized by  $H_2O_2$  catalytically. Initial rates of disappearance of these compounds were measured as a function of  $H_2O_2$  concentration. Hyperbolic dependences obtained (Figure 3.14) were fitted to eq 1, which is consistent with the mechanism in Scheme 3.1, and the corresponding rate constants  $k_I$  and  $k_{II}$  are collected in Table 1.

Dual behavior of 1,4-naphthoquinone  $NO_2$  was discovered. It is presumably oxidized by  $H_2O_2$  through two parallel pathways leading to two different products. Direct oxidation of  $NO_2$  by  $H_2O_2$  affords the epoxide  $NO_2epo$  via the second-order pathway (eq 3.2). Interestingly, no  $NO_2(OH)$  was detected in this non-catalytic oxidation. However, oxidation of propranolol catalyzed by **1c** and **5** clearly showed the formation of  $NO_2(OH)$ . Therefore, it was assumed that  $NO_2(OH)$  is produced from  $NO_2$  catalytically according the rate law in eq 3.1.

$$\frac{d[NO_2epo]}{dt} = k_2[H_2O_2][NO_2] \quad (3.2)$$

1,4-Dihydroxynaphthalene is rapidly oxidized under the reaction conditions without **1c**. The reaction is sufficiently fast that its rate could not be reliably measured by conventional techniques.

Table 3.1 Experimentally measured ( $k_I$  and  $k_{II}$ ), theoretical ( $k_{II,S}$ ) rate constants (both for **1c**-catalyzed oxidation of propranolol, NOH, NO<sub>2</sub>epo, and NO<sub>2</sub>(OH); experimental ( $k_2$ ) and theoretical ( $k_{2,S}$ ) second order rate constants for direct oxidation of N(OH)<sub>2</sub> and NO<sub>2</sub> by H<sub>2</sub>O<sub>2</sub>. All rate constants are in M<sup>-1</sup> s<sup>-1</sup> at pH 7 and 25 °C.

Compound	$k_I$	$10^{-2} \times k_{II}$	$10^{-2} \times k_{II,S}$	$k_2$	$k_{2,S}$	LC <sub>50</sub> / mg L <sup>-1</sup> (ref)
Propranolol <sup>a)</sup>	90±10	146±2	170			2.48 ( <sup>17</sup> )
1-Naphthol (NOH)	112±7	500±200	930			3.96 ( <sup>18</sup> )
1,4-Dihydroxynaphthalene N(OH) <sub>2</sub>					3.5×10 <sup>3</sup>	
1,4-Naphthoquinone (NO <sub>2</sub> ) <sup>b)</sup>			35			
1,4-Naphthoquinone (NO <sub>2</sub> ) <sup>c)</sup>				(36±2)×10 <sup>-3</sup>	34×10 <sup>-3</sup>	0.11 ( <sup>19</sup> ) <sup>e)</sup>
2,3-Dihydro-2,3-epoxy-naphthalene-1,4-dione (NO <sub>2</sub> epo) <sup>d)</sup>	5.0±0.7	0.40±0.07	0.70			
2-Hydroxynaphthalene-1,4-dione (NO <sub>2</sub> (OH)) <sup>d)</sup>	107±2	200±10	500			25.7 ( <sup>20</sup> )

<sup>a)</sup> Data are from ref. <sup>4</sup>

<sup>b)</sup> NO<sub>2</sub>(OH) product.

<sup>c)</sup> NO<sub>2</sub>epo product via eq 2.

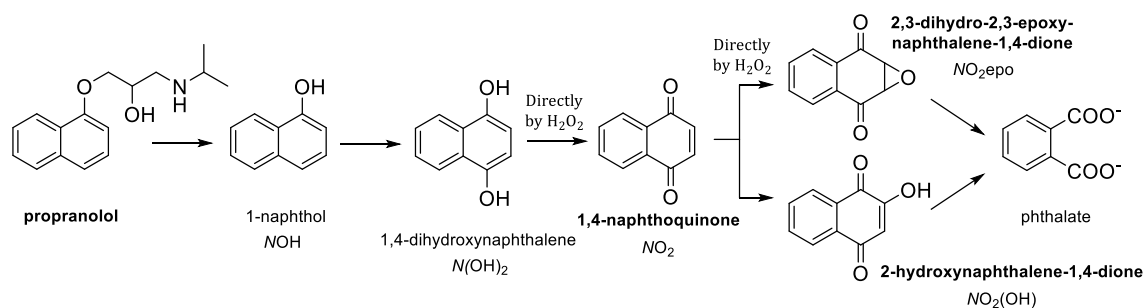
<sup>d)</sup> Phthalic acid product.

<sup>e)</sup> Value for 2-methy-1,4-naphthoquinone.

### 3.2.6 Computer Simulation of the Concentration/Time Profiles of Propranolol and Its Degradation Fragments.

The results presented above prove a chain of events in Scheme 3.2 during the TAML-catalyzed oxidative degradation of propranolol. Strictly speaking, Scheme 3.2 illustrates transformations of a naphthalene unit of the drug. The compounds set in bold were quantified by UPLC. The formation of 1-naphthol was qualitatively confirmed by GC-MS. 1,4-Dihydroxynaphthalene, a postulated intermediate separating 1-naphthol and 1,4-naphthoquinone, is rapidly non-catalytically oxidized into the latter under the reaction conditions.<sup>15,16</sup> It thus became feasible to simulate using a KinTek program the entire "naphthalene" sub-story of the **1c**-catalyzed oxidation of propranolol orienting at the values of available rate constants  $k_{II}$  and  $k_2$  for the compounds shown in Scheme 3.2 and Table 1

Scheme 3.2 Chain of events associated with the **1c**-catalyzed oxidative degradation of the naphthalene unit of propranolol by  $H_2O_2$  at pH 7 and 25 °C. Intermediates quantified against standard compounds are set in bold; 1-naphthol was identified by GC-MS. 1,4-Dihydroxynaphthalene is a postulated intermediate separating 1-naphthol and 1,4-naphthoquinone. See text for details.



. A veracity criterion used was the best visual match between the experimental data points for the quantified compounds set in bold and the calculated concentration versus time profiles. The TAML catalytic mechanism as in Scheme 3.1 was applied using the previously obtained rate constant  $k_I$  ( $90 \text{ M}^{-1} \text{ s}^{-1}$ ) measured with propranolol as an electron donor.<sup>4</sup> The value of  $k_{II}$  was not

available for 1,4-naphthoquinone and therefore an arbitrary value of  $k_{\text{IL,S}}$  was used. Preliminary efforts were made on the assumption that the catalytic activity of the TAML catalyst **1c** *does not* change through the entire time span of Figure 3.3.

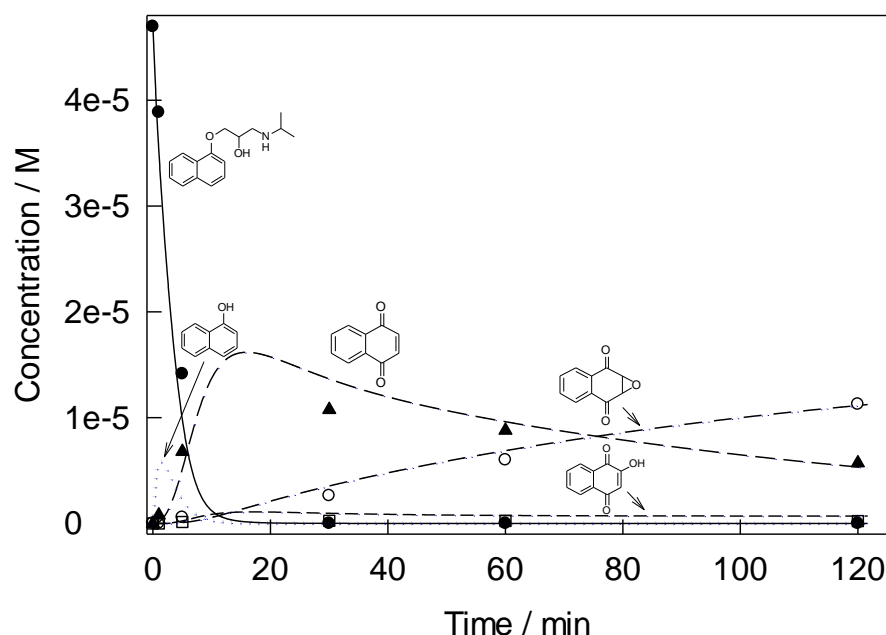


Figure 3.4 Concentration versus time profiles for propranolol and its fragments during **1c**-catalyzed oxidation of propranolol by  $\text{H}_2\text{O}_2$ . Lines are calculated using rate constants  $k_{\text{IL,S}}$  estimated using KinTek software which gave the best visual match with the experimental data points. The operational instability of **1c** (eq *iii*) with  $k_i$  of  $1.7 \times 10^{-3} \text{ s}^{-1}$  was taken into account. See legend to Figure 3.3 for conditions and text for more details.

However, if the operational instability of TAML catalysts was neglected in the analyses satisfactory matches between experimental and computed data could not be obtained. Much better agreement (Figure 3.4) was reached when the operational instability<sup>21–23</sup> was taken into account, i.e. step (*iii*) was added to the mechanism in Scheme 3.1, with the rate constant  $k_i$  of  $1.7 \times 10^{-3} \text{ s}^{-1}$ , which is very close to  $1.1 \times 10^{-3} \text{ s}^{-1}$  measured for **1c** under the same conditions.<sup>22</sup> The lines here are



calculated concentration vs time profiles using the catalytic rate constants  $k_{II,S}$  or the values of  $k_{2,S}$  when intermediates are directly oxidized by  $H_2O_2$ .



### 3.2.7 "Dark (Toxic) Side of the Moon".

At first glance, the concentration versus time profiles in Figure 3.4 leave the impression that the research goal has been successfully achieved — the primary target, propranolol, is rapidly destroyed, aromatic fragments are generated in lower concentrations and eventually disappear after 24 h. However, no one should conclude from the data in Figure 3.4 that we have established a successful degradation because of potential toxicity issues. While it is true that concentrations of intermediate compounds presented in Scheme 3.2 are lower than that of propranolol, in theory their toxicities could be higher and their impact on the environment could be seriously negative especially if incomplete degradation and high toxicity were to come together in a real treatment process. If the toxicity is developmental, it would be hard to detect by current regulatory approaches. This concern can be addressed systematically by first examining the acute toxicities of the intermediates and how the overall toxicity evolves as the process proceeds. Concentration profiles such as in Figure 3.4 should be accompanied by toxicity profiles in which the changing concentrations of intermediates over time are mapped on to the corresponding toxicities of preferably all compounds prior to their complete breakdown.

Just as the toxicities of chemicals to one and the same model (species, embryos, plants, etc.) are different;<sup>24</sup> the toxicities of one and the same chemical to various models can also be different. Thus, individual chemical toxicity comparisons will always be limited by the choice of the toxicity assay. The correspondence between the toxicity evolution of an individual compounds decay and the real world implications can be enhanced by choosing a model with respect to which

the toxicities of a broad spectrum of chemicals have been determined under comparable conditions, since even solution pH may affect toxicity.<sup>25</sup> Such information is, unfortunately, very limited. Although the data base of the Environmental Protection Agency (EPA) is colossal,<sup>24</sup> the specified above information is missing. We have previously operated with the toxicity of chemicals and the products of their decomposition toward zebrafish development,<sup>14,26,27</sup> a widely used model.<sup>28</sup> A SciFinder search was performed to find the LC<sub>50</sub> (lethal concentration, 50%) values for compounds listed in Scheme 3.2. Partial success was achieved by the finding of LC<sub>50</sub> values (Table 1) for propranolol<sup>17</sup>, 1-naphthol<sup>18</sup> and 2-hydroxynaphthalene-1,4-dione.<sup>20</sup> The toxicity versus time profile has been built, in which LC<sub>50</sub> for 2-methy-1,4-naphthoquinone<sup>19</sup> was used as an approximation for the toxicity of 1,4-naphthoquinone.

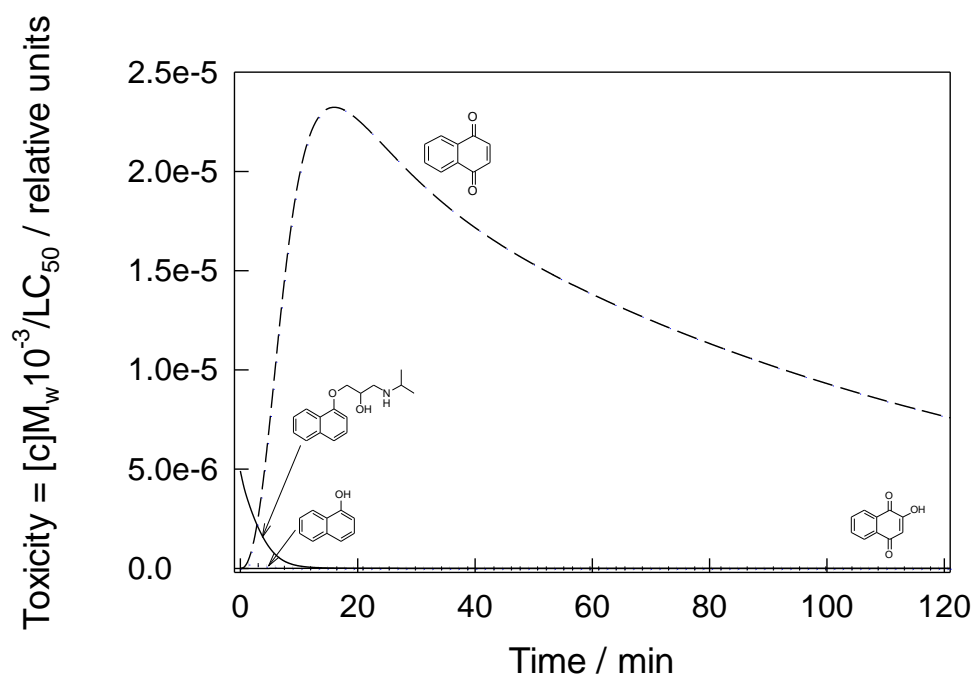


Figure 3.5 Calculated toxicity versus time profile for propranolol and its fragments during **1c**-catalyzed oxidation of propranolol by H<sub>2</sub>O<sub>2</sub>. See caption to Figure 3.4 for conditions and text for details.

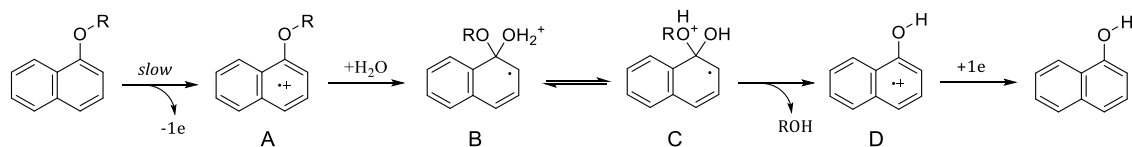
The toxicity versus time profile in Figure 3.5 was calculated using the data in Figure 3.4 and  $LC_{50}$  values in Table 1. Concentrations in Figure 3.4 were converted to  $mg\ L^{-1}$  and then divided by a respective  $LC_{50}$  value. Toxicities in Figure 3.5 are thus normalized values that show numbers of 50% lethal events at given concentrations. Although the calculated toxicity profile is incomplete because only four of seven participants in Scheme 3.2 were taken into account, its significance is obvious. The concentration of a targeted threat, propranolol, goes down whereas zebrafish toxicity increases almost five-fold due to accumulation of 1,4-naphthoquinone. Fortunately, it is a temporary increase since 1,4-naphthoquinone is not detectable after 8 h of the  $H_2O_2$ /TAML treatment (Figure 3.6).

Needless to say, a toxicity profile will not be as in Figure 3.5, if a model other than zebrafish is selected, though any alternative should indicate a potential environmental threat, if such exists. Therefore, data as in Figure 3.5 (toxicity profile) are similarly valuable as data in Figure 3.4 (mass profile) particularly when toxicology is prioritized. It is also worth mentioning that a real situation is surely more complicated because the profiles as in Figure 3.5 are made on the assumption that toxicity is proportional to concentration. Such model cannot predict low-dose effects, the nonlinear relationships between dose and effect which are most vividly revealed for endocrine system disrupting chemicals.<sup>29</sup> In the case of TAML catalysis, changing solution species also brings the potential complication of changing catalyst inhibitions showing just how complicated the impact of these systems on the real world could be at least before the processes reach mineralization. This highlights the argument that an ideal TAML process should be completed prior to release of the treated water to the environment and that the systems should be set up to maximize the mineralization of the treated pollutants.

### 3.2.8 Mechanistic Considerations.

As postulated by several groups,<sup>10–12</sup> a key initial step in the degradation of propranolol is its conversion to 1-naphthol as a result of a cleavage of either the O–C<sub>aryl</sub> or O–C<sub>alkyl</sub> bond. Note that the nature of this step has never been mechanistically discussed in any detail. Propranolol, as in this study, is destroyed oxidatively, though by stoichiometry if not mechanism, 1-naphthol formation is a hydrolytic non-redox substitution reaction in which hydroxide is an incoming group. TAMLs catalyze the reaction at pH 7 and therefore the concentration of OH<sup>–</sup> is extremely low. Water as a nucleophile is insufficiently reactive toward propranolol—otherwise the drug should be degraded in pure water. Our data reported here and previously,<sup>4</sup> show (see also Scheme 3.1) that the rate of propranolol degradation is limited by its interaction with an oxidized TAML activator (Active catalyst), which is presumably involved in a one-electron transfer opening a door for succeeding hydrolytic transformation. The naphthalene ring of propranolol is a plausible target for electron abstraction. If this is the case, electron transfer from propranolol at presumably TAML iron(IV)oxo intermediate should afford radical-cation **A** (Scheme 3) which might be more electrophilic than propranolol itself. Hypothetically, radical-cation **A** may be a subject of the ipso attack by H<sub>2</sub>O to afford **B**. The tautomeric equilibrium should create a better leaving group ROH within **C**. 1-Naphthol is finally produced after one electron transfer at **D**; iron(III) in the resting state of TAML could be a plausible electron donor.

Scheme 3.3 Postulated mechanism of oxidatively induced hydrolysis of propranolol to 1-naphthol during **1c**-catalyzed oxidative degradation of former by H<sub>2</sub>O<sub>2</sub>.



Formally, the mechanism in Scheme 3 is *oxidatively assisted (ether) hydrolysis*. Provided "ether" is ignored, the term is not entirely new and has previously been used in connection with

hydrolysis of allylic iodides.<sup>30</sup> Applied to nucleophilic substitution in aromatic series, first Alder<sup>31</sup> and later Eberson<sup>32</sup> used alternative, S<sub>ON</sub>2 terminology (nucleophilic substitution catalyzed by an oxidant), which corresponds exactly to the events in Scheme 3. In all cases an oxidant increases electrophilicity of a substrate due to an abstraction of electron and a subsequent nucleophilic attack becomes more feasible.

The mechanism in Scheme 3 assumes a radical-cation intermediate. Though no radical species were so far detected by EPR spectroscopy in the propranolol/**1c**/H<sub>2</sub>O<sub>2</sub> system, a radical species was trapped in the case of 1-naphthol (Figure 3.15), which in deprotonated form should obviously form more stable radicals compared to parent propranolol. Here TAML activators match catalysis by horseradish peroxidase, in which the generation of naphthoxy or a naphthoxy-derived radical was reported.<sup>33</sup> It is very likely that oxidatively assisted non-redox processes occur in other TAML-catalyzed environmentally important transformations.<sup>34</sup> Characterizing such mechanisms is challenging and these options should always be considered in future studies.

### 3.3 CONCLUSIONS

Deep analytical and kinetic studies made it possible to quantify the aromatic products of energy-saving oxidative degradation of propranolol by  $\text{H}_2\text{O}_2$  catalyzed by the TAML activator **1c** at ambient temperature and neutral pH. Time-dependent mass and toxicity profiles have been constructed from kinetics and toxicity data to illustrate for the first time that a substantial decrease in concentrations of a targeted substrate and its products of its degradation does not guarantee environmental security, at least while the process is in motion, because the overall toxicity of the reaction soup may temporally increase due to the accumulation of more toxic degradation intermediates. Therefore, mass/toxicity versus time profiles should be considered together to provide more complete information on potential environmental effects of decontamination procedures.

### 3.4 EXPERIMENTAL

#### 3.4.1 Materials.

TAML activator **1a** was obtained from GreenOx; other activators were synthesized according to the published procedures.<sup>35–37</sup> Buffer solutions were made using  $\text{KH}_2\text{PO}_4$  (Acros) or  $\text{K}_2\text{HPO}_4$  (Merck); the pH was adjusted with concentrated solutions of KOH or  $\text{H}_3\text{PO}_4$ . Hydrogen peroxide (30%) was purchased from Fischer. Catalase from bovine liver (lyophilized powder, 2000-5000 units  $\text{mg}^{-1}$  of protein) was purchased from Sigma. ( $\pm$ )-Propranolol hydrochloride (>99%), sodium nitrite, sodium nitrate, sodium acetate, phthalic acid dipotassium salt, sodium pyruvate, sodium oxalate, sodium oxamate, maleic acid disodium salt, and sodium chloride were purchased from Sigma and used as received. Methanol and water (both HPLC grade) were obtained from Fischer and used for liquid or ion chromatography without additional purification.

#### 3.4.2 Instrumentation.

UV-vis measurements were performed using an Agilent 8453 instrument with an attached temperature controller. The pH measurements were made using an Accumet Basic AB15 pH meter from Fischer Scientific. UPLC studies were performed with a Shimadzu LC system with LC 20AB pump, SIL 20A autosampler, CTO 20A column oven, and an RF 20A XS fluorescence detector. A Kinetex (Phenomenex) 5  $\mu\text{M}$  EVO C18 100A column ( $4.6 \times 50$  mm) was used for all kinetic analyses. The LC method consisted of 1  $\text{mL min}^{-1}$  flow rate, 35% methanol in pH 3 phosphate buffer (0.01 M), 40 °C column temperature, and fluorescence detection with 230 nm excitation and 340 nm emission. The sample injection volume for the analyses was 10  $\mu\text{L}$  and the data was automatically integrated and analyzed using Lab Solutions software. Ion chromatography analyses were performed using the Thermoscientific Dionex Ion chromatography system (ICS) 5000+ with Dionex ICS-5000+ dual pump, Dionex ICS-5000+ eluent generator, Dionex ICS-5000+ detector/chromatography module housing a conductivity

detector, and a Thermo Scientific Dionex AS-AP autosampler. A Dionex IonPac CG12 A  $4 \times 50$  mm guard column and a Dionex AS11HC  $4 \times 250$  mm column were used throughout. Analyses were performed under gradient conditions with concentration of KOH (mobile phase) being 1 (5 min), 15 (14 min), 30 (23 min) and 60 mM (40 min). The IC method under gradient conditions comprised of  $0.9 \text{ mL min}^{-1}$  flow rate, and an oven temperature of  $30^\circ\text{C}$  and  $25 \text{ }\mu\text{L}$  injection volume. The mobile phase was prepared with deionized water from a Barnstead Nanopure system. Data were analyzed using Chromeleon Chromatography Version 7 software. Gas chromatography-mass spectrometry analyses were performed with a Restek Rxi® -XLB (30 m,  $0.25 \text{ mm ID}$ ,  $0.25 \text{ }\mu\text{M}$ ) column using a Thermo Finnigan gas chromatograph (GC) equipped with a Trace DSQ mass spectrometer, a programmable temperature vaporization (PTV) injector, and a COMBI PAL autosampler (LEAP technologies, CTC Analytics). Helium was used as a carrier gas in a constant flow mode of  $1 \text{ mL min}^{-1}$ . Each GC-MS analysis took 22 min. The chromatographic oven temperature first 4 min was  $40^\circ\text{C}$ , increased to  $300^\circ\text{C}$  at a speed of  $20^\circ\text{C min}^{-1}$  till 17<sup>th</sup> minute and then was kept at  $300^\circ\text{C}$ . An injection port temperature of  $240^\circ\text{C}$  and a transfer line temperature of  $300^\circ\text{C}$  were employed. The ion source was kept at  $200^\circ\text{C}$ . The mass spectrometer was operated in a scan mode (scan range  $m/z$  50-1000) and it was turned on after 4 min and ended at 22 min for each analysis. The electron ionization mode was applied (70 eV). All samples were analyzed in a positive ionization mode. The sample ( $10 \text{ }\mu\text{L}$ ) was injected in a split mode (split ratio 10). GC-MS data was processed with Xcalibur software.  $^1\text{H}$  NMR data were collected at  $25^\circ\text{C}$  on a Bruker Avance III 500 MHz spectrometer and processed with Bruker TopSpin 3.5 software.

#### ***3.4.3 Analyses for Propranolol Fragments.***

Experiments for TAML-catalyzed oxidation of Propranolol using HPLC has been previously described in chapter 2. Aliquots of the reaction mixture, at suitable time intervals, were analyzed



by UPLC, IC, GC-MS and  $^1\text{H}$  NMR. Intermediates and product ions were confirmed either by spiking standards to the reaction mixtures or by running a standard separately under similar conditions. A small change in retention times were observed for Propranolol and its fragment compounds post UPLC instrumental servicing and tubes replacement (Figure 3.1 and Figure 3.8). However, the trend of peak appearance and their spacing ratio remained consistent throughout.

#### ***3.4.4 Kinetics of Oxidation of Propranolol Fragments.***

Kinetics studies of **1c**-catalyzed oxidation of 2,3-dihydro-2,3-epoxy-naphthalene-1,4-dione ( $\text{NO}_2\text{epo}$ ) and 2-hydroxynaphthalene-1,4-dione ( $\text{NO}_2(\text{OH})$ ) were performed by UV/vis spectroscopy. Initial rates were determined by monitoring a decrease in absorbance at 275 ( $\epsilon = 5840 \text{ M}^{-1} \text{ cm}^{-1}$ ) and 460 nm ( $\epsilon = 3000 \text{ M}^{-1} \text{ cm}^{-1}$ ) for  $\text{NO}_2\text{epo}$  and  $\text{NO}_2(\text{OH})$ , respectively. The oxidation of 1-naphthol was followed by measuring absorbance accumulation at 520 nm<sup>38</sup> using the estimated value  $\epsilon = 3000 \text{ M}^{-1} \text{ cm}^{-1}$ . Kinetics of non-catalyzed oxidation of 1,4-naphthoquinone by  $\text{H}_2\text{O}_2$  was monitored by a decrease in absorbance at 345 nm ( $\epsilon = 3320 \text{ M}^{-1} \text{ cm}^{-1}$ ). Reaction mixtures were prepared by adding suitable amounts of the stock solutions of naphthalene derivative **1c** (for catalyzed reactions) and phosphate buffer and a reaction was initiated by adding  $\text{H}_2\text{O}_2$ . Runs were conducted at 25 °C in 0.01 M phosphate buffer. Stock solutions of **1c** ( $5 \times 10^{-3} \text{ M}$ ), naphthalene derivative ( $5 \times 10^{-3} \text{ M}$ ), and  $\text{H}_2\text{O}_2$  (1 M) were prepared in HPLC grade water. Solutions of  $\text{H}_2\text{O}_2$  were standardized by UV spectroscopy at 230 nm in water ( $\epsilon = 72.4 \text{ M}^{-1} \text{ cm}^{-1}$ ).<sup>39</sup> All the simulations were developed using the software KinTek Explorer ver. 6.<sup>40</sup>

#### ***3.4.5 Isolation of 1,4-Naphthoquinone.***

Degradation of propranolol was conducted by dissolving 100 mg (0.34 mmol) propranolol hydrochloride in 200 mL of HPLC grade water. An appropriate volume of the catalyst stock solution was added to give the catalyst concentration of  $1 \times 10^{-6} \text{ M}$ . Hydrogen peroxide solution

was added in multiple aliquots every ca. 24 h over 10 days (total amount added 15.2 mmol). 1,4-Naphthoquinone was then isolated by performing a solid-phase extraction(SPE) of the aqueous degradation mixture into 80 mL methanol and the solvent was removed by rotary evaporation. The brownish-red residue was dissolved in a minimum amount of ethanol and loaded onto a basic silica flash column. The elution was performed using a gradient method starting with 60:40:1 EtOAc:petroleum ether:NEt<sub>3</sub> progressing incrementally to the 50:50:1 ethanol: EtOAc:NEt<sub>3</sub>. Yellow fractions containing 1,4-naphthoquinone were eluted first, combined and the solvent was removed by rotary evaporation. The yellow liquid obtained was further purified by flash column chromatography using a solvent gradient from 10:90 EtOAc:petroleum ether to 100% ethyl acetate. The solution of 1,4-naphthoquinone was dried in air, the product dissolved in *d*<sub>4</sub>-methanol and analyzed by <sup>1</sup>H NMR and GC-MS (see Appendix).

### 3.5 APPENDIX

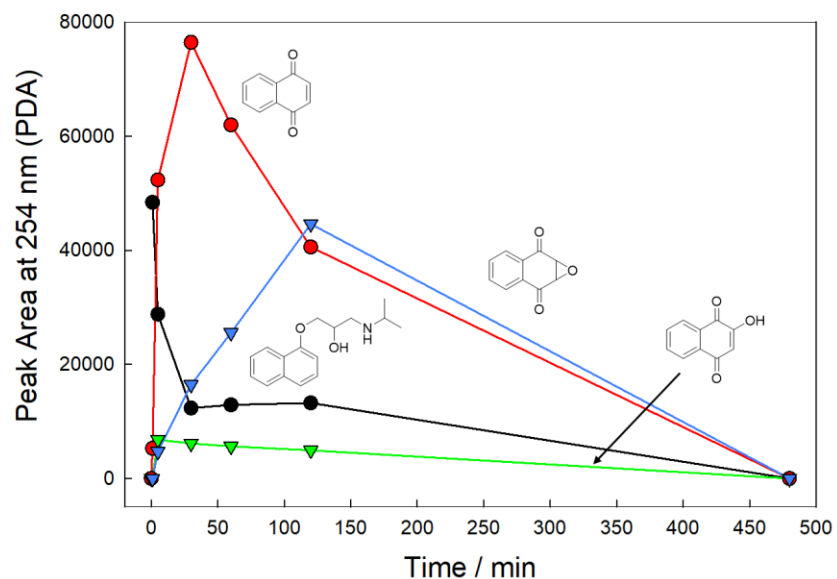


Figure 3.6 Peak areas at 254 nm, using photo-diode array detector, of peaks 1–4 in Figure 3.1 for **1c**-catalyzed degradation of propranolol by  $\text{H}_2\text{O}_2$  after 8 h. Lines are for emphasis only. Reaction conditions:  $[\mathbf{1c}] = 1 \times 10^{-6} \text{ M}$ ,  $[\text{H}_2\text{O}_2] = 5 \times 10^{-3} \text{ M}$ ,  $[\text{propranolol}] = 50 \times 10^{-6} \text{ M}$ . 0.01 M phosphate buffer, pH 7, 25 °C

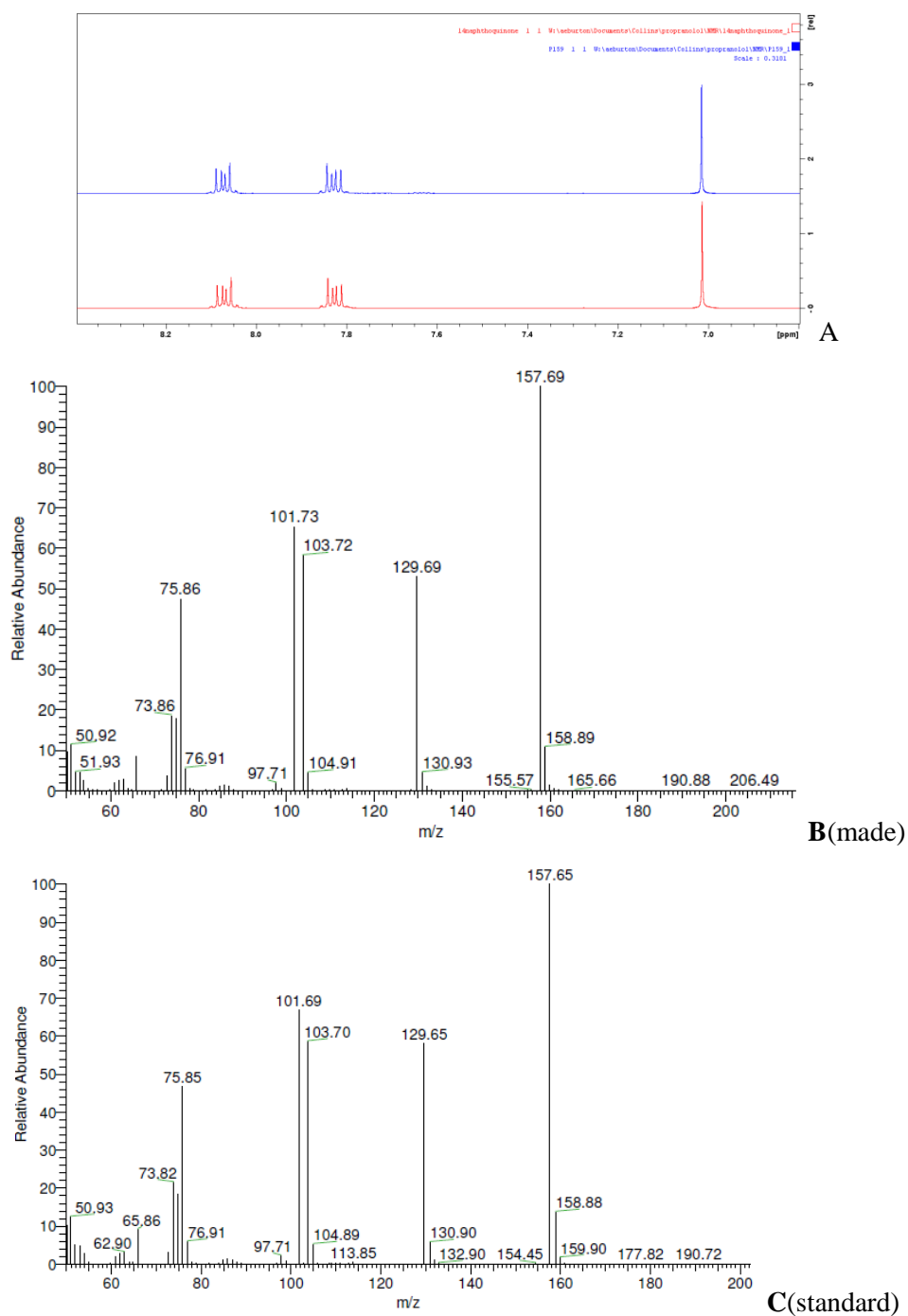


Figure 3.7 **(A)**  $^1\text{H}$  NMR spectra (in methanol- $\text{d}_4$ ) of experimentally obtained (blue, top) and standard (red, bottom) 1,4-naphthoquinone. **(B and C)** Mass spectra of 1,4-naphthoquinone obtained from propranolol **(B)** and standard sample **(C)** in a positive ionization mode.

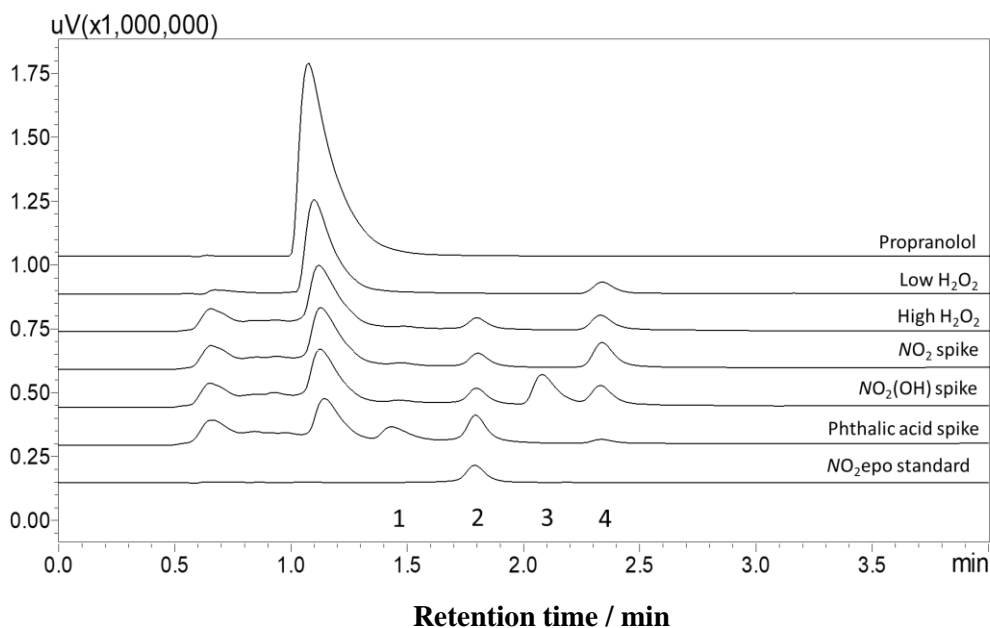


Figure 3.8 HPLC chromatograms of the products of degradation of propranolol by  $\text{H}_2\text{O}_2$  catalyzed by **1c**, identified at 254 nm using a photo-diode array detector, under different reaction conditions and upon spiking with different chemical standards. Reaction conditions: [**1c**] =  $1 \times 10^{-6}$  M,  $[\text{H}_2\text{O}_2]$  =  $5 \times 10^{-4}$  M (low) and  $5 \times 10^{-3}$  M (high), [propranolol] =  $50 \times 10^{-6}$  M. 0.01 M phosphate buffer, pH 7, 25 °C. [Stock solutions of Intermediate standards] =  $5 \times 10^{-4}$  M.

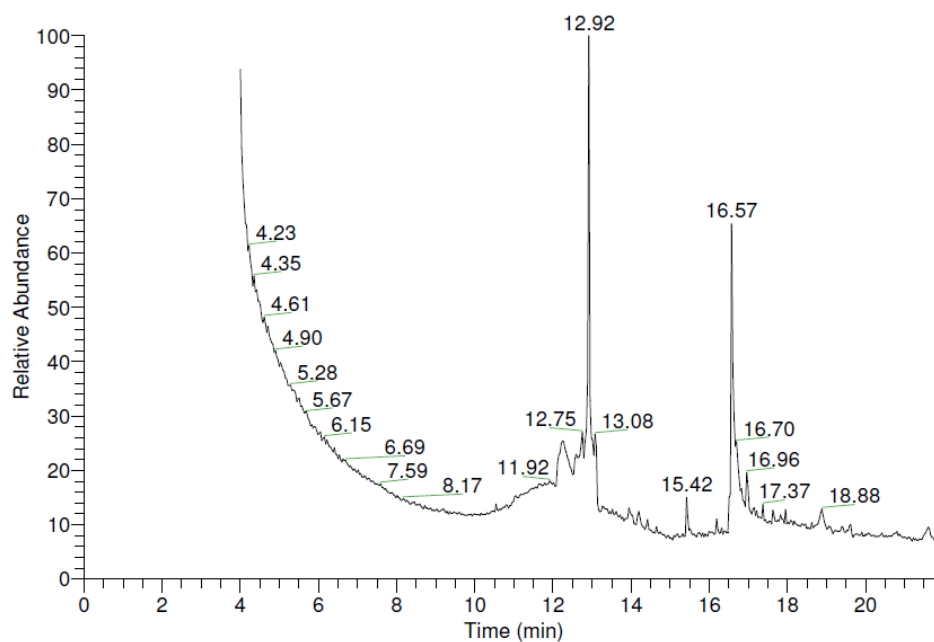


Figure 3.9 Gas chromatogram of the products of **1c**-catalyzed oxidation of propranolol by  $\text{H}_2\text{O}_2$  after the solid phase extraction into methanol. Conditions: [propranolol] =  $1.7 \times 10^{-3}$  M, [**1c**] =  $1 \times 10^{-6}$  M,  $[\text{H}_2\text{O}_2]_{\text{total}}$  =  $76 \times 10^{-3}$  M, unbuffered HPLC water, 25 °C. Aliquots of Hydrogen peroxide were added over 10 days. The aqueous mixture after 10 days was solid phase extracted into methanol.

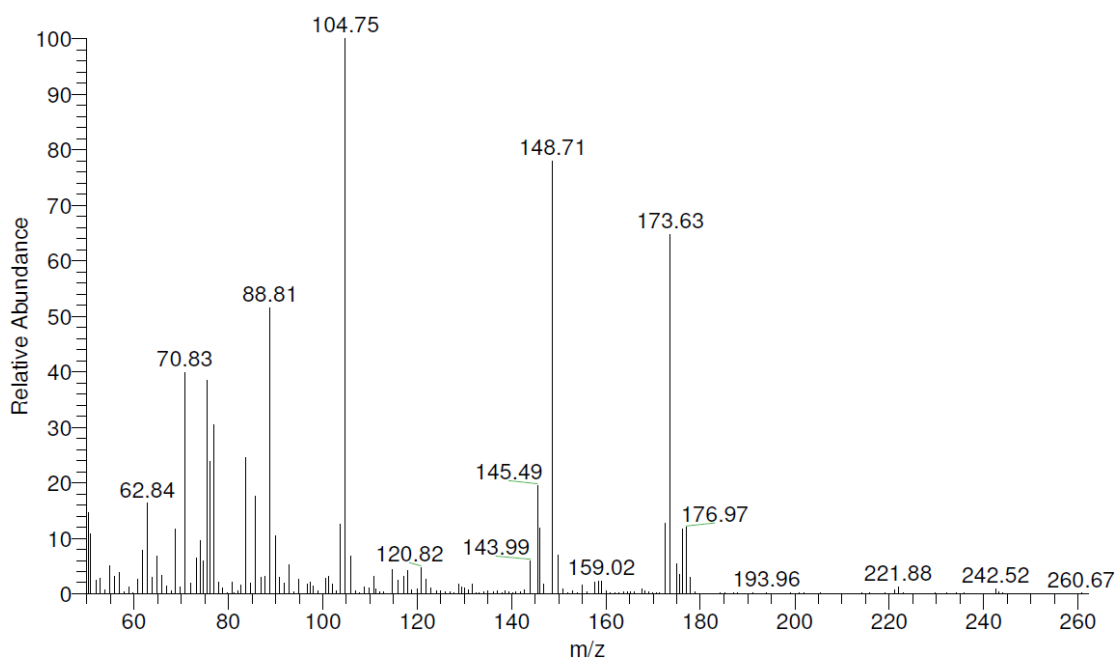


Figure 3.10 Mass spectrum of the peak with retention time 12.92 min ascribed to 2,3-dihydro-2,3-epoxy-naphthalene-1,4-dione.

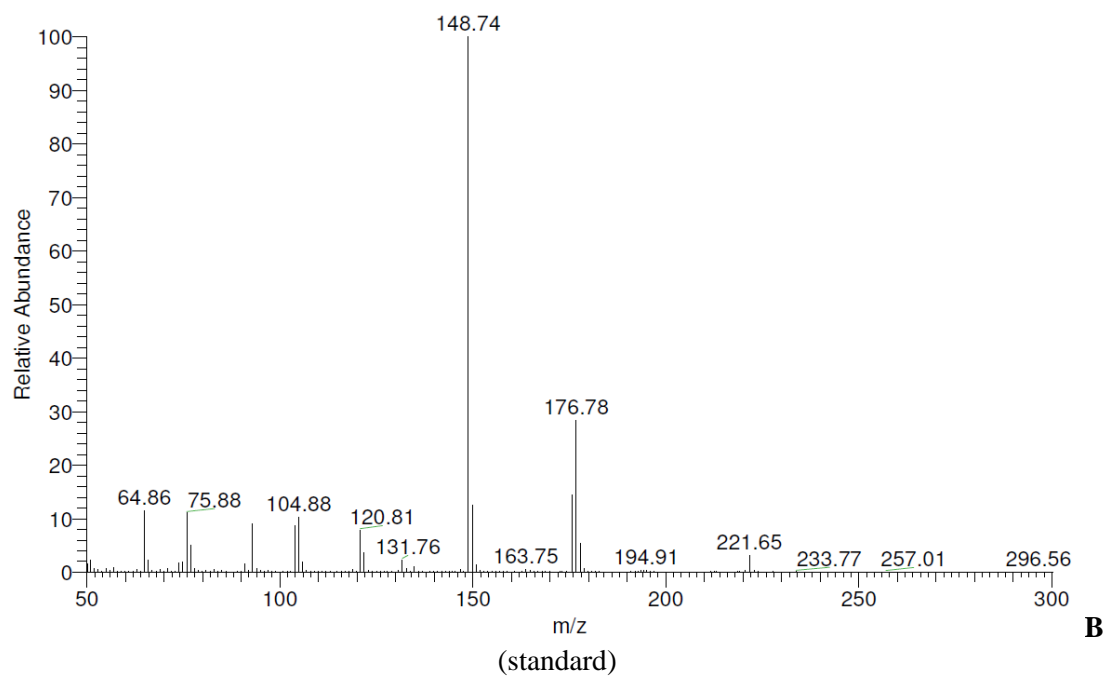
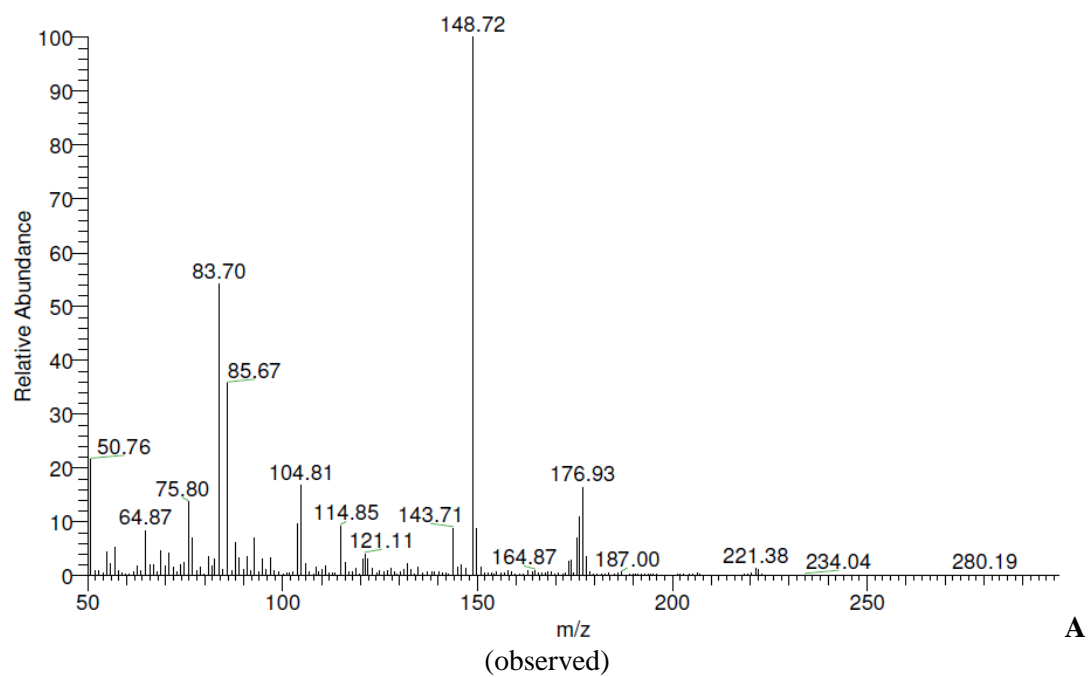


Figure 3.11 (A) Mass spectrum of the peak with retention time 13.08 min ascribed to 2-hydroxynaphthalene-1,4-dione. (B) The spectrum of 2-hydroxynaphthalene-1,4-dione standard

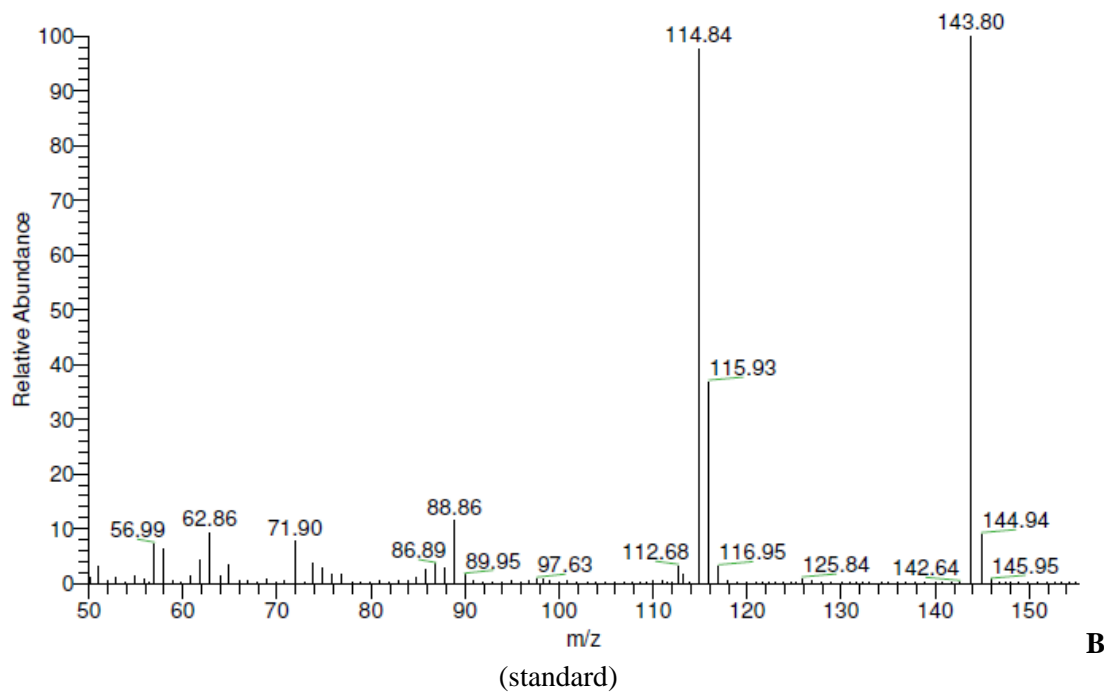
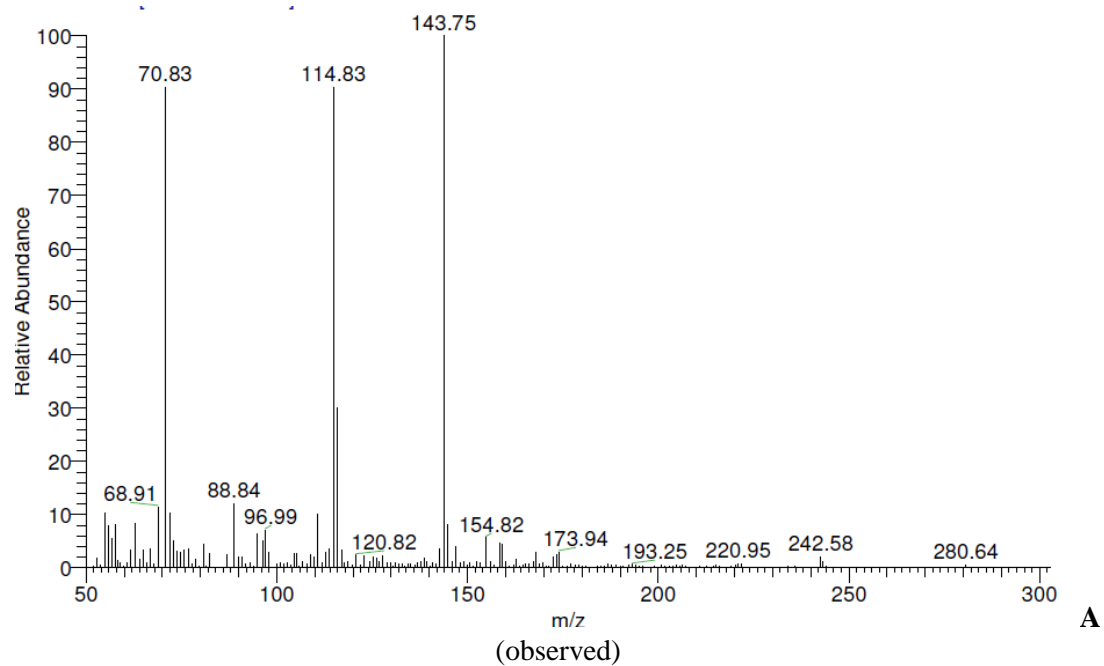


Figure 3.12 (A) Mass spectrum of the peak with retention time 12.75 min ascribed to 1-naphthol. (B) The spectrum of 1-naphthol standard.



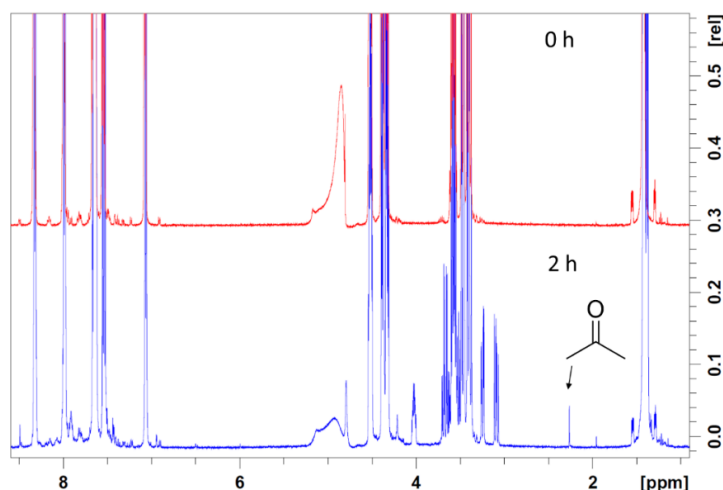


Figure 3.13  $^1\text{H}$  NMR spectra (in  $\text{D}_2\text{O}$ ) of propranolol before (red, top) and after 2 h of **1c**-catalyzed hydrogen peroxide oxidation (blue, bottom) Conditions:  $[\mathbf{1c}] = 1 \times 10^{-6} \text{ M}$ ,  $[\text{propranolol}] = 1.3 \times 10^{-2} \text{ M}$ ,  $[\text{H}_2\text{O}_2] = 0.3 \text{ M}$ , pH 7 (0.01 M phosphate in  $\text{D}_2\text{O}$ ).

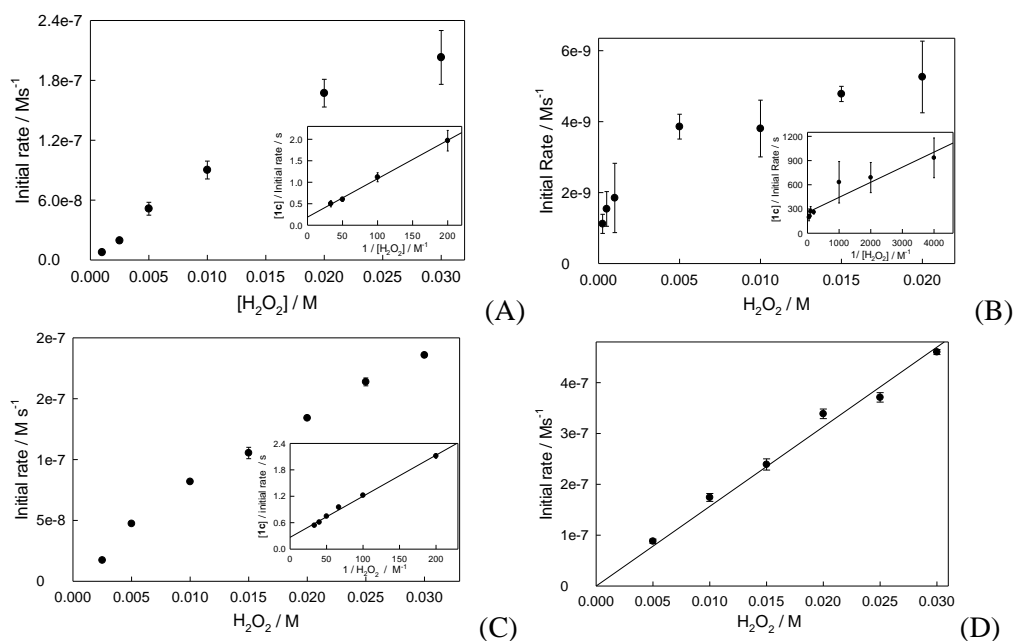


Figure 3.14 . Initial rates versus  $[\text{H}_2\text{O}_2]$  for **1c**-catalyzed oxidation by  $\text{H}_2\text{O}_2$  of products of propranolol degradation: 1-naphthol (A), 2,3-dihydro-2,3-epoxy-naphthalene-1,4-dione (B), 2-hydroxynaphthalene-1,4-dione (C). Initial rates versus  $[\text{H}_2\text{O}_2]$  for uncatalyzed oxidation by  $\text{H}_2\text{O}_2$  of 1,4-naphthoquinone (D). Insets to (A), (B) and (C) show the corresponding double inverse plots,  $[\mathbf{1c}]/(\text{initial rate})$  versus  $[\text{H}_2\text{O}_2]^{-1}$ .

General Reaction Conditions: pH 7 (0.01 M phosphate) and  $25^\circ\text{C}$ .

Specific Conditions for (A):  $[\mathbf{1c}] 1 \times 10^{-7} \text{ M}$ ,  $[\text{H}_2\text{O}_2] (1-30) \times 10^{-3} \text{ M}$ ,  $[\text{NOH}] 1.2 \times 10^{-4} \text{ M}$

Specific Conditions for (B):  $[\mathbf{1c}] 1 \times 10^{-6} \text{ M}$ ,  $[\text{H}_2\text{O}_2] (0.25-20) \times 10^{-3} \text{ M}$ ,  $[\text{NO}_2 \text{ epo}] 1.3 \times 10^{-4} \text{ M}$

Specific Conditions for (C):  $[\mathbf{1c}] 1 \times 10^{-7} \text{ M}$ ,  $[\text{H}_2\text{O}_2] (2.5-30) \times 10^{-3} \text{ M}$ ,  $[\text{NO}_2(\text{OH})] 2 \times 10^{-4} \text{ M}$

Specific Conditions for (D):  $[\text{H}_2\text{O}_2] (5-30) \times 10^{-3} \text{ M}$ ,  $[\text{NO}_2] 4.3 \times 10^{-4} \text{ M}$

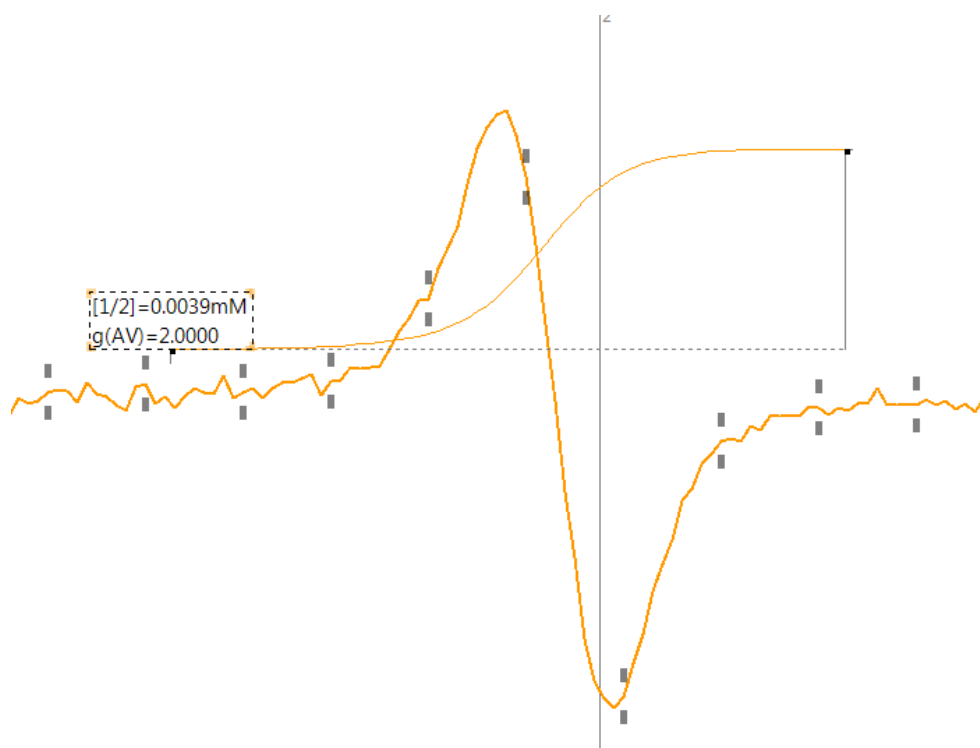


Figure 3.15 EPR spectrum of the reaction mixture 1-naphthol/**1c**/H<sub>2</sub>O<sub>2</sub>. The concentration of the radical at  $g = 2.003$  is  $\sim 4 \times 10^{-6}$  M.

### 3.6 REFERENCES

- (1) Carson, R. *Silent Spring*; Houghton Mifflin Harcourt, 2002.
- (2) Schug, T. T.; Abagyan, R.; Blumberg, B.; Collins, T. J.; Crews, D.; DeFur, P. L.; Dickerson, S. M.; Edwards, T. M.; Gore, A. C.; Guillet, L. J. Designing Endocrine Disruption out of the next Generation of Chemicals. *Green Chem.* **2013**, *15* (1), 181–198.
- (3) Stapleton, M. P. Sir James Black and Propranolol. The Role of the Basic Sciences in the History of Cardiovascular Pharmacology. *Tex Hear. Inst J* **1997**, *24* (4), 336–342.
- (4) Somasundar, Y.; Shen, L. Q.; Hoane, A. G.; Tang, L. L.; Mills, M. R.; Burton, A. E.; Ryabov, A. D.; Collins, T. J. Structural, Mechanistic, and Ultradilute Catalysis Portrayal of Substrate Inhibition in the TAML–Hydrogen Peroxide Catalytic Oxidation of the Persistent Drug and Micropollutant, Propranolol. *J. Am. Chem. Soc.* **2018**, *140* (38), 12280–12289.
- (5) Collins, T. J. TAML Oxidant Activators: A New Approach to the Activation of Hydrogen Peroxide for Environmentally Significant Problems. *Acc. Chem. Res.* **2002**, *35* (9), 782–790.
- (6) Ryabov, A. D.; Collins, T. J. Mechanistic Considerations on the Reactivity of Green FeIII-TAML Activators of Peroxides. *Adv. Inorg. Chem.* **2009**, *61*, 471–521.
- (7) Collins, T. J.; Ryabov, A. D. Targeting of High-Valent Iron-TAML Activators at Hydrocarbons and Beyond. *Chem. Rev.* **2017**.
- (8) Collins, T. J.; Khetan, S. K.; Ryabov, A. D. Chemistry and Applications of Iron–TAML Catalysts in Green Oxidation Processes Based on Hydrogen Peroxide. *Handb. Green Chem. Online* **2010**, 39–77.
- (9) Chahbane, N.; Popescu, D. L.; Mitchell, D. A.; Chanda, A.; Lenoir, D.; Ryabov, A. D.; Schramm, K. W.; Collins, T. J. FeIII-TAML-Catalyzed Green Oxidative Degradation of the Azo Dye Orange II by H<sub>2</sub>O<sub>2</sub> and Organic Peroxides: Products, Toxicity, Kinetics, and Mechanisms. *Green Chem.* **2007**, *9* (1), 49–57.
- (10) Isarain-Chavez, E.; Cabot, P. L.; Centellas, F.; Rodriguez, R. M.; Arias, C.; Garrido, J. A.; Brillas, E. L. B.-I.-C. Electro-Fenton and Photoelectro-Fenton Degradations of the Drug Beta-Blocker Propranolol Using a Pt Anode: Identification and Evolution of Oxidation Products. *J. Hazard. Mater.* **2011**, *185*, 1228–1235.
- (11) Anquandah, G. A. K.; Sharma, V. K.; Panditi, V. R.; Gardinali, P. R.; Kim, H.; Oturan, M. A. Ferrate(VI) Oxidation of Propranolol: Kinetics and Products. *Chemosphere* **2013**, *91* (1), 105–109.
- (12) Ganiyu, S. O.; Oturan, N.; Raffy, S.; Esposito, G.; Van Hullebusch, E. D.; Cretin, M.; Oturan, M. A. Use of Sub-Stoichiometric Titanium Oxide as a Ceramic Electrode in Anodic Oxidation and Electro-Fenton Degradation of the Beta-Blocker Propranolol: Degradation Kinetics and Mineralization Pathway. *Electrochim. Acta* **2017**, *242*, 344–354.

- (13) Ghosh, A.; Mitchell, D. A.; Chanda, A.; Ryabov, A. D.; Popescu, D. L.; Upham, E. C.; Collins, G. J.; Collins, T. J. Catalase-Peroxidase Activity of Iron(III)-TAML Activators of Hydrogen Peroxide. *J. Am. Chem. Soc.* **2008**, *130* (45), 15116–15126.
- (14) Onundi, Y.; Drake, B. A.; Malecky, R. T.; DeNardo, M. A.; Mills, M. R.; Kundu, S.; Ryabov, A. D.; Beach, E. S.; Horwitz, C. P.; Simonich, M. T.; et al. A Multidisciplinary Investigation of the Technical and Environmental Performances of TAML/Peroxide Elimination of Bisphenol A Compounds from Water. *Green Chem.* **2017**, *19* (18), 4234–4262.
- (15) Cason, J. Synthesis of Benzoquinones by Oxidation. *Org. React.* **2004**, *4*, 305–361.
- (16) Takata, T.; Tajima, R.; Ando, W. Oxidation of Dihydroxyaromatics by Hypervalent Iodine Oxides: A Facile Quinone Synthesis. *J. Org. Chem.* **1983**, *48* (24), 4764–4766.
- (17) Sun, L.; Xin, L.; Peng, Z.; Jin, R.; Jin, Y.; Qian, H.; Fu, Z. Toxicity and Enantiospecific Differences of Two B-blockers, Propranolol and Metoprolol, in the Embryos and Larvae of Zebrafish (*Danio Rerio*). *Environ. Toxicol.* **2014**, *29* (12), 1367–1378.
- (18) Dong-dong, Q. U. Study on the Enrichment Rules of 1-Naphthol in Zebra Fish. *J. Anhui Agric. Sci.* **2012**, *2012* (20), 72.
- (19) Knöbel, M.; Busser, F. J. M.; Rico-Rico, A.; Kramer, N. I.; Hermens, J. L. M.; Hafner, C.; Tanneberger, K.; Schirmer, K.; Scholz, S. Predicting Adult Fish Acute Lethality with the Zebrafish Embryo: Relevance of Test Duration, Endpoints, Compound Properties, and Exposure Concentration Analysis. *Environ. Sci. Technol.* **2012**, *46* (17), 9690–9700.
- (20) Song, W. H.; Ding, F.; Guo, J.; Li, L. Y.; Zhang, J. H.; Lian, J.; Hu, W. X.; Gao, M. L. Study on Acute Toxicity and Structure-Activity Relationship of Zebrafish (*Danio Rerio*) Exposed to Naphthoquinones. *J. Environ. Sci. Heal. Part B* **2010**, *45* (7), 601–605.
- (21) Chanda, A.; Ryabov, A. D.; Mondal, S.; Alexandrova, L.; Ghosh, A.; Hangun-Balkir, Y.; Horwitz, C. P.; Collins, T. J. Activity-Stability Parameterization of Homogeneous Green Oxidation Catalysts. *Chem. - A Eur. J.* **2006**, *12* (36), 9336–9345.
- (22) DeNardo, M. A.; Mills, M. R.; Ryabov, A. D.; Collins, T. J. Unifying Evaluation of the Technical Performances of Iron-Tetra-Amido Macrocyclic Ligand Oxidation Catalysts. *J. Am. Chem. Soc.* **2016**, *138* (9), 2933–2936.
- (23) Emelianenko, M.; Torrejon, D.; DeNardo, M. A.; Socolofsky, A. K.; Ryabov, A. D.; Collins, T. J. Estimation of Rate Constants in Nonlinear Reactions Involving Chemical Inactivation of Oxidation Catalysts. *J. Math. Chem.* **2014**, *52* (5), 1460–1476.
- (24) EPA. Ecotox knowledgebase <https://cfpub.epa.gov/ecotox/>.
- (25) Bittner, L.; Teixido, E.; Seiwert, B.; Escher, B. I.; Klüver, N. Influence of PH on the Uptake and Toxicity of  $\beta$ -Blockers in Embryos of Zebrafish, *Danio Rerio*. *Aquat. Toxicol.* **2018**, *201*, 129–137.
- (26) Truong, L.; DeNardo, M. A.; Kundu, S.; Collins, T. J.; Tanguay, R. L. Zebrafish Assays

as Developmental Toxicity Indicators in the Green Design of TAML Oxidation Catalysts. *Green Chem.* **2013**, *15* (9), 2339–2343.

- (27) Truong, L.; Reif, D. M.; St Mary, L.; Geier, M. C.; Truong, H. D.; Tanguay, R. L. Multidimensional in Vivo Hazard Assessment Using Zebrafish. *Toxicol. Sci.* **2013**, *137* (1), 212–233.
- (28) McCollum, C. W.; Ducharme, N. A.; Bondesson, M.; Gustafsson, J. Developmental Toxicity Screening in Zebrafish. *Birth Defects Res. Part C Embryo Today Rev.* **2011**, *93* (2), 67–114.
- (29) Vandenberg, L. N.; Colborn, T.; Hayes, T. B.; Heindel, J. J.; Jacobs, D. R.; Lee, D. H.; Shioda, T.; Soto, A. M.; vom Saal, F. S.; Welshons, W. V.; et al. Hormones and Endocrine-Disrupting Chemicals: Low-Dose Effects and Nonmonotonic Dose Responses. *Endocr. Rev.* **2012**, *33* (3), 378–455.
- (30) Yamamoto, S.; Itani, H.; Tsuji, T.; Nagata, W. Oxidatively Assisted Hydrolysis of Allylic Iodides to Rearranged Allylic Alcohols. A New Example of [2, 3] Sigmatropic Rearrangement. *J. Am. Chem. Soc.* **1983**, *105* (9), 2908–2909.
- (31) Alder, R. W. Electron-Transfer Chain Catalysis of Substitution Reactions. *J. Chem. Soc. Chem. Commun.* **1980**, No. 24, 1184–1186.
- (32) Ebersson, L. Catalysis by Electron Transfer in Organic Chemistry. *J. Mol. Catal.* **1983**, *20* (1), 27–52.
- (33) Doherty, M. d'Arcy; Wilson, I.; Wardman, P.; Basra, J.; Patterson, L. H.; Cohen, G. M. Peroxidase Activation of 1-Naphthol to Naphthoxy or Naphthoxy-Derived Radicals and Their Reaction with Glutathione. *Chem. Biol. Interact.* **1986**, *58*, 199–215.
- (34) Ryabov, A. D. Green Challenges of Catalysis via Iron(IV)Oxo and Iron(V)Oxo Species. *Adv. Inorg. Chem.* **2013**, *65*, 117–163.
- (35) Ghosh, A. *Design, Synthesis and Mechanistic Studies of Iron-TAML Catalytic Activators of Hydrogen Peroxide and a New Activation Chemistry of Dioxygen by Iron*; Carnegie Mellon University, 2004.
- (36) Popescu, D. L.; Chanda, A.; Stadler, M. J.; Mondal, S.; Tehranchi, J.; Ryabov, A. D.; Collins, T. J. Mechanistically Inspired Design of Fe(III)-TAML Peroxide-Activating Catalysts. *J Am Chem Soc* **2008**, *130* (37), 12260–12261.
- (37) Ellis, W. C.; Tran, C. T.; Roy, R.; Rusten, M.; Fischer, A.; Ryabov, A. D.; Blumberg, B.; Collins, T. J. Designing Green Oxidation Catalysts for Purifying Environmental Waters. *J. Am. Chem. Soc.* **2010**, *132* (28), 9774–9781.
- (38) Das, T. N.; Neta, P. Reduction Potentials of Naphthoxyl and Pyridoxyl Radicals in Aqueous Solutions. *J. Phys. Chem. A* **1998**, *102* (35), 7081–7085.
- (39) George, P. L. B.-Ol. The Chemical Nature of the Second Hydrogen Peroxide Compound Formed by Cytochrome c Peroxidase and Horseradish Peroxidase. *Biochem. J.* **1953**, *54*,

267–276.

- (40) Johnson, K. A.; Simpson, Z. B.; Blom, T. Global Kinetic Explorer: A New Computer Program for Dynamic Simulation and Fitting of Kinetic Data. *Anal. Biochem.* **2009**, 387 (1), 20–29.

**Use of the micropollutant, propranolol, as a test system for comparative evaluation of the technical performances of TAMLs and NewTAMLs to identify the best overall candidate for real waste water treatment**





RightsLink®



Home



Help



Email Support



Sign in



Create Account

**Bioinspired, Multidisciplinary, Iterative Catalyst Design Creates the Highest Performance Peroxidase Mimics and the Field of Sustainable Ultradilute Oxidation Catalysis (SUDOC)****Author:** Genoa R. Warner, Yogesh Somasundar, Kyle C. Jansen, et al**Publication:** ACS Catalysis**Publisher:** American Chemical Society**Date:** Aug 1, 2019*Copyright © 2019, American Chemical Society***PERMISSION/LICENSE IS GRANTED FOR YOUR ORDER AT NO CHARGE**

This type of permission/license, instead of the standard Terms & Conditions, is sent to you because no fee is being charged for your order. Please note the following:

- Permission is granted for your request in both print and electronic formats, and translations.
- If figures and/or tables were requested, they may be adapted or used in part.
- Please print this page for your records and send a copy of it to your publisher/graduate school.
- Appropriate credit for the requested material should be given as follows: "Reprinted (adapted) with permission from (COMPLETE REFERENCE CITATION). Copyright (YEAR) American Chemical Society." Insert appropriate information in place of the capitalized words.
- One-time permission is granted only for the use specified in your request. No additional uses are granted (such as derivative works or other editions). For any other uses, please submit a new request.

[BACK](#)[CLOSE WINDOW](#)



## 4.1 INTRODUCTION

As discussed in previous chapters, TAML activators are fully functional small molecule mimics of peroxidase and cytochrome P450 enzymes.<sup>1-3</sup> Over the past two decades, TAML activators have shown to be effective at oxidizing a broad range of micropollutants (MPs) at nM concentrations of TAML and mM concentrations of H<sub>2</sub>O<sub>2</sub>.<sup>4-12</sup> However, the best performing TAML was a fluorinated catalyst<sup>7,11,13</sup> and this initiated the search for next generation TAML activators devoid of halogens. Additionally, the mechanistic understanding of TAMLs led us to move away from the carbonyl moiety in the macrocyclic ligand which we discovered was the reason for inactivation of TAMLs via perhydrolysis.<sup>6,14,15</sup> Thirty-five years of iterative design provided us the best performing next generation of TAMLs – NewTAMLs devoid of halogens and with sulfonyl groups substituting two of the carbonyl groups.<sup>6,15</sup> As with the norm in the research group, the reactivities of NewTAMLs were evaluated using a reference dye Orange II using UV-vis for quick measurements.<sup>14,16,17</sup> While kinetic rate constants for Orange II serves the purpose for initial comparison of the catalysts, there are certain disadvantages associated with Orange II. Orange II is a relatively easy substrate to oxidize,<sup>14</sup> therefore the true potential of NewTAMLs is never observed. Secondly, Orange II is not considered to be a micropollutant (MP) and when it is used as the demonstration substrate this makes the case of NewTAML/H<sub>2</sub>O<sub>2</sub> as a MP treatment technology harder to sell.

Propranolol, a persistent drug<sup>18</sup> and MP<sup>19-22</sup>, is much more resistant to oxidation than Orange II<sup>6,7,15</sup> such that its study assists in examining important features of catalyst performance over longer process time scales. Propranolol has been reported widely to be present in surface, ground and wastewaters.<sup>23-29</sup> Therefore, oxidation of propranolol at its environmentally relevant concentrations (ppt-ppb) will serve the purpose of NewTAML/H<sub>2</sub>O<sub>2</sub> as an MP treatment technology. Additionally, exploring various types of water, viz., buffered pH 7 solution versus unbuffered real waters with high dissolved organic carbon (DOC) will stress the catalytic process

affecting its reactivity as well as effective lifetime providing a realistic test to identify the full potential of NewTAMLs.<sup>6,15</sup> This technical performance, when combined with already established safety aspects of NewTAML,<sup>6</sup> will help identify the best candidate catalyst for real wastewater treatment.

In this chapter, we present a comparative evaluation of TAMLs and NewTAMLs for oxidation of propranolol. We have identified the best performing NewTAML through a sequential approach from higher [propranolol] to dilute [propranolol] extending into the ultradilute regime.

## 4.2 RESULTS AND DISCUSSION

Chart 4.1 Structures of TAML and NewTAML activators, substrates used or discussed in this chapter

TAML	X <sub>1</sub>	X <sub>2</sub>	R <sub>1</sub>	R <sub>2</sub>
<b>1a</b>	H	H	Me	Me
<b>1b</b>	NO <sub>2</sub>	H	Me	Me
<b>1c</b>	NO <sub>2</sub>	H	F	F
<b>2a</b>	H	H	H	H
<b>2b</b>	NO <sub>2</sub>	H	H	H
<b>2c</b>	H	H	Me	H
<b>2d</b>	NO <sub>2</sub>	H	Me	H
<b>4</b>	-	-	H	H
<b>5</b>	NO <sub>2</sub>	H	Me	Me
<b>6</b>	H	H	H	H
<b>7</b>	H	H	-	-

Y = CO (1), SO<sub>2</sub> (2)

Y = CO (3), SO<sub>2</sub> (4)

Y = CO (5), SO<sub>2</sub> (6)

Propranolol

Orange II

Y = SO<sub>2</sub> (7)

### 4.2.1 Buffered studies at propranolol $5 \times 10^{-5}$ M (~15 ppm) at pH 7

I have previously introduced water purification by TAML/H<sub>2</sub>O<sub>2</sub> of the persistent MP propranolol at higher concentrations ( $5 \times 10^{-5}$  M) in chapter 2.<sup>7</sup> It was important that we evaluate NewTAMLs at higher concentrations first in order to evaluate the best performing NewTAMLs and optimize its catalytic system properties for oxidation of propranolol at dilute concentrations (15 ppb,  $\sim 5.3 \times 10^{-8}$  M). As shown in Figure 4.1, NewTAMLs **2** (chart 4.1) showed a superior performance compared to analogous **1** (chart 4.1). NewTAMLs **6**, **7** (Diaromatic) and **4** (non-aromatic) showed no oxidation of propranolol, similar to a control reaction with only H<sub>2</sub>O<sub>2</sub>. This is in contrast to the prototype TAML **1a** which showed an approximate 20% oxidation of propranolol at 120 min under similar conditions. While the performance of **4** and **7** were on expected lines from Orange II experiments,<sup>6,14</sup> lack of catalyzed oxidation of propranolol by **6**, which had a comparable  $k_{II}$  ( $1300 \pm 100 \text{ M}^{-1} \text{ s}^{-1}$ ) to **1a** ( $4950 \pm 20 \text{ M}^{-1} \text{ s}^{-1}$ )<sup>6</sup> reaffirmed two things: (i) Propranolol is a harder to oxidize substrate as established earlier and (ii)  $k_{II}$  is not the only determining factor in the

technical performance of the catalyst. As discussed in detail in a recently published paper,<sup>6</sup> the ratio  $k_{II}/k_i$  that signifies the ratio of reactivity/lifetime of the activated TAML (Ac)<sup>6,30</sup> (Scheme 4.1) is what ultimately determines the technical efficiency of TAMLs/NewTAMLs in operating

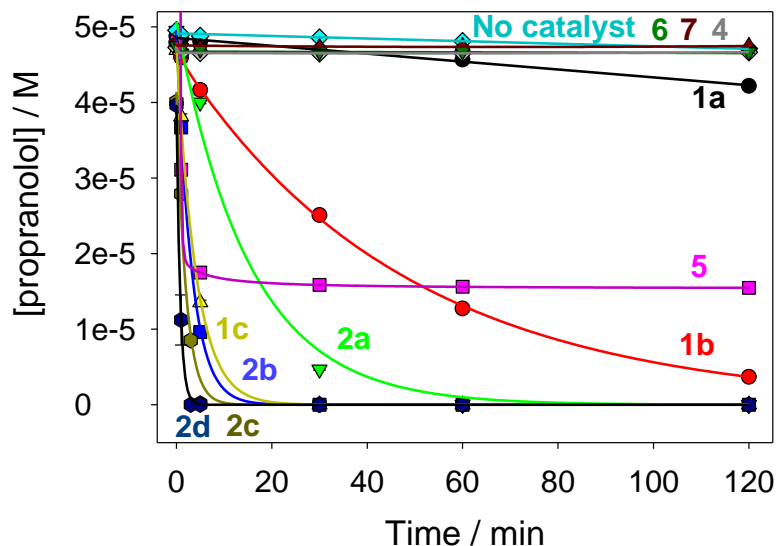


Figure 4.1 Degradation of propranolol by  $H_2O_2$  catalyzed by TAML (**1** and **5**) and NewTAML activators (**2**, **4**, **6** and **7**) at pH 7 measured by UPLC. Conditions: [TAML or NewTAML] =  $1 \times 10^{-6}$  M, [propranolol] =  $5 \times 10^{-5}$  M, [ $H_2O_2$ ] =  $5 \times 10^{-3}$  M, 0.01 M phosphate, 25 °C. All points are an average of three values; standard deviation error bars are mostly not visible as the triplicate points are tightly grouped. Lines are for emphasis only.

solutions. In order to better explain the observed reactivities in Figure 4.1, detailed kinetic evaluations were performed to determine the rate constants  $k_I$ ,  $k_{II}$  and  $k_i$  for NewTAMLs catalyzed hydrogen peroxide oxidation of propranolol.

#### 4.2.2 Determination of kinetic rate constants for NewTAMLs at pH 7

Initial rates for **2a** catalyzed hydrogen peroxide oxidation of propranolol at pH 7 showed a hyperbolic dependence on [ $H_2O_2$ ], consistent with eq 4.1 (when  $k_{-I}$  is negligible) derived from the TAML catalytic mechanism in Scheme 4.1.

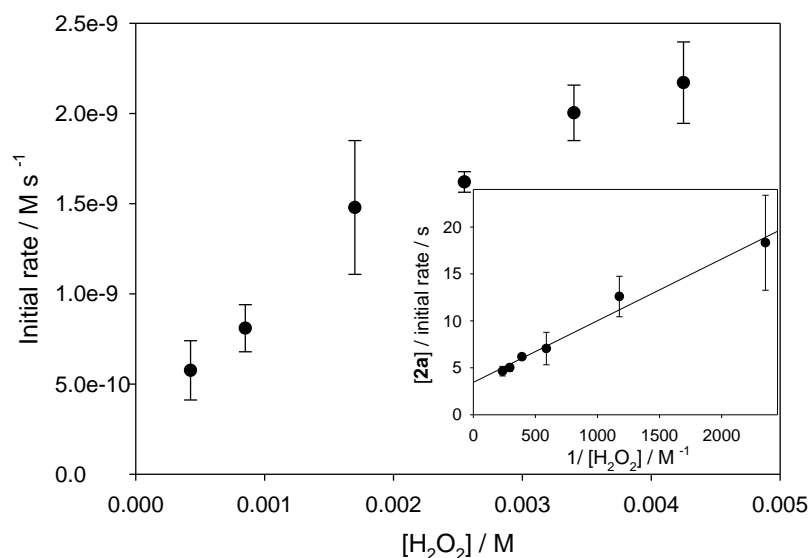
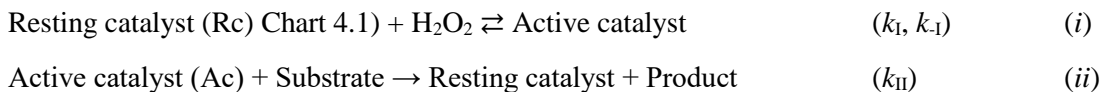


Figure 4.2 Initial rate of propranolol degradation by H<sub>2</sub>O<sub>2</sub> catalyzed by **2a** as a function of [H<sub>2</sub>O<sub>2</sub>] measured by UPLC. Inset shows the double inverse linear plot, [2a]/(initial rate) versus [H<sub>2</sub>O<sub>2</sub>]<sup>-1</sup>. Conditions: [2a] = 1 × 10<sup>-8</sup> M, [propranolol] = 5 × 10<sup>-5</sup> M, pH 7 (0.01 M phosphate), 25 °C. All the data points are an average of three values with standard deviations shown.

Secondary rate constants,  $k_I$  and  $k_{II}$  for **2a** were calculated from a linear double inverse plot  $dt/d[\text{propranolol}]$  versus  $[\text{H}_2\text{O}_2]^{-1}$  (Figure 4.2 inset) and were found to be  $150 \pm 40 \text{ M}^{-1} \text{ s}^{-1}$  and  $5500 \pm 200 \text{ M}^{-1} \text{ s}^{-1}$ , respectively. The first order substrate independent catalyst inactivation rate constant,  $k_i$ , was determined from the same reaction (figure 4.2) via incomplete oxidation of propranolol following a protocol described elsewhere.<sup>14</sup> The  $k_i$  for **2a** was determined to be  $(3.7 \pm 0.3) \times 10^{-4} \text{ s}^{-1}$ . Rate constants  $k_I$ ,  $k_{II}$ ,  $k_i$  were similarly obtained for **2b**, **2c**, **2d** at pH 7 and have been summarized along with rate constants for TAMLs (**1a**, **1b**, **1c**, **5**)<sup>7</sup> reported in Chapter 2, in Table 4.1.

Scheme 4.1 Typical stoichiometric mechanism of oxidative catalysis by TAML/NewTAML activators



$$-\frac{d[S]}{dt} = \frac{k_I k_{II} [H_2O_2][S]}{k_{-I} + k_I [H_2O_2] + k_{II} [S]} [Fe_t^{III}] \quad (4.1)$$

$k_{II} / k_I$  ratios for TAMLs and NewTAMLs were calculated from the experimentally determined  $k_{II}$  and  $k_I$  and have been summarized in Table 4.1 as well. Catalysts **1c**, **2b**, **2c** and **2d** reduced [propranolol] =  $5 \times 10^{-5}$  M to BDL concentrations in ~ 20 min while **2a** achieved the same feat in 60 min. Catalyst **1b** on the other hand achieved 90% propranolol reduction in 120 min. The  $k_{II}/k_I$  ratios for **1a**, **1b**, **1c**, **2a**, **2b**, **2c**, **2d** were found to be [0.95, 0.23, 9.73, 1.5, 3.3, 2.0, 3.6]  $\times 10^7$  M<sup>-1</sup> respectively. As a general case, it can be observed that higher the  $k_{II}/k_I$  ratio, the better was TAML/NewTAML performance. Analogous to **1a**, **2a** had a 1.5 times the  $k_{II}/k_I$  ratio of **1a** (Table 4.1). This superiority was clearly displayed in their performance for propranolol oxidation (Figure 4.1).

Table 4.1 . Rate constants  $k_I$  and  $k_{II}$  and  $k_i$  for oxidation of propranolol catalyzed by various TAML activators at pH 7 (0.01 M phosphate buffer) and 25 °C.

TAML	$k_I / M^{-1} s^{-1}$	$k_{II} / M^{-1} s^{-1}$	$10^4 \times k_i^* / s^{-1}$	$10^{-7} \times k_{II} / k_I / M^{-1}$	Reference
<b>1a</b>	$2 \pm 0.1$	$70 \pm 20$	$0.0735 \pm 0.0009$	0.95	7
<b>1b</b>	$5.0 \pm 0.2$	$140 \pm 20$	$0.6 \pm 0.04$	0.23	7
<b>1c</b>	$90 \pm 10$	$14600 \pm 200$	$1.5 \pm 0.02$	9.73	7
<b>2a</b>	$150 \pm 40$	$5500 \pm 200$	$3.7 \pm 0.3$	1.5	This work
<b>2b</b>	$132 \pm 2.0$	$63000 \pm 18500$	$18.9 \pm 3.5$	3.3	This work
<b>2c</b>	$78 \pm 2.1$	$16000 \pm 3900$	$8.0 \pm 1.1$	2.0	This work
<b>2d</b>	$134 \pm 5.9$	$26000 \pm 8800$	$7.2 \pm 1.5$	3.6	This work
<b>5</b>	$200 \pm 10$	$5300 \pm 2400$	$11.6 \pm 1.6$	0.46	7

\*  $k_i$  measured at  $[H_2O_2] = 2.5 \times 10^{-3}$  M; All  $k_i$  values are from this work, not published earlier. Reference mentioned on top is only for  $k_I$  and  $k_{II}$ .

Similarly, analogous catalysts **1b** and **2b** showed a superior performance for **2b** which has 14 times the  $k_{II}/k_I$  ratio of **1b**. The superiority of **2c** over **2a** by the virtue of 1.3 times better  $k_{II}/k_I$  ratio for **2c** compared to **2a** was also observed for propranolol oxidation. The  $k_{II}/k_I$  ratio for **1a** is higher than **1b** in spite of **1b** containing a nitro group in the ligand. This is mainly as a result of an order

of magnitude lower  $k_i$  value for **1a**. In practicality, what this means is **1a** would last longer in solution and perform very slow catalysis and might be able to outperform **1b** after several days of reaction, which is not practical from a water treatment perspective. The  $k_{II}/k_i$  ratio of 9.73 for **1c** suggests it outperforms **2d** if we purely go by numbers, which may not say the complete story. For a slower acting substrate, **2d** may lose ground compared to **1c**. because, the kill switch in **2** activators has its own locked in dynamics and the longer it takes to destroy a pollutant, the more it winnows out the NewTAML, **2d** in this case. In fact, for the **2** catalysts,  $k_i$  is actually a composite of the amide perhydrolysis and the kill switch. If the kill switch can be completely shut off, for which there are ongoing efforts in the group, we can make relative comparisons of lifetime impacted by perhydrolysis alone. We will not know the answer until we have a kill switch off catalyst—when we have one, it can be projected to be much more effective than **1c** against propranolol.

While several TAML/NewTAMLs performed really well in catalyzing oxidation of propranolol at  $5 \times 10^{-5}$  M, we were still far from identifying the best performing TAML/NewTAML for wastewater treatment from these catalysts at this point in time, with only the performance data at  $\mu\text{M}$  [propranolol]. In order to truly test and differentiate between the performance levels of **1c**, **2b**, **2c** and **2d**, it was necessary to stretch the performance of catalyst under stressful conditions. To achieve this, two separate experiments were designed: (i) Assess the reactivities of better performing catalysts (**1b**, **1c**, **2a**, **2b**, **2c** and **2d**) at oxidizing  $5 \times 10^{-5}$  M of propranolol under low [propranolol] =  $5.3 \times 10^{-8}$  M in pH 7 buffered water (ii) Identify the top performing catalysts at oxidizing  $5.3 \times 10^{-8}$  M of propranolol in pH 7 buffered water and perform analogous experiments, by spiking propranolol ( $5.3 \times 10^{-8}$  M) in unbuffered high DOC real water.

#### 4.2.3 Buffered studies at propranolol $5.3 \times 10^{-8}$ M (~15 ppb)

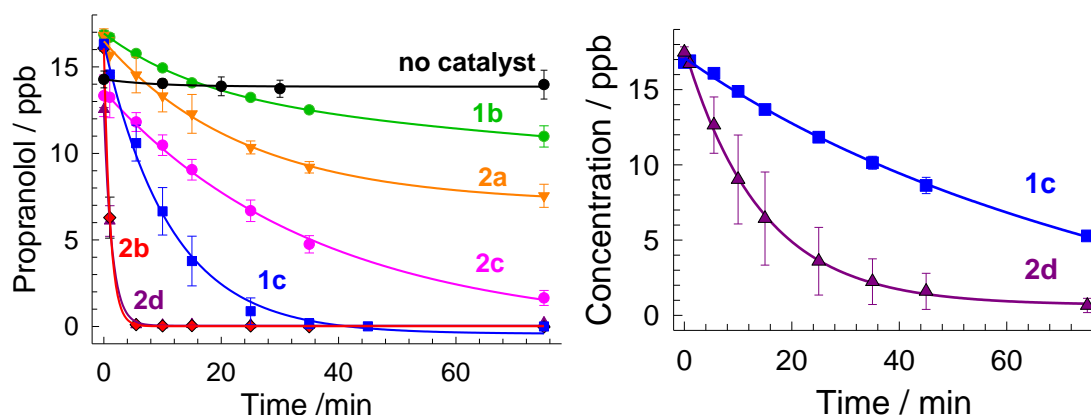


Figure 4.3 Comparisons of propranolol degradation by TAML/ $\text{H}_2\text{O}_2$  and NewTAML/ $\text{H}_2\text{O}_2$ . (Left) Degradation of propranolol ( $5.3 \times 10^{-8}$  M) by TAMLs **1b** and **1c** and NewTAMLs **2a - 2d** ( $1.0 \times 10^{-7}$  M) with  $\text{H}_2\text{O}_2$  ( $3.3 \times 10^{-4}$  M) at pH 7 (0.01 M phosphate), 25 °C, and ambient pressure. Lines were not calculated and are for emphasis only. (Right) Degradation of propranolol ( $5.7 \times 10^{-8}$  M) under ultradilute conditions by TAML **1c** and NewTAML **2d** ( $1.0 \times 10^{-8}$  M, 10 nM!) with  $\text{H}_2\text{O}_2$  ( $3.3 \times 10^{-4}$  M) at pH 7 (0.01 M phosphate) and 25 °C.

TAML **1a** has already been shown to exhibit very low catalytic activity against propranolol at high concentrations,<sup>7</sup> so the low concentration study was not conducted here. Here TAML- and NewTAML-catalyzed oxidations were compared for **1b**, **1c**, **2a-2d**, starting at low concentrations ( $5.3 \times 10^{-8}$  M, ~15.6 ppb) of propranolol and passing through the ultradilute regime. This was done to get as closer to the real world concentrations of propranolol in waters, typically in ppt-low ppb.<sup>23,29</sup> The data in Figure 4.3, left, compare the performances of 100 nM TAML/NewTAMLs using 0.33 mM  $\text{H}_2\text{O}_2$  (11.2 ppm) at pH 7. The data in Figure 4.3, right, shows analogous experiments with 10 nM **1c** and **2d**. TAML **1b**/ $\text{H}_2\text{O}_2$  gives 35% propranolol reduction in 75 min. Fluorinated **1c** removes propranolol to below the limit of detection in 35 min, illustrating the power of the fluorine effect that, in part, NewTAMLs have been designed to replace. NewTAMLs **2a** and **2c** were less effective than **1c** (figure 4.3, left), because of a much smaller  $k_{\text{II}}$  (lack of nitro head group) and an overall smaller  $k_{\text{II}}/k_{\text{i}}$  ratio compared to **1c** (table 4.1).



The superior performance of **2c** over **2a** is purely a consequence of its less active kill switch (1 versus 2 methylene protons respectively), as explained in chapter 1. Remarkably, nitro-substituted **2b** and **2d** achieve propranolol removal to below the detection limit in under 5 min. Here also the higher activities imparted by the electron-withdrawing nitro group to the **2b** and **2d** iron catalytic sites over those of **2a** and **2c** dominates, even while more active kill switches winnow the former catalyst pair more rapidly. Such substantial increases in technical performance over **1b** and **1c** promised to improve the cost performances of NewTAML/H<sub>2</sub>O<sub>2</sub> over TAML/H<sub>2</sub>O<sub>2</sub> for MP water treatments. In this NewTAML/H<sub>2</sub>O<sub>2</sub> propranolol treatment, the [catalyst]/substrate molar ratio starts at ~2. This is unusual from the synthetic perspective. However, the destruction goal of water treatment is to remove MPs like propranolol to below detection limits. If the system is working correctly, the concentration ratio of [catalyst]/[substrate] approaches infinity as the process proceeds. Note in Figure 4.3, right, that 10 nM (6.21 ppb) **2d** removes 96% of propranolol in 75 min vs 69% for **1c**. This would translate to 1 kg of **2d** being able to treat 161 000 tonnes of water were it to be used in this way for just this purpose. While 100 nM **2b** and **2d** showed very similar performances at oxidizing applications ( $5.3 \times 10^{-8}$  M, ~15.6 ppb) of propranolol at pH 7, it was necessary to identify the superior performing catalyst of the two to be taken forward as the best overall candidate for real wastewater treatment.

#### ***4.2.4 Unbuffered studies in Allegheny river water***

##### ***4.2.4.1 Significance of pH.***

In the recently published study introducing NewTAMLs,<sup>6</sup> a clear case was established for the evidence of a kill switch (2 methylene protons) that increases in sensitivity and the resulting catalyst decay with increasing pH of the solution.<sup>30</sup> Progressing towards alkaline pH,  $k_i$  for **2b** increased sharply beyond pH 7 in the catalytic oxidation of Orange II.<sup>6</sup> To illustrate this kill switch activity, catalytic oxidation of  $5.3 \times 10^{-8}$  M, ~15.6 ppb of propranolol was performed

with  $1 \times 10^{-7}$  M **2b** using  $\text{H}_2\text{O}_2$  ( $3.3 \times 10^{-4}$  M) in unbuffered Allegheny river water at different initial pH of water, viz., pH 8.5 and pH 7.2.

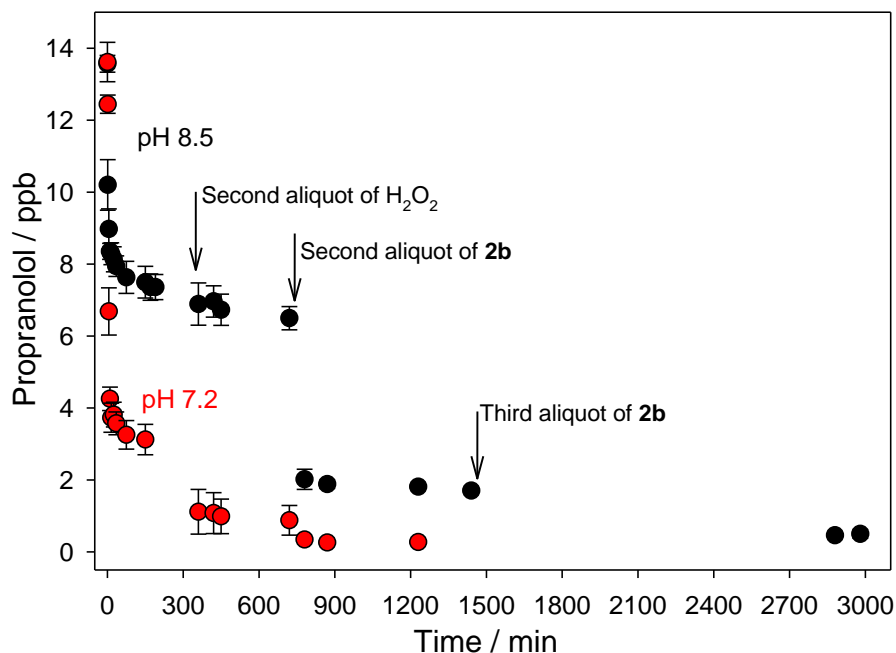


Figure 4.4 Degradation of propranolol ( $5.3 \times 10^{-8}$  M) by **2b** ( $1.0 \times 10^{-7}$  M) with  $\text{H}_2\text{O}_2$  ( $3.3 \times 10^{-4}$  M) in 25 °C, in unbuffered propranolol-spiked Allegheny River water at pH 7 and pH 8.5 and ambient pressure. Aliquots of  $\text{H}_2\text{O}_2$  and **2b** were added to determine the limiting factor for reaction progress. Multiple aliquots of **2b** were added to oxidize propranolol to below detection limit concentrations

As suspected, the performance of **2b** was superior at pH 7.2 compared to pH 8.5. At 360 min, a 93 % reduction in propranolol was achieved with **2b** at pH 7.2 as opposed to 50 % removal at pH 8.5. Since there was no experimentally obtained  $k_{\text{II}}$  and  $k_{\text{i}}$  at pH 8.5 for **2b** for propranolol oxidation, observations were extrapolated from the Orange II oxidation experiments. Although pH 8.5 provided a near highest  $k_{\text{II}}$  for oxidation of Orange II, a nearly 5 times higher  $k_{\text{i}}$  at pH 8.5 rendered the  $k_{\text{II}}/k_{\text{i}}$  ratio extremely low at pH 8.5 compared to pH 7. We believe the kill switch is more active at pH 8.5 causing inactivation of **2b** and an overall decrease in [**2b**] at alkaline pH, leading to a reduced performance. For a wastewater treatment to be effective, it was necessary to be able to reduce the concentration of MPs to BDL concentrations. By addition of  $\text{H}_2\text{O}_2$ , it was

confirmed that  $\text{H}_2\text{O}_2$  was not the limiting factor in propranolol oxidation, rather it was inactivation of **2b**. By addition of multiple aliquots of **2b** ( $1 \times 10^{-7}$  M) after each inactivation, propranolol was able to be oxidized to BDL concentrations both at pH 7 and pH 8.5 over 50h.

#### 4.2.4.2 Significance of a partially muted kill switch at pH 7

Having established that the two best performing catalysts at ppb [propranolol] were **2b** and **2d** and also having observed the effect of activated kill switch at alkaline pH, comparative experiments were performed for **2b** and **2d** in unbuffered Allegheny river water adjusted to pH 7 at the beginning of reaction using diluted HCl solution. A control experiment with  $\text{H}_2\text{O}_2$  did not show any removal. While 100 nM **2b** reduced propranolol ( $5.3 \times 10^{-8}$  M) to BDL concentrations in 5 min under buffered conditions (figure 4.3); **2b** was inactivated in 20 min and achieved 70 % of propranolol reduction. In contrast, 100 nM **2d** reduced propranolol to BDL concentrations in 20 min.

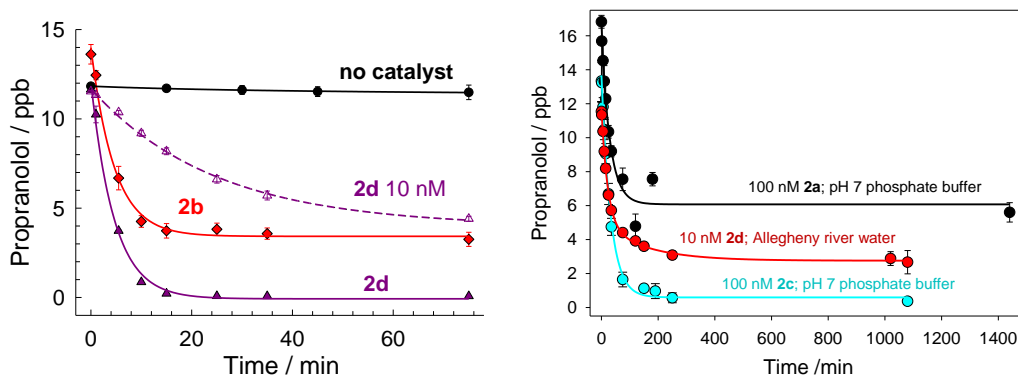


Figure 4.5 (Left) Degradation of propranolol ( $5.3 \times 10^{-8}$  M) by **2b** and **2d** ( $1.0 \times 10^{-7}$  M) with  $\text{H}_2\text{O}_2$  ( $3.3 \times 10^{-4}$  M) in 25 °C, in unbuffered propranolol-spiked Allegheny River water at pH 7 and ambient pressure. Under the most difficult oxidation conditions assessed in this study, **2d** gave a significantly improved performance over **2b** at  $1.0 \times 10^{-7}$  M; **2d** at  $1.0 \times 10^{-8}$  M performs comparably to **2b** at  $1.0 \times 10^{-7}$  M. (Right) Propranolol degradation with **2a** and **2c** at  $1.0 \times 10^{-7}$  M from Figure 4.3 in buffered conditions and **2d** at  $1.0 \times 10^{-8}$  M in unbuffered river water from the figure on the left over 1400 min of reaction. Lines are for emphasis only.

While the superiority of **2d** over **2b** was clearly established with this experiment alone, it was important to see how much of a significant effect does partially muting the kill switch (1 methylene proton) have on the technical performance of **2d**. At 10 nM, **2d** showed an almost similar performance to **2b** in Allegheny river water – the most stressed, high DOC real water studied in the group till date. This can also be explained by the virtue of the higher  $k_{II}/k_I$  ratio for **2d** –  $3.6 \times 10^7 \text{ M}^{-1}$  as opposed to  $3.3 \times 10^7 \text{ M}^{-1}$  for **2b**. While the magnitude of superiority of  $k_{II}/k_I$  ratio for **2d** over **2b** is not huge, but when combined with the active kill switch in **2b**, the effect is significant as observed in the Allegheny river water studies. Just by the virtue of having more active catalyst in the reaction, the rate and progress of reaction is greatly enhanced since any TAML/NewTAML catalytic reaction is linearly dependent on the [TAML/NewTAML] as in eq 4.1. When the experiments were evaluated over longer times, viz., 24h the effect of the kill switch becomes even more evident (figure 4.5, right). At 100 nM, **2c** (with a partially muted kill switch) reduced propranolol ( $5.3 \times 10^{-8} \text{ M}$ ) to BDL concentrations after 18 h of reaction while **2a**, with a fully active kill switch, was inactivated after 3.5 h of reaction after reducing propranolol by 60 %. At  $1/10^{\text{th}}$  the concentration of **2b** in Allegheny river water, **2d** showed a slightly better performance of 75 % over 70 % reduction with 10 times more **2b** in reaction. Even in river water, the performance of **2d** at 10 nM performed better than **2a** at 100 nM and was only slightly lower in performance than **2c** at 100 nM in clean buffered water (figure 4.5, right).

#### **4.2.5 Safety perspective:**

Although no toxicity experiments were performed as part of my thesis work, it is important to point to the previous study published by the group<sup>6,30</sup> focused on including mouse uterotrophic assays to better understand the safety of NewTAMLs (using **2a**) to bring a holistic picture of technical and safety performance as part of finalizing a candidate for real wastewater treatment. Catalyst **2a** was shown to reduce the estrogenicity induced in prepubertal mice by using drinking water containing 84 nM ethynylestradiol (EE2) where different mice cohorts received (i) EE2, (ii)

**2a**, (iii) **2a**/H<sub>2</sub>O<sub>2</sub>/EE2 and (iv) water alone. EE2 produces a uterotrophic response in the mice, viz., 6.2-fold enlargement in uterus when drinking EE2 containing water to result in a 5–9 ppt daily intake as opposed to drinking uncontaminated water. When the EE2 containing drinking water was treated with 4 nM **2a**/1 mM H<sub>2</sub>O<sub>2</sub> the uterotrophic response was reduced to ~ 40 % and at 40 nM **2a**/1 mM H<sub>2</sub>O<sub>2</sub> it was reduced to ~ 3 %, the same value as a negative control with plain water. This also approved of the **2a** catalytic oxidation process since the known estrogenic oxidation products of EE2 produced during **2a**/H<sub>2</sub>O<sub>2</sub> oxidations had to be completely destroyed with EE2 to achieve this result. While **2a**/H<sub>2</sub>O<sub>2</sub> were very effective at reducing the estrogenicity induced by EE2 in mice, control experiments with just **2a** (4nM or 40 nM)/1mM H<sub>2</sub>O<sub>2</sub> did not induce any estrogenicity

### 4.3 CONCLUSIONS

The utilitarian aspect of NewTAMLs was better assessed for practical applications using the harder to oxidize substrate propranolol as compared to Orange II. NewTAMLs outperform analogous TAMLs in oxidation of propranolol at higher concentrations such as  $5 \times 10^{-5}$  M as well as at environmentally relevant dilute concentration  $5.3 \times 10^{-8}$  M. The critical parameter in the reactivity of a TAML/NewTAML is the  $k_{II}/k_i$  ratio at any point in time for their catalyzed oxidations of substrates. However, the kill switch component in **2** activators complicate the simple analyses. Only when a *kill switch off* **2** activator is synthesized, changes can be incorporated in the kinetic scheme to tell a holistic catalyst inactivation mechanism. For easier interpretations at this point, we will continue to use the existing reaction schemes which use an overall inactivation rate constant,  $k_i$  as opposed to a differentiated perhydrolysis and kill switch inactivations.

Nitro substituted TAML **1b** and Nitro substituted NewTAMLs **2b** outperformed their non-substituted analogs **1a** and **2a**. Inactivation pathway in NewTAML, viz., “the kill switch” contributes significantly at alkaline pH for **2b** and also affects its life and overall reactivity at pH 7. This significance was illustrated with comparative experiments involving **2a**, **2b** with their structural analogs **2c** and **2d** (having a partially muted kill switch - 1 methyl group substituted for 1 methylene proton). Catalysts **2c** and **2d** outperformed **2a** and **2b** respectively in both buffered solution and unbuffered Allegheny river water at pH 7. At 100 nM, **2b** was inactivated within 20 min (70 % propranolol reduction) while 100 nM **2d** reduced propranolol  $5.3 \times 10^{-8}$  M to BDL concentrations in 20 min. The partially muted kill switch in **2d** enabled greater life of **2d** which resulted in 10 nM **2d** providing similar performance to 100 nM **2b** in the oxidation of propranolol  $5.3 \times 10^{-8}$  M in Allegheny river water. From a safety perspective, **2a**/H<sub>2</sub>O<sub>2</sub> treatment process was found to be safe to mice by itself and it reduced or eliminated the estrogenicity induced in mice, by drinking EE2 spiked water, when the drinking water was treated with 4 nM or 40 nM/1mM

H<sub>2</sub>O<sub>2</sub>, respectively. While experiments were not performed specifically for **2d** because of the time consuming and expensive nature of the toxicity experiments, extrapolating from safety experiments involving **1a** and **1c**<sup>10,31,32</sup> and now **2a**/H<sub>2</sub>O<sub>2</sub> treatments, it is safe to conclude that **2d**/H<sub>2</sub>O<sub>2</sub> treatment process will not produce estrogenic products or induce toxicity in mice. Combining the technical and safety performances together, **2d** was determined to be the current best overall candidate for real waste water treatment considering technical, cost, health, and environmental and fairness performances for parameterizing sustainable technologies.

## 4.4 EXPERIMENTAL

### 4.4.1 Materials.

TAML activator **1a**, **1b**, **1c**, **5** were obtained from IGS supplies; NewTAML activators **2a-2d**, **6**, **7** were obtained from Dr. Genoa R. Warner and NewTAML activator 4 was obtained from Dr. Matthew R. Mills. Buffer solutions were made using KH<sub>2</sub>PO<sub>4</sub> (Acros) or K<sub>2</sub>HPO<sub>4</sub> (Merck); the pH was adjusted with concentrated solutions of KOH or H<sub>3</sub>PO<sub>4</sub>. Hydrogen peroxide (30%) was purchased from Fischer. Catalase from bovine liver (lyophilized powder, 2000-5000 units mg<sup>-1</sup> of protein) was purchased from Sigma. (±)-Propranolol hydrochloride (>99%), were purchased from Sigma and used as received. Methanol and water (both HPLC grade) were obtained from Fischer and used for liquid chromatography without additional purification.

### 4.4.2 Catalyzed Degradation of Propranolol by H<sub>2</sub>O<sub>2</sub>

Stock solutions of catalyst ( $1 \times 10^{-5}$  M), propranolol ( $4 \times 10^{-6}$  M or  $5 \times 10^{-3}$  M), and H<sub>2</sub>O<sub>2</sub> (1 M) were prepared in HPLC-grade water. Appropriate volumes of phosphate buffer (0.01 M), propranolol, and catalyst stock solutions were combined and equilibrated to  $25 \pm 2$  °C in a water bath. The reaction was initiated by the addition of an appropriate volume of the peroxide stock solution to give a final volume of 10 mL. At predetermined time intervals, aliquots were withdrawn, and the concentration of propranolol was determined using HPLC. The LC method consisted of 1 mL/min flow rate, 35% methanol/65% pH 3 0.01 M phosphate buffer, 40 °C column temperature, and fluorescence detection by excitation at 230 nm and monitoring of the 340 nm emission wavelength. For the measurements of parts per million of propranolol, the sensitivity was set to low and the sample injection volume for the analyses was 10 µL. For the measurement of parts per billion concentrations of propranolol, the sensitivity was set to medium with 4× gain for the signal and the sample injection volume for the analysis was 100 µL. All



propranolol peaks were integrated automatically, and the data was analyzed using Lab Solutions software. All reported values are the mean of three determinations.

#### ***4.4.3 Instrumentation.***

UV-vis measurements were performed using an Agilent 8453 instrument with an attached temperature controller. The pH measurements were made using an Accumet Basic AB15 pH meter from Fischer Scientific. UPLC studies were performed with a Shimadzu LC system with LC 20AB pump, SIL 20A autosampler, CTO 20A column oven, and an RF 20A XS fluorescence detector. A Kinetex (Phenomenex) 5  $\mu$ M EVO C18 100A column (4.6  $\times$  50 mm) was used for all kinetic analyses. The LC method consisted of 1 mL min<sup>-1</sup> flow rate, 35% methanol in pH 3 phosphate buffer (0.01 M), 40 °C column temperature, and fluorescence detection with 230 nm excitation and 340 nm emission. The sample injection volume for the analyses was 10  $\mu$ L and the data was automatically integrated and analyzed using Lab Solutions software.

#### 4.5 REFERENCES

- (1) Collins, T. J. Designing Ligands for Oxidizing Complexes. *Acc. Chem. Res.* **1994**, 27 (9), 279–285.
- (2) Collins, T. J. TAML Oxidant Activators: A New Approach to the Activation of Hydrogen Peroxide for Environmentally Significant Problems. *Acc. Chem. Res.* **2002**, 35 (9), 782–790.
- (3) Ryabov, A. D.; Collins, T. J. Mechanistic Considerations on the Reactivity of Green FeIII-TAML Activators of Peroxides. *Adv. Inorg. Chem.* **2009**, 61, 471–521.
- (4) Shen, L. Q.; Beach, E. S.; Xiang, Y.; Tshudy, D. J.; Khanina, N.; Horwitz, C. P.; Bier, M. E.; Collins, T. J. Rapid, Biomimetic Degradation in Water of the Persistent Drug Sertraline by TAML Catalysts and Hydrogen Peroxide. *Env. Sci Technol* **2011**, 45 (18), 7882–7887.
- (5) Kundu, S.; Chanda, A.; Khetan, S. K.; Ryabov, A. D.; Collins, T. J. TAML Activator/Peroxide-Catalyzed Facile Oxidative Degradation of the Persistent Explosives Trinitrotoluene and Trinitrobenzene in Micellar Solutions. *Env. Sci Technol* **2013**, 47 (10), 5319–5326.
- (6) Warner, G. R.; Somasundar, Y.; Jansen, K. C.; Kaaret, E. Z.; Weng, C.; Burton, A. E.; Mills, M. R.; Shen, L. Q.; Ryabov, A. D.; Pros, G.; Pintauer, T.; Biswas, S.; Hendrich, M. P.; Taylor, J. A.; Vom Saal, F. S.; Collins, T. J. Bioinspired, Multidisciplinary, Iterative Catalyst Design Creates the Highest Performance Peroxidase Mimics and the Field of Sustainable Ultradilute Oxidation Catalysis (SUDOC). *ACS Catal.* **2019**, 7023–7037.
- (7) Somasundar, Y.; Shen, L. Q.; Hoane, A. G.; Tang, L. L.; Mills, M. R.; Burton, A. E.; Ryabov, A. D.; Collins, T. J. Structural, Mechanistic, and Ultradilute Catalysis Portrayal of Substrate Inhibition in the TAML–Hydrogen Peroxide Catalytic Oxidation of the Persistent Drug and Micropollutant, Propranolol. *J. Am. Chem. Soc.* **2018**, 140 (38), 12280–12289.
- (8) Chanda, A.; Khetan, S. K.; Banerjee, D.; Ghosh, A.; Collins, T. J. Total Degradation of Fenitrothion and Other Organophosphorus Pesticides by Catalytic Oxidation Employing Fe-TAML Peroxide Activators. *J Am Chem Soc* **2006**, 128 (37), 12058–12059.
- (9) Deboshri, B.; L., M. A.; Toshihiro, Y.; Anindya, G.; B., B. P.; G., M. E.; K., K. S.; J., C. T. “Green” Oxidation Catalysis for Rapid Deactivation of Bacterial Spores. *Angew. Chemie Int. Ed.* **2006**, 45 (24), 3974–3977.
- (10) Onundi, Y.; Drake, B. A.; Malecky, R. T.; DeNardo, M. A.; Mills, M. R.; Kundu, S.; Ryabov, A. D.; Beach, E. S.; Horwitz, C. P.; Simonich, M. T.; Truong, L.; Tanguay, R. L.; Wright, L. J.; Singhal, N.; Collins, T. J. A Multidisciplinary Investigation of the Technical and Environmental Performances of TAML/Peroxide Elimination of Bisphenol A Compounds from Water. *Green Chem.* **2017**, 19 (18), 4234–4262.
- (11) Mills, M. R.; Arias-Salazar, K.; Baynes, A.; Shen, L. Q.; Churchley, J.; Beresford, N.; Gayathri, C.; Gil, R. R.; Kanda, R.; Jobling, S.; Collins, T. J. Removal of Ecotoxicity of 17 $\alpha$ -Ethinylestradiol Using TAML/Peroxide Water Treatment. *Sci Rep* **2015**, 5, 10511.
- (12) Collins, T. J.; Ryabov, A. D. Targeting of High-Valent Iron-TAML Activators at

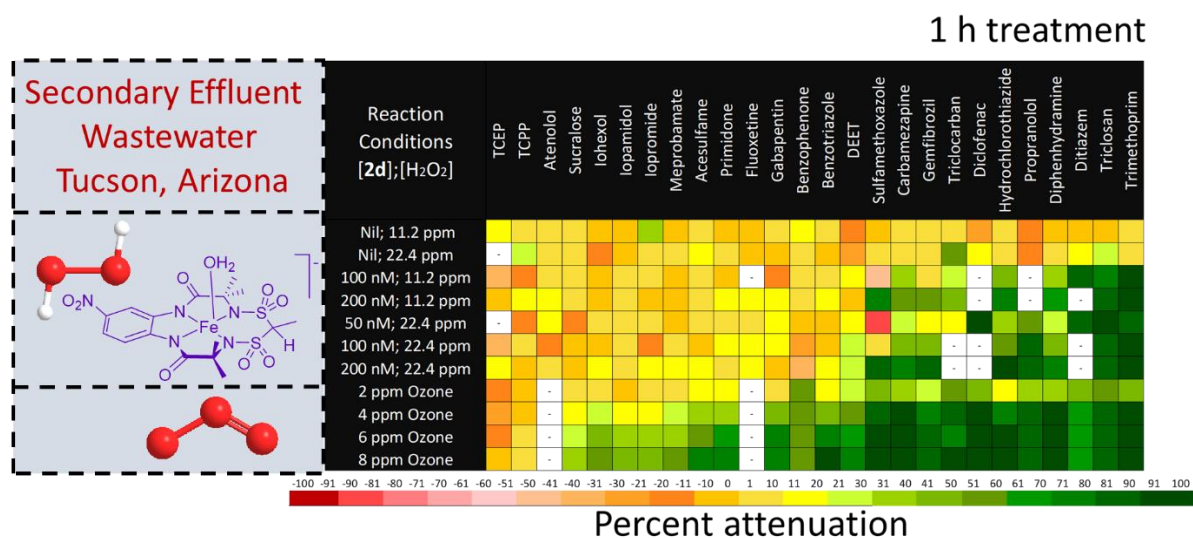
Hydrocarbons and Beyond. *Chem. Rev.* **2017**.

- (13) Tang, L. L.; DeNardo, M. A.; Schuler, C. J.; Mills, M. R.; Gayathri, C.; Gil, R. R.; Kanda, R.; Collins, T. J. Homogeneous Catalysis Under Ultradilute Conditions: TAML/NaClO Oxidation of Persistent Metaldehyde. *J. Am. Chem. Soc.* **2017**, *139* (2), 879–887.
- (14) DeNardo, M. A.; Mills, M. R.; Ryabov, A. D.; Collins, T. J. Unifying Evaluation of the Technical Performances of Iron-Tetra-Amido Macrocyclic Ligand Oxidation Catalysts. *J. Am. Chem. Soc.* **2016**, *138* (9), 2933–2936.
- (15) Collins, T. J.; DeNardo, M. A.; Warner, G. R.; Gordon-Wylie, S. W.; Ellis, W. C.; Somasundar, Y. Far Superior Oxidation Catalysts Based on Macrocyclic Compounds, October 25, 2018.
- (16) Chahbane, N.; Popescu, D. L.; Mitchell, D. A.; Chanda, A.; Lenoir, D.; Ryabov, A. D.; Schramm, K. W.; Collins, T. J. FeIII-TAML-Catalyzed Green Oxidative Degradation of the Azo Dye Orange II by H<sub>2</sub>O<sub>2</sub> and Organic Peroxides: Products, Toxicity, Kinetics, and Mechanisms. *Green Chem.* **2007**, *9* (1), 49–57.
- (17) Warner, G.; Mills, M.; Enslin, C.; Pattanayak, S.; Panda, C.; Sen Gupta, S.; Ryabov, A. D.; Collins, T. J. Reactivity of N-Tailed ('Biuret') TAMLs in Water: Kinetics of the Catalyzed Oxidation of Orange II by H<sub>2</sub>O<sub>2</sub>. Synthesis and X-Ray Characterization of an N-Phenyl Biuret TAML. *Chem. - Eur. J.* **2015**, *21* (16), 6226–6233.
- (18) Stapleton, M. P. Sir James Black and Propranolol. The Role of the Basic Sciences in the History of Cardiovascular Pharmacology. *Tex Hear. Inst J* **1997**, *24* (4), 336–342.
- (19) Huggett, D. B.; Brooks, B. W.; Peterson, B.; Foran, C. M.; Schlenk, D. Toxicity of Select Beta Adrenergic Receptor-Blocking Pharmaceuticals (B-Blockers) on Aquatic Organisms. *Arch Env. Contam Toxicol* **2002**, *43* (2), 229–235.
- (20) Escher, B. I.; Bramaz, N.; Eggen, R. I. L.; Richter, M. In Vitro Assessment of Modes of Toxic Action of Pharmaceuticals in Aquatic Life. *Environ. Sci. Technol.* **2005**, *39* (9), 3090–3100.
- (21) Soeter, M.; Kindt, M. An Abrupt Transformation of Phobic Behavior After a Post-Retrieval Amnesic Agent. *Biol Psychiatry* **2015**, *78* (12), 880–886.
- (22) Fent, K.; Weston, A. A.; Caminada, D. Ecotoxicology of Human Pharmaceuticals. *Aquat. Toxicol.* **2006**, *76* (2), 122–159.
- (23) Miege, C.; Favier, M.; Brosse, C.; Canler, J. P.; Coquery, M. Occurrence of Betablockers in Effluents of Wastewater Treatment Plants from the Lyon Area (France) and Risk Assessment for the Downstream Rivers. *Talanta* **2006**, *70* (4 LB-Miège2006), 739–744.
- (24) Yamamoto, H.; Nakamura, Y.; Moriguchi, S.; Nakamura, Y.; Honda, Y.; Tamura, I.; Hirata, Y.; Hayashi, A.; Sekizawa, J. Persistence and Partitioning of Eight Selected Pharmaceuticals in the Aquatic Environment: Laboratory Photolysis, Biodegradation, and Sorption Experiments. *Water Res* **2009**, *43* (2), 351–362.
- (25) Petrovic, M.; Skrbic, B.; Zivancev, J.; Ferrando-Climent, L.; Barcelo, D. Determination of 81 Pharmaceutical Drugs by High Performance Liquid Chromatography Coupled to Mass Spectrometry with Hybrid Triple Quadrupole-Linear Ion Trap in Different Types of Water in Serbia. *Sci. Total Environ.* **2014**, *468*, 415–428.

- (26) Ashton, D.; Hilton, M.; Thomas, K. V. Investigating the Environmental Transport of Human Pharmaceuticals to Streams in the United Kingdom. *Sci Total Env.* **2004**, 333 (1–3), 167–184.
- (27) Birch, G. F.; Drage, D. S.; Thompson, K.; Eaglesham, G.; Mueller, J. F. Emerging Contaminants (Pharmaceuticals, Personal Care Products, a Food Additive and Pesticides) in Waters of Sydney Estuary, Australia. *Mar. Pollut. Bull.* **2015**, 97 (1), 56–66.
- (28) Pochodylo, A.; Helbling, D. E. *Target and Suspect Screening for Micropollutants in the Hudson River Estuary during the 2015 Recreational Season*; Cornell University, 2015.
- (29) Huggett, D. B.; Khan, I. A.; Foran, C. M.; Schlenk, D. Determination of Beta-Adrenergic Receptor Blocking Pharmaceuticals in United States Wastewater Effluent. *Environ. Pollut.* **2002**, 121, 199–205.
- (30) Warner, G. R. SYNTHESIS, PROPERTIES, AND REACTIVITY OF SULFONAMIDE NEWTAML OXIDATION CATALYSTS, Carnegie Mellon University, 2017.
- (31) Truong, L.; DeNardo, M. A.; Kundu, S.; Collins, T. J.; Tanguay, R. L. Zebrafish Assays as Developmental Toxicity Indicators in the Green Design of TAML Oxidation Catalysts. *Green Chem.* **2013**, 15 (9), 2339–2343.
- (32) Shappell, N. W.; Vrabel, M. A.; Madsen, P. J.; Harrington, G.; Billey, L. O.; Hakk, H.; Larsen, G. L.; Beach, E. S.; Horwitz, C. P.; Ro, K.; Hunt, P. G.; Collins, T. J. Destruction of Estrogens Using Fe-TAML/Peroxide Catalysis. *Environ. Sci. Technol.* **2008**, 42 (4), 1296–1300.

# Chapter 5

## Sustainable Ultra-Dilute Oxidation Catalysis (SUDOC) utilizing NewTAML activators for Global water treatment: A Landmark study with Tucson wastewater.



## 5.1 INTRODUCTION

Water pollution is an everyday problem which is ubiquitous around the world.<sup>1</sup> Recent advancement in science have led to a massive production and subsequent disposal of pharmaceuticals, consumer products, hormones, industrial chemicals, research supplies, etc. into our water bodies.<sup>2-8</sup> Several of these compounds behave as micropollutants, exhibiting adverse effects at low doses (ppt-ppb).<sup>9-11</sup> Conventional wastewater treatment methods are ineffective in removing these micropollutants (MPs) at their low concentrations.<sup>5,12</sup> To address the micropollutant menace, Switzerland mandated a 50% reduction in their releases and added an additional step of ozone and activated carbon treatment in ca. 100 of their ca. 650 wastewater treatment plants.<sup>13,14</sup> However, this is a solution viable for rich nations and does not transfer to less wealthy jurisdictions across world.

TAML (Tetra amido macrocyclic ligand, **1**) activators are bio inspired, small molecule, fully functional (mechanism copying) replicas of the peroxidase and cytochrome P450 enzymes<sup>15,16</sup> at 1% the size of the enzymes. Over the last two decades, TAMLs have been shown to be effective in destroying a broad range of MPs including pharmaceuticals, pesticides, artificial estrogens, explosives, bacterial spores, dyes, industrial chemicals, and many more.<sup>17-24</sup> In one of the studies on London wastewaters, the best performing TAML **1c** was shown to be effective in oxidizing MPs at ppt-ppb concentrations.<sup>25</sup> However, **1c** is an organofluorine catalyst and despite being safety tested in low dose zebrafish developmental toxicity experiments,<sup>19,26</sup> we decided to not develop it for commercialization as a precautionary safety measure for considering the continuous long term use at global scale that we are targeting.<sup>27</sup> Over 25 years, our continued iterations in design, focused on the performance and safety parameters, have provided us with a superior, long lasting, non-halogenated next generation of catalysts called “NewTAMLs”, **2**.

The technical performance for any of **1** or **2** activators, viz., reactivity and lifetime, adheres to the mechanism shown in Figure 5.1.

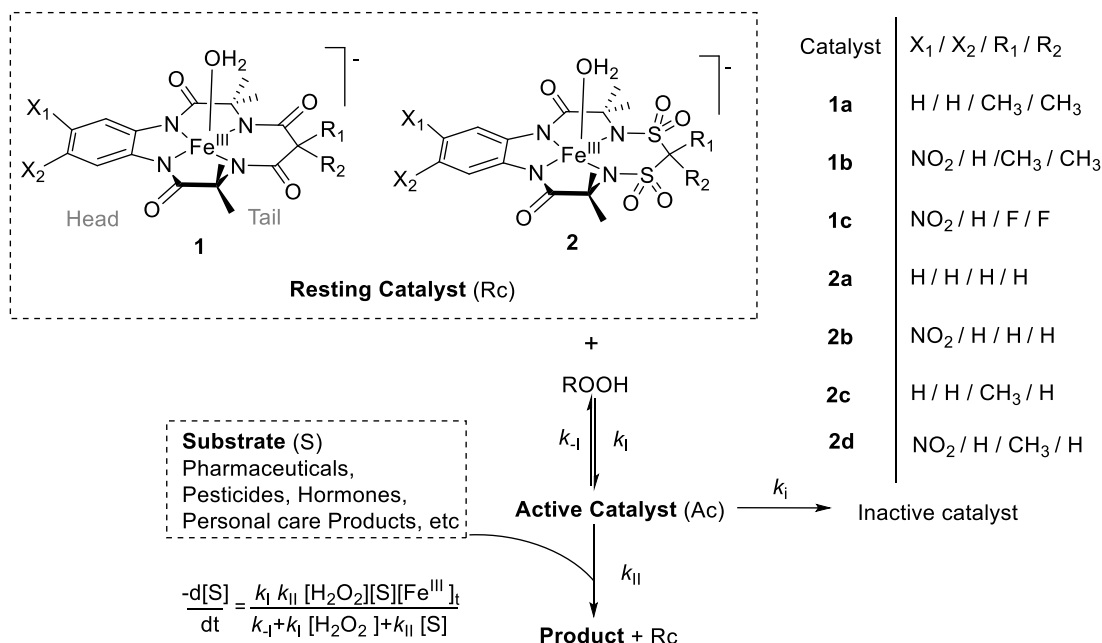


Figure 5.1 : Structures of TAMLs **1** and NewTAMLs **2** used or discussed in this paper and general mechanism for **1** or **2** catalyzed oxidation of substrates (micropollutants). \* ROOH in this study is H<sub>2</sub>O<sub>2</sub>

As discussed in detail in the recently published introductory paper on **2** activators, a bigger ratio of  $k_{II}$  (reactivity)/ $k_i$  (lifetime) correlates with a superior catalyst.<sup>28</sup> Prior to **2**, **1** activators exhibited a linear free energy relationship (LFER) between  $k_{II}$  and  $k_i$  with a slope  $\approx 1$ . This meant that the most reactive **1** activator always had the lowest lifetime in a catalytic oxidation process.<sup>29</sup> Through detailed mechanistic understanding and iterative design over 25 years, we were able to develop **2** activators which are non-halogenated and fell slightly below the linear  $\log k_{II}/\log k_i$  line followed by **1** activators and certain **2** activators (**2a, 2b**), resulting in more reactive, and equally long-lived **2d**. (see Table 2) This was made possible in the iterative process by first discovering and then controlling a new tunable lifetime control design element called a *kill switch* (CH<sub>2</sub>

bridging acidifying sulfonamide ligands in **2a,2b** versus less acidic C(CH<sub>3</sub>)H in **2c,2d**) in the tail region of **2** activators which gave us greater ability to control the functional lifetime and offered the potential to balance this against persistence in the environment. Although only marginally off the line, the resulting enhanced effect for **2c** and **2d** was clearly visible under stressed conditions (harder to oxidize substrate, multiple contaminants and high DOC water) as in the oxidation of a persistent pharmaceutical propranolol (active ingredient of beta blocker drug Inderal), a concentration (~15 ppb) that is close to environmentally relevant concentrations ( $\leq 2$  ppb) in Allegheny river water. At 100 nM catalyst loading and fish-safe 0.33 mM (11.2 ppm) H<sub>2</sub>O<sub>2</sub>, while **2b** deactivated after 77% attenuation, **2d** removed propranolol to below detection limits after 25 min. Pushing the system a notch higher, analogous experiments with 10% catalyst loading (10 nM), **2d** achieved 77 % attenuation of propranolol before inactivation at ~6h. This translates to treating ca. 160,000 tonnes of wastewater with one kilogram of **2d** (our best performing **2** activator).

With respect to safety, the TAML prototype catalyst **1a** in conjunction with 4mM H<sub>2</sub>O<sub>2</sub> completely removed the estrogenicity in BPA (43.8  $\mu$ M) solutions and despite being an organofluorine catalyst, our best performing **1** TAML, **1c**, passed zebrafish developmental toxicity studies.<sup>26</sup> However as a precautionary measure, we decided to move beyond halogenated **1c**. Recently, **2a** (analogous to **1a**) in conjunction with 1mM H<sub>2</sub>O<sub>2</sub> completely removed the uterotrophic response (increase in uterine weight by 6.2 fold) induced in mice, by feeding of EE2 spiked water (84 nM). Additionally, no uterotrophic response was observed when water containing only **2a** at 4 nM and 40 nM was fed to mice.<sup>28</sup> Building on the state of the art catalysis for water purification, here we present an economic, efficient, rapid and a safe (by all measures to date) alternative to ozone and other technologies for wastewater treatment- *NewTAML hydrogen peroxide catalytic oxidation*.



## 5.2 RESULTS AND DISCUSSION

### 5.2.1 Comparative evaluation of **2d**/H<sub>2</sub>O<sub>2</sub> treatments and Ozone treatments

The superior technical and safety performances of **2** activators have enabled a novel, first of its kind, domain of catalysis that we have named *Sustainable Ultradilute Oxidation catalysis* (SUDOC).<sup>28</sup> With SUDOC at our disposal, in collaboration with the group of Shane Snyder at University of Arizona, we performed an extensive study on the attenuation of 38 MPs (in triplicate separate experiments), kinetically over 6 h, with five different treatment conditions using our best performing **2d**/H<sub>2</sub>O<sub>2</sub> with two control H<sub>2</sub>O<sub>2</sub> experiments. For comparison, we have performed analogous non-kinetic experiments to evaluate the comparative endpoint performance of 2, 4, 6 and 8 ppm ozone treatment (analyzed after **72** hours of addition of ozone aliquot – this is not the effective exposure time since ozone decays rapidly) of the same water samples from a municipal wastewater treatment plant: Agua Nueva. The bulk composition of the organic matrix of the wastewater was also evaluated to understand the effectiveness of the **2d**/H<sub>2</sub>O<sub>2</sub> treatment in different wastewaters. Herein, we present SUDOC treatment as an economic, efficient, rapid and safe alternative for wastewater treatment.

Of the 38 compounds that were analyzed (Table 5.5), compounds selected based on a priority scoring system published previously,<sup>30</sup> during the treatment studies, only 26 compounds were detected in the Tucson wastewater across experiments. The technical performance after 1h of **2d**/H<sub>2</sub>O<sub>2</sub> treatment is shown in Figure 5.2. Percent attenuation here refers to the percent reduction of the MP in reference to its 0 min time point.. The rest of the kinetic profile can be found in the Appendix (Figure 5.8). For easier interpretation, compounds have been arranged from left to right with increasing ease or extent of oxidation, with the most easily oxidized compounds by **2d**/H<sub>2</sub>O<sub>2</sub> and ozone treatments being on the right of the heat map (green zone, DEET-trimethoprim). The compounds on the left (amber zone, TCEP-benzotriazole) show little to no oxidation with

**2d**/H<sub>2</sub>O<sub>2</sub> treatments under the various conditions and with 2 ppm ozone. However, they show slightly more oxidation at higher ozone concentrations. What is important to note here is the mechanism of

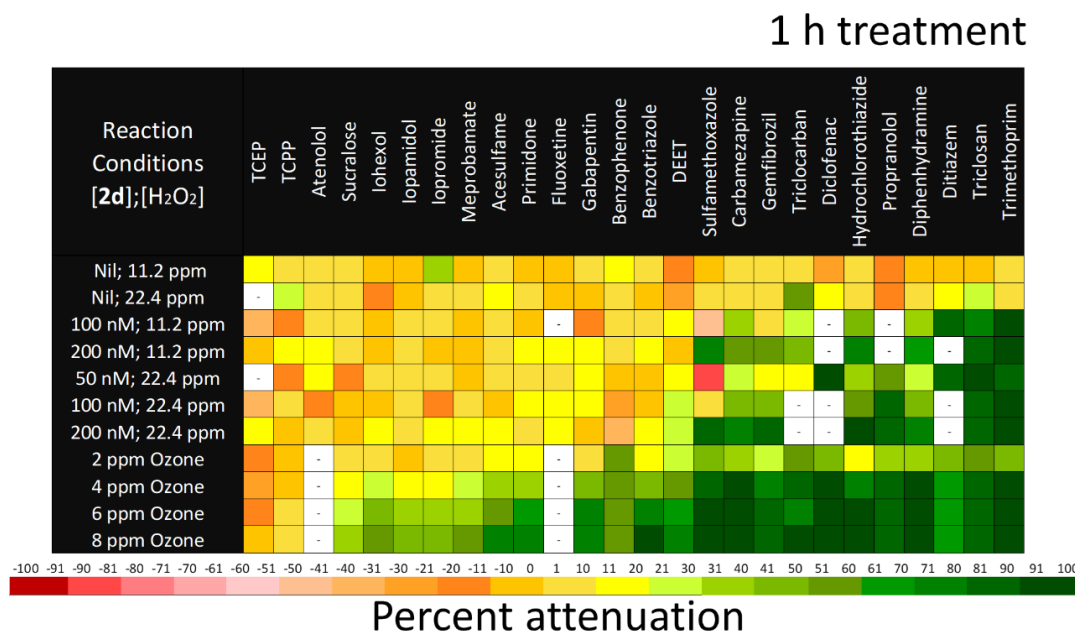


Figure 5.2 Attenuation in percentage (average of triplicate separate measurements) for micropollutants after 1h treatment with various concentrations of (i) H<sub>2</sub>O<sub>2</sub>, (ii) **2d**/H<sub>2</sub>O<sub>2</sub> and (iii) ozone (from the endpoint concentration, no kinetics performed). \*White boxes indicate below detection level concentrations for compounds prior to and at all stages of experimentation.

oxidation by ozone is very different to the mechanism of oxidation by **2d**/H<sub>2</sub>O<sub>2</sub> treatment. Probably, these compounds cannot be typically oxidized by conventional peroxide based treatment.

There was practically no change in the heat map between 1h until 6h (Figure 5.8). We believe under high DOC, multi compound wastewater conditions, the kill switch in **2d** served to winnow out the catalyst almost completely at 1h. This indicates that H<sub>2</sub>O<sub>2</sub> by itself and no secondary oxidants that might have been generated could oxidize the MPs. Although not performed here, we have shown in chapter 4 that adding a second aliquot of catalyst helps in taking the reaction further down to get

non detect concentrations of MPs. Given the superior reactivity of **2d** at pH 7, we expected most of the attenuation to happen in the first 30 min. The treatment time is very important here because it directly influences holding tanks volumes and thus capital and operational costs with shorter process times being better.

### 5.2.2 Improvement factor of 200 nM **2d** /22.4 ppm H<sub>2</sub>O<sub>2</sub> over 2 ppm ozone

We have summarized the performance of our best treatment condition, viz., 200 nM **2d**/22.4 ppm H<sub>2</sub>O<sub>2</sub> alongside the current industry standard dose 2 ppm ozone (table 5.1). Since there was practically no differences between these two processes under the prescribed conditions in the amber zone, only MPs in the green zone are discussed below.

Table 5.1 Percent attenuation for MPs in the green zone for 200 nM **2d** /22.4 ppm H<sub>2</sub>O<sub>2</sub> over 6h. 2 ppm ozone endpoint attenuation percent added for comparison.

Treatment time, min	Percent Attenuation								
	DEET	Sulfamethoxazole	Carbamazepine	Gemfibrozil	Hydrochlorothiazide	Propranolol	Diphenhydramine	Triclosan	Trimethoprim
6	21.6	-26	25.8	25.8	31.6	83.8	19.5	77.1	74.3
12	22.8	43.2	34.9	45.1	54.2	86.2	37.2	75.6	95.7
20	31.7	72.1	51	55.7	67.2	86.6	54.2	84.2	98
30	23.1	86.2	61.8	68.9	83.2	88.4	63	84.2	98
60	25	88.8	73.5	88.6	92.2	88.4	77.1	84.2	98
360	26.2	87.8	72.7	85.5	90	88.4	83.3	84.2	98
2 ppm ozone*	28	48.7	37.3	29.7	11.2	31	35.5	54.1	43.2

\*Ozone measurements were non kinetic and only attenuation percent based on endpoint concentration is shown here.

Using 2 ppm ozone showed an attenuation percent between ~11-55% at its endpoint value for the above MPs. Barring sulfamethoxazole, even in the first 6 min, 200 nM **2d**/22.4 ppm H<sub>2</sub>O<sub>2</sub> treatment gave a percent removal between ~20-84%. The removal percent was ~ 22-96%, 23-98%, 25-98% and 26-98% after 12, 30, 60 and 360 min of treatment time. Widely used and priority MPs like propranolol, triclosan and trimethoprim showed an attenuation of ~84, 77 and 74 % respectively in the first 6 min as opposed to an end point attenuation of ~ 31, 54 and 43 % respectively with 2 ppm ozone treatment. Although not shown in this table due to lack of experimental data, diclofenac is another priority MP discussed in the European Union with respect to wastewater remediation. In London wastewater studies, diclofenac was the most successfully removed of 11 micropollutants thought to be of highest priority by the United Kingdom Water Industry Research (UKWIR) Association.

Table 5.2 Improvement factors for 200 nM **2d**/22.4 ppm H<sub>2</sub>O<sub>2</sub> over 2 ppm ozone treatment over 6h for MPs in the green zone of Figure 5.2.

Time, min	DEET	Sulfamethoxazole	Carbamazepine	Gemfibrozil	Hydrochlorothiazide	Propranolol	Diphenhydramine	Triclosan	Trimethoprim
6	0.8	-0.5	0.7	0.9	2.8	2.7	0.5	1.4	1.7
12	0.8	0.9	0.9	1.5	4.8	2.8	1.0	1.4	2.2
20	1.1	1.5	1.4	1.9	6.0	2.8	1.5	1.6	2.3
30	0.8	1.8	1.7	2.3	7.4	2.9	1.8	1.6	2.3
60	0.9	1.8	2.0	3.0	8.2	2.9	2.2	1.6	2.3
360	0.9	1.8	1.9	2.9	8.0	2.9	2.3	1.6	2.3

Diclofenac could be assessed using the data obtained with 50 nM **2d**/22.4 ppm H<sub>2</sub>O<sub>2</sub> treatment and showed a maximum attenuation percent of 92% in the first 6 min which remained constant thereafter. This can be compared with 41% attenuation by 2 ppm ozone thus providing a ~2.3-fold improvement over 2 ppm ozone treatment. Extrapolating to 200 nM **2d**, would translate to ~9.2-fold improvement over 2 ppm ozone treatment. Similarly, for diltiazem an improved performance

factor of ~2.1-fold and ~8.4-fold was obtained with 50 nM and 100 nM **2d**, respectively. The improved performances compared to ozone for the other MPs are summarized in table 5.2. From table 5.1, most MPs obtained a maximum attenuation at 30 min with 200 nM **2d**/22.4 ppm H<sub>2</sub>O<sub>2</sub> treatment. To give a holistic picture, we can see that, at all times, 200 nM **2d**/22.4 ppm H<sub>2</sub>O<sub>2</sub> performance is comparable (barring an outlier for sulfamethoxazole) or superior to ozone. After 60 min, for DEET, sulfamethoxazole, carbamazepine, gemfibrozil, hydrochlorothiazide, propranolol, diphenhydramine, triclosan, trimethoprim, 200 nM **2d**/22.4 ppm H<sub>2</sub>O<sub>2</sub> gave improved performance of ~ 1, 2, 2, 3, 8, 3, 2, 2, and 2-fold respectively (table 5.2) over 2 ppm ozone. This remained virtually identical even after 360 min (6 h) of 200 nM **2d**/ 22.4 ppm H<sub>2</sub>O<sub>2</sub> treatment. Because of the difficulties of the analyses, the estrogen estradiol, estrone and ethinylestradiol (EE2) were not followed. However, it is well established that these are rapidly and effectively destroyed by TAML/peroxide.<sup>19,25,28</sup>

### ***5.2.3 Kinetic analyses of 2d / H<sub>2</sub>O<sub>2</sub> and Ozone treatments utilizing trimethoprim as a model MP***

To help understand the **2d**/H<sub>2</sub>O<sub>2</sub> mechanisms and make reasonable comparisons with ozone, trimethoprim was chosen as a model compound for deeper kinetics analysis because it was observed across spectrum of conditions, at all kinetic time points and had a good attenuation percent for all treatments. Trimethoprim, typically used as an antibiotic in treating bladder infections and pneumonia for people infected with HIV, has taken its place in WHO's list of essential medicines. However, this leads to its profuse usage, greater disposal quantities and higher water contamination. In May 2019, in a news article published by University of York, trimethoprim was found to be the most prevalent antibiotic contaminating rivers.<sup>31</sup> This significance added to the case for studying this particular compound in deeper detail.

The experiments with 11.2 ppm and 22.4 ppm H<sub>2</sub>O<sub>2</sub> were evaluated at 100 nM and 200 nM of **2d** in triplicate separate experiments. The 22.4 ppm H<sub>2</sub>O<sub>2</sub> process showed a superior performance

across the board in oxidizing MPs (Figure 5.2), but the 11.2 ppm conditions are approximately equal (50 nM **2d**) or superior to (100 and 200 nM **2d**) 2 ppm ozone. In studying the kinetics of the model compound trimethoprim (Figure 5.3a, 5.3b), we observed: (i) maximum attenuation at 60 min and 30 min respectively for both 11.2 ppm and 22.4 ppm H<sub>2</sub>O<sub>2</sub> with 100 nM and 200 nM **2d** respectively, (ii) hyperbolic dependence on [H<sub>2</sub>O<sub>2</sub>], adhering to eq 1 as is typical of any TAML/NewTAML catalyst (Figure 5.1), and (iii) a near first order dependence in [H<sub>2</sub>O<sub>2</sub>] and treatment time (for the first 20 min – insets to Figure 5.3a,5.3b).

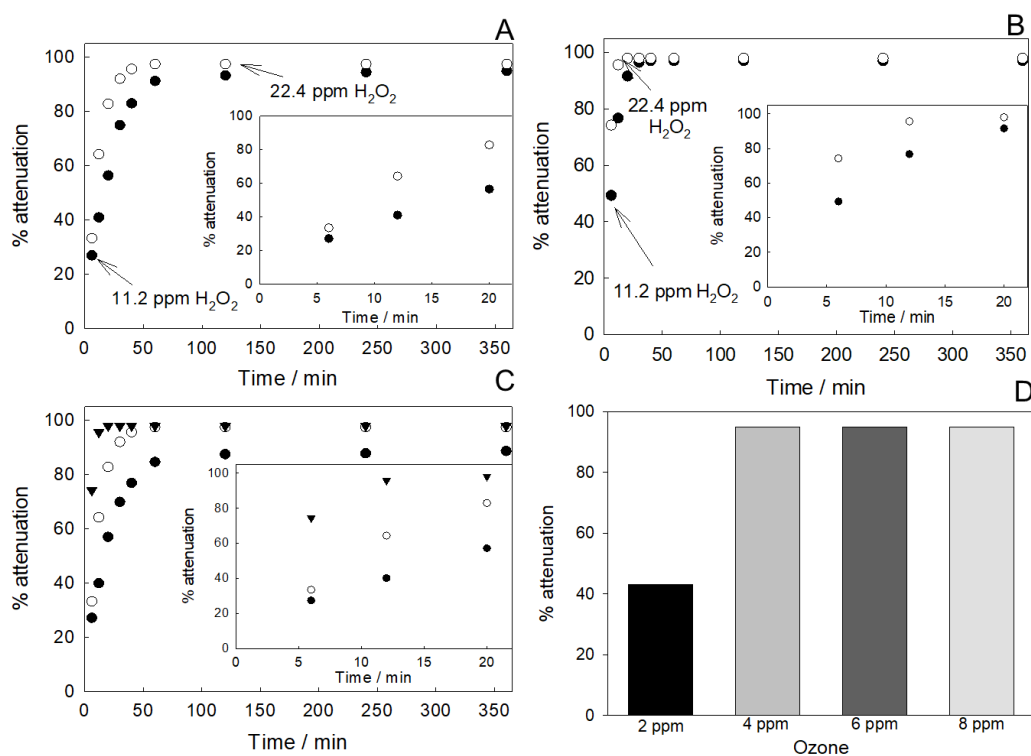


Figure 5.3 Percent attenuation (average of triplicate separate experiments) for trimethoprim over 6h with various **2d**/H<sub>2</sub>O<sub>2</sub> treatments: (A) 100 nM **2d** /11.2 and 22.4 ppm H<sub>2</sub>O<sub>2</sub> (B) 200 nM **2d** /11.2 and 22.4 ppm H<sub>2</sub>O<sub>2</sub> (C) 50, 100 and 200 nM **2d**/22.4 ppm H<sub>2</sub>O<sub>2</sub> and (D) 2, 4, 6 and 8 ppm ozone (non-kinetic, endpoint). Insets to A, B and C show percent attenuation in the first 20 min of treatment.

Given the rapid reactivity of **2d** at pH 7, this early saturation/maximization of attenuation was not surprising and better linearity with respect to [H<sub>2</sub>O<sub>2</sub>] could have been observed if more sampling

points were taken < 6 min in all cases. Detailed kinetic profiles for all MPs and treatments can be found in Figure 5.8

As with catalytic treatments, 2, 4, 6, and 8 ppm of ozone were explored to analyze the attenuation dependency on the [ozone]. Not surprisingly, while 6 ppm and 8 ppm of ozone performed extremely well compared to 2 and 4 ppm, the difference in performance between them was negligible across all compounds. The effect of [Ozone] on the attenuation of various MPs (carbamazepine and beyond in the green zone) have been shown in Figure 5.9. In some cases, like carbamazepine (Figure 5.9) and trimethoprim (Figure 5.3D), the attenuation increased almost linearly from 2 ppm to 4 ppm and saturated after this. Greater linear dependency with attenuation could probably be observed at lower concentrations of ozone (< 2 ppm). While 6 ppm and 8 ppm of ozone show great attenuations at first glance, they also add significantly to the operational and capital costs for wastewater treatment. Just to give a more practical relevance, the flagship ozone MP wastewater treatment plant at the Neugat Palant in Dübendorf Switzerland uses 2 ppm ozone in typical operations (Prof. Urs Von Gunten to Prof. Collins, private communication).

Adhering to the defined TAML catalysis mechanisms (eq 1, Figure 1), a first order dependency in [2d] was observed for trimethoprim (Figure 5.3c) in the first 20 min (Figure 5.3c-inset).

Additionally, at 22.4 ppm H<sub>2</sub>O<sub>2</sub>, 50 nM, 100 nM and 200 nM of **2d** showed maximum attenuation at ~120, 60, and 20 min, respectively, corresponding to ~84 %, 98% and 98%, respectively again. The [2d] dependency for MPs in the green zone for the first 6 min has been shown in Figure 5.10. Once oxidized intermediates are formed, they compete with parent MPs for the active **2d**. For the seven compounds shown in Figure 5.10, everything except triclosan exhibited a first order dependency on [2d] (eq 1, Figure 1) with R<sup>2</sup> varying from 0.95 to 0.98. This is a significant linear dependence on [2d] considering a small amount of activated **2d** is constantly being consumed by oxidizing undetermined compounds in the wastewater matrix. Not surprisingly, easier to oxidize MPs like triclosan, propranolol and trimethoprim deviated slightly from linearity due to faster

maximum attenuation of the MPs. The intercept in most cases was non-zero suggesting background oxidation with  $\text{H}_2\text{O}_2$  alone (negligible) and faster oxidation kinetics. Better linearity would be observed if kinetic measurements were to be performed at lower time points (< 6 min)—nevertheless, this is a massive water treatment study already.

#### 5.2.4 Correlating structure of MPs with their attenuation.

Unfortunately, given the diverse structures of MPs, developed for their varying applications, it was really difficult to find a common property or a structural moiety within MPs which could account for their differences in reactivity with **2d** /  $\text{H}_2\text{O}_2$  treatments. Efforts were made to develop a correlation between % attenuation and  $\text{p}K_{\text{a}1}$  of the MPs wherever available (Figure 5.4).<sup>32</sup>

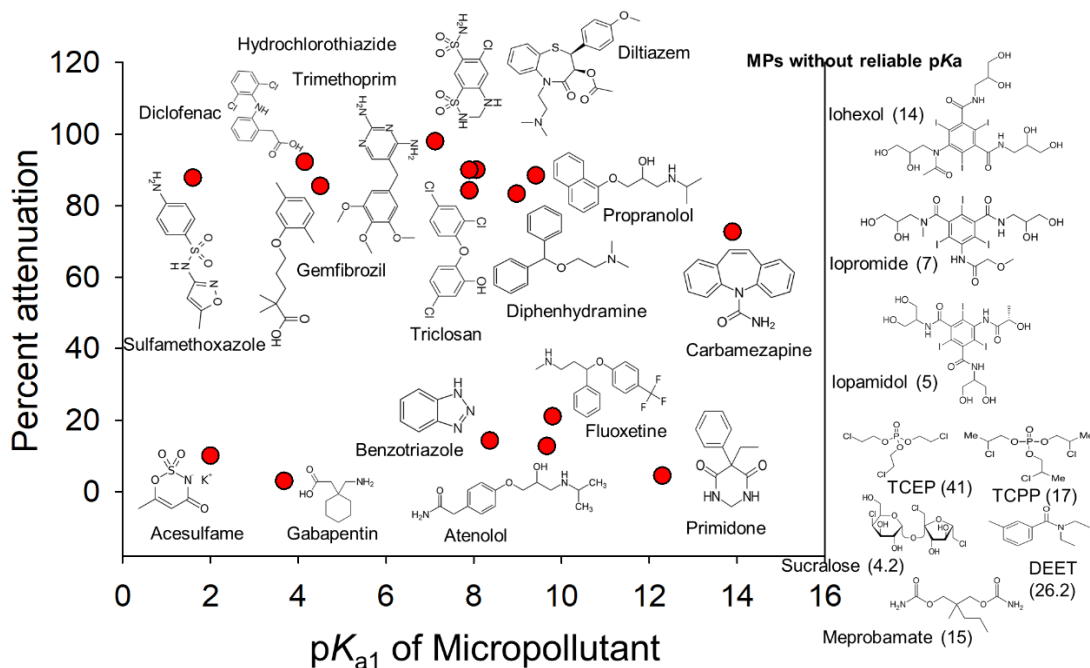


Figure 5.4 Correlation of the percent attenuations, after 6h of 200 nM **2d**/22.4 ppm  $\text{H}_2\text{O}_2$  treatment, with the  $\text{p}K_{\text{a}1}$  of the micropollutants. No reliable  $\text{p}K_{\text{a}1}$  could be obtained for MPs mentioned on the right. The attenuation percent for each of them is mentioned in the brackets.



The resulting correlation populated into two clear bands viz., green zone and amber zone MPs from Figure 5.1 with no clear trend. Acesulfame and sulfamethoxazole have very similar  $pK_{a1}$  values of 2.0 and 1.6 respectively, but there was a massive difference in their attenuation percent of 10 and 88 % respectively. Similarly, propranolol and atenolol, structurally very similar, with  $pK_{a1}$  of 9.42 and 9.67 respectively showed attenuation percent of 88.4 and 12.7 % respectively.

To understand various other factors that might be influencing the attenuation of MPs, DFT calculations of MPs were performed and correlations were developed between attenuation percent and the Highest Occupied Molecular Orbital (HOMO) energy levels in electron volt (eV) for MPs (Figure 5.5).

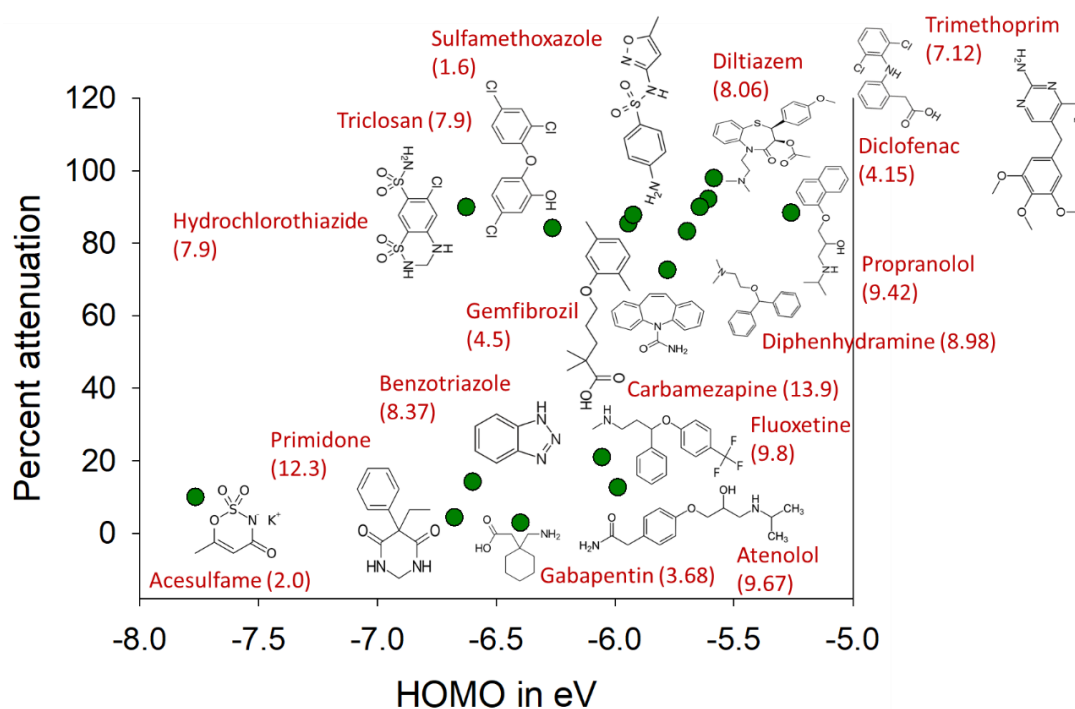


Figure 5.5 Correlation of the percent attenuation, after 6h of 200 nM **2d**/22.4 ppm  $H_2O_2$  treatment, with the HOMO energy levels of MPs. The  $pK_{a1}$  values of MPs are noted in the brackets. The values for diltiazem and diclofenac have been used from 50 nM **2d**/22.4 ppm  $H_2O_2$  treatment.

Although we could see some sort of an exponential trend, with greater attenuation of MPs having a higher HOMO value, there were still discrepancies. While this allowed to explain for the difference in reactivity of **2d** towards propranolol (-5.26 eV, 88.4%) vs atenolol (-5.99 eV, 12.7%) and sulfamethoxazole (-5.92 eV, 88%) vs acesulfame (-7.76 eV, 10%) pairs, it still could not account for the difference in attenuation of triclosan (-6.26 eV, 84.2 %), hydrochlorothiazide (-6.63 eV, 90 %), primidone (-6.68 eV, 4.42 %), benotriazole (-6.60 eV, 14.23 %) and gabapentin (-6.40 eV, 2.96 %) which have very similar HOMO values.

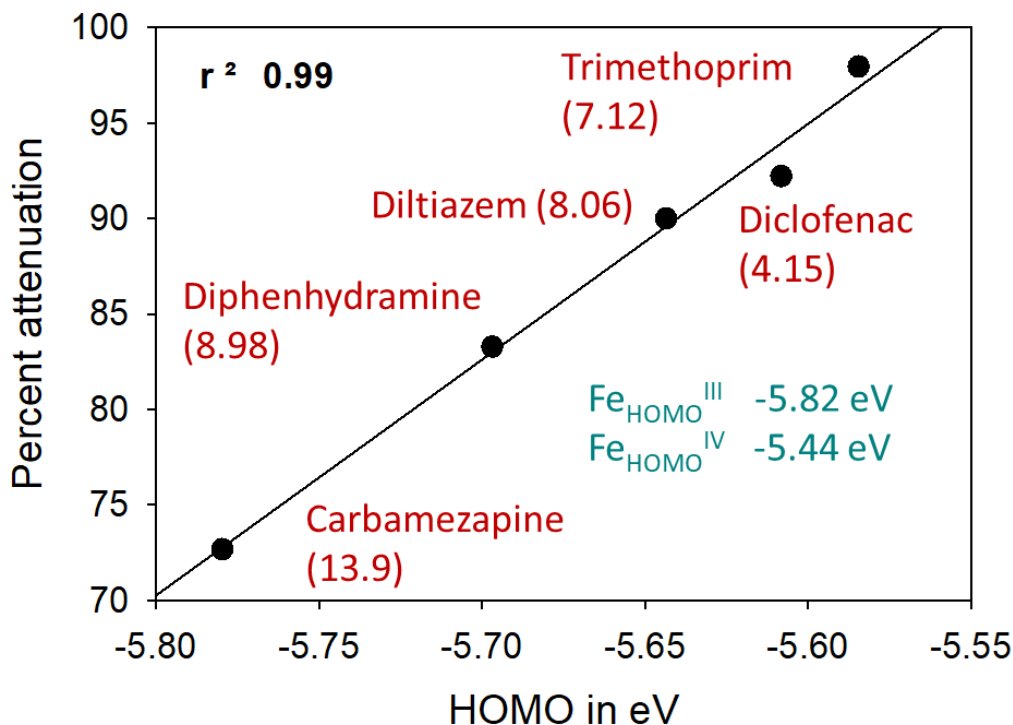


Figure 5.6 Correlation of the attenuation percent, after 6h of 200 nM **2d**/22.4 ppm H<sub>2</sub>O<sub>2</sub> treatment, with MPs whose HOMO energies lie within the range of **2d** HOMO energy levels, viz., Fe<sub>HOMO</sub><sup>III</sup>-5.82 eV and Fe<sub>HOMO</sub><sup>IV</sup> -5.44 eV. The values for diltiazem and diclofenac have been used from 50 nM **2d**/22.4 ppm H<sub>2</sub>O<sub>2</sub> treatment. The pK<sub>a1</sub> values of MPs are noted in the brackets.

There is a sharp linear trend ( $r^2=0.98$ ) for a very small region with MPs showing great attenuation viz., carbamazepine (-5.78 eV, 72.7 %), diphenhydramine (-5.70 eV, 83.3 %), diltiazem (-5.64

eV, 90 %), diclofenac (-5.60 eV, 92.2 %) and trimethoprim (-5.58 eV, 97.9 %) (Figure 5.6). Interestingly, this lies right within the range of the **2d** HOMO energy levels, viz.,  $\text{Fe}_{\text{HOMO}}^{\text{III}}$ -5.82 eV and  $\text{Fe}_{\text{HOMO}}^{\text{IV}}$  -5.44 eV. So there could exist a linear correlation as long it is within the HOMO energy levels for two electron oxidation of resting **2d** state. Our previous work has dealt in detail on the substrate catalyst interactions which cannot be ruled out here although it seems from all we know<sup>17</sup> that such interactions would be negligible at the operating concentrations. In general, most of the MPs with a greater than 50% attenuation by **2d**/H<sub>2</sub>O<sub>2</sub> treatment had structures with electron rich moieties such as aromatic rings (naphthyl ether substituents, electron donating substituents connected to the benzene ring), or basic functionalities like aniline, secondary amines, etc. Most easily oxidized MPs like diclofenac, trimethoprim, triclosan, and diphenhydramine, showed a basic diphenylmethane like moiety in their structure although trimethoprim and triclosan contained heteroatoms like N and O in their structure (Figure 5.11). In totality, there seems to be multiple contributing factors in MP attenuation and a detailed study focusing on the structure activity relationships for the MPs analyzed in this study is in consideration.

#### ***5.2.5 Effect of 2d/H<sub>2</sub>O<sub>2</sub> treatments on Dissolved Organic Carbon in Water.***

Fluorescence spectroscopy over the years has been used extensively as an analytical tool to characterize dissolved organic matter (DOM). Fluorescence excitation-emission matrix (EEM) - 3 dimensional plot of excitation, emission and fluorescence intensity, helps characterize the various types of fluorophores and their concentrations in water (Table 5.3). Excitation-emission pairs are characteristic of a type of fluorophore. There are 5 operational regional boundaries for calculating total fluorescence (TF) of wastewater.<sup>33,34</sup>

Table 5.3 – Regional fluorescence integration boundaries used in this study<sup>34,35</sup> (reproduced from reference 34)

Regional fluorescence type	Region I (Tyrosine-like aromatic protein)	Region II (Tryptophan-like aromatic protein)	Region III (Fulvic acid-like matter)	Region IV (Soluble microbial byproduct-like matter)	Region V (Humic acid-like matter)
Exc boundary (nm)	200-250	200-250	200-250	250-400	250-400
Emm boundary (nm)	280-330	330-380	380-550	280-380	380-550

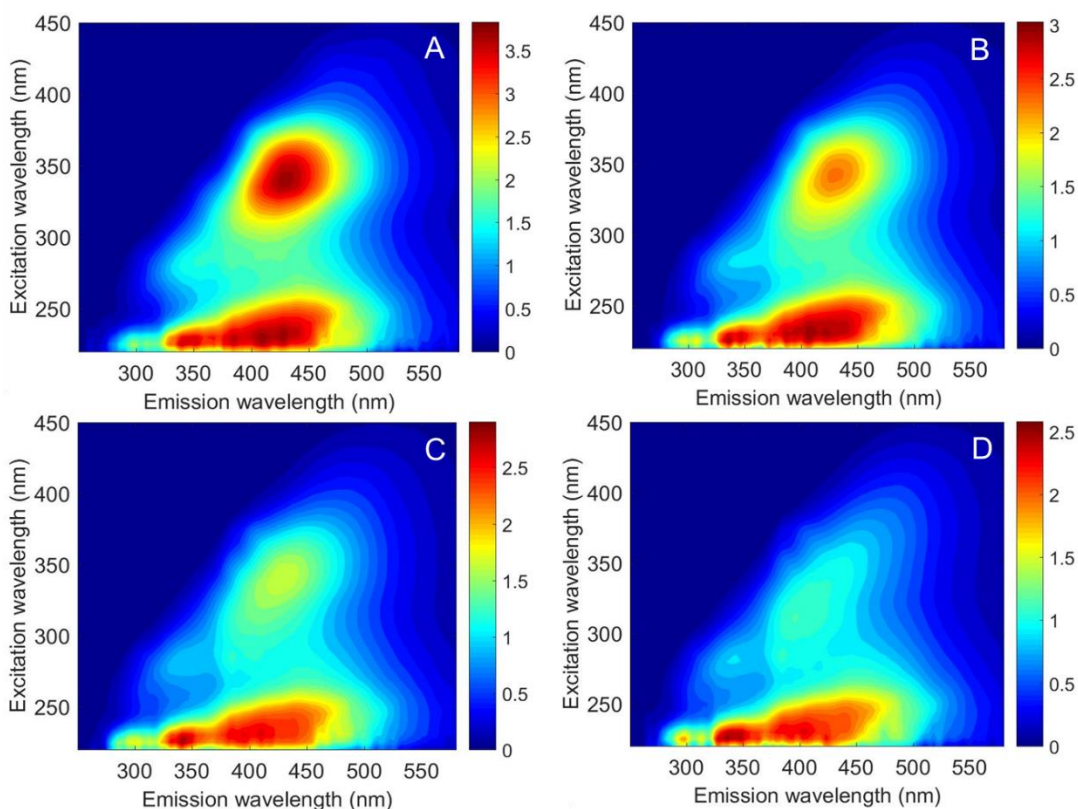


Figure 5.7 Excitation-emission spectra of wastewater after treatment with 22.4 ppm  $\text{H}_2\text{O}_2$  and (A) 0 nM **2d** (Control) (B) 50 nM **2d** (C) 100 nM **2d** (D) 200 nM **2d**

An excitation emission spectrum of plain wastewater could not be obtained. Hence, a control spectrum with just 22.4 ppm hydrogen  $\text{H}_2\text{O}_2$  treated wastewater (negligible attenuation, Figure

5.2) was used as a zero attenuation reference henceforth. As it was shown in the previous work<sup>35</sup>, there are three maximums for the control spectrum (Figure 5.7a) viz., (i) exc ~ 230 nm, emm 340 nm (tryptophan like aromatic proteins) (ii) exc ~ 230 nm, emm 420 nm (hydrophobic fulvic acid-like compounds) (iii) exc ~ 340 nm, emm 420 nm (hydrophobic humic acid-like matter).

Table 5.4 Percent decrease in total fluorescence(TF) and in fluorescence regions II, III and V using a control 22.4 ppm H<sub>2</sub>O<sub>2</sub> treatment (0 nM **2d**) as a zero attenuation reference point.

<b>2d</b> / H <sub>2</sub> O <sub>2</sub>	Region II (% decrease in fluorescence)	Region III (% decrease in fluorescence)	Region V (% decrease in fluorescence)	Total Fluorescence TF (% decrease in fluorescence)
50 nM / 22.4ppm	23.2	20.8	28.8	23.3
100 nM / 22.4ppm	27.5	29	41.6	30.8
200 nM / 22.4ppm	34	39.6	54	40.3

At 22.4 ppm hydrogen H<sub>2</sub>O<sub>2</sub>, in reference to a control water (0 nM **2d**), Tucson wastewater treated with 50, 100 and 200 nM of **2d** showed a total fluorescence (TF) decrease of 23.3, 30.8 and 40.3 % respectively (Table 5.4, Figure 5.7). A 200 nM **2d**/22.4 ppm H<sub>2</sub>O<sub>2</sub> treatment showed a fluorescence decrease of 34, 39.6 and 54 % in Region II, III and V, respectively, indicating the greater effectiveness of **2d**/H<sub>2</sub>O<sub>2</sub> in oxidizing humic acid like matter (Region V, Figure 5.7D).

As with the fluorescence EEM, the UV 254 absorbance of wastewater<sup>35,36</sup> also showed an overall decrease post **2d**/H<sub>2</sub>O<sub>2</sub> treatment. At 22.4 ppm H<sub>2</sub>O<sub>2</sub>, 50, 100 and 200 nM of **2d** effected a 10.9, 14.3 and 17. 7% decrease in UV 254 absorbance respectively (Figure 5.12) from an initial absorbance of 0.145 for only 22.4 ppm H<sub>2</sub>O<sub>2</sub> treated water (0 nM **2d**). Both the UV vis and EEM studies confirmed that in addition to oxidizing MPs in presence of DOC, NewTAML/H<sub>2</sub>O<sub>2</sub> treatment was also effective in oxidizing the DOC.

### ***5.2.6 How many tonnes of wastewater can be treated?***

Dubendorf, Switzerland which is the birth of ozone as a technology for wastewater treatment for micropollutants, utilizes 2 ppm ozone for its wastewater treatment. For every 150,000 Europeans, an output of 22,500 tonnes of wastewater is produced each day. The costing for **2d** has been approximated based on the manufacturing and operational costs for prototype catalyst **1a**. From this extensive study, it can be approximated that 70 nM **2d**/15 ppm of H<sub>2</sub>O<sub>2</sub> can treat 22,500 tonnes of wastewater and the performance can be approximated to that of 3.5 ppm ozone. These numbers can magnify further when considered the fact that wastewaters in Switzerland are much cleaner (mostly tertiary effluent) than the secondary effluent in Tucson that has been utilized in this study. We predict an even superior performance (comparable to 6-8 ppm ozone) when a similar extensive study can be performed with tertiary effluents of Switzerland. We predict this can extrapolate to treating 22,500 tonnes of wastewater with < 50 nM **2d**/15 ppm H<sub>2</sub>O<sub>2</sub>.

### 5.3 CONCLUSIONS

Catalytic **2d**/H<sub>2</sub>O<sub>2</sub> treatments outperformed 2 ppm ozone (current industrial dose in certain WWTPs), even at a minimal 50 nM [**2d**], in the oxidation of the 25 MPs in the secondary effluent of a wastewater treatment plant (WWTP) in Tucson, Arizona. Overall, 200 nM **2d**/22.4 ppm H<sub>2</sub>O<sub>2</sub> was determined to be the optimal treatment conditions for best attenuation of MPs. Compounds in the green zone, viz., DEET, sulfamethoxazole, carbamazepine, gemfibrozil, triclocarban, diclofenac, hydrochlorothiazide, propranolol, diphenhydramine, diltiazem, triclosan, trimethoprim, are easily oxidized by **2d**/H<sub>2</sub>O<sub>2</sub> treatments as well as ozone treatments with ca. > 72 % attenuation across the board, except for 26 % attenuation for DEET with 200 nM **2d**/22.4 ppm H<sub>2</sub>O<sub>2</sub> treatment. No straight forward correlations relating structure of MPs and reactivity could be established although MPs with diphenylmethane like moieties in their structure exhibited greater reactivity towards **2d**/H<sub>2</sub>O<sub>2</sub> treatments. There is an ongoing effort to develop correlations utilizing structure based properties like Ionization potential, substrate – catalyst interactions, derived from detailed DFT modelling, with the attenuation of MPs. Iodinated contrast agents, viz., iopamidol, iohexol and iopromide and other MPs like primidone, meprobamate, sucralose, acesulfame, are hard to oxidize using **2d**/H<sub>2</sub>O<sub>2</sub> treatments under the utilized treatment conditions. However, at higher ozone treatments of 4, 6, 8 ppm, they were found to experience 10-50 % attenuation. The higher concentrations of ozone add to the operational costs considerably. For MPs in the green zone, 200 nM **2d**/22.4 ppm H<sub>2</sub>O<sub>2</sub> gave an approximate improvement between 1-8 fold compared to 2ppm ozone treatment. The kinetics of **2d**/H<sub>2</sub>O<sub>2</sub> treatments were in agreement with the equation shown in Figure 5.1, showing a linear dependence on [**2d**] and an approximate hyperbolic dependence on [H<sub>2</sub>O<sub>2</sub>]. However, more studies with varying [H<sub>2</sub>O<sub>2</sub>] are needed to resolve the complete trend. The total DOC content of wastewater was characterized using fluorescence excitation emission matrix (EEM) as an analytical tool. The 200 nM **2d**/22.4 ppm H<sub>2</sub>O<sub>2</sub> process showed an overall 40 % reduction in total fluorescence with maximum reduction of

54 % in region V, which primarily covers hydrophobic humic acid-like matter. Considering the performance with the secondary effluent used in this study for the costing analysis, we predict a treatment of 22,500 tonnes of wastewater utilizing 70 nM **2d**/15 ppm of H<sub>2</sub>O<sub>2</sub> would approximate 3.5 ppm ozone, but be far easier to use and overall much cheaper.



## 5.4 EXPERIMENTAL

### 5.4.1 Materials, Chemicals and Reagents

**2d** was prepared as described elsewhere.<sup>28,37</sup> H<sub>2</sub>O<sub>2</sub> (50 wt% solution in water, stabilized) was purchased from ACROS Organics™ and standardized using ferric thiocyanate method.<sup>38</sup> Colorimetric measurements were performed using a H<sub>2</sub>O<sub>2</sub> Single-Analyte Photometer (SAM) Kit (I-2016) which consisted of Vacu-vials® and a SAM photometer. Catalase enzyme from bovine liver (aqueous suspension, 45 mg / mL – 10,000-40,000 units / mg protein) was purchased from Sigma Aldrich and used without further purification. Analytical standards from Sigma Aldrich (St. Louis, MO), Alfa Aesar (Ward Hill, MA), and US Pharmacopeia (Washington, DC) of >97% purity were used in this study. Isotopically labeled surrogate standards were purchased from Cambridge Isotope Laboratories (Andover, MA), Toronto Research Chemicals (Ontario, Canada), C/D/N Isotopes (Quebec, Canada) and Santa Cruz Biotechnology (Dallas, TX). Nanopure water was produced in house using a Barnstead Pure system. HPLC grade acetonitrile, methanol and ACS grade acetic acid were purchased from Fisher Scientific (Fair Lawn, NJ, USA). Whatmann GF/F filters were purchased from Waters Corporations.

### 5.4.2 Sample Collection and Preparation

Secondary effluent from The Agua Nueva Water Reclamation Facility (WRF), Tucson, Arizona was filtered using a Whatman® glass microfiber filters, (Grade GF/F, mm and 0.7-µm pore size) and stored at 4° C. All experiments were performed within 2 weeks of water collection. Post experiments, samples were filtered and 100 µl of 2 µg/L of isotopically labelled surrogates were added to 900 µl of samples in a 2 ml vial prior to analyses. UVA 254nm, TF, and EEM analysis were performed with 20 mL of samples.

### 5.4.3 Indicator Micropollutants for Analyses

An indicator list of 38 chemicals of emerging concern (CECs) (Table 5.5) comprising pharmaceuticals, personal care products, industrial or commercial chemicals, household chemicals, steroids or hormones (synthetic and natural) and pesticides were chosen based on a priority scoring system (PSS) involving (i) frequency of detection in wastewaters (ii) mean concentration in wastewaters (iii) number of published literature (2000-2015) for compounds detected in wastewater.<sup>30</sup>

Table 5.5 Micropollutants, categorized by their primary utility in daily usage, that were analyzed in all **2d** / H<sub>2</sub>O<sub>2</sub> and Ozone treatment experiments.

Household chemical	Industrial/ Commercial chemical	Personal care product	Pesticide	Steroid/ Hormone
Acesulfame	Benzotriazole	Benzophenone	Atrazine	Dexamethasone
Bisphenol A	Bisphenol A	DEET	Simazine	Hydrocortisone
Caffeine	Iohexol	Triclocarban		Prednisone
TCEP	Iopamidol	Triclosan		Testosterone
TCPP	Iopromide			
	Propylparaben			
Pharmaceutical				
Atenolol	Carbamazepine	Clofibric acid	Diclofenac	Diphenhydramine
Diltiazem	Fluoxetine	Gemfibrozil	Ibuprofen	Hydrochlorothiazide
Meprobamate	Naproxen	Primidone	Propranolol	Sulfamethoxazole
Gabapentin	Trimethoprim			

### 5.4.4 Instrumentation

All LC-MS-MS analyses were performed using an Agilent 1290 UHPLC coupled with an Agilent 6490 Triple Quadrupole (QQQ). Separation of compounds were achieved on a non-polar Agilent Zorbax eclipse Plus C8 column (2.1 x 100 mm, 1.8  $\mu$ m (particle size), Rapid Resolution HD column) using a combination of water with 0.1 % Acetic acid (A) and ACN with 0.1 % Acetic acid (B) as the mobile phases. The LC-MS/MS method developed here was a modification of the

previous work.<sup>30</sup> The LC method comprised of a gradient elution of A and B, beginning with 5 % B for the first minute and then gradually increasing to a 100% after 10 minutes. This was maintained for 4 minutes until shifting back to the starting condition of 5%. A flow rate of 0.35 ml / min and a sample injection volume of 80  $\mu$ L was used for all samples. The mass spectrometer was run in dynamic multiple reaction monitoring (MRM) mode, with analytes being ionized using electrospray ionization (ESI-both positive and negative), selected with triple quadrupoles (QQQ), and quantified using a high energy dynode.

The instrument detection limits (IDLs) were determined by the lowest standard in calibration curve with a signal to noise ratio of at least 3 ( $S/N > 3$ ) and with at least 80% accuracy. The calibration points were at 0.1, 0.2, 0.5, 1.0, 2.0, 5.0, 10, 20, 50, 100, 200, 500 and 1,000  $\mu$ g/L. Depending on where the analyte concentration within the sample fell, irrelevant calibrations points on either end of the curve were dropped to increase linearity. All concentrations that were above the highest point in the calibration curve were diluted and re-analyzed. All analytes were calibrated externally using linear or power regression with 1/x weighting. Correlation coefficients were required to be at least 0.990 and typically exceeded 0.995. Isotope dilution was used for quantification of all analytes<sup>39</sup>. The data was then processed with MassHunter Quantitative Analysis B.04.00. At least one lab blank, lab fortified blank, and QC sample were carried out for every 10 samples.

#### ***5.4.5 Ozone treatments***

Ozonation was performed as described in a previous study.<sup>36</sup> A concentrated ozone stock was prepared by bubbling gaseous ozone into ultrapure water in a specialized liquid-jacketed vessel that was precooled to 1 °C using a recirculating chiller. An aliquot from this stock was added to wastewater to be treated to yield a starting ozone concentrations of 2, 4, 6 and 8 mg /L. No kinetic analyses were performed like in the case of **2d** / H<sub>2</sub>O<sub>2</sub> treatments and only the end point [MPs]

from ozone treatments were used for comparison with several **2d** / H<sub>2</sub>O<sub>2</sub> treatments. The ozone concentration of stock solution and residual ozone concentration of samples were determined using indigotrisulfonate (ITS) method and the detailed procedure is described in the literature.<sup>40</sup>

#### ***5.4.6 2d / H<sub>2</sub>O<sub>2</sub> treatment:***

Stock solutions of **2d** ( $1 \times 10^{-5}$  M) and H<sub>2</sub>O<sub>2</sub> (1 M) were prepared in HPLC grade water. The secondary effluent sample was equilibrated to 25 °C in a water bath and reaction was initiated by adding appropriate aliquots of **2d** and H<sub>2</sub>O<sub>2</sub>. At pre-determined time intervals, aliquots were drawn and analyzed by LC-MS using the method described above.

## 5.5 APPENDIX

Table 5.6 Electrospray ionization (ESI) Mass spectrometry parameters utilized for compounds and their isotopic surrogates in positive and negative ESI modes.

Compound Name	Precursor Ion (m/z)	Product Ion (m/z)	Ret Time (min)	Delta Ret Time (min)	Fragmentor (V)	Collision Energy (V)	Cell Accelerator (V)
<b>ESI Positive Compounds</b>							
Atenolol	267.1	190.1	3.13	1.48	380	15	2
Atenolol	267.1	145	3.13	1.48	380	20	2
<i>Atenolol-d7</i>	274	190.1	3.08	2.08	380	15	2
Atrazine	218	176	7.86	0.77	380	15	2
Atrazine	216	174	7.86	0.77	380	15	2
<i>Atrazine-d5</i>	221	179	7.84	1.22	380	15	2
Benzophenone	183	105.1	9.03	0.59	380	10	2
<i>Benzophenone-d10</i>	193	110.1	8.98	0.86	380	10	2
Caffeine	195.1	138	4.82	1.11	380	16	2
Caffeine	195.1	110.1	4.82	1.11	380	24	2
<i>Caffeine-13C3</i>	198.1	140	4.82	1.18	380	16	2
Carbamezapine	237	194	7.27	0.82	380	15	2
Carbamezapine	237	179	7.27	0.82	380	35	2
<i>Carbamezapine-d10</i>	247	204	7.22	0.74	380	15	2
DEET	192	119	7.96	0.97	380	15	2
DEET	192	91	7.96	0.97	380	30	2
<i>DEET-d6</i>	198	119	7.94	0.79	380	15	2
Diphenhydramine	256.2	167.1	6.42	1.34	380	4	2
Diphenhydramine	256.2	165.1	6.42	1.34	380	44	2
<i>Diphenhydramine-d5</i>	261.2	172.1	6.42	1.19	380	4	2
Diltiazem	415.2	178	6.49	1.56	380	24	2
Diltiazem	415.2	150	6.49	1.56	380	48	2
<i>Diltiazem-d3</i>	418.2	178	6.49	1.71	380	24	2
Fluoxetine	310	148	7.07	1.49	380	5	2
<i>Fluoxetine-d5</i>	315	153	7.07	1.62	380	5	2
Gabapentin	172	55.1	4.35	2	380	24	2
Gabapentin	172	44.1	4.35	2	380	60	2
Gabapentin	172	41.1	4.35	2	380	60	2
Iohexol	821.9	803.8	2.48	1.64	380	20	2
<i>Iohexol-d5</i>	826.9	809	2.48	1.45	380	20	2
Iopamidol	777.9	558.9	2.06	1.34	380	22	2
Iopamidol	777.9	387	2.06	1.34	380	42	2
<i>Iopamidol-d3</i>	781	562	2.06	1.49	380	22	2
Iopromide	791.8	572.8	4.24	0.97	380	22	2
Iopromide	791.8	558.8	4.24	0.97	380	28	2
Meprobamate	219	158	6.4	0.8	380	5	2
Meprobamate	219	55	6.4	0.8	380	20	2

<i>Meprobamate-d3</i>	222.1	161.1	6.38	0.97	380	5	2
Primidone	219.3	162.1	5.71	0.74	380	9	2
Primidone	219.3	91.1	5.71	0.74	380	25	2
<i>Primidone-d5</i>	224	167	5.68	0.89	380	9	2
Propranolol	260	116	6.2	1.45	380	13	2
Propranolol	260	56	6.2	1.45	380	29	2
Simazine	202.1	68.1	7.12	1.19	380	36	2
Simazine	202.1	132	7.12	1.19	380	16	2
Sucralose	419	239	5.3	0.62	380	15	2
Sucralose	419	221	5.3	0.62	380	15	2
<i>Sucralose-d6</i>	425	243	5.3	0.66	380	15	2
Sulfamethoxazole	254	156	6.45	0.74	380	10	2
Sulfamethoxazole	254	92	6.45	0.74	380	30	2
<i>Sulfamethoxazole-13C6</i>	260	162	6.45	0.74	380	10	2
TCEP	285	223	7.74	1.04	380	10	4
<i>TCEP-d12</i>	297	232	7.74	0.59	380	13	2
TCPP	327	99	8.85	1.34	380	16	4
TCPP	327	81	8.85	1.34	380	70	4
Testosterone	289.2	109.1	8.08	1.26	380	24	4
Testosterone	289.2	97.2	8.08	1.26	380	28	4
Trimethoprim	291	261	4.91	1.11	380	25	2
Trimethoprim	291	230	4.91	1.11	380	25	2
<i>Trimethoprim-d3</i>	294	264	4.89	0.93	380	25	2

---

#### ESI Negative Compounds

---

Acesulfame	162	82.1	2.77	1.78	380	13	2
<i>Acesulfame-d4</i>	166.1	86.1	2.77	2.53	380	10	2
Benzotriazole	118	90.1	5.38	0.79	380	16	7
Benzotriazole	118	50	5.38	0.79	380	28	7
<i>Benzotriazole-d4</i>	122	94.1	5.33	1.19	380	16	7
Bisphenol A	227	212	7.98	0.74	380	11	7
Bisphenol A	227	133	7.98	0.74	380	19	7
<i>Bisphenol A-13C12</i>	239	224	7.97	0.53	380	11	7
Clofibric Acid	213	127	8.22	0.89	380	10	7
Dexamethasone	451.2	361.1	7.3	1.19	380	16	4
Dexamethasone	451.2	307.1	7.3	1.19	380	36	4
<i>Dexamethasone-d4</i>	455.2	363.1	7.3	1.19	380	16	4
Diclofenac	294	250	9.11	1.19	380	4	7
Diclofenac	294	214	9.11	1.19	380	16	7
<i>Diclofenac-13C6</i>	300	256	9.14	0.81	380	4	7
Gemfibrozil	249.2	121	9.73	1.31	380	6	7
<i>Gemfibrozil-d6</i>	255	121	9.71	0.82	380	6	7
Hydrochlorothiazide	296	204.7	4.95	1.11	380	15	2
Hydrochlorothiazide	296	268.9	4.95	1.11	380	10	2
Hydrocortisone	421.2	331.3	6.8	0.8	380	16	4

Hydrocortisone	421.2	297.3	6.8	0.8	380	36	4
<i>Hydrocortisone-d2</i>	423.2	333	6.8	0.74	380	16	4
Ibuprofen	205	161	9.29	0.97	380	0	7
<i>Ibuprofen-d3</i>	208	164	9.29	0.74	380	0	7
Naproxene	229	170	8.2	0.82	380	4	7
Naproxene	229	169	8.2	0.82	380	24	7
<i>Naproxene-13C,d3</i>	233	169	8.3	0.5	380	4	7
Prednisone	417.2	357.3	6.81	0.82	380	4	4
Prednisone	417.2	327.2	6.81	0.82	380	12	4
<i>Prednisone-d8</i>	425.2	333.2	0.81	0.57	380	16	4
Propylparaben	179.1	137.1	7.95	1.04	380	7	7
Propylparaben	179.1	92	7.95	1.04	380	20	7
<i>Propylparaben-d4</i>	183.1	141.1	7.88	0.7	380	12	7
Triclocarban	313	160	9.98	1.06	380	5	7
Triclocarban	313	126	9.98	1.06	380	25	7
<i>Triclocarban-13C6</i>	318.9	160	9.98	1.11	380	5	7
Triclosan	289	37	10.1	0.81	380	5	7
Triclosan	287	35	10.1	0.81	380	5	7
<i>Triclosan-13C12</i>	299	35	10.1	0.82	380	5	7

Table 5.7 Instrumental parameters for triple quadrupole (QQQ) operations.

Parameter	ESI Positive	ESI Negative
Gas Temperature (°C)	275	275
Gas Flowrate (L/min)	18	18
Nebulizer (psi)	45	45
Sheath Gas Temperature (°C)	350	350
Sheath Gas Flowrate (L/min)	11	11
Capillary (V)	3000	3000
Nozzle Voltage (V)	1500	500
Delta EMV (V)	250	250

## 6 h treatment

Reaction Conditions [2d];[H <sub>2</sub> O <sub>2</sub> ]	TCEP	TCPP	Atenolol	Sucralose	Iohexol	Iopamidol	Iopromide	Meprobamate	Acesulfame	Primidone	Fluoxetine	Gabapentin	Benzophenone	Benzotriazole	DEET	Sulfamethoxazole	Carbamazepine	Gemfibrozil	Triclocarban	Diclofenac	Hydrochlorothiazide	Propranolol	Diphenhydramine	Diltiazem	Triclosan	Trimethoprim
Nil; 11.2 ppm																										
Nil; 22.4 ppm	•																									
100 nM; 11.2 ppm																										
200 nM; 11.2 ppm																										
50 nM; 22.4 ppm	•																									
100 nM; 22.4 ppm																										
200 nM; 22.4 ppm																										
2 ppm Ozone																										
4 ppm Ozone																										
6 ppm Ozone																										
8 ppm Ozone																										

## 4 h treatment

Reaction Conditions [2d];[H <sub>2</sub> O <sub>2</sub> ]	TCEP	TCPP	Atenolol	Sucralose	Iohexol	Iopamidol	Iopromide	Meprobamate	Acesulfame	Primidone	Fluoxetine	Gabapentin	Benzophenone	Benzotriazole	DEET	Sulfamethoxazole	Carbamazepine	Gemfibrozil	Triclocarban	Diclofenac	Hydrochlorothiazide	Propranolol	Diphenhydramine	Diltiazem	Triclosan	Trimethoprim
Nil; 11.2 ppm																										
Nil; 22.4 ppm	•																									
100 nM; 11.2 ppm																										
200 nM; 11.2 ppm																										
50 nM; 22.4 ppm	•																									
100 nM; 22.4 ppm																										
200 nM; 22.4 ppm																										
2 ppm Ozone																										
4 ppm Ozone																										
6 ppm Ozone																										
8 ppm Ozone																										



## 2 h treatment

Reaction Conditions [2d];[H <sub>2</sub> O <sub>2</sub> ]	TCEP	TCPP	Atenolol	Sucralose	Iohexol	Iopamidol	Iopromide	Meprobamate	Acesulfame	Primidone	Fluoxetine	Gabapentin	Benzophenone	Benzotriazole	DEET	Sulfamethoxazole	Carbamazepine	Gemfibrozil	Triclocarban	Diclofenac	Hydrochlorothiazide	Propranolol	Diphenhydramine	Ditiazem	Triclosan	Trimethoprim
Nil; 11.2 ppm																										
Nil; 22.4 ppm	.																									
100 nM; 11.2 ppm											.															
200 nM; 11.2 ppm																										
50 nM; 22.4 ppm	.																									
100 nM; 22.4 ppm																										
200 nM; 22.4 ppm																										
2 ppm Ozone			.								.															
4 ppm Ozone			.								.															
6 ppm Ozone			.								.															
8 ppm Ozone			.								.															

## 40 min treatment

Reaction Conditions [2d];[H <sub>2</sub> O <sub>2</sub> ]	TCEP	TCPP	Atenolol	Sucralose	Iohexol	Iopamidol	Iopromide	Meprobamate	Acesulfame	Primidone	Fluoxetine	Gabapentin	Benzophenone	Benzotriazole	DEET	Sulfamethoxazole	Carbamazepine	Gemfibrozil	Triclocarban	Diclofenac	Hydrochlorothiazide	Propranolol	Diphenhydramine	Ditiazem	Triclosan	Trimethoprim
Nil; 11.2 ppm																										
Nil; 22.4 ppm	.																									
100 nM; 11.2 ppm																										
200 nM; 11.2 ppm																										
50 nM; 22.4 ppm	.																									
100 nM; 22.4 ppm																										
200 nM; 22.4 ppm																										
2 ppm Ozone			.								.															
4 ppm Ozone			.								.															
6 ppm Ozone			.								.															
8 ppm Ozone			.								.															

## 30 min treatment

Reaction Conditions [2d];[H <sub>2</sub> O <sub>2</sub> ]	TCEP	TCPP	Atenolol	Sucralose	Iohexol	Iopamidol	Iopromide	Meprobamate	Acesulfame	Primidone	Fluoxetine	Gabapentin	Benzophenone	Benzotriazole	DEET	Sulfamethoxazole	Carbamazepine	Gemfibrozil	Triclocarban	Diclofenac	Hydrochlorothiazide	Propranolol	Diphenhydramine	Diltiazem	Triclosan	Trimethoprim
Nil; 11.2 ppm																										
Nil; 22.4 ppm	•																									
100 nM; 11.2 ppm											•											•				
200 nM; 11.2 ppm																						•				
50 nM; 22.4 ppm	•																					•				
100 nM; 22.4 ppm																						•				
200 nM; 22.4 ppm																						•				
2 ppm Ozone			•								•															
4 ppm Ozone			•								•	•														
6 ppm Ozone			•								•	•														
8 ppm Ozone			•								•	•														

## 20 min treatment

Reaction Conditions [2d];[H <sub>2</sub> O <sub>2</sub> ]	TCEP	TCPP	Atenolol	Sucralose	Iohexol	Iopamidol	Iopromide	Meprobamate	Acesulfame	Primidone	Fluoxetine	Gabapentin	Benzophenone	Benzotriazole	DEET	Sulfamethoxazole	Carbamazepine	Gemfibrozil	Triclocarban	Diclofenac	Hydrochlorothiazide	Propranolol	Diphenhydramine	Ditiazem	Triclosan	Trimethoprim
Nil; 11.2 ppm																										
Nil; 22.4 ppm	•																									
100 nM; 11.2 ppm											•															
200 nM; 11.2 ppm																										
50 nM; 22.4 ppm	•																									
100 nM; 22.4 ppm																										
200 nM; 22.4 ppm																										
2 ppm Ozone			•								•	•														
4 ppm Ozone			•								•	•														
6 ppm Ozone			•								•	•														
8 ppm Ozone			•								•	•														

## 12 min treatment



## 6 min treatment

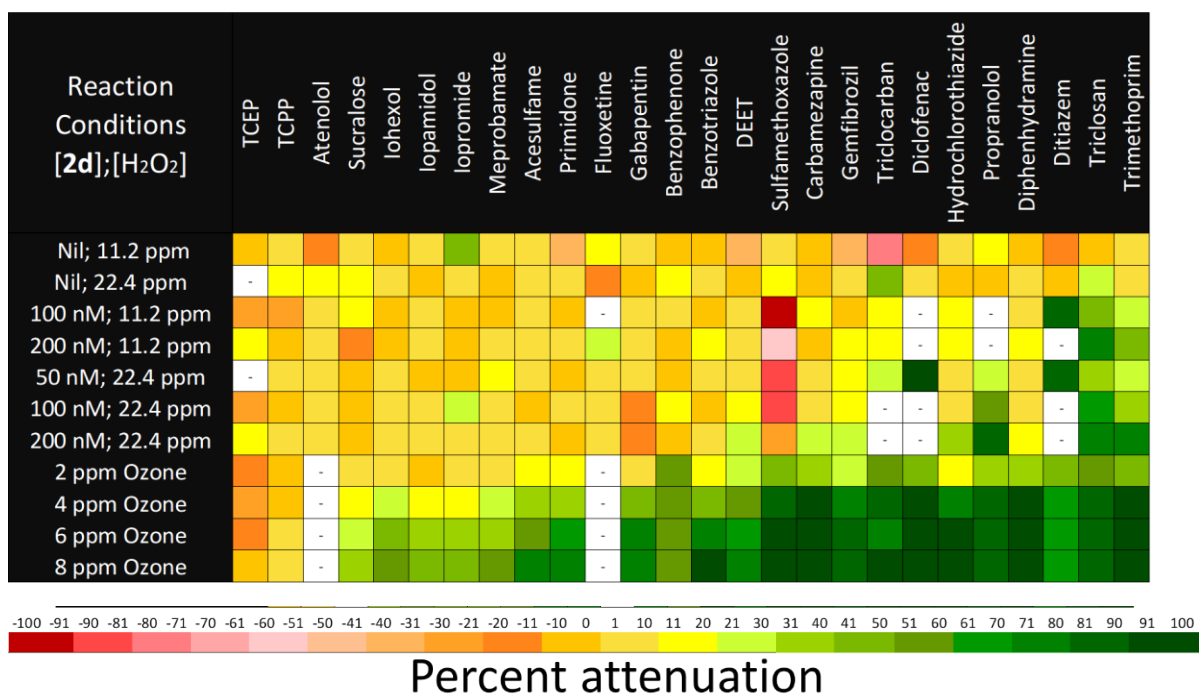


Figure 5.8 Attenuation in percentage (average of triplicate separate measurements) for micropollutants after 6h, 4h, 2h, 40 min, 30 min, 20 min, 12min and 6 min treatment times with various **2d** / H<sub>2</sub>O<sub>2</sub> and ozone treatments. \*White boxes indicate below detection level concentrations for compounds prior to and at all stages of experimentation.

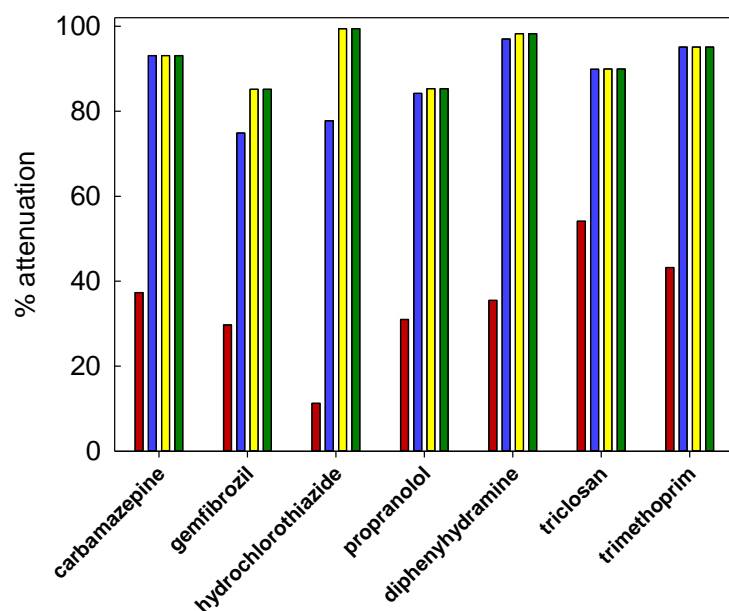


Figure 5.9 Attenuation in percentage (average of triplicate separate measurements) for various micropollutants after 72h endpoint (not exposure time) with (A) 2ppm-brown (B) 4 ppm-blue (C) 6 ppm-yellow and (D) 8 ppm-green of ozone treatment.

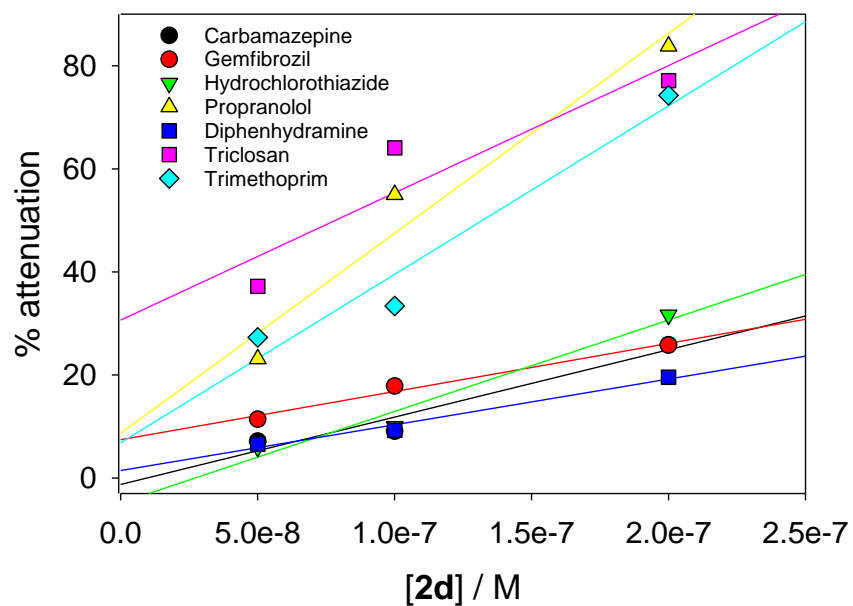


Figure 5.10 Attenuation in percentage (average of triplicate separate experiments) for various micropollutants with 22.4 ppm  $H_2O_2$  and various  $[2d]$  after 6 min treatment.

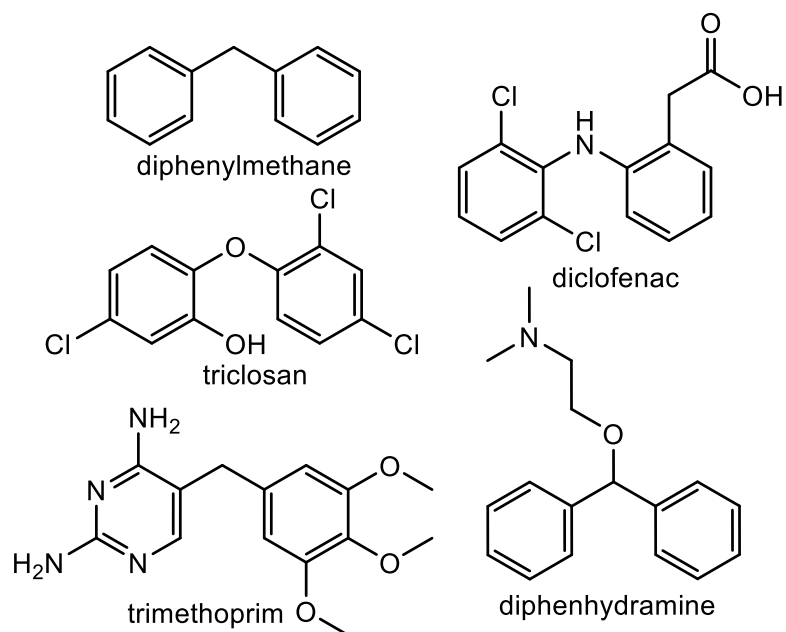


Figure 5.11 Structure of Diphenylmethane Triclosan Diclofenac Diphenhydramine and Trimethoprim

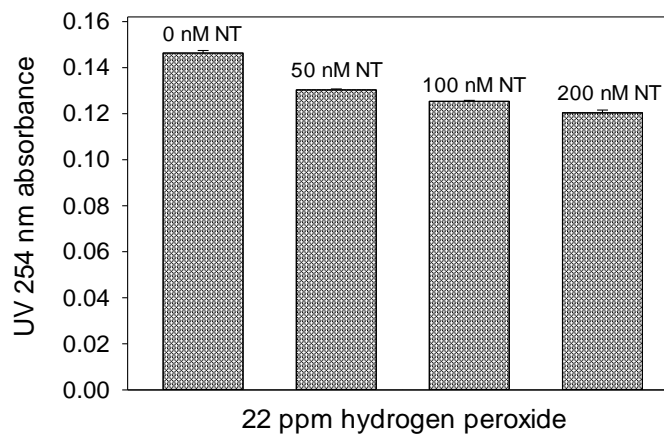


Figure 5.12 UV 254 absorbances of wastewater after treatment with 22.4 ppm H<sub>2</sub>O<sub>2</sub> and (A) 0 nM **2d** (B) 50 nM **2d** (C) 100 nM **2d** (D) 200 nM **2d**

## 5.6 REFERENCES

- (1) Schwarzenbach, R. P.; Egli, T.; Hofstetter, T. B.; von Gunten, U.; Wehrli, B. Global Water Pollution and Human Health. *Annu. Rev. Environ. Resour.* **2010**, *35* (1), 109–136.
- (2) CAS-A Division of the American Chemical Society <https://www.cas.org/>.
- (3) Benotti, M. J.; Trenholm, R. A.; Vanderford, B. J.; Holady, J. C.; Stanford, B. D.; Snyder, S. A. Pharmaceuticals and Endocrine Disrupting Compounds in U.S. Drinking Water. *Environ. Sci. Technol.* **2009**, *43* (3), 597–603.
- (4) Schwarzenbach, R. P.; Escher, B. I.; Fenner, K.; Hofstetter, T. B.; Johnson, C. A.; von Gunten, U.; Wehrli, B. The Challenge of Micropollutants in Aquatic Systems. *Science* (80-. ). **2006**, *313* (5790), 1072 LP – 1077.
- (5) Luo, Y.; Guo, W.; Ngo, H. H.; Nghiem, L. D.; Hai, F. I.; Zhang, J.; Liang, S.; Wang, X. C. A Review on the Occurrence of Micropollutants in the Aquatic Environment and Their Fate and Removal during Wastewater Treatment. *Sci Total Env.* **2014**, *473–474*, 619–641.
- (6) Snyder, S. A. Occurrence of Pharmaceuticals in U.S. Drinking Water. In *Contaminants of Emerging Concern in the Environment: Ecological and Human Health Considerations*; ACS Symposium Series; American Chemical Society, 2016; Vol. 1048, pp 69–80.
- (7) Bexfield, L. M.; Toccalino, P. L.; Belitz, K.; Foreman, W. T.; Furlong, E. T. Hormones and Pharmaceuticals in Groundwater Used As a Source of Drinking Water Across the United States. *Environ. Sci. Technol.* **2019**, *53* (6), 2950–2960.
- (8) Khetan, S. K.; Collins, T. J. Human Pharmaceuticals in the Aquatic Environment: A Challenge to Green Chemistry. *Chem. Rev.* **2007**, *107* (6), 2319–2364.
- (9) Colborn, T.; vom Saal, F. S.; Soto, A. M. Developmental Effects of Endocrine-Disrupting Chemicals in Wildlife and Humans. *Environ. Health Perspect.* **1993**, *101* (5), 378–384.
- (10) Vandenberg, L. N.; Colborn, T.; Hayes, T. B.; Heindel, J. J.; Jacobs, D. R.; Lee, D. H.; Shioda, T.; Soto, A. M.; vom Saal, F. S.; Welshons, W. V.; et al. Hormones and Endocrine-Disrupting Chemicals: Low-Dose Effects and Nonmonotonic Dose Responses. *Endocr. Rev.* **2012**, *33* (3), 378–455.
- (11) United Nations Environment Programme (UNEP); World Health Organisation (WHO). *State of the Science of Endocrine Disrupting Chemicals - 2012*; Geneva, Switzerland, 2013.
- (12) Rogowska, J.; Cieszyńska-Semenowicz, M.; Ratajczyk, W.; Wolska, L. Micropollutants in Treated Wastewater. *Ambio* **2019**.
- (13) Eggen, R. I. L.; Hollender, J.; Joss, A.; Schärer, M.; Stamm, C. Reducing the Discharge of Micropollutants in the Aquatic Environment: The Benefits of Upgrading Wastewater Treatment Plants. *Environ. Sci. Technol.* **2014**, *48* (14), 7683–7689.
- (14) Margot, J.; Kienle, C.; Magnet, A.; Weil, M.; Rossi, L.; de Alencastro, L. F.; Abegglen, C.; Thonney, D.; Chevre, N.; Scharer, M.; et al. Treatment of Micropollutants in Municipal Wastewater: Ozone or Powdered Activated Carbon? *Sci Total Env.* **2013**, *461–462*, 480–498.
- (15) Collins, T. J. TAML Oxidant Activators: A New Approach to the Activation of Hydrogen

Peroxide for Environmentally Significant Problems. *Acc. Chem. Res.* **2002**, *35* (9), 782–790.

- (16) Ryabov, A. D.; Collins, T. J. Mechanistic Considerations on the Reactivity of Green FeIII-TAML Activators of Peroxides. *Adv. Inorg. Chem.* **2009**, *61*, 471–521.
- (17) Somasundar, Y.; Shen, L. Q.; Hoane, A. G.; Tang, L. L.; Mills, M. R.; Burton, A. E.; Ryabov, A. D.; Collins, T. J. Structural, Mechanistic, and Ultradilute Catalysis Portrayal of Substrate Inhibition in the TAML–Hydrogen Peroxide Catalytic Oxidation of the Persistent Drug and Micropollutant, Propranolol. *J. Am. Chem. Soc.* **2018**, *140* (38), 12280–12289.
- (18) Kundu, S.; Chanda, A.; Espinosa-Marvan, L.; Khetan, S. K.; Collins, T. J. Facile Destruction of Formulated Chlorpyrifos through Green Oxidation Catalysis. *Catal. Sci. Technol.* **2012**, *2* (6), 1165–1172.
- (19) Mills, M. R.; Arias-Salazar, K.; Baynes, A.; Shen, L. Q.; Churchley, J.; Beresford, N.; Gayathri, C.; Gil, R. R.; Kanda, R.; Jobling, S.; et al. Removal of Ecotoxicity of 17 $\alpha$ -Ethinylestradiol Using TAML/Peroxide Water Treatment. *Sci Rep* **2015**, *5*, 10511.
- (20) Kundu, S.; Chanda, A.; Khetan, S. K.; Ryabov, A. D.; Collins, T. J. TAML Activator/Peroxide-Catalyzed Facile Oxidative Degradation of the Persistent Explosives Trinitrotoluene and Trinitrobenzene in Micellar Solutions. *Env. Sci Technol* **2013**, *47* (10), 5319–5326.
- (21) Deboshri, B.; L., M. A.; Toshihiro, Y.; Anindya, G.; B., B. P.; G., M. E.; K., K. S.; J., C. T. “Green” Oxidation Catalysis for Rapid Deactivation of Bacterial Spores. *Angew. Chemie Int. Ed.* **2006**, *45* (24), 3974–3977.
- (22) Chahbane, N.; Popescu, D. L.; Mitchell, D. A.; Chanda, A.; Lenoir, D.; Ryabov, A. D.; Schramm, K. W.; Collins, T. J. FeIII-TAML-Catalyzed Green Oxidative Degradation of the Azo Dye Orange II by H<sub>2</sub>O<sub>2</sub> and Organic Peroxides: Products, Toxicity, Kinetics, and Mechanisms. *Green Chem.* **2007**, *9* (1), 49–57.
- (23) Onundi, Y.; Drake, B. A.; Malecky, R. T.; DeNardo, M. A.; Mills, M. R.; Kundu, S.; Ryabov, A. D.; Beach, E. S.; Horwitz, C. P.; Simonich, M. T.; et al. A Multidisciplinary Investigation of the Technical and Environmental Performances of TAML/Peroxide Elimination of Bisphenol A Compounds from Water. *Green Chem.* **2017**, *19* (18), 4234–4262.
- (24) Sen Gupta, S.; Stadler, M.; Noser, C. A.; Ghosh, A.; Steinhoff, B.; Lenoir, D.; Horwitz, C. P.; Schramm, K.-W.; Collins, T. J. Rapid Total Destruction of Chlorophenols by Activated Hydrogen Peroxide. *Sci. (Washington, DC, U. S.)* **2002**, *296* (5566), 326–328.
- (25) Churchley, J.; Collins, T.; Jobling, S. *Catalytic Oxidation of Pharmaceutical Compounds in Wastewater Effluents*; UKWIR: London, 2013.
- (26) Truong, L.; DeNardo, M. A.; Kundu, S.; Collins, T. J.; Tanguay, R. L. Zebrafish Assays as Developmental Toxicity Indicators in the Green Design of TAML Oxidation Catalysts. *Green Chem.* **2013**, *15* (9), 2339–2343.
- (27) Collins, T. Toward Sustainable Chemistry. *Science (80-. )*. **2001**, *291* (5501), 48 LP – 49.
- (28) Warner, G. R.; Somasundar, Y.; Jansen, K. C.; Kaaret, E. Z.; Weng, C.; Burton, A. E.; Mills, M. R.; Shen, L. Q.; Ryabov, A. D.; Pros, G.; et al. Bioinspired, Multidisciplinary,

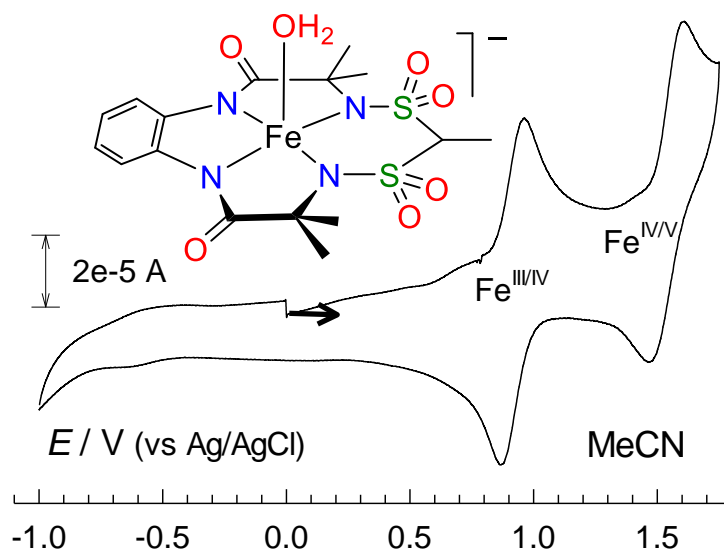
Iterative Catalyst Design Creates the Highest Performance Peroxidase Mimics and the Field of Sustainable Ultradilute Oxidation Catalysis (SUDOC). *ACS Catal.* **2019**, 7023–7037.

- (29) DeNardo, M. A.; Mills, M. R.; Ryabov, A. D.; Collins, T. J. Unifying Evaluation of the Technical Performances of Iron-Tetra-Amido Macrocyclic Ligand Oxidation Catalysts. *J. Am. Chem. Soc.* **2016**, 138 (9), 2933–2936.
- (30) Anumol, T.; Wu, S.; Marques dos Santos, M.; Daniels, K. D.; Snyder, S. a. Rapid Direct Injection LC-MS/MS Method for Analysis of Prioritized Indicator Compounds in Wastewater Effluent. *Environ. Sci. Water Res. Technol.* **2015**, 1 (5), 632–643.
- (31) University of York. Antibiotics found in some of the world’s rivers exceed “safe” levels, global study finds <https://www.sciencedaily.com/releases/2019/05/190527094120.htm>.
- (32) U.S. National Library of Medicine. PubChem <https://pubchem.ncbi.nlm.nih.gov/>.
- (33) Chen, W.; Westerhoff, P.; Leenheer, J. A.; Booksh, K. Fluorescence Excitation-Emission Matrix Regional Integration to Quantify Spectra for Dissolved Organic Matter. *Environ. Sci. Technol.* **2003**, 37 (24), 5701–5710.
- (34) Park, M.; Snyder, S. A. Sample Handling and Data Processing for Fluorescent Excitation-Emission Matrix (EEM) of Dissolved Organic Matter (DOM). *Chemosphere* **2018**, 193, 530–537.
- (35) Merel, S.; Anumol, T.; Park, M.; Snyder, S. A. Application of Surrogates, Indicators, and High-Resolution Mass Spectrometry to Evaluate the Efficacy of UV Processes for Attenuation of Emerging Contaminants in Water. *J. Hazard. Mater.* **2015**, 282, 75–85.
- (36) Park, M.; Anumol, T.; Daniels, K. D.; Wu, S.; Ziska, A. D.; Snyder, S. A. Predicting Trace Organic Compound Attenuation by Ozone Oxidation: Development of Indicator and Surrogate Models. *Water Res.* **2017**, 119, 21–32.
- (37) Collins, T. J.; DeNardo, M. A.; Warner, G. R.; Gordon-Wylie, S. W.; Ellis, W. C.; Somasundar, Y. Far Superior Oxidation Catalysts Based on Macrocyclic Compounds, October 25, 2018.
- (38) Boltz, D. F.; Howell, J. A. *Colorimetric Determination of Nonmetals*; 1978.
- (39) Vanderford, B. J.; Snyder, S. A. Analysis of Pharmaceuticals in Water by Isotope Dilution Liquid Chromatography/Tandem Mass Spectrometry. *Environ. Sci. Technol.* **2006**, 40 (23), 7312–7320.
- (40) Rakness, K. L.; Wert, E. C.; Elovitz, M.; Mahoney, S. Operator-Friendly Technique and Quality Control Considerations for Indigo Colorimetric Measurement of Ozone Residual. *Ozone Sci. Eng.* **2010**, 32 (1), 33–42.



## Chapter 6

# Predicting Properties of Iron(III) TAML Activators of Peroxides from Their III/IV and IV/V Reduction Potentials

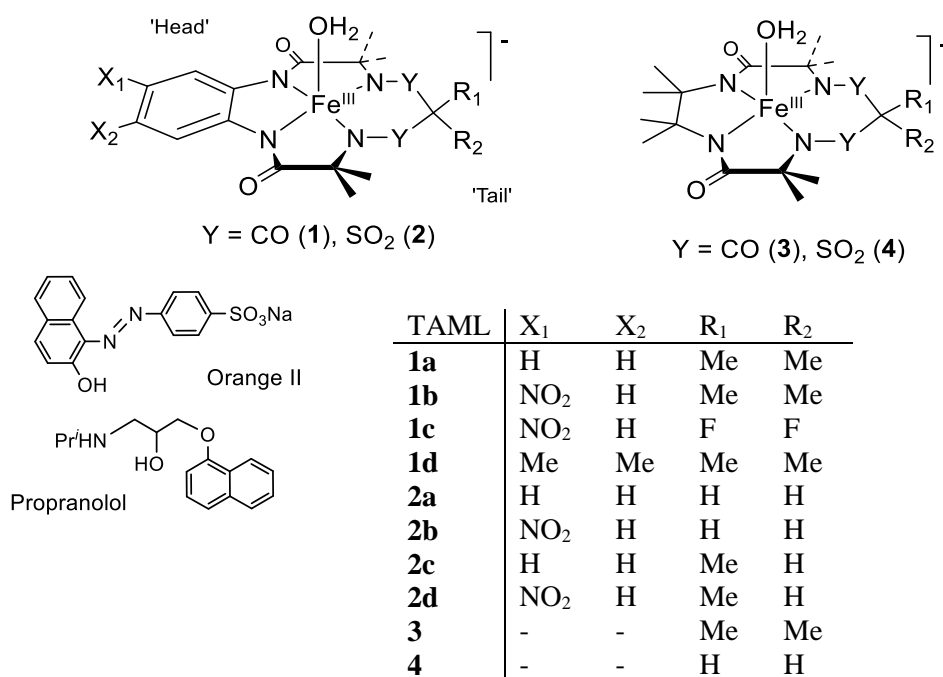


## 6.1 INTRODUCTION

Linear free energy relationship (LFER) methodology<sup>1</sup> is a fundamental tool for analyzing and predicting various properties of iron TAML activators of peroxides (Chart 6.1).<sup>2</sup> Inter alia, LFERs have proven to be particularly useful for establishing relations between the oxidative reactivity of TAMLs ( $\log k_{II}$ ) and their acid-base properties ( $pK_a$ ) in aqueous media<sup>3</sup> and between  $\log k_{II}$  and the operational instability ( $\log k_i$ ).<sup>4</sup> LFERs assisted in detailing intimate mechanistic features of C–H bond activation of hydrocarbons by TAML iron(V)oxo species in an organic solvent.<sup>5</sup> LFER becomes a particularly attractive and useful provided a standard set of parameters, like free energies, rate constants,  $pK_a$ , etc. which are related to the properties of TAML activators, is available. As such in TAML cases, we have previously used the free energies of the C–H activation ( $\Delta G^\ddagger$ )<sup>5</sup> and the  $pK_a$  values.<sup>3</sup> However, calculations of both  $\Delta G^\ddagger$  and  $pK_a$  are rather laborious and therefore we were challenged to find alternative, easier to access parameters that would allow us to analyze and predict the reactivity of both iron(IV) and iron(V) TAML species both involved in numerous TAML catalyzed or promoted transformations.<sup>2,6,7</sup> Therefore, we turned to cyclic voltammetry studies of TAML activators in acetonitrile which can be measured with low effort for both  $Fe^{III/IV}$  and  $Fe^{IV/V}$  transitions and, as explained in this chapter, can support revealing LFER correlations.

Iron(III/IV) reduction potentials of the first series of TAML activators (TAMLs **1** of first generation<sup>8</sup>) obtained by cyclic voltammetry in acetonitrile were reported a decade ago.<sup>9</sup> A complex speciation of iron(IV) TAMLs in water precludes in most of the cases accurate determination of reduction potentials using cyclic voltammetry. The  $Fe^{III/IV}$  and  $Fe^{IV/V}$  values were obtained under basic conditions using differential pulse voltammetry.<sup>10</sup> A recent electrochemical study of the “beheaded” TAML activator **3** revealed that its  $Fe^{III/IV}$  and  $Fe^{IV/V}$  reduction potentials are measurable by cyclic voltammetry over a broad pH range.<sup>11</sup> This finding gave confidence that  $Fe^{III/IV}$  and  $Fe^{IV/V}$  reduction potentials of TAML activators of several generations could be easily

Chart 6.1 TAML activators of peroxides and donors of electrons mentioned or used in this work.



measured at least in an organic solvent (MeCN) and further be used as parameters for LFER predictions of diverse inherent catalytically relevant properties. Thus, in this work we report the cyclic voltammetry data for **1-3**, TAMLs of several generations, the values of Fe<sup>III/IV</sup> and Fe<sup>IV/V</sup> reduction potentials in MeCN; LFER correlations of the potentials with (i) theoretically calculated ionization potentials (IP) and the HOMOs of Fe<sup>III</sup> and Fe<sup>IV</sup> TAMLs and with (ii) the oxidative reactivity (log  $k_{II}$ ), (iii) the acid-base properties (p*K*<sub>a</sub>), and (iv) the Stern-Volmer quenching constants (log  $K_{SV}$ ).

## 6.2 RESULTS AND DISCUSSION

### 6.2.1 Cyclic Voltammetry Measurements.

Cyclic voltammograms of iron(III) TAML activators listed in Chart 6.1 were obtained using a glassy carbon working electrode in MeCN over a broad potential range, usually from  $-1$  to  $+2$  V versus the Ag/AgCl reference electrode. Particularly useful information has been collected in the anodic region above  $0.0$  V, where two clear cut one-electron features were cleanly observed. A representative cyclic voltammogram of **2c** in Figure 6.1 is consistent with  $\text{Fe}^{\text{III/IV}}$  and  $\text{Fe}^{\text{IV/V}}$  one electron processes, since the fact that  $\text{Fe}^{\text{IV}}$  and  $\text{Fe}^{\text{V}}$  species can be generated in organic solvents is a matter of common knowledge.<sup>12,13</sup> Similar behavior has been reported for the iron(III) TAML **3** in aqueous medium where the corresponding  $\text{Fe}^{\text{IV}}$  and  $\text{Fe}^{\text{V}}$  species generated, inter alia, by bulk electrolysis were characterized by spectral techniques.<sup>11,14</sup>

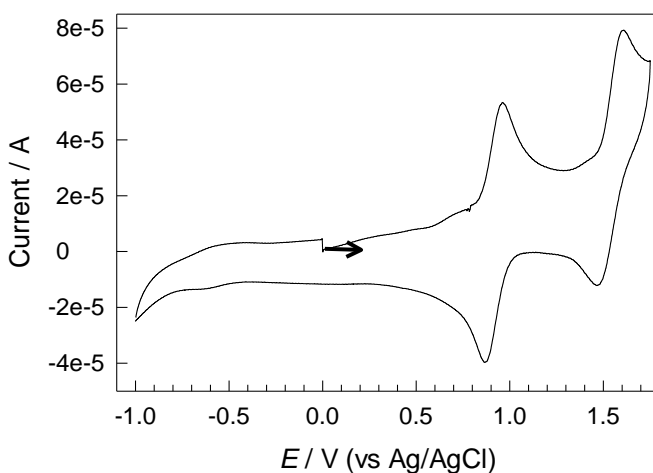


Figure 6.1 Cyclic voltammogram of argon-deaired solution of **2c** ( $0.001$  M) in MeCN containing  $0.1$  M  $(n\text{-Bu})_4\text{NPF}_6$  at a scan rate  $1 \text{ V s}^{-1}$  (glassy carbon electrode,  $30^\circ\text{C}$ ).

Running cyclic voltammograms of **2c** at scan rates  $0.05\text{--}1.0 \text{ V s}^{-1}$  in the potential range of  $0.4\text{--}1.8$  V (Figure 6.8) showed that the  $\text{Fe}^{\text{III/IV}}$  process is reversible at lower scan rates ( $\Delta E$  between anodic and cathodic peaks is  $60 \text{ mV}$ ) although  $\Delta E$  increases to  $100 \text{ mV}$  at higher scan rates indicating a quasi-reversible behavior. The  $\text{Fe}^{\text{IV/V}}$  reversibility is lower and  $\Delta E$  increases from  $90$

to 170 mV as the scan rate rises from 0.05 to 1.0 V s<sup>-1</sup>, as anticipated for a quasi-reversible process.<sup>15</sup> Anodic peak currents depend linearly on the square root of the scan rate for both Fe<sup>III/IV</sup> and Fe<sup>IV/V</sup> features (Figure 6.9).

Table 6.1 Reduction potentials (III/IV and IV/V, vs Ag/AgCl) of iron(III) TAML activators measured in MeCN in the presence of 0.1 M (*n*-Bu)<sub>4</sub>NPF<sub>6</sub> at a glassy carbon electrode, at 30 °C, calculated ionization potentials (IP) and HOMOs of iron(III) and iron(IV) TAMLs.

TAML (X <sub>1,2</sub> , R <sub>1</sub> , R <sub>2</sub> )	<i>E</i> <sup>o'</sup> / V		IP / eV		HOMO / eV	
	Fe <sup>III/IV</sup>	Fe <sup>IV/V</sup>	Fe <sup>III</sup>	Fe <sup>IV</sup>	Fe <sup>III</sup>	Fe <sup>IV</sup>
<b>1a</b> (H, Me, Me)	0.725	1.45	5.09	4.70	-5.25	-4.87
<b>1b</b> (NO <sub>2</sub> , Me, Me)	0.971	1.535	5.45	4.91	-5.60	-5.09
<b>1c</b> (NO <sub>2</sub> , F, F)	1.16	1.64	5.60	5.14	-5.75	-5.29
<b>1d</b> (Me <sub>2</sub> , Me, Me)	0.44 <sup>a</sup>		5.00	4.64	-5.16	-4.82
<b>2a</b> (H, H, H)	0.89	1.52	5.31	4.98	-5.47	-5.15
<b>2b</b> (NO <sub>2</sub> , H, H)	1.17	1.59	5.68	5.30	-5.83	-5.47
<b>2c</b> (H, Me, H)	0.918	1.53	5.27	4.96	-5.43	-5.13
<b>2d</b> (NO <sub>2</sub> , Me, H)	1.19	1.59	5.67	5.28	-5.82	-5.44
<b>3</b> (-, Me, Me)	0.52	~1.5 <sup>b</sup>	5.50	4.58	-5.60	-4.77
<b>4</b> (-, H, H)	0.96	~1.4 <sup>b</sup>	5.89	5.07	-6.01	-5.27

<sup>a</sup> From ref. <sup>9</sup>; <sup>b</sup> anodic peak.

The Fe<sup>III/IV</sup> and Fe<sup>IV/V</sup> features are clearly observed for all iron(III) TAML activators shown in Chart 6.1. The corresponding formal reduction potentials *E*<sup>o'</sup> are collected in Table 6.1. They both increase gradually as the TAML ligand system becomes more electron-demanding due to adding electron-withdrawing groups to the head (usually NO<sub>2</sub>) and tail (usually F) parts of the molecule (see Chart 6.1). It is worth noting that the Fe<sup>III/IV</sup> potentials are more sensitive to the electronic properties of ligands than the Fe<sup>IV/V</sup> values. The slope of a linear plot in Figure 6.2, which compares Fe<sup>III/IV</sup> and Fe<sup>IV/V</sup> potentials, is just ca. 0.33 reflecting the fact that *E*<sup>o'</sup> vary in the ranges of ca. 0.8 and ca. 0.2 V, respectively. This observation may suggest that the TAML system plays

a bigger role in the  $\text{Fe}^{\text{III/IV}}$  transition whereas the second electron transfer ( $\text{Fe}^{\text{IV/V}}$ ) is to a larger extent an iron-centered phenomenon.

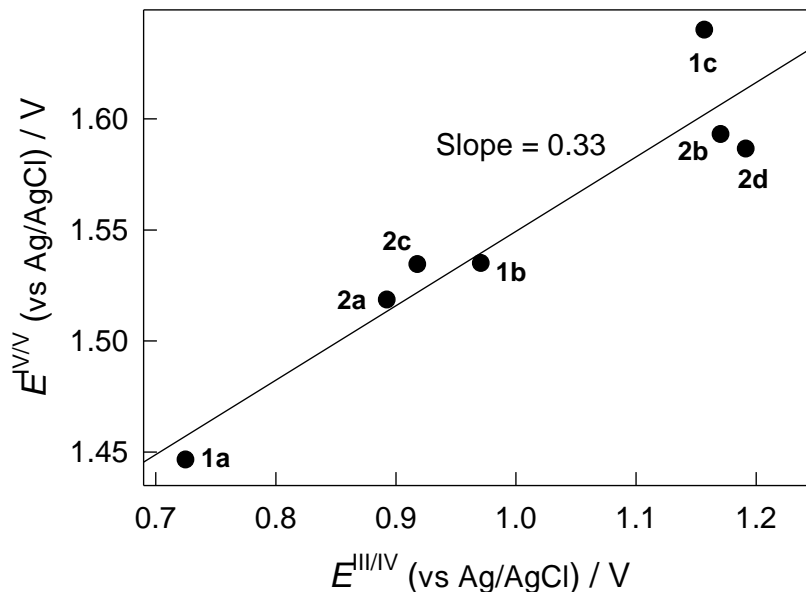


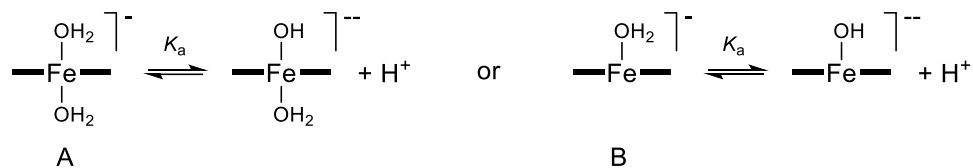
Figure 6.2 Formal IV/V reduction potentials of various TAML activators versus corresponding III/IV reduction potentials obtained in MeCN containing 0.1 M  $(n\text{-Bu})_4\text{NPF}_6$  at a scan rate  $1 \text{ V s}^{-1}$  (glassy carbon electrode,  $30^\circ\text{C}$ ).

The data in Figure 6.1 for **2c** shows no redox effects in the cathodic region. There are no cathodic peaks for **1a** as well above  $-1 \text{ V}$  (vs Ag/AgCl). This, however, is not a general feature since broader peaks were detected for some TAMLs. In particular, there are such for **2b** (Figure 6.10) and **2a**. They are usually irreversible and depend on the scan range applied. Additional irreversible peaks were detected when the applied potential was reversed at  $-2 \text{ V}$  as compared to that at  $-1 \text{ V}$ . The variability of these effects leads us to assume that they are most likely due to ligand-centered reductions rather than due to the  $\text{Fe}^{\text{II/III}}$  transitions because in the latter case one could anticipate such peaks for all iron(III) TAMLs studied as it is observed for  $\text{Fe}^{\text{III/IV}}$  and  $\text{Fe}^{\text{IV/V}}$  transitions. This was not the case and therefore no further analysis of cathodic peaks was made.

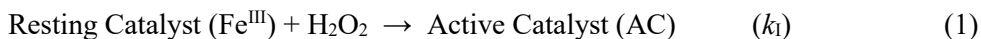
### 6.2.2 Formal Reduction Potentials $E^{\circ'}$ and $pK_a$ 's.

All known iron(III) TAML activators are five coordinate square pyramidal species in the solid phase.<sup>7,8,16</sup> Despite the nature of an axial ligand, which is usually water, they transform into diaqua six- or monoaqua five-coordinate complexes (cases A and B in Scheme 6.1, respectively).<sup>16-18</sup> In turn, both A and B undergo deprotonation in the pH range of 8–11.5. The corresponding values of  $K_a$  reflect the Lewis acidity of the metal center, which determines the oxidative reactivity of TAMLs in aqueous solution. In fact, there are linear dependencies between  $pK_a$  and  $\log k$ , where, as shown in Scheme 6.2,  $k$  are rate constants for activation of  $H_2O_2$  by iron(III) TAMLs ( $k_I$ ) to form an active TAML or for reactions of the latter with an electron donor ( $k_{II}$ ).<sup>3</sup> It was therefore tempting to establish a correlation of  $pK_a$  with  $E^{\circ'}$  for  $Fe^{III/IV}$  and  $Fe^{IV/V}$  features because the  $E^{\circ'}$  values could be diagnostic for estimating the reactivity of TAMLs in aqueous media.

Scheme 6.1 Deprotonation options for TAML activators: of six- (A) and five-coordinate (B) aqua iron(III) complexes.



Scheme 6.2 General mechanism of catalysis by TAML activators



The data presented in Figure 6.3 confirmed that the values of  $pK_a$  measured in water correlate satisfactorily with the formal reduction potentials  $E^{\circ'}$  for both  $Fe^{III/IV}$  and  $Fe^{IV/V}$  features despite the fact that  $E^{\circ'}$  were measured in an organic solvent. The corresponding analytical expressions for the III/IV and IV/V lines are equations 6.1 and 6.2, respectively.

$$E^{\circ'}(\text{III/IV}) = (3.1 \pm 0.4) - (0.22 \pm 0.05) \times \text{p}K_a \quad (6.1)$$

$$E^{\circ'}(\text{IV/V}) = (2.0 \pm 0.2) - (0.05 \pm 0.02) \times \text{p}K_a \quad (6.2)$$

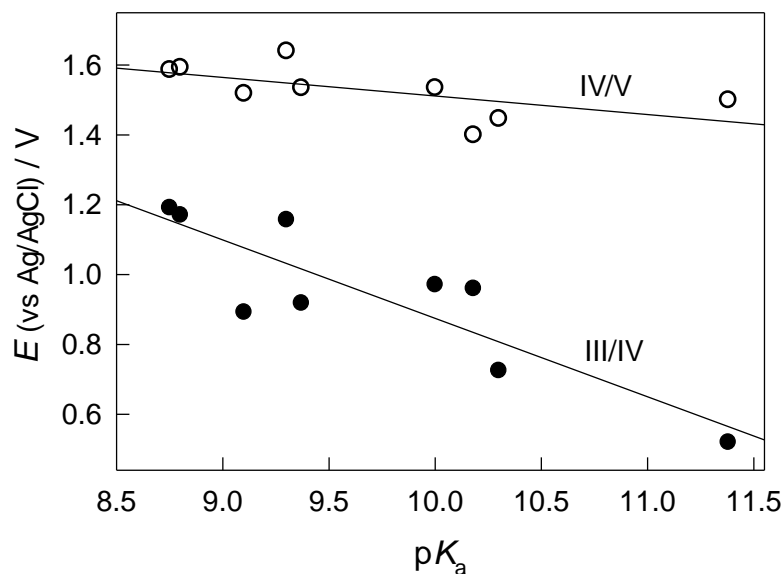


Figure 6.3 . . Formal III/IV and IV/V reduction potentials of various TAML activators in MeCN (0.1 M (*n*-Bu)<sub>4</sub>NPF<sub>6</sub>; glassy carbon electrode, 30 °C) versus pK<sub>a</sub> values of the corresponding iron(III) aqua complexes in water (see text for details).

Equations 6.1 and 6.2 show that the  $E^{\circ'}(\text{III/IV})$  values are more than four times more sensitive to pK<sub>a</sub> than the  $E^{\circ'}(\text{IV/V})$  ones. This is not surprising in view that the proton dissociation and removal of the first electron both involve one and the same species, i.e. iron(III), whereas that the second electron transfer involves an iron(IV) complex, which is not the iron(III) center (from which the proton dissociates).



### 6.2.3 Formal Reduction Potentials $E^\circ$ and Stern-Volmer Quenching Constants $K_{SV}$ .

We have recently found that TAML activators **1** quench the fluorescence of propranolol (P), which is a micropollutant of broad concern.<sup>19</sup> The quenching is a non-linear, upright curved function of TAML concentrations and therefore the Stern-Volmer constants  $K_{SV}$  were calculated at low loadings of quenchers when the  $I_0/I$  versus [TAML] plot could be approximated by a straight line. The value of  $K_{SV}$  for **1a** of  $(60 \pm 1) \times 10^2 \text{ M}^{-1}$  exceeds by two orders of magnitude  $K_{SV}$  for iodide, the benchmark fluorescence quencher. Our previous goals were to find (i) evidence for the interaction between propranolol and iron(III) TAMLs in the ground state and (ii) establish LFERs between  $K_{SV}$  and rate constants  $k_{II}$  (Scheme 6.2). The former goal was achieved though no  $K_{SV}$ – $k_{II}$  correlations were found. Moreover, attempts to correlate  $K_{SV}$  to any other property of TAMLs failed as well. Therefore, it was motivating to find that the values of  $\log(K_{SV})$  are proportional to formal reduction potentials  $E^\circ$  for both  $\text{Fe}^{\text{III/IV}}$  and  $\text{Fe}^{\text{IV/V}}$  features (Figure 6.4).

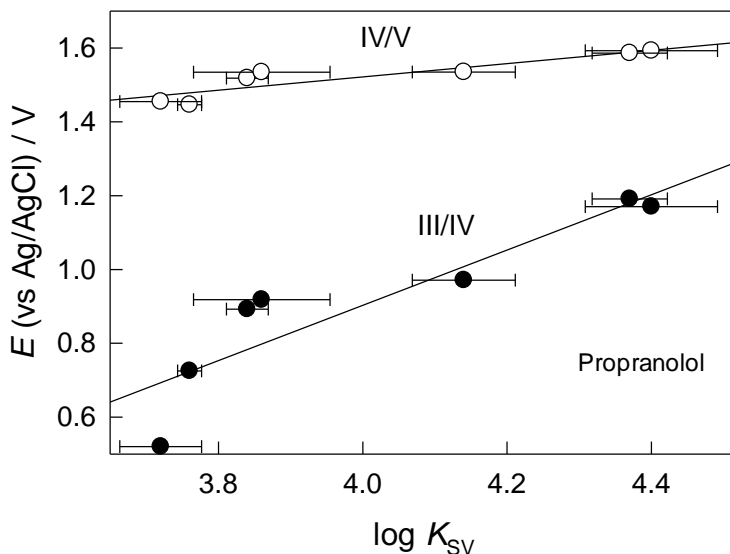


Figure 6.4 Formal III/IV and IV/V reduction potentials of various TAML activators in MeCN (0.1 M  $(n\text{-Bu})_4\text{NPF}_6$ ; glassy carbon electrode, 30 °C) versus Stern-Volmer constants  $K_{SV}$  (Table 6.2) measured for propranolol and corresponding iron(III) aqua TAMLs in water (see text for details).

Positive slopes in Figure 6.4 confirm further our previous observation that the Stern-Volmer constants  $K_{SV}$  are larger for iron(III) TAMLs with higher Lewis acidity of the metal center, which parallels with respective reduction potentials.

The data presented in Figure 6.4 may be indicative of the electron-transfer mechanism of quenching of propranolol fluorescence by TAMLs. This hypothesis encouraged us to calculate theoretically IP, HOMOs and LUMOs of iron (III, IV and V) TAML activators for comparing them with the experimentally measured reduction potentials. The results of theoretical analysis are presented in the next section.

#### **6.2.4 Calculated Ionization Potentials (IPs), HOMOs of Iron(III, IV and V) TAMLs and Formal Reduction Potentials $E^\circ$ .**

Structures of TAML activators with iron in different oxidation states, which were selected for computation, are presented in Chart 6.2. The following assumptions were applied. TAML iron(III) resting was associated with a five coordinate, square pyramidal species; iron(IV) and iron(V) were considered as the corresponding monomeric ironoxo derivatives. The calculated values of IPs for two step-wise oxidations and HOMOs are collected in Table 6.1.

Chart 6.2 . Structures of TAML activators with iron in different oxidation states used for computation.

.

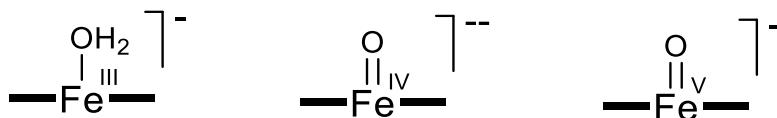


Figure 6.5 shows that calculated IPs of iron(III) and iron(IV) TAML activators both depend linearly on  $E^{III/IV}$  with positive slopes confirming that TAMLs with higher IPs are to oxidized at higher potentials, i.e. have higher reduction potentials. It is worth noting that both lines in Figure

6.5 are near parallel, the gap between them being ca.  $0.40 \pm 0.08$  eV. This may indicate that similar factors control one electron oxidation of both  $\text{Fe}^{\text{III}}$  and  $\text{Fe}^{\text{IV}}$  species. It was rather surprising for us to find higher IPs for  $\text{Fe}^{\text{III}}$  than for  $\text{Fe}^{\text{IV}}$  derivatives. Perhaps this fact deserves special attention but as a first tentative rationale it can be ascribed to a higher reorganizational term in the case of the  $\text{Fe}^{\text{III}} \rightarrow \text{Fe}^{\text{IV}}$  transition because the initial electron transfer should result in an iron(IV)aqua species which should drop two protons to achieve the iron(IV)oxo state. Note that the  $\text{Fe}^{\text{IV}} \rightarrow \text{Fe}^{\text{V}}$  transition is a clean one electron oxidation.

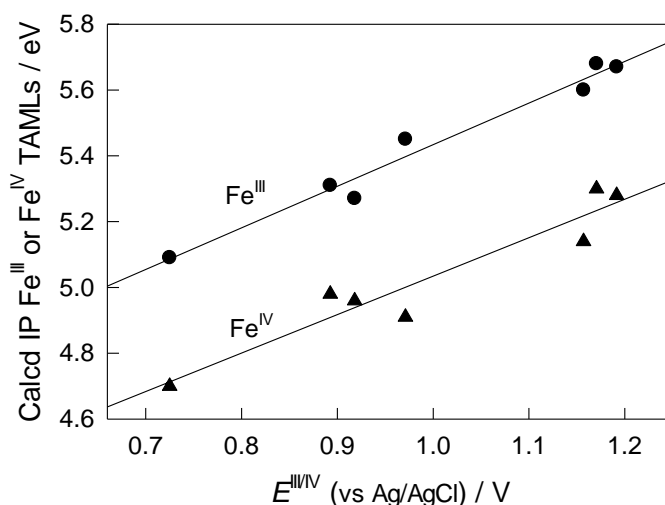


Figure 6.5 Calculated IPs of iron(III) TAMLs versus their measured  $\text{Fe}^{\text{III/IV}}$  reduction potentials. See text for details.

Similar graph comparing calculated IPs of iron(IV) TAML and  $E^{\text{IV/V}}$  reduction potentials presented in Figure 6.11 shows the same tendency as the data in Figure 6.5. Calculated IPs and HOMOs for  $\text{Fe}^{\text{III}}$  and  $\text{Fe}^{\text{IV}}$  TAMLs all correlate with each other as it could be anticipated (Figure 6.12). It is worth noting that the data for ‘beheaded’ TAML **3** are somewhat off regression lines which are tentatively due to its higher conformational perturbations compared to TAMLs **1** and **2**.

### 6.2.5 Reactivity Comparisons.

The general mechanism of catalysis by TAMLs in Scheme 6.2 implies that the catalytic activity is determined by the values of rate constants  $k_I$  and  $k_{II}$ . The former is substrate independent in the absence of substrate inhibition<sup>19</sup> though the latter is always a function of an electron donor substrate S. The reactivities of S are different and S compounds are customarily classified as easy-to-oxidize and hard-to-oxidize substrates.<sup>20</sup> Corresponding  $k_{II}$  values are different as well. Needless to say that for one and the same S, the  $k_{II}$  values depend on the nature of the TAML catalyst. The dependence is strong. Some TAML activators are inactive toward hard-to-oxidize substrates. In particular, **1a** does not catalyze oxidation of propranolol by  $H_2O_2$  but **1c** does;<sup>19</sup> **1c** is inactive toward imidacloprid while **2d** is active.<sup>21</sup> Note that these four TAMLs catalyze the oxidation of easy-to-oxidize Orange II dye.<sup>16,22</sup> Reduction potentials provide a convenient tool for quantitative rationalization of this property of TAML activators. One needs just to compare rate constants  $k_I$  and  $k_{II}$  with reduction potentials  $E^{III/IV}$  as it is suggested in Figure 6.6. Here,  $\log k_{II}$  for both propranolol and Orange II are plotted against  $E^{III/IV}$ . The slopes of both straight lines are positive (i.e. higher oxidizing power delivers higher catalytic activity), but the tangent for propranolol is by a factor of ca. 3 higher than that for Orange II! The corresponding analytical expressions for  $\log k_{II}$  equal  $(3.2 + 1.5 \times E^{III/IV})$  and  $(-1.3 + 4.9 \times E^{III/IV})$  for Orange II and propranolol, respectively; they forecast a particular value of  $\log k_{II}$  provided  $E^{III/IV}$  is known. For example,  $k_{II}$  for **1d** and propranolol should be around  $7.2 \text{ M}^{-1} \text{ s}^{-1}$ , i.e. too low to be experimentally measurable at nM concentrations of the catalyst. Easy-to-oxidize donors of electrons S have smaller slopes in plots such as in Figure 6.6. Hard-to-oxidize S, in contrast, have larger slopes. For smaller-slope, easy-to-oxidize S, the values of  $k_{II}$  could never be very high even if  $E^{III/IV}$  of TAML is large. In contrast, TAMLs with higher  $E^{III/IV}$  can be substantially more reactive toward hard-to-oxidize S. As an illustration of convenience of these simple LFERs, let us consider a couple of hypothetical examples. The linear regressions mentioned above reveal that the  $E^{III/IV}$

reduction potential of a TAML having diffusion-controlled  $k_{II}$  (ca.  $10^{10} \text{ M}^{-1} \text{ s}^{-1}$ ) in the oxidation of Orange II should equal 4.5 V; the same for propranolol is noticeably lower, around 2.3 V. The latter is hard to achieve, but the former is unrealistic! Orange II and propranolol will be oxidized with identical  $k_{II}$  when  $E^{\text{III/IV}}$  of a TAML activator equals 1.27 V (vs Ag/AgCl). Above that propranolol is always more reactive than Orange II.

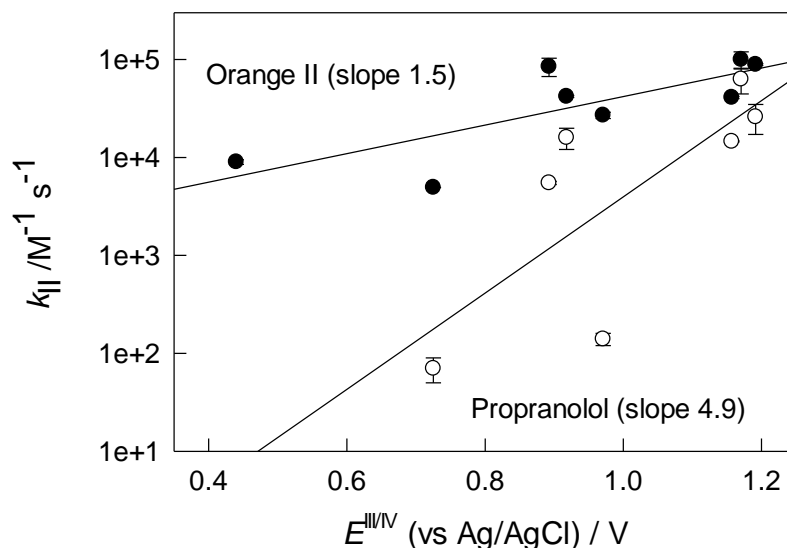


Figure 6.6 Values of  $\log k_{II}$  (pH 7, 25 °C) against  $E^{\text{III/IV}}$  for propranolol and Orange II. Data are from Tables 6.3 and 6.4, respectively.

The dependence of  $\log k_I$  against  $E^{\text{III/IV}}$  is presented in Figure 6.7. The data point for 'beheaded' TAML **3**, which is rather off the line, increases the slope ( $\log k_I = -0.39 + 2.75 \times E^{\text{III/IV}}$ ). The regression without it is  $0.80 + 1.65 \times E^{\text{III/IV}}$ , i.e. the sensitivity of  $k_I$  to the nature of TAML is low. The extension to the  $k_I$  level of horseradish peroxidase (ca.  $10^7 \text{ M}^{-1} \text{ s}^{-1}$ )<sup>23</sup> requires a TAML activator with  $E^{\text{III/IV}}$  of ca. 3.8 V (vs Ag/AgCl), i.e. the peroxidase performs better with respect to  $k_I$  as compared to TAML chemistry. However,  $k_I$  alone partially represents the overall reactivity of a TAML. TAMLs more than make up for this with orders of magnitude higher  $k_{II}$ , leading to oxidation of persistent pollutants which bounces right off the peroxidase enzymes

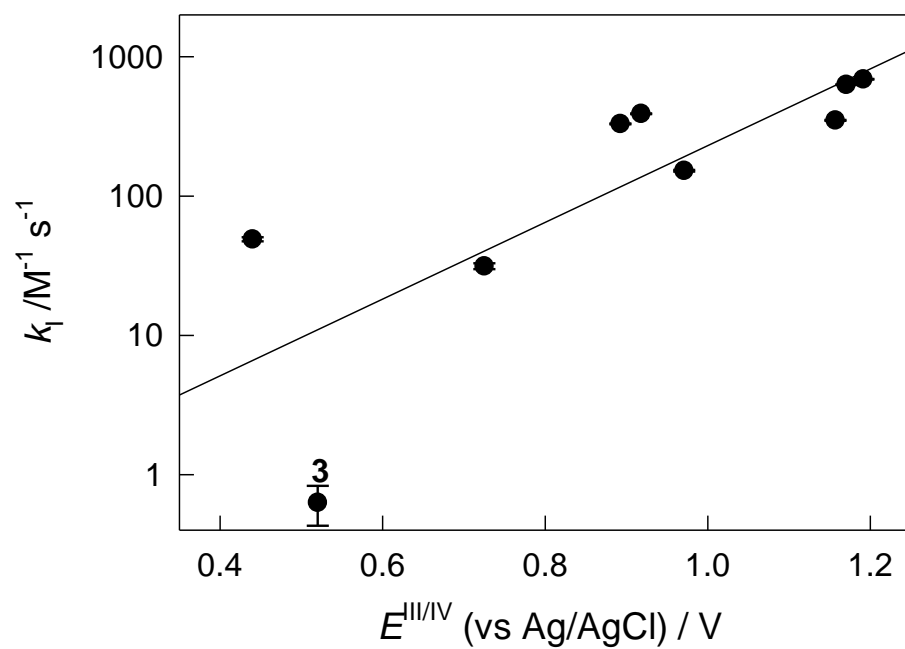


Figure 6.7 Values of  $\log k_I$  (pH 7, 25 °C) against  $E^{\text{III/IV}}$ . The data were obtained using Orange II as an electron donor.

### 6.3 CONCLUSION.

Reversible or quasi-reversible  $\text{Fe}^{\text{III/IV}}$  and  $\text{Fe}^{\text{IV/V}}$  formal reduction potentials of TAML activators are rather useful for predictions of several properties of iron(III) TAML activators of peroxides in terms of LFERs. The values of  $E^{\circ'}(\text{III/IV})$  and  $E^{\circ'}(\text{IV/V})$  correlate with  $\text{p}K_{\text{a}}$ 's of the axial aqua ligand at iron(III), the Stern-Volmer constants  $K_{\text{SV}}$  for the quenching of a fluorescence of propranolol, calculated ionization potentials of  $\text{Fe}^{\text{III}}$  and  $\text{Fe}^{\text{IV}}$  TAMLs, rate constants  $k_{\text{I}}$  and  $k_{\text{II}}$  for the oxidation of the resting iron(III) TAML state by  $\text{H}_2\text{O}_2$  and reactions of the active forms of TAMLs formed with donors of electrons S. Used as a tool for reactivity predictions, they provide valuable estimates of the catalytic activity of man-made TAML catalysts in comparison with peroxidase enzymes.

## 6.4 EXPERIMENTAL

### 6.4.1 Materials

Iron(III) TAML complex **1a** was obtained from GreenOx Catalysts, Inc.; complexes **1c** and **1b** were prepared as described elsewhere.<sup>24–26</sup> The preparation of Fe<sup>III</sup> NewTAML **2a–d** complexes recently described<sup>16</sup> “Beheaded” TAMLs **3** and **4** were prepared as described elsewhere.<sup>4,16</sup> (*n*-Bu)<sub>4</sub>NPF<sub>6</sub> was purchased from Aldrich. Acetonitrile (HPLC grade) was a Fischer reagent; it was used as received.

### 6.4.2 Instrumentation and Measurements.

Electrochemical studies were performed with an Autolab PGSTAT100. The working electrode was a glassy carbon disk, with a Ag/AgCl reference electrode and platinum wire counter electrode. Unless otherwise stated, all potentials indicated in the text are versus Ag/AgCl. The working electrode was always polished with a diamond paste (Struers) before each measurement. The electrochemical cell, acetonitrile solvent, and solutions were all degassed with N<sub>2</sub> for 10–30 min. All measurements were performed using 10<sup>–3</sup> M solutions of TAML activators in the presence of 0.1 M (*n*-Bu)<sub>4</sub>NPF<sub>6</sub>. Fluorescence measurements were performed at 25 °C using a Cary Eclipse Varian instrument (excitation wavelength 230 nm, emission range from 250 to 800 nm, slit width 5 nm). Concentrations of propranolol, concentrations of TAML activators and procedures used for calculating the Stern-Volmer constants *K*<sub>SV</sub>, which are collected in Table 6.2, were as described in our previous work.<sup>19</sup> Kinetic data for the TAML-catalyzed oxidation of propranolol used for calculating second-order rate constants *k*<sub>II</sub> (Table 6.3) were collected as described in detail previously.

### 6.4.3 Theoretical Calculations.

HOMOs of iron(III), iron(IV) and iron(V) TAML activators were calculated using Becke’s three parameter hybrid functional (B3)<sup>27,28</sup> along with the Lee–Yang–Parr correlation functional



(LYP)<sup>29</sup> implemented in the computational suite Gaussian 09, rev. D.01.<sup>30</sup> Basis set 6-31+G(d) was employed for the sulfur element and 6-311G for all others. The solvent effect was considered using the SMD continuum model.<sup>31</sup> Molecular geometries were obtained upon numerical convergence at the default criteria. Vertical ionization energy for each species in the study was computed by taking differences of the electronic energies between its oxidation state and reduction state while maintaining the geometry of the latter.

## 6.5 APPENDIX

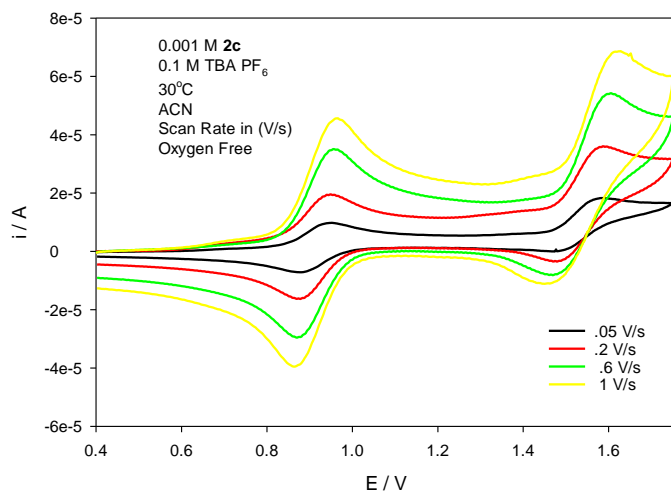


Figure 6.8 Cyclic voltammograms of TAML **2c** at different scan rates. Conditions: MeCN (0.1 M  $(n\text{-Bu})_4\text{NPF}_6$ ; glassy carbon electrode, 30 °C. Potentials are against Ag/AgCl reference electrode.

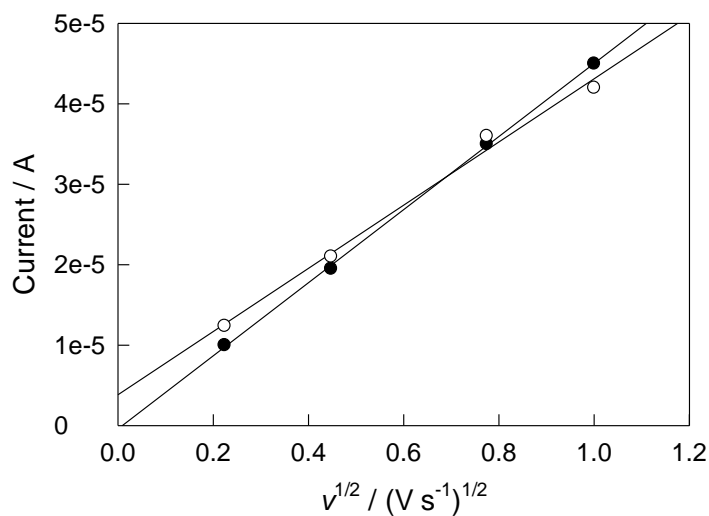


Figure 6.9 Anodic peak currents versus square root of scan rate for III/IV (●) and IV/V (○) features of TAML **2c** in MeCN (0.1 M  $(n\text{-Bu})_4\text{NPF}_6$ ; glassy carbon electrode, 30 °C.

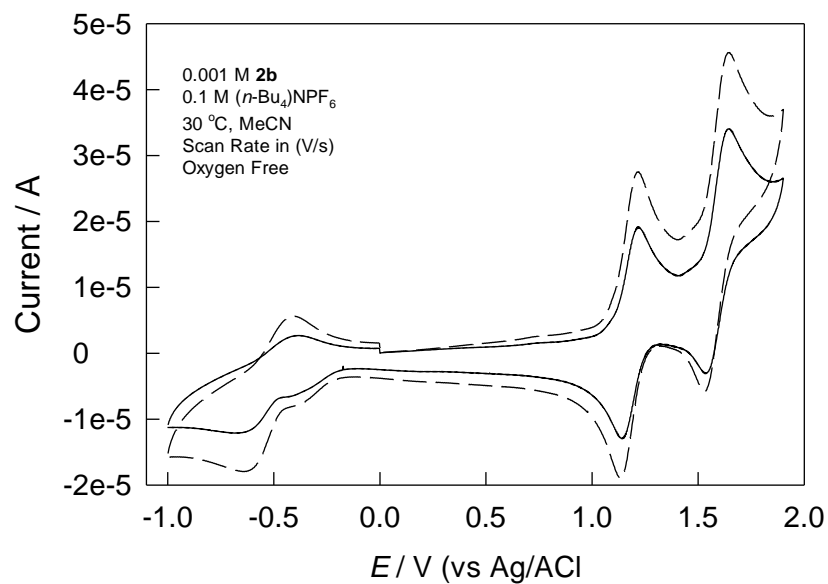


Figure 6.10 Cyclic voltammogram of argon-deaerated solution of **2b** (0.001 M) in MeCN containing 0.1 M (n-Bu)<sub>4</sub>NPF<sub>6</sub> at scan rates 0.1 (solid line) and 0.2 V s<sup>-1</sup> (dash line) at a glassy carbon electrode, 30 °C.

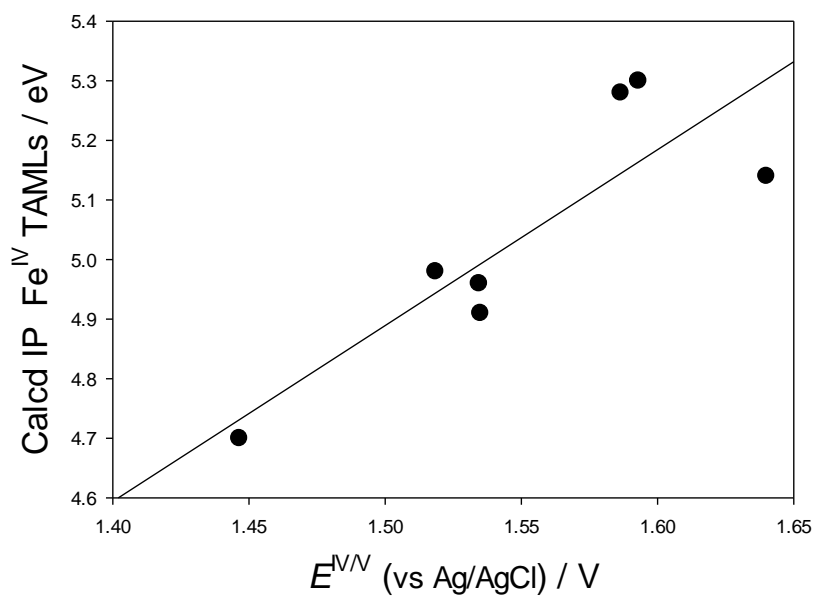


Figure 6.11 Calculated IPs of iron(IV) TAMLs versus their measured Fe<sup>IV/III</sup> reduction potentials.

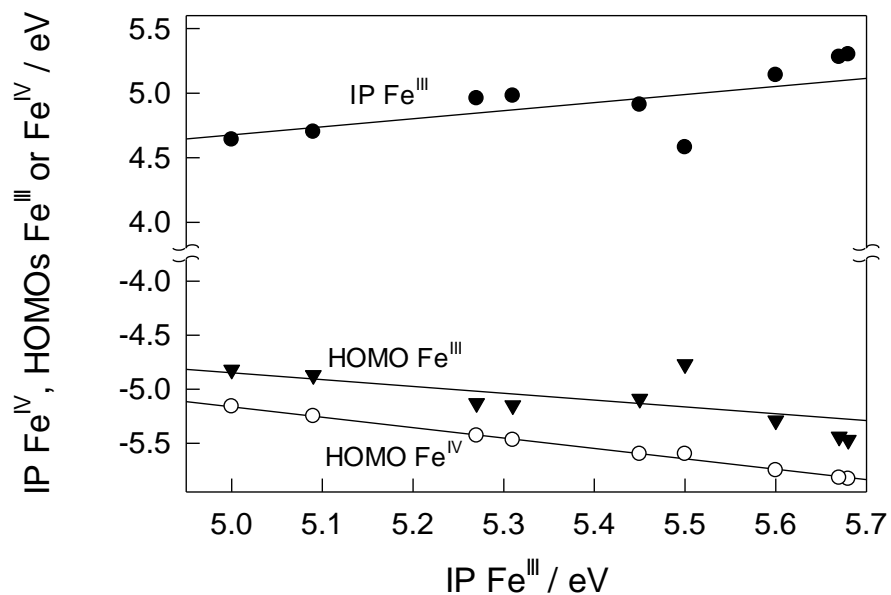


Figure 6.12 Correlations between computed ionization potentials and HOMOs (in V) for Fe<sup>III</sup> and Fe<sup>IV</sup> TAML species (data are from Table 6.1).

Table 6.2 Stern-Volmer constants  $K_{sv}$  of measured for quenching propranolol fluorescence by TAML activators at pH 7 (0.01 M phosphate buffer) and 25 °C

TAML	$K_{sv} / \text{M}^{-1}$	Reference
<b>1a</b>	$6000 \pm 100$	19
<b>1b</b>	$14000 \pm 1000$	19
<b>2a</b>	$6900 \pm 200$	This work
<b>2b</b>	$26200 \pm 2400$	This work
<b>2c</b>	$7400 \pm 700$	This work
<b>2d</b>	$23700 \pm 1200$	This work
<b>3</b>	$5300 \pm 300$	This work

Table 6.3 Second order rate constants  $k_I$  and  $k_{II}$  for oxidation of propranolol catalyzed by various TAML activators at pH 7 (0.01 M phosphate buffer) and 25 °C.

TAML	$k_I / \text{M}^{-1} \text{s}^{-1}$	$k_{II} / \text{M}^{-1} \text{s}^{-1}$	Reference
<b>1a</b>	$2 \pm 0.1$	$70 \pm 20$	19
<b>1b</b>	$5.0 \pm 0.2$	$140 \pm 20$	19
<b>1c</b>	$90 \pm 10$	$14600 \pm 200$	19
<b>2a</b>	$150 \pm 40$	$5500 \pm 200$	This work
<b>2b</b>	$132 \pm 2.0$	$63000 \pm 18500$	This work
<b>2c</b>	$78 \pm 2.1$	$16000 \pm 3900$	This work
<b>2d</b>	$134 \pm 5.9$	$26000 \pm 8800$	This work

Table 6.4 Second order rate constants,  $k_I$  and  $k_{II}$  in  $\text{M}^{-1} \text{s}^{-1}$  for oxidation of Orange II catalyzed by various TAML activators at pH 7 (0.01 M phosphate buffer) and 25 °C.

TAML	$k_I / \text{M}^{-1} \text{s}^{-1}$	$k_{II} / \text{M}^{-1} \text{s}^{-1}$	Reference
<b>1a</b>	$31.4 \pm 0.1$	$4950 \pm 20$	4
<b>1b</b>	$152 \pm 5$	$27000 \pm 2000$	4
<b>1c</b>	$350 \pm 2$	$41000 \pm 1000$	4
<b>1d</b>	$49 \pm 3$	$9000 \pm 500$	4
<b>2a</b>	$330 \pm 20$	$85000 \pm 18000$	16
<b>2b</b>	$630 \pm 50$	$100000 \pm 20000$	16
<b>2c</b>	$390 \pm 4$	$42000 \pm 1000$	16
<b>2d</b>	$690 \pm 20$	$89000 \pm 2000$	16
<b>3</b>	$0.63 \pm 0.02$	$1.19 \pm 0.03$	4

## 6.6 REFERENCES

- (1) Hammett, L. P. The Effect of Structure upon the Reactions of Organic Compounds. Benzene Derivatives. *J. Am. Chem. Soc.* **1937**, *59* (1), 96–103.
- (2) Collins, T. J.; Ryabov, A. D. Targeting of High-Valent Iron-TAML Activators at Hydrocarbons and Beyond. *Chem. Rev.* **2017**.
- (3) Mills, M. R.; Weitz, A. C.; Zhang, D. Z.; Hendrich, M. P.; Ryabov, A. D.; Collins, T. J. A “Beheaded” TAML Activator: A Compromised Catalyst That Emphasizes the Linearity between Catalytic Activity and PKa. *Inorg. Chem.* **2016**, No. 23, 12263–12269.
- (4) DeNardo, M. A.; Mills, M. R.; Ryabov, A. D.; Collins, T. J. Unifying Evaluation of the Technical Performances of Iron-Tetra-Amido Macrocyclic Ligand Oxidation Catalysts. *J. Am. Chem. Soc.* **2016**, *138* (9), 2933–2936.
- (5) Kundu, S.; Van Thompson, J. K.; Shen, L. Q.; Mills, M. R.; Bominaar, E. L.; Ryabov, A. D.; Collins, T. J. Activation Parameters as Mechanistic Probes in the TAML Iron(V)-Oxo Oxidations of Hydrocarbons. *Chem. - A Eur. J.* **2015**, *21* (4), 1803–1810.
- (6) Collins, T. J.; Khetan, S. K.; Ryabov, A. D. Chemistry and Applications of Iron–TAML Catalysts in Green Oxidation Processes Based on Hydrogen Peroxide. *Handb. Green Chem. Online* **2010**, 39–77.
- (7) Ryabov, A. D.; Collins, T. J. Mechanistic Considerations on the Reactivity of Green FeIII-TAML Activators of Peroxides. *Adv. Inorg. Chem.* **2009**, *61*, 471–521.
- (8) Warner, G.; Mills, M.; Enslin, C.; Pattanayak, S.; Panda, C.; Sen Gupta, S.; Ryabov, A. D.; Collins, T. J. Reactivity of N-Tailed (“Biuret”) TAMLs in Water: Kinetics of the Catalyzed Oxidation of Orange II by H<sub>2</sub>O<sub>2</sub>. Synthesis and X-Ray Characterization of an N-Phenyl Biuret TAML. *Chem. - Eur. J.* **2015**, *21* (16), 6226–6233.
- (9) Ghosh, A.; Mitchell, D. A.; Chanda, A.; Ryabov, A. D.; Popescu, D. L.; Upham, E. C.; Collins, G. J.; Collins, T. J. Catalase-Peroxidase Activity of Iron(III)-TAML Activators of Hydrogen Peroxide. *J. Am. Chem. Soc.* **2008**, *130* (45), 15116–15126.
- (10) Popescu, D. L.; Vrabel, M.; Brausam, A.; Madsen, P.; Lente, G.; Fabian, I.; Ryabov, A. D.; van Eldik, R.; Collins, T. J. Thermodynamic, Electrochemical, High-Pressure Kinetic, and Mechanistic Studies of the Formation of Oxo Fe(IV)-TAML Species in Water. *Inorg Chem* **2010**, *49* (24), 11439–11448.
- (11) Weitz, A. C.; Mills, M. R.; Ryabov, A. D.; Collins, T. J.; Guo, Y.; Bominaar, E. L.; Hendrich, M. P. A Synthetically Generated LFeIVO H<sub>2</sub>O Complex. *Inorg. Chem.* **2019**, *58* (3), 2099–2108.
- (12) de Oliveira, F. T.; Chanda, A.; Banerjee, D.; Shan, X.; Mondal, S.; Que, L.; Bominaar, E. L.; Münck, E.; Collins, T. J. Chemical and Spectroscopic Evidence for an FeV-Oxo Complex. *Science* (80-. ). **2007**, *315* (5813), 835–838.
- (13) Ren, Q. Z.; Guo, Y. S.; Mills, M. R.; Ryabov, A. D.; Collins, T. J. On the Iron(V) Reactivity of an Aggressive Tail-Fluorinated Tetraamido Macrocyclic Ligand (TAML) Activator. *Eur. J. Inorg. Chem.* **2015**, *2015* (8), 1445–1452.
- (14) Mills, M. R.; Weitz, A. C.; Hendrich, M. P.; Ryabov, A. D.; Collins, T. J. NaClO-Generated Iron(IV)Oxo and Iron(V)Oxo TAMLs in Pure Water. *J Am Chem Soc* **2016**,

138 (42), 13866–13869.

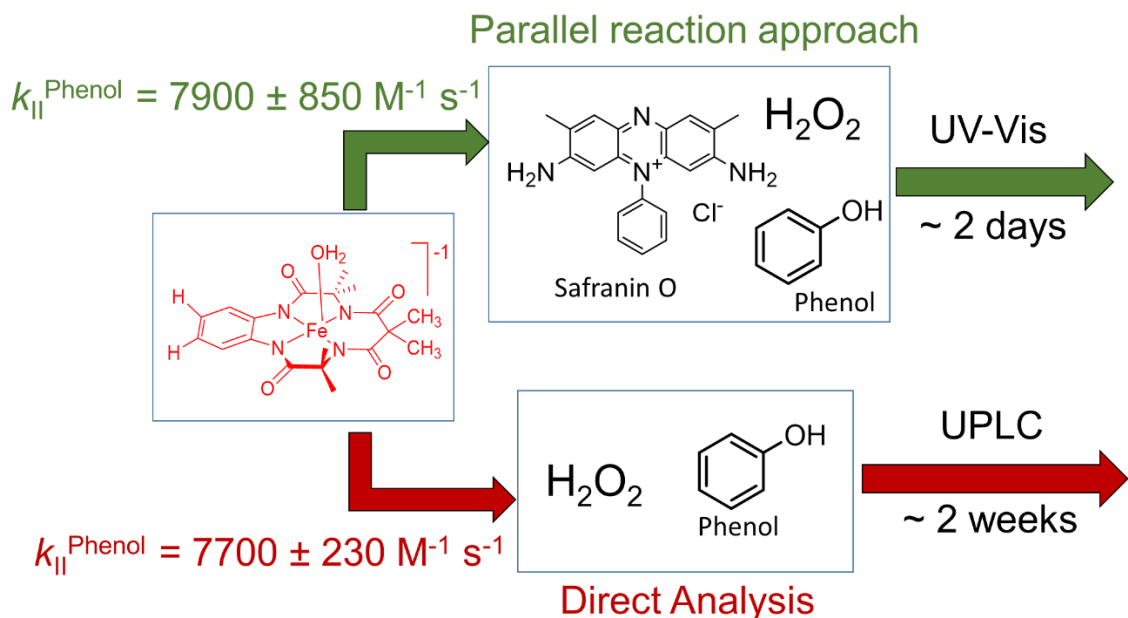
- (15) Bard, A. J.; Faulkner, L. R.; Leddy, J.; Zoski, C. G. *Electrochemical Methods: Fundamentals and Applications*; Wiley New York, 1980; Vol. 2.
- (16) Warner, G. R.; Somasundar, Y.; Jansen, K. C.; Kaaret, E. Z.; Weng, C.; Burton, A. E.; Mills, M. R.; Shen, L. Q.; Ryabov, A. D.; Pros, G.; et al. Bioinspired, Multidisciplinary, Iterative Catalyst Design Creates the Highest Performance Peroxidase Mimics and the Field of Sustainable Ultradilute Oxidation Catalysis (SUDOC). *ACS Catal.* **2019**, 7023–7037.
- (17) Ghosh, A.; Ryabov, A. D.; Mayer, S. M.; Horner, D. C.; Prasuhn Jr, D. E.; Sen Gupta, S.; Vuocolo, L.; Culver, C.; Hendrich, M. P.; Rickard, C. E. F.; et al. Understanding the Mechanism of H<sup>+</sup>-Induced Demetalation as a Design Strategy for Robust Iron(III) Peroxide-Activating Catalysts. *J. Am. Chem. Soc.* **2003**, 125 (41), 12378–12379.
- (18) Mills, M. R.; Shen, L. Q.; Zhang, D. Z.; Ryabov, A. D.; Collins, T. J. Iron(III) Ejection from a “Beheaded” TAML Activator: Catalytically Relevant Mechanistic Insight into the Deceleration of Electrophilic Processes by Electron Donors. *Inorg. Chem.* **2017**, 56 (17), 10226–10234.
- (19) Somasundar, Y.; Shen, L. Q.; Hoane, A. G.; Tang, L. L.; Mills, M. R.; Burton, A. E.; Ryabov, A. D.; Collins, T. J. Structural, Mechanistic, and Ultradilute Catalysis Portrayal of Substrate Inhibition in the TAML–Hydrogen Peroxide Catalytic Oxidation of the Persistent Drug and Micropollutant, Propranolol. *J. Am. Chem. Soc.* **2018**, 140 (38), 12280–12289.
- (20) Tang, L. L.; Gunderson, W. A.; Weitz, A. C.; Hendrich, M. P.; Ryabov, A. D.; Collins, T. J. Activation of Dioxygen by a TAML Activator in Reverse Micelles: Characterization of an Fe(III)Fe(IV) Dimer and Associated Catalytic Chemistry. *J Am Chem Soc* **2015**, 137 (30), 9704–9715.
- (21) Warner, G. R.; Somasundar, Y.; Weng, C.; Akin, M. H.; Ryabov, A. D.; Collins, T. J. *Zero-Order Catalysis in the TAML-Catalyzed Oxidations of Imidacloprid and 3-Methyl-4-Nitrophenol by H<sub>2</sub>O<sub>2</sub> or Should a Catalyst Always Increase a Reaction Rate?*
- (22) Chahbane, N.; Popescu, D. L.; Mitchell, D. A.; Chanda, A.; Lenoir, D.; Ryabov, A. D.; Schramm, K. W.; Collins, T. J. Fe(III)-TAML-Catalyzed Green Oxidative Degradation of the Azo Dye Orange II by H<sub>2</sub>O<sub>2</sub> and Organic Peroxides: Products, Toxicity, Kinetics, and Mechanisms. *Green Chem.* **2007**, 9 (1), 49–57.
- (23) Dunford, H. B. *Heme Peroxidases*; Wiley-VCH: NY, Chichester, Weinheim, 1999.
- (24) Ghosh, A. *Design, Synthesis and Mechanistic Studies of Iron-TAML Catalytic Activators of Hydrogen Peroxide and a New Activation Chemistry of Dioxygen by Iron*; Carnegie Mellon University, 2004.
- (25) Popescu, D. L.; Chanda, A.; Stadler, M. J.; Mondal, S.; Tehranchi, J.; Ryabov, A. D.; Collins, T. J. Mechanistically Inspired Design of Fe(III)-TAML Peroxide-Activating Catalysts. *J Am Chem Soc* **2008**, 130 (37), 12260–12261.
- (26) Institute for Green Science <https://www.cmu.edu/igs/>.
- (27) Becke, A. D. A New Mixing of Hartree–Fock and Local Density-functional Theories. *J. Chem. Phys.* **1993**, 98 (2), 1372–1377.

- (28) Becke, A. D. Density-Functional Exchange-Energy Approximation with Correct Asymptotic Behavior. *Phys. Rev. A* **1988**, 38 (6), 3098.
- (29) Lee, C.; Yang, W.; Parr, R. G. Development of the Colle-Salvetti Correlation-Energy Formula into a Functional of the Electron Density. *Phys. Rev. B* **1988**, 37 (2), 785.
- (30) Frisch, M. J.; Trucks, G. W.; Schlegel, H. B.; Scuseria, G. E.; Robb, M. A.; Cheeseman, J. R.; Scalmani, G.; Barone, V.; Petersson, G. A.; Nakatsuji, H.; et al. Gaussian 09, Revision D.01. *Gaussian, Inc., Wallingford CT*. 2009.
- (31) Marenich, A. V.; Cramer, C. J.; Truhlar, D. G. Universal Solvation Model Based on Solute Electron Density and on a Continuum Model of the Solvent Defined by the Bulk Dielectric Constant and Atomic Surface Tensions. *J. Phys. Chem. B* **2009**, 113 (18), 6378–6396.



## Chapter 7

### Determination by UV-vis spectroscopy of rate constants for colorless substrates for their TAML catalyzed oxidations by $\text{H}_2\text{O}_2$



## 7.1 INTRODUCTION

Water across globe is contaminated profusely.<sup>1,2,11–13,3–10</sup> Unfortunately in a way, contaminated water may not look dirty leaving no reason for people to comprehend the dangers within. Several colorless chemicals determined in surface and ground waters have been shown to be micropollutants that cause undesired effects at low concentrations, typically at low ppt–low ppb (ng/L–μg/L).<sup>2,6,7,14</sup> To make the situation worse, several of the micropollutants behave as endocrine disruptors – chemicals that interfere with the biosynthesis, metabolism or action of hormones resulting in a deviation from normal homeostatic control or development.<sup>11,15–22</sup> Recent research published worldwide has called for the imminent decontamination of water bodies and there are ongoing efforts towards that goal.<sup>9,10,19,23</sup> Liquid chromatography tandem mass spectrometry (LC-MS/MS) is the most commonly used analytical technique for quantification of micropollutants in water and for following the kinetics of their removal or degradation.<sup>19,24–26</sup> While LC-MS/MS offers great sensitivity (ppt), repeatability and capability to detect multiple chemicals at the same time, it is accompanied by certain drawbacks. The analyses require sample preparation in most cases, run times are typically long and each compound requires a new instrumental method to be developed.<sup>27</sup> Although an instrumental method can be developed to monitor multiple compounds, it requires constant updating with the addition of each new compound to the existing instrumental method and care has to be taken to ensure non-overlap of the compounds in the chromatogram. This is a time consuming process that often requires expert training of the operators for successful methods development.<sup>28</sup> Advanced techniques like high throughput screening LC-MS/MS provide excellent sensitivity,<sup>29</sup> but are extremely expensive and require libraries of compounds for quick determinations.<sup>30,31</sup>

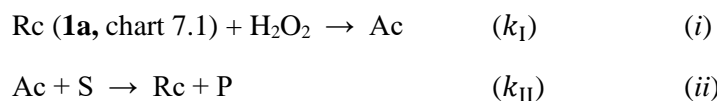
Chemical kinetics<sup>32–34</sup> is an integral part of scientific studies across disciplines. Rate laws provide evidence for mechanisms of reactions.<sup>33–37</sup> From an environmental perspective, kinetics evaluates the efficiency of a decontamination process— how quickly can a pollutant be degraded or

removed? The kinetics of a reaction also provide valuable information regarding the mechanism of decontamination and can guide development of pathways for faster decontaminations. While diagnosis alone of pollutants by LC-MS/MS is a time-consuming process, the time, cost and labor compounds when the kinetics of the degradation of pollutants is analyzed by LC-MS/MS. Given the exponential increase in the number of anthropogenic compounds<sup>38</sup> and the increase in the number of compounds being detected in surface waters,<sup>2</sup> water analytical scientists could be assisted in their work by the development of a simple and inexpensive analytical tool for quick evaluation of compounds for their reactivity towards decontamination processes. In contrast with LC-MS/MS, UV-vis spectroscopy (i) requires high concentrations of compounds ( $\mu\text{M}$ - $\text{mM}$ ) for detection and (ii) cannot differentiate between compounds with similar chromophores.<sup>39</sup> Additionally, the technique decreases in utility when analyzing compounds without significant absorption in the visible region. In a decontamination or disinfection process, such as chlorination, ozonation or peroxide based treatments, key reagents and many oxidation products do or may absorb in the UV region<sup>40,41</sup> making this technique inappropriate for colorless chemicals. Having noted this, UV-vis is a remarkably inexpensive, easy to use, and portable technique that can be deployed to perform fast analyses.<sup>39</sup> Provided that a colored substrate of interest is in the reaction media, UV-vis can perform analyses in seconds to aid in rapidly assembling kinetic profiles for decontamination processes, typically over the span of few hours.

TAML (Tetraamido macrocyclic ligand) activators are full functional (mimic the enzymatic mechanism), small molecule mimics of peroxidase and short circuited cytochrome P450 enzymes.<sup>42-47</sup> Over the past two decades, they have been shown to be effective in oxidizing a broad range of micropollutants including pharmaceuticals,<sup>14,48</sup> pesticides,<sup>49,50</sup> plasticizers,<sup>18</sup> synthetic estrogens,<sup>19</sup> dyes,<sup>51-53</sup> explosives,<sup>54</sup> hormones,<sup>55</sup> etc. to identify but a few classes. The degradations of the majority of these micropollutants were kinetically characterized via High Performance Liquid Chromatography (HPLC), Ultra Performance Liquid Chromatography

(UPLC) or LC-MS<sup>19,48,56</sup> over UV-vis approaches because (i) the pollutant and system lacked a significant absorbance in the visible region of the spectrum, (ii) HPLC or LC-MS could differentiate oxidation products from starting compounds. This extended the time needed to complete a single pollutant study to typically over several months.

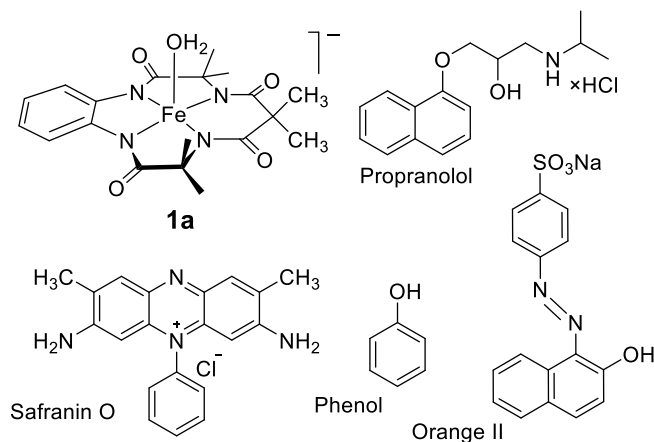
Scheme 7.1 Mechanism of a typical TAML-catalyzed hydrogen peroxide oxidation of a substrate (S). Rc= Resting catalyst; Ac = Active catalyst; P = Products.



For any TAML catalyzed reaction, the second order rate constant,  $k_{\text{II}}$  determines the efficiency of the TAML activator in catalyzing peroxide oxidation of a substrate.<sup>57,58</sup> This is a useful parameter for (i) comparing the potential effectiveness of various TAMLs in catalyzing oxidation of a particular substrate and (ii) comparing different substrates in their reactivities towards a particular TAML catalyzed oxidation. For simple determination of the second order rate constant,  $k_{\text{II}}$  for a given substrate, a universally applicable UV-vis technique would allow for the analysis of a large number of substrates without the need for developing a UPLC methods for each one.

Parallel or competing reactions are reactions wherein a starting compound or an active intermediate can react in more than one way to provide parallel outcomes. These parallel pathways compete for the same starting compound or active intermediate. For example, if an active oxidant reacts with substrates A and B in parallel pathways, the rate of oxidation of substrate A is impacted by the parallel rate of oxidation of substrate B.<sup>32</sup> If substrate A is colored, it is easy to follow the impact on its oxidation by substrate B via UV-visible spectroscopy. The extent of this impact can be indirectly correlated to the oxidation rate of substrate B.

Chart 7.1 Structure of TAML (**1a**) and other compounds used or discussed in this study.



Here we show (i) that bleaching rates for Orange II and Safranin O dyes are reduced in presence of the invisible substrates propranolol and phenol; (ii) that the rate constant,  $k_{II}^{IS}$  for oxidation of the colorless or invisible substrates (IS) such as propranolol and phenol can be determined via this indirect method using UV-vis spectroscopy and compared to the rate constant  $k_{II}$  obtained via direct measurements by UPLC; (iii) that substrate inhibition of **1a**, as a function of lowered second order rate constant  $k_I$ , for the activation of **1a**, plays a significant role in determining the rate constants  $k_{II}^{IS}$ ; and (iv) that the oxidation products formed can interfere with these indirect measurements and thereby preventing the applicability of this technique for colorless MPs that can form oxidations products which interfere with the absorbance measurements.

## 7.2 RESULTS AND DISCUSSION

### 7.2.1 Direct determination of second order rate constant, $k_{II}$

A typical TAML catalyzed reaction mechanism for oxidation of a single substrate is shown in Scheme 7.1. The rate of the oxidation of substrate is given by Equation 7.1.

$$-\frac{d[S]}{dt} = k_{II}[Ac][S] \quad (7.1)$$

Applying the Steady State Approximation to Active catalyst (Ac) provides

$$\frac{d[Ac]}{dt} = 0 = k_I[Rc][H_2O_2] - k_{II}[Ac][S] \quad (7.2)$$

Mass balance with respect to Resting catalyst (Rc) with [Fe] being the total catalyst concentration provides

$$[Rc] = [Fe] - [Ac] \quad (7.3)$$

Inputting Equations 7.2 and 7.3 into Equation 7.1, yields Equation 7.4.

$$-\frac{d[S]}{dt} = \frac{k_I k_{II} [Fe] [H_2O_2] [S]}{k_I [H_2O_2] + k_{II} [S]} \quad (7.4)$$

**1a**-catalyzed hydrogen peroxide oxidation of phenol was followed kinetically by monitoring a decrease in [phenol] over time by UPLC. Consistent with Equation 7.1, initial rates of phenol oxidation showed a rising hyperbolic dependence on [phenol] (Figure 7.1). The second order rate constants  $k_I$  and  $k_{II}$  for activation of **1a** and oxidation of phenol, respectively, were calculated from a linearized double inverse plot  $dt/d[S]$  versus  $[\text{phenol}]^{-1}$  (inset to Figure 7.1) as described elsewhere<sup>14</sup> and were determined to be  $50 \pm 10$  and  $7700 \pm 230 \text{ M}^{-1} \text{ s}^{-1}$ , respectively. The rate

constants  $k_I$  and  $k_{II}$  have been obtained in a similar manner previously for Orange II (UV-vis),<sup>58</sup> Safranin O (UV-vis)<sup>59</sup> and propranolol (UPLC)<sup>14</sup> and are summarized in Table 7.1.

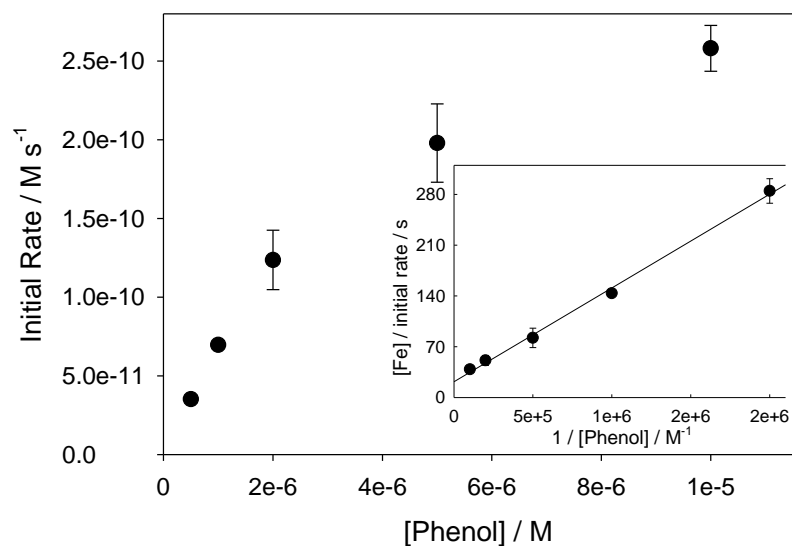


Figure 7.1 Initial rate of phenol degradation by H<sub>2</sub>O<sub>2</sub> catalyzed by **1a** as a function of [phenol]. Reaction Conditions: [phenol] = (0.05–1) × 10<sup>-5</sup> M, [**1a**] = 1 × 10<sup>-8</sup> M, [H<sub>2</sub>O<sub>2</sub>] 1 × 10<sup>-3</sup> M, pH 7 (0.01 M phosphate), 25 °C.

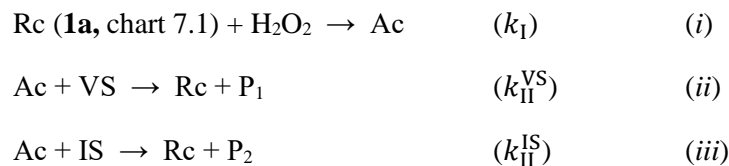
Table 7.1 Rate constants by direct analyses for 1a-catalyzed oxidation of various substrates in 0.01 M phosphate pH 7 buffer at 25 °C.

Substrate	$k_I$ (M <sup>-1</sup> s <sup>-1</sup> )	$k_{II}$ (M <sup>-1</sup> s <sup>-1</sup> )	Reference
Orange II	31.4 ± 0.1	4950 ± 20	58
Safranin O	4.0 ± 0.4	800 ± 390	59
propranolol	2 ± 0.1	70 ± 20	14
phenol	50 ± 10	7700 ± 230	This work

### 7.2.2 Indirect determination of second order rate constant, $k_{II}^{IS}$

#### 7.2.2.1 Kinetics of a TAML catalyzed parallel oxidation of two substrates.

Scheme 7.2 Reaction mechanism of TAML-catalyzed oxidation of visible substrate (VS) and invisible substrate (IS) wherein VS and IS are competing for Active catalyst (Ac). Rc = Resting catalyst; Ac = Active catalyst; P<sub>1</sub> or P<sub>2</sub> are Products.



The TAML catalysis mechanism for a simple 2 substrate parallel oxidation can be described by steps (i)–(iii) in Scheme 7.2. Henceforth in the discussion, we will refer to Orange II and Safranin O as the visible substrate (VS) and the second order rate constant for their bleaching as  $k_{II}^{\text{VS}}$ . The colorless (no absorption in the visible region) substrate (propranolol and phenol) will be referred to as the invisible substrate (IS) and the second order rate constant for their bleaching as  $k_{II}^{\text{IS}}$ .

Again, utilizing the initial rate approach the rate of oxidation of the visible substrate can be expressed by Equation 7.5

$$-\frac{d[\text{VS}]}{dt} = k_{II}^{\text{VS}}[\text{Ac}][\text{VS}] \quad (7.5)$$

Applying steady-state approximation with respect to Ac provides Equation 7.6.

$$\frac{d[\text{Ac}]}{dt} = 0 = k_I[\text{Rc}][\text{H}_2\text{O}_2] - k_{II}^{\text{VS}}[\text{Ac}][\text{VS}] - k_{II}^{\text{IS}}[\text{Ac}][\text{IS}] \quad (7.6)$$

Applying mass balance with respect to Rc (Equation 7.3) gives Equation 7.7, with [Fe] being total catalyst concentration.



$$-\frac{d[\text{VS}]}{dt} = \frac{k_1 k_{\text{II}}^{\text{VS}} [\text{Fe}][\text{H}_2\text{O}_2][\text{VS}]}{k_1 [\text{H}_2\text{O}_2] + k_{\text{II}}^{\text{VS}} [\text{VS}] + k_{\text{II}}^{\text{IS}} [\text{IS}]} \quad (7.7)$$

Taking the inverse of Equation 7.7 and multiplying by  $k_1 k_{\text{II}}^{\text{VS}} [\text{Fe}][\text{H}_2\text{O}_2][\text{VS}]$  gives Equation 7.8.

$$-\frac{dtk_1 k_{\text{II}}^{\text{VS}} [\text{Fe}][\text{H}_2\text{O}_2][\text{VS}]}{d[\text{VS}]} = k_{\text{II}}^{\text{IS}} [\text{IS}] + k_1 [\text{H}_2\text{O}_2] + k_{\text{II}}^{\text{VS}} [\text{VS}] \quad (7.8)$$

By keeping all conditions constant except for [IS], Equation 7.8 should yield a straight line with an intercept when the inverse of the initial rate of VS bleaching is plotted against the [IS].

#### 7.2.2.2 Determination of second order rate constant $k_{\text{II}}^{\text{IS}}$ for oxidation of propranolol:

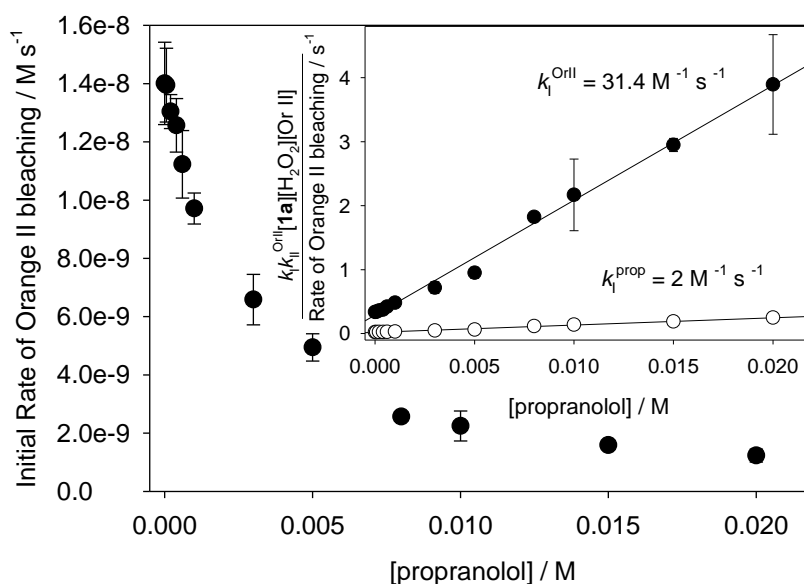


Figure 7.2 Initial rate of Orange II bleaching as a function of [propranolol]. Inset: Plot of  $\frac{dtk_1 k_{\text{II}}^{\text{Or II}} [\text{Fe}][\text{H}_2\text{O}_2][\text{Or II}]}{d[\text{Or II}]}$  versus [propranolol] with  $k_{\text{I}}^{\text{prop}}$  and  $k_{\text{I}}^{\text{Or II}}$ . Reaction Conditions:  $2 \times 10^{-5}$  M Orange II,  $3 \times 10^{-3}$  M  $\text{H}_2\text{O}_2$ ,  $5 \times 10^{-7}$  M **1a**, 0.01 M phosphate buffer, pH 7 25 °C.

The second order rate constant  $k_{II}^{IS}$  was determined for propranolol by following the disappearance of Orange II dye at 484 nm using UV-vis spectroscopy in a **1a**-catalyzed hydrogen peroxide oxidation of a solution of Orange II and propranolol.

Consistent with Equation 7.7, there is a decreasing hyperbolic dependence of initial rate of Orange II bleaching on the [phenol] (Figure 7.2). The second order rate constant  $k_{II}^{IS}$  for oxidation of propranolol was determined from Equation 7.8 as shown in inset to Figure 7.2 and was found to be  $180 \pm 7 \text{ M}^{-1} \text{ s}^{-1}$  when the rate constant  $k_I^{Or II}$  value of  $31.4 \text{ M}^{-1} \text{ s}^{-1}$ , for activation of **1a** in the catalytic oxidation of Orange II, was utilized for developing the linear plot based on Equation 7.8 (inset to Figure 7.2). This is in close alignment with the rate constant  $k_{II}$  value of  $70 \pm 20 \text{ M}^{-1} \text{ s}^{-1}$ , measured directly by UPLC.<sup>14</sup> This provided experimental support for the validity of Equation 7.8.

However, when the  $k_I^{prop}$  value of  $2 \text{ M}^{-1} \text{ s}^{-1}$ , for activation of **1a** in the catalytic oxidation of propranolol, was utilized in developing the linear plot based on Equation 7.8 (inset to Figure 7.2), the rate constant  $k_{II}^{IS}$  for oxidation of propranolol was determined to be  $11.4 \pm 0.4 \text{ M}^{-1} \text{ s}^{-1}$ . This value was approximately a factor of 7 lower than the rate constant  $k_{II}$  value of  $70 \pm 20 \text{ M}^{-1} \text{ s}^{-1}$ , measured directly by UPLC.<sup>14</sup> Thus, while the parallel reaction model was found to be capable of determining the second order rate constant  $k_{II}^{IS}$  for oxidation of an invisible substrate, it was dependent strongly on the **1a** activation rate constant  $k_I$ .

However, to ensure the viability of this technique with more than one VS, experiments were performed with a persistent, recalcitrant dye Safranin O as the VS in presence of propranolol under similar conditions (not shown here). Analogous experiments were also performed to determine  $k_{II}^{IS}$  for the oxidation of phenol with both Orange II and Safranin O as the VS in separate studies. Separate calculations were performed utilizing  $k_I^{VS}$  and  $k_I^{IS}$  to see if a significant

impact of  $k_1$  is observed in all cases. The second order rate constants,  $k_{II}^{\text{prop}}$  and  $k_{II}^{\text{phenol}}$  for oxidation of phenol and propranolol respectively utilizing Orange II and Safranin O as the VS have been summarized in Table 7.2 alongside rate constants,  $k_{II}$  obtained from direct analyses using UPLC.

Table 7.2 Rate constants  $k_{II}$  and  $k_{II}^{\text{IS}}$  for **1a**-catalyzed hydrogen peroxide oxidations of propranolol and phenol by direct and indirect analyses respectively at pH7, 25 °C.

Invisible Substrate	Visible Substrate	$k_{\text{II}}^{\text{IS}}$ ( $\text{M}^{-1} \text{ s}^{-1}$ ) from indirect analysis using UV-vis			$k_{\text{II}}$ ( $\text{M}^{-1} \text{ s}^{-1}$ ) from direct kinetic analysis using UPLC
		Using $k_{\text{I}}^{\text{VS}}$	Using $k_{\text{I}}^{\text{IS}}$	Using $*k_{\text{I,eff}}$ ( $\text{M}^{-1} \text{ s}^{-1}$ )	
		( $\text{M}^{-1} \text{ s}^{-1}$ )	( $\text{M}^{-1} \text{ s}^{-1}$ )		
		$k_{\text{I}}^{\text{Or II}} = 31.4$	$k_{\text{I}}^{\text{prop}} = 2$		
		or	or		
		$k_{\text{I}}^{\text{Saf O}} = 4$	$k_{\text{I}}^{\text{phenol}} = 50$		
propranolol	Orange II	$180 \pm 7$	$11.4 \pm 0.4$	$40 \pm 7$	$70 \pm 20$
	Safranin O	$120 \pm 7$	$60 \pm 3.4$	$40 \pm 13$	
phenol	Orange II	$4100 \pm 520$	$7000 \pm 900$	$4400 \pm 580$	$7700 \pm 230$
	Safranin O	$5000 \pm 540$	$62300 \pm 700$	$7900 \pm 850$	

\*  $k_{I,\text{eff}}$  for Orange II – Phenol =  $31.3 \text{ M}^{-1} \text{s}^{-1}$ ;  $k_{I,\text{eff}}$  for Safranin O – Phenol =  $6.3 \text{ M}^{-1} \text{s}^{-1}$ ; \*  $k_{I,\text{eff}}$  for Orange II – propranolol and Safranin O – propranolol is variable (see text)

Columns 3 and 4 in Table 7.2 showcase the rate constants  $k_{II}^{\text{prop}}$  and  $k_{II}^{\text{phenol}}$  obtained utilizing **1a** activation rate constants  $k_1^{\text{VS}}$  (Or II and Saf O) and  $k_1^{\text{IS}}$  (propranolol and phenol), respectively. Column 6 contains  $k_{II}$  values for propranolol and phenol oxidation obtained from direct analyses using UPLC. Some general observations can be made from the data in Table 7.2 as follows: (i) Utilizing either  $k_1^{\text{VS}}$  (column 3, Table 7.2) or  $k_1^{\text{IS}}$  (column 4, Table 7.2) alone did not give  $k_{II}^{\text{IS}}$  values consistent with directly measured rate constants  $k_{II}$  for propranolol and phenol in all cases. Thus, there was no universal  $k_1$  that could be utilized for all calculations. (ii) There is a greater alignment of  $k_{II}^{\text{IS}}$  values in column 3 and column 4 when the  $k_1^{\text{VS}}$  and  $k_1^{\text{IS}}$  are closer to each other. For example, **1a** activation rate constants  $k_1^{\text{Or II}}$  and  $k_1^{\text{phenol}}$  in catalytic oxidations of Orange II

and phenol are  $31.4$  and  $50 \text{ M}^{-1} \text{ s}^{-1}$  respectively. The subsequent indirect rate constant  $k_{\text{II}}^{\text{phenol}}$  utilizing the above  $k_{\text{I}}^{\text{Or II}}$  and  $k_{\text{I}}^{\text{phenol}}$  values were found to be  $4100 \pm 520$  and  $7000 \pm 900 \text{ M}^{-1} \text{ s}^{-1}$  respectively. These are in good agreement with the second order rate constant,  $k_{\text{II}}$  value of  $7700 \pm 230 \text{ M}^{-1} \text{ s}^{-1}$  for phenol oxidation determined from direct measurements. The same was observed for the Safranin O – propranolol system wherein  $k_{\text{I}}^{\text{Saf O}}$  and  $k_{\text{I}}^{\text{prop}}$  values of  $4$  and  $2 \text{ M}^{-1} \text{ s}^{-1}$  provided the second order rate constant  $k_{\text{II}}^{\text{prop}}$  values of  $120 \pm 7$  and  $60 \pm 3.4 \text{ M}^{-1} \text{ s}^{-1}$ , respectively. As observed with the Orange II–phenol system, the above  $k_{\text{II}}^{\text{prop}}$  values were in close agreement with the second order rate constant  $k_{\text{II}}$  value of  $70 \pm 20 \text{ M}^{-1} \text{ s}^{-1}$  for oxidation of propranolol determined directly using UPLC. (iii) Wherever the differences in  $k_{\text{I}}^{\text{VS}}$  and  $k_{\text{I}}^{\text{IS}}$  values are large, there is a significant difference in the determined  $k_{\text{II}}^{\text{IS}}$  values. For example, in the Safranin O – phenol system wherein  $k_{\text{I}}^{\text{Saf O}}$  and  $k_{\text{I}}^{\text{phenol}}$  were  $4$  and  $50 \text{ M}^{-1} \text{ s}^{-1}$ , respectively, subsequently determined indirect rate constant  $k_{\text{II}}^{\text{phenol}}$  values utilizing the above  $k_{\text{I}}^{\text{Saf O}}$  and  $k_{\text{I}}^{\text{phenol}}$  values were found to be  $5000 \pm 540$  and  $62300 \pm 700 \text{ M}^{-1} \text{ s}^{-1}$ , respectively. There was an order of magnitude difference between the two  $k_{\text{II}}^{\text{phenol}}$  values. A similar trend was also observed for the Orange II – propranolol system.

This clearly shows that the second order rate constant  $k_{\text{I}}$ , for activation of **1a**, is crucial to determining the  $k_{\text{II}}^{\text{IS}}$  for oxidation of any invisible substrate. Thus, for the viability of this indirect method for application across colorless substrates with varying functionalities, it was important to take into consideration the impact of a substrate on the activation of **1a**, which in turn impacts the indirect determination of the second order rate constant  $k_{\text{II}}^{\text{IS}}$  for the oxidation of any invisible substrate.

### 7.2.3 Significance of substrate inhibition of **1a**.

As shown in Scheme 7.2,  $k_I$  explains the dynamics of formation of Ac which oxidizes VS and IS. It has been shown in recent studies that  $k_I$  is not independent of substrate and **1a** is inhibited via hydrogen bonding and other non-covalent interactions at higher [substrate].<sup>14</sup> Substrate inhibition manifests itself as a decrease in the uninhibited  $k_I$  for **1a**. The  $k_I$  values obtained from direct analyses were  $31.4 \pm 0.1$  (Orange II),  $4.0 \pm 0.4$  (Safranin O),  $2 \pm 0.1$  (propranolol) and  $50 \pm 10 \text{ M}^{-1} \text{ s}^{-1}$  (phenol) (Table 7.1). It can be clearly seen that propranolol and Safranin O inhibit **1a** more than Orange II and phenol. For easier interpretations, henceforth we will consider propranolol and Safranin O as inhibiting substrates while phenol and Orange II as non-inhibiting substrates.

As discussed in Chapter 2, when a substrate inhibits resting TAML catalyst (Rc) and the resulting substrate – TAML adduct is inert to activation, the rate constant  $k_I$  in Equation 7.4 becomes an effective value  $k_{I,\text{eff}} = k_I / (1 + K[S])$ , where  $K$  is the binding constant between Rc and the substrate. Thus, the rate law for substrate oxidation is better presented as Equation 7.9.

$$-\frac{d[S]}{dt} = \frac{k_{I,\text{eff}}k_{II}[\text{H}_2\text{O}_2][S]}{k_{I,\text{eff}}[\text{H}_2\text{O}_2] + k_{II}[S]}[\text{Fe}] \quad (7.9)$$

The resultant inhibited  $k_I$  viz.,  $k_{I,\text{eff}}$  decreases as a function of [inhibiting substrate]. This can be observed for any of our above systems where an inhibiting substrate is involved.

For example, in the Orange II – propranolol system, a projected impact on uninhibited  $k_I^{\text{Or II}}$  over [low to high propranolol] is depicted in Figure 7.3. The impact is huge,  $k_{I,\text{eff}}$  at  $\mu\text{M}$  [propranolol] is projected to be  $\text{ca. } 10 \text{ M}^{-1} \text{ s}^{-1}$  (inset to Figure 7.3), which represents a  $\text{ca. } 66 \%$  decrease from an uninhibited  $k_I^{\text{Or II}}$  value of  $31.4 \text{ M}^{-1} \text{ s}^{-1}$ . Thus, at any [propranolol],  $k_I$  for activation of **1a** in the Orange II – propranolol system, will neither be  $k_I^{\text{Or II}}$  nor  $k_I^{\text{prop}}$  exclusively. Thus,  $k_{I,\text{eff}}$  is a more realistic rate constant to be utilized for calculations for determining  $k_{II}^{\text{IS}}$  for oxidation of

propranolol and phenol via this indirect method. Similar projected  $k_{I,eff}$  plots were also developed for Safranin O – phenol, Orange II – phenol, and Safranin O – propranolol systems and the inhibiting effect was observed in all cases (Figure 7.7-7.9). With respect to phenol, because it is non-inhibiting ( $k_I^{phenol} = 50 \text{ M}^{-1} \text{ s}^{-1}$ ), compared to Safranin O and Orange II ( $k_I^{Saf O} = 4 \text{ M}^{-1} \text{ s}^{-1}$

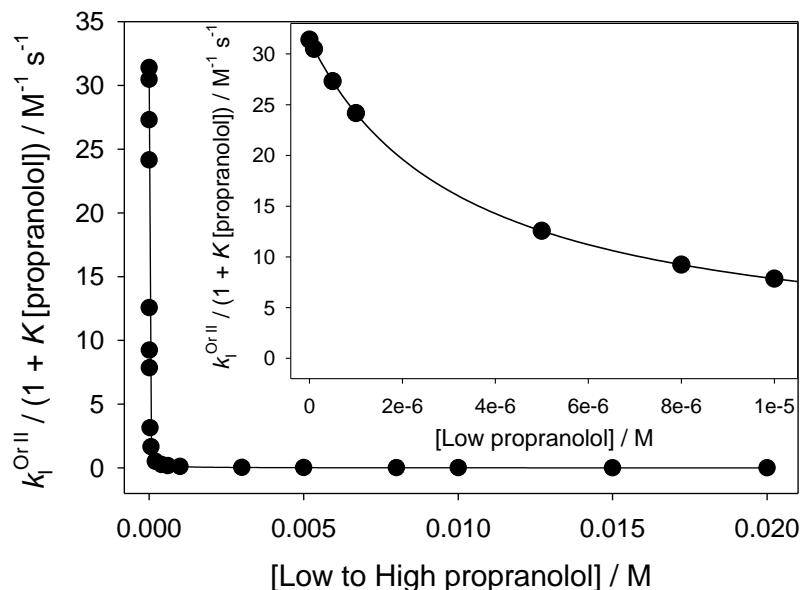


Figure 7.3 Plot depicting the projected impact of propranolol substrate inhibition on the less inhibited  $k_I^{Or II}$  from [propranolol] = 0 to low mM. Note,  $k_{I,eff} = k_I^{Or II} / (1 + K[\text{propranolol}]) \approx 0$  when [propranolol]  $\geq 3 \times 10^{-3} \text{ M}$ . Inset shows the same projection until [propranolol] =  $1 \times 10^{-5} \text{ M}$

and  $k_I^{Or II} = 31.4 \text{ M}^{-1} \text{ s}^{-1}$ ),  $k_{I,eff}$  plots are drawn showing the impact of Orange II and Safranin O on  $k_I^{phenol}$ . In our experiments although, only [phenol] is varied and not the other way. These plots are only to show the significance of substrate inhibition on uninhibited  $k_I^{phenol}$ . The work described henceforth discusses various scenarios involving inhibiting and non-inhibiting VS and IS.

### 7.2.3.1 Case 1: When both VS (Orange II) and IS (phenol) are non-inhibiting in nature

(similar rate constants,  $k_1^{\text{Or II}}$  and  $k_1^{\text{phenol}}$  values of 31.4 and 50  $\text{M}^{-1} \text{s}^{-1}$  respectively)

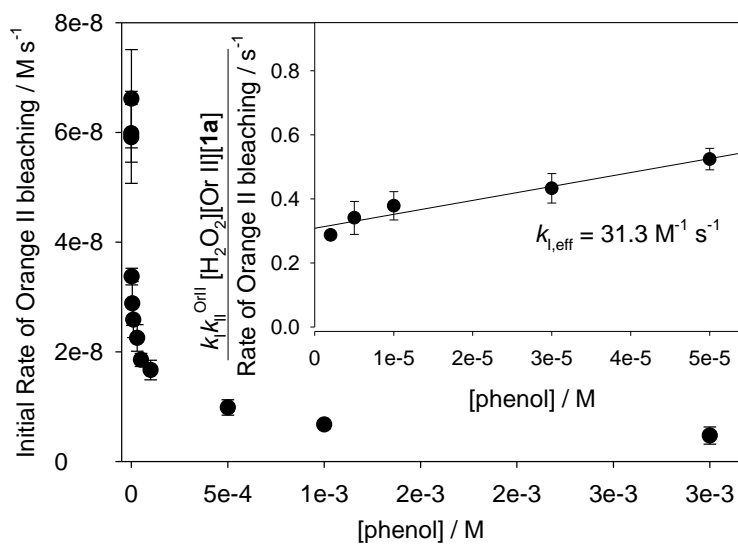


Figure 7.4 : Initial rate of Orange II bleaching as a function of [phenol]. Inset: Plot of  $\frac{dk_{l,\text{eff}} k_1^{\text{Or II}} [\text{Fe}][\text{H}_2\text{O}_2][\text{Or II}]}{d[\text{Or II}]}$  versus [phenol] with  $k_{l,\text{eff}} = 31.3 \text{ M}^{-1} \text{s}^{-1}$ . Reaction Conditions:  $5 \times 10^{-5} \text{ M}$  Orange II,  $2.5 \times 10^{-3} \text{ M}$   $\text{H}_2\text{O}_2$ ,  $5 \times 10^{-7} \text{ M}$  **1a**, 0.01 M phosphate buffer, pH 7, 25 °C.

Although both Orange II and phenol have very similar  $k_1$  values of 31.4 and 50  $\text{M}^{-1} \text{s}^{-1}$  respectively, Orange II could be considered slightly inhibiting as compared to phenol from these values. The second order rate constant,  $k_{l,\text{eff}}$  at  $5 \times 10^{-5} \text{ M}$  Orange II was determined to be 31.3  $\text{M}^{-1} \text{s}^{-1}$  which is identical to  $k_1^{\text{Or II}}$  (31.4  $\text{M}^{-1} \text{s}^{-1}$ ). It is important to observe here that since phenol is non-inhibiting, as the [phenol] goes from lower to higher, there is no additional substrate inhibition experienced by **1a**. The second order rate constant  $k_{\text{II}}^{\text{phenol}}$  was determined by following the disappearance of Orange II dye at 484 nm UV-vis spectroscopy in a **1a**-catalyzed hydrogen peroxide oxidation of Orange II and phenol. The second order rate constant  $k_{\text{II}}^{\text{phenol}}$  for

oxidation of phenol was determined from the positive slope (inset to Figure 7.4 ) and was found to be  $4400 \pm 580 \text{ M}^{-1} \text{ s}^{-1}$ , which is in close agreement with the  $k_{\text{II}}$  value of  $7700 \pm 230 \text{ M}^{-1} \text{ s}^{-1}$  determined from direct analysis using UPLC.<sup>14</sup> Only the slope of the initial linear region was considered for calculations since the entire plot of

$\frac{dt k_{\text{I,eff}} k_{\text{II}}^{\text{Or II}} [\text{Fe}] [\text{H}_2\text{O}_2] [\text{Or II}]}{d[\text{Or II}]}$  versus [phenol] yields a hyperbola (Figure 7.10 ). In comparison, rate

constants  $k_{\text{I}}^{\text{phenol}}$  and  $k_{\text{I}}^{\text{Or II}}$  provided  $k_{\text{II}}^{\text{phenol}}$  values of  $7000 \pm 900 \text{ M}^{-1} \text{ s}^{-1}$  and  $4100 \pm 520 \text{ M}^{-1} \text{ s}^{-1}$  respectively. These are in good agreement with  $k_{\text{II}}$  values from UPLC as well. Therefore, substrate inhibition did not impact the indirect measurements of  $k_{\text{II}}^{\text{IS}}$  when VS and IS are non-inhibiting in nature.

#### **7.2.3.2 Case 2: When both VS (Safranin O) and IS (propranolol) are equally inhibiting in nature**

(similar values of 4 and  $2 \text{ M}^{-1} \text{ s}^{-1}$  for second rate constants,  $k_{\text{I}}^{\text{Saf O}}$  and  $k_{\text{I}}^{\text{Prop}}$ , respectively).

Propranolol and Safranin O were both determined to inhibit **1a** to a similar extent based on their  $k_{\text{I}}$  values of  $2 \text{ M}^{-1} \text{ s}^{-1}$  and  $4 \text{ M}^{-1} \text{ s}^{-1}$ , respectively. As with Orange II – phenol, a hyperbolic decrease in the initial rate of Safranin O bleaching is observed. However, since propranolol ( $k_{\text{I}}^{\text{Prop}} = 2 \text{ M}^{-1} \text{ s}^{-1}$ ) is relatively more inhibiting as compared to Safranin O ( $k_{\text{I}}^{\text{Saf O}} = 4 \text{ M}^{-1} \text{ s}^{-1}$ ), there is an effective slight additional inhibition with the increase in [propranolol]. Thus, the  $k_{\text{I,eff}}$  is reduced at each [propranolol] unlike phenol which was found to be non-inhibiting. This leads to a negative slope in the linearization plot in the inset to Figure 7.5. The entire plot of



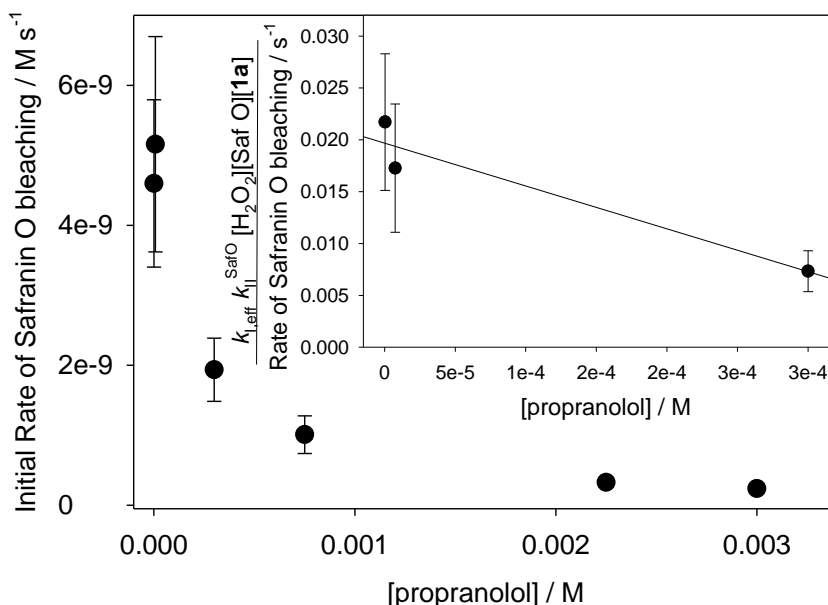


Figure 7.5 : Initial rate of safranin O bleaching as a function of propranolol concentration. Inset: Plot of  $\frac{dk_{I,eff} k_{II}^{Saf O} [Fe][H_2O_2][Saf O]}{d[Saf O]}$  versus [propranolol] with varying  $k_{I,eff}$ . Reaction Conditions:  $3 \times 10^{-5}$  M Safranin O,  $3 \times 10^{-3}$  M  $H_2O_2$ ,  $3.3 \times 10^{-7}$  M **1a**, 0.01 M phosphate buffer, pH 7, 25 °C.

$\frac{dk_{I,eff} k_{II}^{Saf O} [Fe][H_2O_2][Saf O]}{d[Or II]}$  versus [propranolol] was a decreasing hyperbola (Figure 7.11). and

as before only the value from the negative slope of the initial linear portion of the plot is

considered for calculations (inset to Figure 7.5). This provided us with a rate constant  $k_{II}^{prop}$  value of  $40 \pm 13 \text{ M}^{-1} \text{ s}^{-1}$ . This is in agreement with the value of  $70 \pm 20 \text{ M}^{-1} \text{ s}^{-1}$  determined directly via

UPLC. Similar rate constants  $k_{II}^{prop}$  values of  $120 \pm 7 \text{ M}^{-1} \text{ s}^{-1}$  and  $60 \pm 3 \text{ M}^{-1} \text{ s}^{-1}$  were obtained

from  $k_I^{Saf O}$  and  $k_I^{Prop}$  respectively, that were in agreement with the second order rate constant,  $k_{II}$

determined by UPLC. This again shows that there is not a significant impact of substrate

inhibition on calculations when two substrates are equally inhibiting in nature.

**7.2.3.3 Case 3: When VS (Orange II) is non-inhibiting and IS (propranolol) is inhibiting in nature**

(large variance in values of 31.4 and 2 M<sup>-1</sup> s<sup>-1</sup> for rate constants,  $k_1^{\text{Or II}}$  and  $k_1^{\text{Prop}}$  respectively).

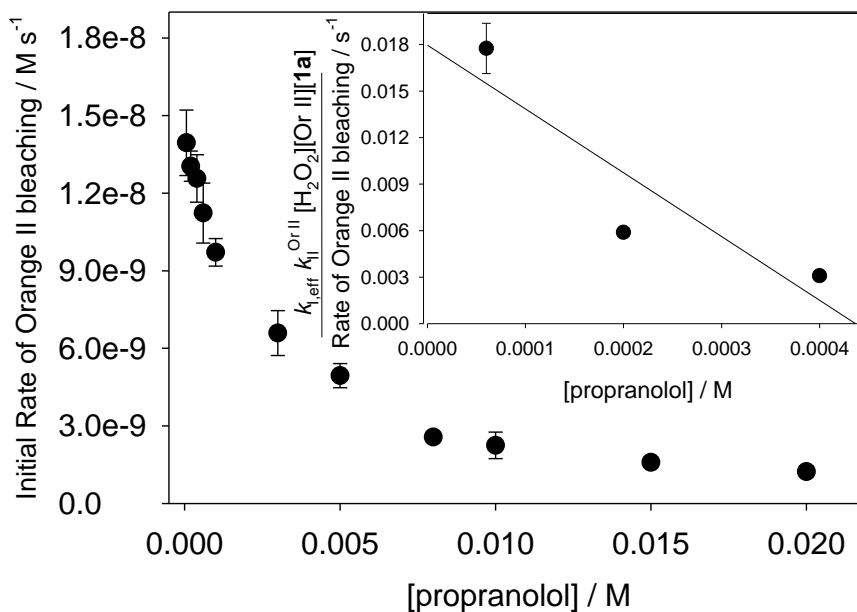


Figure 7.6 : Initial rate of Orange II bleaching as a function of propranolol concentration. Inset: Plot of  $\frac{dk_1^{\text{Or II}}}{d[\text{Or II}]}$  versus [propranolol] with varying  $k_1^{\text{eff}}$ . Reaction Conditions:  $2 \times 10^{-5}$  M Orange II,  $3 \times 10^{-3}$  M H<sub>2</sub>O<sub>2</sub>,  $5 \times 10^{-7}$  M **1a**, 0.01 M phosphate buffer, pH 7, 25 °C.

This large variance in **1a** activation rate constant,  $k_1$  will be the most common scenario specially when the broad range of MPs and their varying functionalities are considered. Thus, it is very important to study scenarios such as this, so that the practical implication of this indirect method can encompass most MPs.

The impact of propranolol on the uninhibited  $k_1^{\text{Or II}}$  is shown in Figure 7.3. As in Case 2,  $k_1^{\text{eff}}$  values decreased with increasing [propranolol]—a negative slope was observed in the linearization plot (inset to Figure 7.6) upon increasing the [propranolol]. As with Case 2, only the

positive value from the negative slope of the linear portion has been considered for calculations.

The second order rate constant  $k_{II}^{prop}$  for oxidation of propranolol was determined to be  $40 \pm 7 \text{ M}^{-1} \text{ s}^{-1}$  via this indirect method utilizing rate constants  $k_{I,eff}$  values for activation of **1a**; this was in close agreement (< factor of 2) with the rate constant  $k_{II}$  value of  $70 \pm 20 \text{ M}^{-1} \text{ s}^{-1}$  obtained with UPLC. In comparison, when rate constants,  $k_I^{Or II}$  and  $k_I^{Prop}$  were used as **1a** activation rate constants, second order rate constant  $k_{II}^{prop}$  values of  $180 \pm 7 \text{ M}^{-1} \text{ s}^{-1}$  and  $11 \pm 0.4 \text{ M}^{-1} \text{ s}^{-1}$  were obtained respectively. While the former value is somewhat in agreement (~ factor of 2.5), the latter is not in agreement (~ factor of 7) with the second order rate constant,  $k_{II}$  obtained from direct measurements. Additionally, the second order rate constant  $k_{II}^{prop}$  when obtained from exclusive rate constants  $k_I^{Or II}$  versus  $k_I^{Prop}$  values, differ by more than an order of magnitude between each other. Thus, utilizing  $k_{I,eff}$  we are able to negate this large difference in the second order rate constant  $k_{II}^{prop}$  values and bring it into greater agreement with directly measured rate constants,  $k_{II}$ .

A similar situation was observed for Safranin O as the VS and phenol as the IS (Figure 7.12). The resulting rate constant  $k_{II}^{phenol}$  values obtained from rate constants  $k_I^{Saf O}$ ,  $k_I^{phenol}$ , and  $k_{I,eff}$  were  $5000 \pm 540 \text{ M}^{-1} \text{ s}^{-1}$ ,  $62300 \pm 700 \text{ M}^{-1} \text{ s}^{-1}$  and  $7900 \pm 850 \text{ M}^{-1} \text{ s}^{-1}$ , respectively. As with the Orange II – propranolol system, the second order rate constant  $k_{II}^{phenol}$  obtained from the rate constant  $k_{I,eff}$  gave the closest alignment to the UPLC  $k_{II}$  value of  $7700 \pm 230 \text{ M}^{-1} \text{ s}^{-1}$ . As with the Orange II – propranolol system, the Safranin O – phenol system also exhibited an order of magnitude difference in the rate constant  $k_{II}^{phenol}$  values when obtained using exclusive  $k_I^{Saf O}$  versus  $k_I^{phenol}$ .

The second order rate constants for oxidation of phenol and propranolol obtained via direct analysis (UPLC),  $k_{II}$  and from indirect analysis using UV-vis,  $k_{II}^{IS}$  utilizing **1a** activation rate

constants  $k_1^{VS}$ ,  $k_1^{IS}$  and  $k_{I,eff}$  have been summarized in Table 7.2. In totality, it can be clearly seen that the closest alignment with UPLC values in all cases were with the rate constants  $k_{I,eff}$  as opposed to using either  $k_1^{VS}$  or  $k_1^{IS}$  rate constants.

#### ***7.2.4 Interference from the oxidation products.***

Propranolol was an excellent IS for this indirect approach (Figure 7.13 A) because of the high solubility even at mM concentrations and lack of immediate formation of oxidation products that absorbed in the visible region. While phenol worked perfectly well across a broad concentration range, it was noticed that upon longer reaction time of a few hours, co-precipitates were observed which were pinkish-brown in color (Figure 7.13 B). Upon peroxide oxidation of only phenol catalyzed by **1a**, a yellowish brown solution was observed, which is a characteristic of quinones, the typical oxidation products of phenols (Figure 7.13 C). Phenol oxidizes to quinones, which co-precipitated with Safranin O at  $10^{-6}$  M of [phenol] and higher. To overcome this, kinetic analyses were always performed using the initial rate approach wherein absorbance of the solution was measured when the reaction had proceeded to < 10 % completion typically in the first few minutes.

In several cases, oxidation products of VS or IS can absorb in the same wavelength region as the targeted absorbance of VS required for  $k_{II}^{IS}$  determination. For example, Safranin O and Orange II have targeted absorbance wavelengths of 484 nm and 520 nm, respectively. Therefore, formation of oxidation products which absorb at similar wavelengths is not favorable for this indirect approach when Orange II and Safranin O are the VS. TAML catalyzed oxidation of 1-Naphthol produces 1,4-dihydroxy naphthalene which has an absorbance at ~ 520 nm (Chapter 3). This prevented outright the possibility of using Safranin O as the VS. Experiments were performed using Orange II as the VS and a net absorbance at 484 nm was explored as a possible way to determine the Orange II bleaching rate. However, an increase in the baseline absorbance of the

solution in the UV-vis spectrum due to oxidation product formation resulted in several negative net absorbance values. This resulted in impractical measurements and subsequently made the determinations of the second order rate constant  $k_{\text{II}}^{1\text{-Naphthol}}$  very cumbersome and unreliable.

### 7.3 CONCLUSIONS

The parallel reaction model can serve as a kinetic tool allowing quick measurements of secondary rate constant,  $k_{II}^{IS}$  for oxidation of IS using UV-vis spectroscopy. The second order rate constants  $k_{II}^{IS}$  values obtained from this indirect approach were consistent with second order rate constants  $k_{II}$  values obtained via direct measurements by UPLC for propranolol and phenol for both VS – Orange II and Safranin O dyes. For an easily oxidizable VS like Orange II, greater [IS] is required in order to keep the reaction competitive, such that  $k_{II}^{IS} [IS] \sim k_{II}^{VS} [VS]$ . Substrate inhibition of **1a**, which manifests in decreased  $k_I$  values is significant for  $k_{II}^{IS}$  calculations. Different substrates inhibit **1a** to different extents, and the most realistic **1a** oxidation rate constant,  $k_I$  is the effective rate constant,  $k_{I,eff}$  which is a value between the exclusive rate constants  $k_I^{VS}$  and  $k_I^{IS}$ . The inhibited rate constant,  $k_{I,eff}$  was calculated taking into account the equilibrium binding constant,  $K$ , between **1a** and the substrate. Compared to using substrate specific exclusive rate constants  $k_I^{VS}$  or  $k_I^{IS}$ , using effective rate constants,  $k_{I,eff}$  for a reaction mixture gave the best agreement between the indirect second order rate constants  $k_{II}^{IS}$  and the directly measured rate constants,  $k_{II}$  for oxidation of propranolol and phenol. It was more accurate to use effective rate constant  $k_{I,eff}$  in scenarios wherein one of the substrates is significantly more inhibiting than the other, such as in Orange II – propranolol and Safranin O – phenol systems. The second rate constant  $k_{II}^{phenol}$  obtained from using rate constants  $k_{I,eff}$  with Orange II and Safranin O as the VS were  $4400 \pm 580$  and  $7900 \pm 850 \text{ M}^{-1} \text{ s}^{-1}$ , respectively. Both these values were in close agreement with second order rate constant,  $k_{II}$  value of  $7700 \pm 230 \text{ M}^{-1} \text{ s}^{-1}$  for oxidation of phenol. Similarly, the second rate constant  $k_{II}^{prop}$  obtained from using rate constants  $k_{I,eff}$  with Orange II and Safranin O as the VS were  $40 \pm 7$  and  $40 \pm 13 \text{ M}^{-1} \text{ s}^{-1}$ , respectively. Again these values were in close agreement with second order rate constant,  $k_{II}$  value of  $70 \pm 20 \text{ M}^{-1} \text{ s}^{-1}$  for propranolol oxidation. It is also important to note here that while the

determination of second order rate constants,  $k_{II}$  by UPLC for both phenol and propranolol took more than two weeks, indirect determination of second order rate constants,  $k_{II}^{\text{phenol}}$  and  $k_{II}^{\text{prop}}$  was completed in 2 days. Care should be taken while working with IS having limited solubilities in water to ensure no precipitation occurs. Similarly, a control experiment with IS should be performed to ensure its oxidation products do not interfere with the peak of interest in the VS.

Although the current work is focused on TAML catalyzed oxidations, the practical implications of this indirect approach can be extended to other catalytic systems. With the ever-growing list of contaminants (that may behave as micropollutants) being detected in water, there is a pressing need for a quick diagnostic technique to study quantitatively the efficiency of wastewater treatment techniques that can be universal and easy to use. With the advancement in portable UV-vis spectrometers, the feasibility of this technique to be universal is further enhanced.

## 7.4 EXPERIMENTAL

### 7.4.1 Materials.

Purified TAML activator **1a** was obtained from the IGS stock supplies. Buffer solutions were prepared from  $\text{KH}_2\text{PO}_4$  (Acros or Sigma) or  $\text{K}_2\text{HPO}_4$  (Merck); the pH of the solutions were adjusted with concentrated solutions of KOH or  $\text{H}_3\text{PO}_4$ . Hydrogen peroxide (30%) was purchased from Fischer. Catalase from bovine liver (lyophilized powder, 2000–5000 units/mg of protein) was purchased from Sigma. Safranin O was purchased from Acros and ( $\pm$ )-propranolol hydrochloride (>99%), Orange II and phenol were purchased from Sigma. HPLC grade methanol and water purchased from Fischer were used for preparing solutions and running chromatographic analyses.

### 7.4.2 Instrumentation.

All analyses involving UV-vis were performed using Agilent UV 8543 spectrophotometer (with Agilent Chemstation software) and Shimadzu UV-1800 double-beam spectrophotometer (with UV probe 2.43 software) with attached temperature controllers. The pH measurements were made using an Accumet Basic AB15 pH meter from Fischer Scientific. UPLC experiments, for determining  $k_{\text{II}}$  from direct analyses, were performed with a Shimadzu LC system with LC 20AB pump, SIL 20A autosampler, CTO 20A column oven, and an RF 20A XS fluorescence detector. A Kinetex (Phenomenex) 5  $\mu\text{M}$  EVO C18 100A column ( $4.6 \times 50$  mm) was used for all kinetic analyses. The LC method (5 min) for phenol analyses (injections 100  $\mu\text{L}$ ) consisted of 1 mL/min flow rate, 20% methanol in pH 3 phosphate buffer (0.01 M), 40 °C column temperature, and fluorescence detection with 260 nm excitation and 305 nm emission, with automatic peak integration and Lab Solutions software data analysis. The LC method for propranolol has been reported previously.<sup>14</sup>



#### **7.4.3 Direct kinetic analyses using UPLC.**

Stock solution of **1a** ( $5 \times 10^{-3}$  M) was prepared in HPLC grade methanol, phenol ( $5 \times 10^{-3}$  M) and  $\text{H}_2\text{O}_2$  (1 M) were prepared in HPLC grade water. Solutions of  $\text{H}_2\text{O}_2$  were stored under refrigeration and standardized daily before use by UV-vis spectroscopy at 230 nm in water ( $\epsilon = 72.4 \text{ M}^{-1} \text{ cm}^{-1}$ ).<sup>60</sup> Reaction mixtures were prepared by adding calculated amounts of phenol, **1a**, and phosphate buffer to make a 10 mL buffered reaction mixture. The reaction mixture was kept at 25 °C in a water bath, and the reaction was initiated by adding a suitable aliquot of the stock solution of  $\text{H}_2\text{O}_2$  to the mixture. After certain time intervals, aliquots of the reaction mixture were quenched with catalase (10  $\mu\text{L}$  of 10 mg  $\text{mL}^{-1}$  solution) and analyzed for phenol using UPLC. Initial rates were calculated from linear plots of [phenol] vs time when the conversion of phenol did not exceed 20 %. Each data point reported is an average of triplicate separate experiments. propranolol direct analyses have been reported previously.<sup>14</sup>

#### **7.4.4 Indirect kinetic analyses via parallel reaction approach using UV-vis spectroscopy.**

Stock solutions of propranolol, phenol, Orange II and Safranin O (all  $10^{-3}$  M) were prepared in HPLC grade water. Corresponding amounts of **1a**, visible substrate (VS) - Orange II, Safranin O; and invisible substrate (IS) - propranolol, phenol; were added to a cuvette and the volume was made up to 2 mL with 0.01 M pH 7 phosphate buffer. Reactions were initiated by adding hydrogen peroxide to the mixture and monitored every 30 s. Initial rates for bleaching of Orange II and Safranin O (in presence of IS) were determined by monitoring a decrease in absorbance at 486 nm ( $\epsilon = 21000 \text{ M}^{-1} \text{ cm}^{-1}$ ) and 520 nm ( $\epsilon = 34000 \text{ M}^{-1} \text{ cm}^{-1}$ ) respectively. Each data point reported for indirect analyses is an average of three separate experiments.

## 7.5 APPENDIX

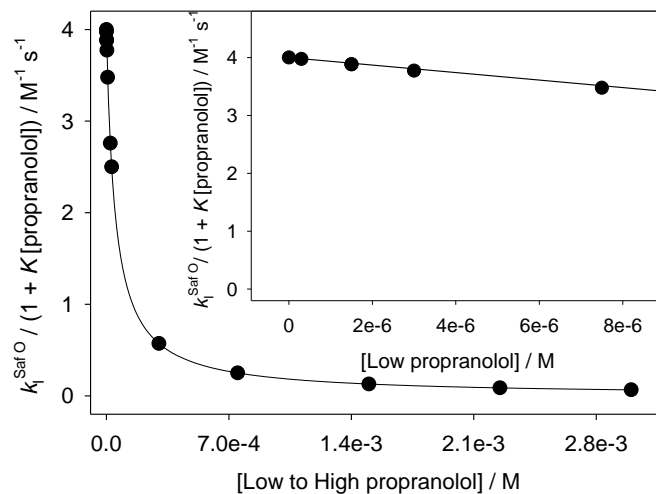


Figure 7.7 : Plot depicting the projected impact of propranolol substrate inhibition on the less inhibited  $k_I^{\text{SafO}}$  from [propranolol] = 0 to low mM. Note,  $k_{I,\text{eff}} = k_I^{\text{SafO}} / (1 + K[\text{propranolol}]) \approx 0$  when [propranolol]  $\geq 3 \times 10^{-3}$  M. Inset shows the same projection until [propranolol] =  $8 \times 10^{-6}$  M

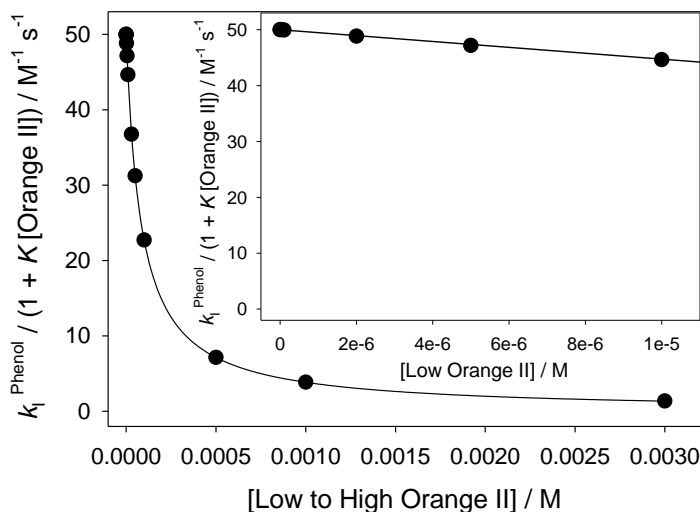


Figure 7.8 Plot depicting the projected impact of Orange II substrate inhibition on the less inhibited  $k_I^{\text{phenol}}$  from [orange II] = 0 to low mM. Note,  $k_{I,\text{eff}} = k_I^{\text{phenol}} / (1 + K[\text{orange II}]) \approx 0$  when [orange II]  $> 3 \times 10^{-3}$  M. Inset shows the same projection until [orange II] =  $1 \times 10^{-5}$  M

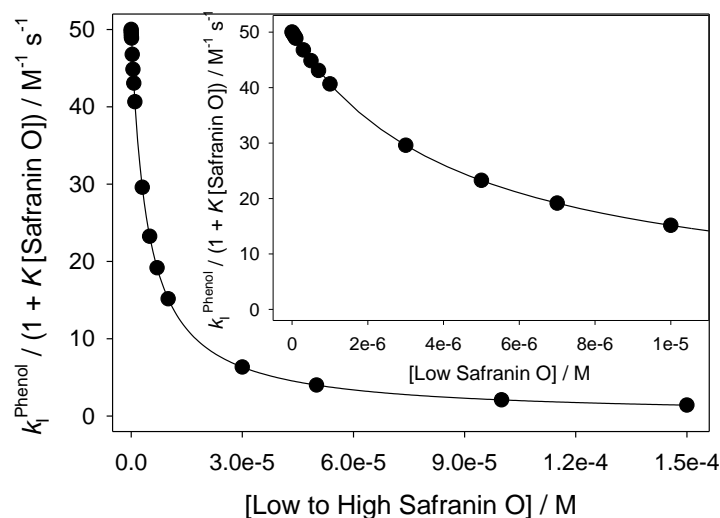


Figure 7.9 Plot depicting the projected impact of Safranin O substrate inhibition on the less inhibited  $k_1^{\text{phenol}}$  from  $[\text{safranin O}] = 0$  to low mM. Note,  $k_{1,\text{eff}} = k_1^{\text{phenol}} / (1 + K[\text{safranin O}]) \approx 0$  when  $[\text{safranin O}] > 1.5 \times 10^{-4} \text{ M}$ . Inset shows the same projection until  $[\text{safranin O}] = 1 \times 10^{-5} \text{ M}$

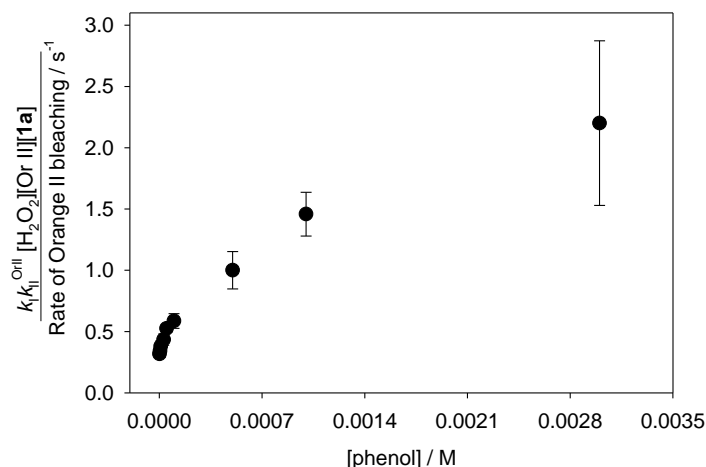


Figure 7.10 Plot of  $\frac{dk_1^{\text{eff}} k_{\text{II}}^{\text{Or II}} [\text{Fe}][\text{H}_2\text{O}_2][\text{Or II}]}{d[\text{Or II}]}$  versus  $[\text{phenol}]$  with  $k_{1,\text{eff}} = 31.3 \text{ M}^{-1} \text{s}^{-1}$ . There is a rising hyperbolic dependence on  $[\text{phenol}]$  when all the data points are taken into account. Reaction Conditions:  $5 \times 10^{-5} \text{ M}$  Orange II,  $2.5 \times 10^{-3} \text{ M}$   $\text{H}_2\text{O}_2$ ,  $5 \times 10^{-7} \text{ M}$  **1a**, 0.01 M phosphate buffer, pH 7, 25 °C.

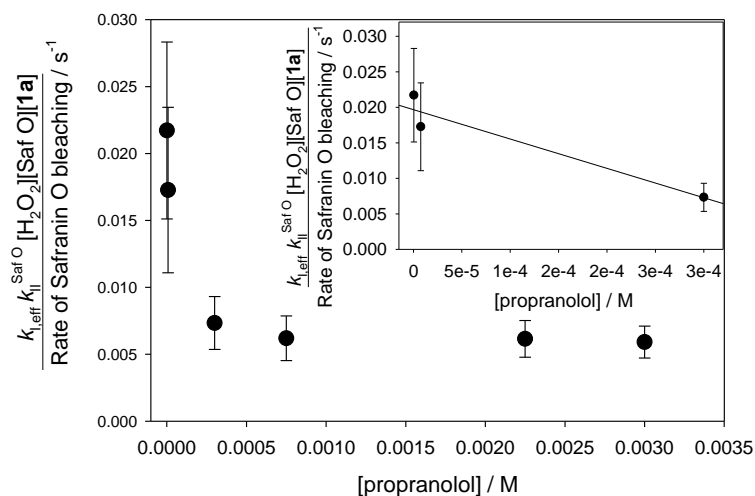


Figure 7.11 Plot of  $\frac{dk_{l,eff} k_{II}^{SafO} [Fe][H_2O_2][SafO]}{d[SafO]}$  versus [propranolol] with varying  $k_{l,eff}$ . Inset: The same plot at [low propranolol]. Reaction Conditions:  $3 \times 10^{-5}$  M Safranin O,  $3 \times 10^{-3}$  M  $H_2O_2$ ,  $3.3 \times 10^{-7}$  M **1a**, 0.01 M phosphate buffer, pH 7, 25 °C.

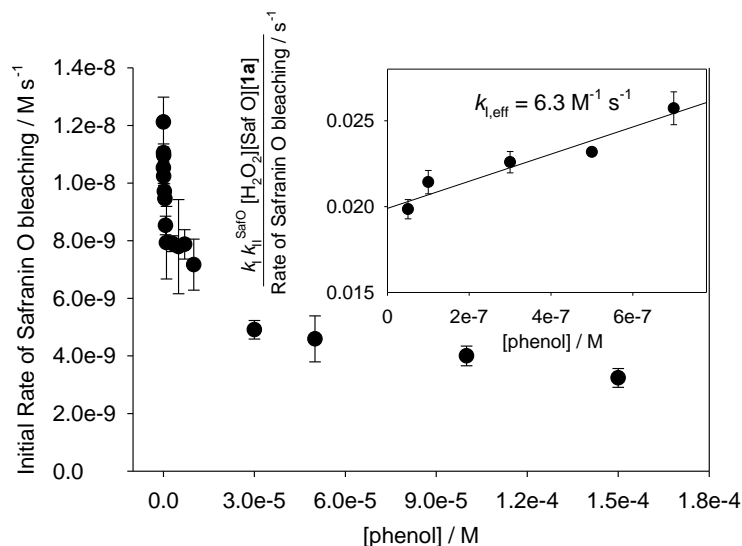


Figure 7.12 Initial rate of Safranin O bleaching as a function of [phenol]. Inset: Linear region of a plot of  $\frac{dk_{l,eff} k_{II}^{SafO} [Fe][H_2O_2][SafO]}{d[SafO]}$  versus [phenol] with  $k_{l,eff} = 31.3 \text{ M}^{-1} \text{ s}^{-1}$ . Reaction Conditions:  $3 \times 10^{-5}$  M Safranin O,  $3 \times 10^{-3}$  M  $H_2O_2$ ,  $5 \times 10^{-7}$  M **1a**, 0.01 M phosphate buffer, pH 7, 25 °C.

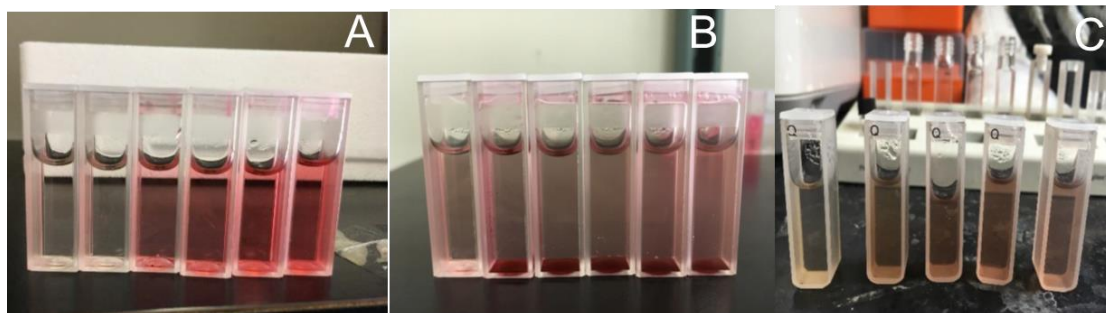


Figure 7.13 (A) Competitive bleaching of Safranin-O, with increasing  $[\text{propranolol}] = (3 \times 10^{-7} - 3 \times 10^{-3} \text{ M})$  on moving from left to right. Reaction Conditions:  $3 \times 10^{-5} \text{ M}$  Safranin O,  $3 \times 10^{-3} \text{ M}$   $\text{H}_2\text{O}_2$ ,  $3.3 \times 10^{-7} \text{ M}$  **1a**, 0.01 M phosphate buffer, pH 7 25 °C. (B) Competitive bleaching of Safranin-O, with increasing  $[\text{phenol}] = (3 \times 10^{-7} - 3 \times 10^{-3} \text{ M})$  on moving from left to right, after several hours of reaction. Reaction Conditions:  $3 \times 10^{-5} \text{ M}$  Safranin O,  $3 \times 10^{-3} \text{ M}$   $\text{H}_2\text{O}_2$ ,  $3.3 \times 10^{-7} \text{ M}$  **1a**, 0.01 M phosphate buffer, pH 7 25 °C. (C) **1a**-catalyzed oxidation of phenol, with increasing  $[\text{phenol}] = (3 \times 10^{-7} - 3 \times 10^{-3} \text{ M})$  on moving from left to right, after several hours of reaction. Reaction Conditions:  $3 \times 10^{-3} \text{ M}$   $\text{H}_2\text{O}_2$ ,  $3.3 \times 10^{-7} \text{ M}$  **1a**, 0.01 M phosphate buffer, pH 7 25 °C.

## 7.6 REFERENCES

- (1) Bexfield, L. M.; Toccalino, P. L.; Belitz, K.; Foreman, W. T.; Furlong, E. T. Hormones and Pharmaceuticals in Groundwater Used As a Source of Drinking Water Across the United States. *Environ. Sci. Technol.* **2019**, *53* (6), 2950–2960.
- (2) Rogowska, J.; Cieszyńska-Semenowicz, M.; Ratajczyk, W.; Wolska, L. Micropollutants in Treated Wastewater. *Ambio* **2019**.
- (3) Snyder, S. A. Occurrence of Pharmaceuticals in U.S. Drinking Water. In *Contaminants of Emerging Concern in the Environment: Ecological and Human Health Considerations*; ACS Symposium Series; American Chemical Society, 2016; Vol. 1048, pp 69–80.
- (4) Khetan, S. K.; Collins, T. J. Human Pharmaceuticals in the Aquatic Environment: A Challenge to Green Chemistry. *Chem. Rev.* **2007**, *107* (6), 2319–2364.
- (5) Schwarzenbach, R. P.; Egli, T.; Hofstetter, T. B.; von Gunten, U.; Wehrli, B. Global Water Pollution and Human Health. *Annu. Rev. Environ. Resour.* **2010**, *35* (1), 109–136.
- (6) Schwarzenbach, R. P.; Escher, B. I.; Fenner, K.; Hofstetter, T. B.; Johnson, C. A.; von Gunten, U.; Wehrli, B. The Challenge of Micropollutants in Aquatic Systems. *Science* (80-. ). **2006**, *313* (5790), 1072 LP – 1077.
- (7) Luo, Y.; Guo, W.; Ngo, H. H.; Nghiem, L. D.; Hai, F. I.; Zhang, J.; Liang, S.; Wang, X. C. A Review on the Occurrence of Micropollutants in the Aquatic Environment and Their Fate and Removal during Wastewater Treatment. *Sci Total Env.* **2014**, *473–474*, 619–641.
- (8) Margot, J.; Rossi, L.; Barry, D. A.; Holliger, C. A Review of the Fate of Micropollutants in Wastewater Treatment Plants. *WIREs Water* **2015**, *2* (5), 457–487.
- (9) Margot, J.; Kienle, C.; Magnet, A.; Weil, M.; Rossi, L.; de Alencastro, L. F.; Abegglen, C.; Thonney, D.; Chevre, N.; Scharer, M.; Barry, D. A. Treatment of Micropollutants in Municipal Wastewater: Ozone or Powdered Activated Carbon? *Sci Total Env.* **2013**, *461–462*, 480–498.
- (10) Patel, M.; Kumar, R.; Kishor, K.; Mlsna, T.; Pittman, C. U.; Mohan, D. Pharmaceuticals of Emerging Concern in Aquatic Systems: Chemistry, Occurrence, Effects, and Removal Methods. *Chem. Rev.* **2019**, *119* (6), 3510–3673.
- (11) Daughton, C. G.; Ternes, T. A. Pharmaceuticals and Personal Care Products in the Environment: Agents of Subtle Change? *Environ. Health Perspect.* **1999**, *107* (Suppl 6), 907–938.
- (12) Chiara, P.; Barbara, M.; Tamar, K.; Anojys, M.; Denis, T.; Nathalie, C. Occurrence and Fate of Micropollutants in the Vidy Bay of Lake Geneva, Switzerland. Part I: Priority List for Environmental Risk Assessment of Pharmaceuticals. *Environ. Toxicol. Chem.* **2010**, *29* (8), 1649–1657.
- (13) Benotti, M. J.; Trenholm, R. A.; Vanderford, B. J.; Holady, J. C.; Stanford, B. D.; Snyder, S. A. Pharmaceuticals and Endocrine Disrupting Compounds in U.S. Drinking Water. *Environ. Sci. Technol.* **2009**, *43* (3), 597–603.
- (14) Somasundar, Y.; Shen, L. Q.; Hoane, A. G.; Tang, L. L.; Mills, M. R.; Burton, A. E.;

- Ryabov, A. D.; Collins, T. J. Structural, Mechanistic, and Ultradilute Catalysis Portrayal of Substrate Inhibition in the TAML–Hydrogen Peroxide Catalytic Oxidation of the Persistent Drug and Micropollutant, Propranolol. *J. Am. Chem. Soc.* **2018**, *140* (38), 12280–12289.
- (15) Vandenberg, L. N.; Colborn, T.; Hayes, T. B.; Heindel, J. J.; Jacobs, D. R.; Lee, D. H.; Shioda, T.; Soto, A. M.; vom Saal, F. S.; Welshons, W. V.; Zoeller, R. T.; Myers, J. P. Hormones and Endocrine-Disrupting Chemicals: Low-Dose Effects and Nonmonotonic Dose Responses. *Endocr. Rev.* **2012**, *33* (3), 378–455.
  - (16) Colborn, T.; vom Saal, F. S.; Soto, A. M. Developmental Effects of Endocrine-Disrupting Chemicals in Wildlife and Humans. *Environ. Health Perspect.* **1993**, *101* (5), 378–384.
  - (17) Huggett, D. B.; Brooks, B. W.; Peterson, B.; Foran, C. M.; Schlenk, D. Toxicity of Select Beta Adrenergic Receptor-Blocking Pharmaceuticals (B-Blockers) on Aquatic Organisms. *Arch. Env. Contam. Toxicol.* **2002**, *43* (2), 229–235.
  - (18) Onundi, Y.; Drake, B. A.; Malecky, R. T.; DeNardo, M. A.; Mills, M. R.; Kundu, S.; Ryabov, A. D.; Beach, E. S.; Horwitz, C. P.; Simonich, M. T.; Truong, L.; Tanguay, R. L.; Wright, L. J.; Singhal, N.; Collins, T. J. A Multidisciplinary Investigation of the Technical and Environmental Performances of TAML/Peroxide Elimination of Bisphenol A Compounds from Water. *Green Chem.* **2017**, *19* (18), 4234–4262.
  - (19) Mills, M. R.; Arias-Salazar, K.; Baynes, A.; Shen, L. Q.; Churchley, J.; Beresford, N.; Gayathri, C.; Gil, R. R.; Kanda, R.; Jobling, S.; Collins, T. J. Removal of Ecotoxicity of 17alpha-Ethinylestradiol Using TAML/Peroxide Water Treatment. *Sci Rep* **2015**, *5*, 10511.
  - (20) Calafat, A. M.; Ye, X.; Wong, L.-Y.; Reidy, J. A.; Needham, L. L. Exposure of the US Population to Bisphenol A and 4-Tertiary-Octylphenol: 2003–2004. *Environ. Health Perspect.* **2007**, *116* (1), 39–44.
  - (21) Grün, F.; Blumberg, B. Environmental Obesogens: Organotins and Endocrine Disruption via Nuclear Receptor Signaling. *Endocrinology* **2006**, *147* (6), s50–s55.
  - (22) Diamanti-Kandarakis, E.; Bourguignon, J.-P.; Giudice, L. C.; Hauser, R.; Prins, G. S.; Soto, A. M.; Zoeller, R. T.; Gore, A. C. Endocrine-Disrupting Chemicals: An Endocrine Society Scientific Statement. *Endocr. Rev.* **2009**, *30* (4), 293–342.
  - (23) Snyder, S. A. Removal of EDCs and Pharmaceuticals in Drinking and Reuse Treatment Processes. **2007**.
  - (24) Anumol, T.; Wu, S.; Marques dos Santos, M.; Daniels, K. D.; Snyder, S. a. Rapid Direct Injection LC-MS/MS Method for Analysis of Prioritized Indicator Compounds in Wastewater Effluent. *Environ. Sci. Water Res. Technol.* **2015**, *1* (5), 632–643.
  - (25) Park, M.; Anumol, T.; Daniels, K. D.; Wu, S.; Ziska, A. D.; Snyder, S. A. Predicting Trace Organic Compound Attenuation by Ozone Oxidation: Development of Indicator and Surrogate Models. *Water Res.* **2017**, *119*, 21–32.
  - (26) Barbara, M.; Florence, B.; Hans, R.; Dominique, G.; Felipe, de A. L.; Chiara, P.; Nathalie, C.; Tamar, K. Occurrence and Fate of Micropollutants in the Vidy Bay of Lake Geneva, Switzerland. Part II: Micropollutant Removal between Wastewater and Raw Drinking Water. *Environ. Toxicol. Chem.* **2010**, *29* (8), 1658–1668.

- (27) Grebe, S. K.; Singh, R. J. LC-MS/MS in the Clinical Laboratory - Where to From Here? *Clin. Biochem. Rev.* **2011**, 32 (1), 5–31.
- (28) Youdim, K. A.; Saunders, K. C. A Review of LC–MS Techniques and High-Throughput Approaches Used to Investigate Drug Metabolism by Cytochrome P450s. *J. Chromatogr. B* **2010**, 878 (17), 1326–1336.
- (29) Chen, X.-H.; Zhao, Y.-G.; Qiu, Q.-L.; Zhu, Y.; Min, J.-Q.; Jin, M.-C. A Fast and High Throughput LC-MS/MS Method for the Determination of 58 Human and Veterinary Drugs in River Water. *Anal. Methods* **2017**, 9 (29), 4228–4233.
- (30) Zedda, M.; Zwiener, C. Is Nontarget Screening of Emerging Contaminants by LC-HRMS Successful? A Plea for Compound Libraries and Computer Tools. *Anal. Bioanal. Chem.* **2012**, 403 (9), 2493–2502.
- (31) Herrera-Lopez, S.; Hernando, M. D.; García-Calvo, E.; Fernández-Alba, A. R.; Ulaszewska, M. M. Simultaneous Screening of Targeted and Non-Targeted Contaminants Using an LC-QTOF-MS System and Automated MS/MS Library Searching. *J. Mass Spectrom.* **2014**, 49 (9), 878–893.
- (32) Ryabov, A. D. *Kinetics and Mechanisms of Chemical and Enzymatic Reactions*; M.V. Lomonosov Moscow State University, Carnegie Mellon University, 2015.
- (33) Cornish-Bowden, A. *Fundamentals of Enzyme Kinetics*; Portland Press: London, UK, 1995.
- (34) Connors, K. A. *Chemical Kinetics: The Study of Reaction Rates in Solution*; John Wiley & Sons, 1990.
- (35) Frost, A.; Pearson, R. Kinetics and Mechanism. *J. Phys. Chem.* **1961**, 65 (2), 384.
- (36) Berezin, I. V.; Martinek, K. *Principles of the Physical Chemistry of Enzymic Catalysis*; Vysshaya Shkola: Moscow, 1977.
- (37) Laidler, K. J.; Bunting, P. S. *The Chemical Kinetics of Enzyme Action*; Clarendon Press Oxford, 1973; Vol. 84.
- (38) CAS-A Division of the American Chemical Society <https://www.cas.org/>.
- (39) Perkampus, H.-H. *UV-VIS Spectroscopy and Its Applications*; Springer Science & Business Media, 2013.
- (40) Roccaro, P.; Chang, H.-S.; Vagliasindi, F. G. A.; Korshin, G. V. Differential Absorbance Study of Effects of Temperature on Chlorine Consumption and Formation of Disinfection By-Products in Chlorinated Water. *Water Res.* **2008**, 42 (8), 1879–1888.
- (41) Kitis, M.; Karanfil, T.; Kilduff, J. E.; Wigton, A. The Reactivity of Natural Organic Matter to Disinfection By-Products Formation and Its Relation to Specific Ultraviolet Absorbance. *Water Sci. Technol.* **2001**, 43 (2), 9–16.
- (42) Collins, T. J.; DeNardo, M. A.; Warner, G. R.; Gordon-Wylie, S. W.; Ellis, W. C.; Somasundar, Y. Far Superior Oxidation Catalysts Based on Macrocyclic Compounds, October 25, 2018.
- (43) Warner, G. R.; Somasundar, Y.; Jansen, K. C.; Kaaret, E. Z.; Weng, C.; Burton, A. E.; Mills, M. R.; Shen, L. Q.; Ryabov, A. D.; Pros, G.; Pintauer, T.; Biswas, S.; Hendrich, M.



- P.; Taylor, J. A.; Vom Saal, F. S.; Collins, T. J. Bioinspired, Multidisciplinary, Iterative Catalyst Design Creates the Highest Performance Peroxidase Mimics and the Field of Sustainable Ultradilute Oxidation Catalysis (SUDOC). *ACS Catal.* **2019**, 7023–7037.
- (44) Collins, T. J. Designing Ligands for Oxidizing Complexes. *Acc. Chem. Res.* **1994**, 27 (9), 279–285.
- (45) Collins, T. J. TAML Oxidant Activators: A New Approach to the Activation of Hydrogen Peroxide for Environmentally Significant Problems. *Acc. Chem. Res.* **2002**, 35 (9), 782–790.
- (46) Ryabov, A. D.; Collins, T. J. Mechanistic Considerations on the Reactivity of Green FeIII-TAML Activators of Peroxides. *Adv. Inorg. Chem.* **2009**, 61, 471–521.
- (47) Ryabov, A. D. Green Challenges of Catalysis via Iron(IV)Oxo and Iron(V)Oxo Species. *Adv. Inorg. Chem.* **2013**, 65, 117–163.
- (48) Shen, L. Q.; Beach, E. S.; Xiang, Y.; Tshudy, D. J.; Khanina, N.; Horwitz, C. P.; Bier, M. E.; Collins, T. J. Rapid, Biomimetic Degradation in Water of the Persistent Drug Sertraline by TAML Catalysts and Hydrogen Peroxide. *Env. Sci Technol* **2011**, 45 (18), 7882–7887.
- (49) Kundu, S.; Chanda, A.; Espinosa-Marvan, L.; Khetan, S. K.; Collins, T. J. Facile Destruction of Formulated Chlorpyrifos through Green Oxidation Catalysis. *Catal. Sci. Technol.* **2012**, 2 (6), 1165–1172.
- (50) Chanda, A.; Khetan, S. K.; Banerjee, D.; Ghosh, A.; Collins, T. J. Total Degradation of Fenitrothion and Other Organophosphorus Pesticides by Catalytic Oxidation Employing Fe-TAML Peroxide Activators. *J Am Chem Soc* **2006**, 128 (37), 12058–12059.
- (51) Chahbane, N.; Popescu, D. L.; Mitchell, D. A.; Chanda, A.; Lenoir, D.; Ryabov, A. D.; Schramm, K. W.; Collins, T. J. FeIII-TAML-Catalyzed Green Oxidative Degradation of the Azo Dye Orange II by H<sub>2</sub>O<sub>2</sub> and Organic Peroxides: Products, Toxicity, Kinetics, and Mechanisms. *Green Chem.* **2007**, 9 (1), 49–57.
- (52) Ellis, W. C.; Tran, C. T.; Denardo, M. A.; Fischer, A.; Ryabov, A. D.; Collins, T. J. Design of More Powerful Iron-TAML Peroxidase Enzyme Mimics. *J. Am. Chem. Soc.* **2009**, 131 (50), 18052–18053.
- (53) Chanda, A.; Ryabov, A. D.; Mondal, S.; Alexandrova, L.; Ghosh, A.; Hangun-Balkir, Y.; Horwitz, C. P.; Collins, T. J. Activity-Stability Parameterization of Homogeneous Green Oxidation Catalysts. *Chem. - A Eur. J.* **2006**, 12 (36), 9336–9345.
- (54) Kundu, S.; Chanda, A.; Thompson, J. V. K.; Diabes, G.; Khetan, S. K.; Ryabov, A. D.; Collins, T. J. Rapid Degradation of Oxidation Resistant Nitrophenols by TAML Activator and H<sub>2</sub>O<sub>2</sub>. *Catal. Sci. Technol.* **2015**, 5 (3), 1775–1782.
- (55) Shappell, N. W.; Vrabell, M. A.; Madsen, P. J.; Harrington, G.; Billey, L. O.; Hakk, H.; Larsen, G. L.; Beach, E. S.; Horwitz, C. P.; Ro, K.; Hunt, P. G.; Collins, T. J. Destruction of Estrogens Using Fe-TAML/Peroxide Catalysis. *Environ. Sci. Technol.* **2008**, 42 (4), 1296–1300.
- (56) Somasundar, Y.; Ryabov, A.; Collins, T. TAML Activators for Green Oxidative Degradation of Propranolol: A Comparative Evaluation. In *ABSTRACTS OF PAPERS OF THE AMERICAN CHEMICAL SOCIETY*; AMER CHEMICAL SOC 1155 16TH ST, NW,

WASHINGTON, DC 20036 USA, 2017; Vol. 253.

- (57) Warner, G.; Mills, M.; Enslin, C.; Pattanayak, S.; Panda, C.; Sen Gupta, S.; Ryabov, A. D.; Collins, T. J. Reactivity of N-Tailed ('Biuret') TAMLs in Water: Kinetics of the Catalyzed Oxidation of Orange II by H<sub>2</sub>O<sub>2</sub>. Synthesis and X-Ray Characterization of an N-Phenyl Biuret TAML. *Chem. - Eur. J.* **2015**, *21* (16), 6226–6233.
- (58) DeNardo, M. A.; Mills, M. R.; Ryabov, A. D.; Collins, T. J. Unifying Evaluation of the Technical Performances of Iron-Tetra-Amido Macrocyclic Ligand Oxidation Catalysts. *J. Am. Chem. Soc.* **2016**, *138* (9), 2933–2936.
- (59) Somasundar, Y.; Lu, I.; Bradley, J.; Hoane, A. G.; Qian, L.; Miller, J.; Ryabov, A. D.; Collins, T. J. *Review of the Kinetic and Mechanistic Parameters of TAML Activators and New TAML Activators in the Oxidation of Persistent Substrates Safranin O and Propranolol.*
- (60) George, P. L. B.-01. The Chemical Nature of the Second Hydrogen Peroxide Compound Formed by Cytochrome c Peroxidase and Horseradish Peroxidase. *Biochem. J.* **1953**, *54*, 267–276.